

# UC Irvine

## UC Irvine Electronic Theses and Dissertations

### Title

Engineering Protein-Based Nanoparticles for Infectious Disease Vaccine Development

### Permalink

<https://escholarship.org/uc/item/97c8d0m4>

### Author

Ramirez, Aaron

### Publication Date

2024

### Copyright Information

This work is made available under the terms of a Creative Commons Attribution License, available at <https://creativecommons.org/licenses/by/4.0/>

Peer reviewed|Thesis/dissertation

UNIVERSITY OF CALIFORNIA,  
IRVINE

Engineering Protein-Based Nanoparticles for Infectious Disease Vaccine Development  
DISSERTATION

submitted in partial satisfaction of the requirements for the degree of

DOCTOR OF PHILOSOPHY  
in Chemical and Biomolecular Engineering

by

Aaron Ramirez

Dissertation Committee:

Professor Szu-Wen Wang, Chair

Associate Professor Han Li

Associate Professor in Residence David Huw Davies

2024

Chapter 1 © 2020 Wiley Periodicals LLC.  
Chapter 2 © 2023 American Chemical Society  
Chapter 3 © 2023 American Chemical Society  
All other materials © 2024 Aaron Ramirez

## DEDICATION

To

My grandparents, Eugenio Beltran, Amelia Beltran, and Teresa Ramirez, who passed during my  
pursuit

My family, Adalberto Rogelio Ramirez, Nelida Beltran-Ramirez, Timoteo Gabriel Ramirez,  
Daniel Benjamin Ramirez, and Elizabeth Ramirez

I have no special talent. I am only passionately curious.

## TABLE OF CONTENTS

	Page
LIST OF ABBREVIATIONS	v
LIST OF FIGURES	viii
LIST OF SCHEMES	x
ACKNOWLEDGMENTS	xi
VITA	xii
ABSTRACT OF THE DISSERTATION	xiv
CHAPTER 1: BACKGROUND	
1.1. Influenza and the Immune System	2
1.2. <i>Coxiella burnetii</i> and the Immune System	4
1.3. Nanoparticles for Infectious Disease Vaccine Platforms	6
1.4. Pyruvate Dehydrogenase E2 and its Use as a Platform for Inducing Immune Responses	8
1.5. Toll-like Receptor (TLR) Agonists as Immune System Adjuvants	9
1.6. Project Goals and Specific Aims of Each Chapter	12
1.7. References	14
CHAPTER 2: PROTEIN NANOPARTICLE-MEDIATED DELIVERY OF RECOMBINANT INFLUENZA HEMAGGLUTININ ENHANCES IMMUNOGENICITY AND BREADTH OF THE ANTIBODY RESPONSE	
2.1. Abstract	23
2.2. Introduction	23
2.3. Methods	26
2.4. Results and Discussion	32
2.5. Conclusions	46
2.6. Acknowledgements	47
2.7. References	48
CHAPTER 3: ENGINEERING PROTEIN NANOPARTICLES FUNCTIONALIZED WITH AN IMMUNODOMINANT <i>COXIELLA BURNETII</i> ANTIGEN TO GENERATE A Q FEVER VACCINE	
3.1. Abstract	56
3.2. Introduction	57
3.3. Methods	59
3.4. Results and Discussion	68
3.5. Conclusions	82
3.6. Acknowledgements	83
3.7. References	84

CHAPTER 4: ENGINEERING PROTEIN NANOPARTICLES CO-DELIVERING MULTIPLE TOLL-LIKE RECEPTOR AGONISTS AND POTENTIAL PANDEMIC INFLUENZA HEMAGGLUTININ H5 TO ENHANCE VACCINE IMMUNOGENICITY AND EFFICACY	
4.1. Abstract	92
4.2. Introduction	93
4.3. Methods	95
4.4. Results and Discussion	103
4.5. Conclusions	124
4.6. Acknowledgements	125
4.7. References	126
CHAPTER 5: CONCLUSIONS AND FUTURE DIRECTIONS	
5.1. Functionalizing E2 protein nanoparticles with whole protein antigens and immunostimulatory agonists	134
5.2. Construction of E2 nanoparticle-based vaccines enhance prophylactic immune responses against infectious disease antigens	136
5.3. <i>In vitro</i> evaluation of co-delivering multiple adjuvants on a single E2 nanoparticle	142
5.4. References	145
APPENDIX A	148
APPENDIX B	172

## LIST OF ABBREVIATIONS

Abs	Absorbance
APC	Antigen presenting cell
BCA	Bicinchoninic acid
BCR	B cell receptor
BMDC	Bone marrow-derived dendritic cell
BMDM	Bone marrow-derived macrophage cell
BMPH	N- $\beta$ -maleimidopropionic acid hydrazide
CHO	Chinese hamster ovary
CpG	Nonmethylated single-stranded DNA with repeating CG motifs
CTL	CD8+ cytotoxic T lymphocyte
D381C	E2 nanoparticle with an internal point mutation to cysteine at amino acid 381
DLS	Dynamic light scattering
DTT	dithiothreitol
E2	Catalytic subunit of the pyruvate dehydrogenase enzyme complex
E279C	E2 nanoparticle with an external point mutation to cysteine at amino acid 279
ELISpot	Enzyme-linked immunospot assay
FliC	Flagellin
FliCc	Cysteine-stabilized flagellin
GAPDH	Glyceraldehyde-3-phosphate dehydrogenase
GFP	Green fluorescent protein
HA	Hemagglutinin
HA0	Full-length hemagglutinin
HA1	Hemagglutinin head region
HA2	Hemagglutinin stem region
His-tag	Polyhistidine-tag

IAV	Influenza A virus
IFN- $\gamma$	Interferon gamma
LAL	Limulus ameocyte lysate
LPS	Lipopolysaccharide
mAbs	Monoclonal antibodies
<i>mal-tNTA</i>	<i>maleimido cyclic tris-NTA</i>
MHC	Major Histocompatibility complex
MPLA	Monophosphoryl lipid A
nAbs	Neutralizing antibodies
NP	Nanoparticle
NTA	Ni(II)-chelated nitrilotriacetic acid
OVA	Chicken ovalbumin
Pam3	Pam3CSK4 lipopeptide when conjugated to E2 nanoparticle
PAMP	Pathogen-associated molecular pattern
PBS	Phosphate buffered saline
PCR	Polymerase chain reactions
PDH	pyruvate dehydrogenase
PEG	Poly(ethylene glycol)
PRR	Pattern recognition receptor
RT	Room temperature
SD	Standard deviation
SEM	Standard error of the mean
SC $\Delta$ N	N-terminus truncated form of SpyCatcher
SDM	Site directed mutagenesis
SDS-PAGE	Sodium dodecyl sulfate polyacrylamide gel electrophoresis
SEAP	Secreted alkaline phosphatase



SEC	Size exclusion column/chromatography
SIIN	SIINFEKL peptide when conjugated to E2 nanoparticle
SIINFEKL	MHC I-restricted epitope from the chicken ovalbumin protein (AA 257-264)
SLS	Sarkosyl, N-Lauroylsarcosine sodium salt
SMCC	Succinimidyl trans-4-(maleimidylmethyl)cyclohexane-1-carboxylate
ST/SC	SpyTag/SpyCatcher bioconjugation system
ST-E2	E2 nanoparticle with SpyTag genetically fused to its N-terminus
TBS	Tris-buffered saline
TEM	Transmission electron microscopy
TLR	Toll-like receptor
T-reg	Regulatory T cell
T-TBS	Tris-buffered saline containing 0.05% Tween 20
VLP	Virus-like particle

## LIST OF FIGURES

	Page	
Figure 1.1	Diagrams of influenza pathogenesis and general immune responses elicited by influenza infection	3
Figure 1.2	Depiction of <i>C. burnetii</i> intracellular infection of macrophage immune cells	5
Figure 1.3	Diagram of the general immune response that is elicited by an infectious pathogen (i.e., bacteria, viruses, fungi, and parasite)	5
Figure 1.4	Representative diagram of the immune response elicited by nanoparticle vaccines	8
Figure 1.5	Diagram showing characteristics of E2 platform and subsequent anti-cancer immune responses elicited by E2 formulations	9
Figure 1.6	Signal pathways of TLRs after activation with agonists	11
Figure 2.1	Hemagglutinin (HA, subtype H1) protein attachment to E2 using mal-tNTA	34
Figure 2.2	Characterization of tNTA-E2 and H1-E2 nanoparticles	35
Figure 2.3	Vaccine groups and immunization schedule	39
Figure 2.4	H1-specific IgG profiling by protein microarray	40
Figure 2.5	Attachment of H1 to E2 (H1-E2) modulates the immune response to H1 towards a more balanced IgG1/IgG2c antibody response	42
Figure 2.6	Attachment of H1 to E2 nanoparticle (H1-E2) engenders homosubtypic and heterosubtypic cross-reactivity that is enhanced by MPLA	44
Figure 3.1	Overview of protein antigen-nanoparticle conjugation strategies	68
Figure 3.2	Conjugating CBU1910 onto E2 protein nanoparticles using a tris-NTA-Ni linker	71
Figure 3.3	Conjugation of CBU1910 onto E2 nanoparticles using the SpyTag/SpyCatcher system	73
Figure 3.4	Antibody responses of protein antigen and nanoparticle formulations	76

Figure 3.5	ELISpot analysis of splenocytes after immunizations with CBU1910 (protein) and CBU1910p (peptide epitope) formulations	81
Figure 4.1	Schematic of nanoparticle synthesis with two adjuvants, CpG and flagellin (FliC), and the immunodominant influenza antigen hemagglutinin (H5)	103
Figure 4.2	Synthesis of ST-E2 nanoparticles conjugated with CpG, SC-FliCc, and/or SC-H5	107
Figure 4.3	Conjugation of SC-FliCc onto ST-E2 NPs increases activation of TLR5 reporter cells and macrophages, relative to SC-FliCc alone	110
Figure 4.4	Antibody response elicited by H5-FliCc-CpG-E2 dual-adjuvant nanoparticle formulations	113
Figure 4.5	Immunization with nanoparticles bound to H5 and TLR adjuvants protect mice from the lethal challenge of influenza and improve morbidity	119
Figure 4.6	Synthesis of E2 nanoparticles conjugated with Pam3CSK4 and <i>in vitro</i> activation studies of HEK-blue reporter cells	120

## LIST OF SCHEMES

	Page
Scheme 2.1 Synthesis route of mal-tNTA	33

## ACKNOWLEDGMENTS

I would like to first thank my advisor, Dr. Szu-Wen Wang, for her guidance and continuous support throughout this journey. Her mentorship has helped mold me into the student and scientist I am today. Thank you for giving this once timid student confidence in his abilities and himself. I wholeheartedly enjoyed the research.

My research was supported by the Defense Threat Reduction Agency (Awards HDTRA11810035 and HDTRA11810036), the National Institutes of Health (R01EB027797), and the National Science Foundation (Graduate Research Fellowship).

I would like to thank my committee members, Dr. Han Li and Dr. Huw Davies, for constructive feedback and helping to direct my research efforts and agreeing to evaluate my competency to enter the world as a PhD scientist.

I would like to thank all of my collaborators, including Dr. Huw Davies, Dr. Philip Felgner, and Dr. Amanda Burkhardt, for their invaluable advice, direction, help on experiments, and contributions to publishing high quality research.

I would like to acknowledge everyone who allowed my use of their facilities/equipment and for providing materials, training, and advice, and for contributing as co-authors to my published work including Alexander J. Badten, Dr. Jenny E. Hernandez-Davies, Dr. Tyler J. Albin, Aarti Jain, Rie Nakajima, Jiin Felgner, Dr. Sharon Jan, Dr. Anthony E. Gregory, and Dr. Algimantas Jasinskas.

I would like to thank Wiley Periodicals LLC. for permission to include portions of Chapter One of my dissertation, which were originally published in *Wiley Interdisciplinary Reviews-Nanomedicine and Nanobiotechnology*.

I would like to thank American Chemical Society for permission to include Chapter Two and Three of my dissertation, which were originally published in *ACS Infectious Diseases* and *Bioconjugate Chemistry*, respectively.

I would like to acknowledge the UCI Flow Cytometry Core Facility at the Institute for Immunology and Dr. Felix Grun and Dr. Benjamin Katz of the Mass Spectrometry Facility.

I would like to acknowledge all of my lab mates, past and present, for useful discussions and assistance, and for maintaining a lab culture of professionalism and friendliness that made going to work engaging each and every day.

I would like to acknowledge Dr. Medea Neek, a former Wang-lab member, for mentoring me and assuring me that I would be a good fit with the lab.

Finally, I will thank my family; My mother, Nelida Beltran-Ramirez, my father, Adalberto Ramirez, my brothers, Timoteo Ramirez and Daniel Ramirez, my sister, Elizabeth (Lizzy) Ramirez, for all their unconditional love and support. Without their support none of this would have been possible.

## VITA

### Aaron Ramirez

#### EDUCATION

- Ph.D., Chemical and Biomolecular Engineering, University of California, Irvine, 2024
- M.S., Chemical and Biomolecular Engineering, University of California, Irvine, 2020
- B.S., Chemical and Environmental Engineering, University of California, Riverside (*magna cum laude* distinction ), 2018

#### RESEARCH EXPERIENCE & INTEREST

- Delivery vehicle-based therapies and vaccines
- Protein engineering-based therapeutics
- Infectious disease and cancer vaccine development

#### HONORS & ACCOMPLISHMENTS

- Recipient of Latino Excellence and Achievement Dinner - Graduate Student Excellence Award, 2023
- Recipient of National Science Foundation (NSF) Graduate Research Fellowship (GRF), 2020-2023
- Recipient of Rose Hills Foundation Science & Engineering Fellowship, 2020-24
- Recipient of the Graduate Assistance in Areas of National Need (GAANN) Fellowship, 2018

#### PUBLICATIONS

- **Ramirez A**, Hernandez-Davies JE, Jain A, Wang L, Strahsburger E, Davies DH, Wang SW. Engineering protein nanoparticles co-delivering multiple toll-like receptor agonists and potential pandemic influenza hemagglutinin H5 to enhance vaccine immunogenicity and efficacy (in preparation).
- **Ramirez A**, Felgner J, Jain A, Jan S, Albin TJ, Badten AJ, Gregory AE, Nakajima R, Jasinskas A, Felgner PL, Burkhardt AM, Davies DH, Wang SW. Engineering Protein Nanoparticles Functionalized with an Immunodominant *Coxiella burnetii* Antigen to Generate a Q Fever Vaccine. *Bioconjugate Chem.* 2023 Sep 20;34(9):1653-1666. doi: 10.1021/acs.bioconjchem.3c00317. Epub 2023 Sep 8. PMID: 37682243; PMCID: PMC10515490.
- Badten AJ\*, **Ramirez A\***, Hernandez-Davies JE, Albin TJ, Jain A, Nakajima R, Felgner J, Davies DH, Wang SW. Protein Nanoparticle-Mediated Delivery of Recombinant Influenza Hemagglutinin Enhances Immunogenicity and Breadth of the Antibody Response. *ACS Infect. Dis.* 2023 Feb 10;9(2):239-252. doi: 10.1021/acsinfecdis.2c00362. Epub 2023 Jan 6. PMID: 36607269; PMCID: PMC9926493.
- Butkovich N, Tucker JA, **Ramirez A**, Li E, Meli VS, Nelson EL, Wang SW. Nanoparticle vaccines can be designed to induce pDC support of mDCs for increased antigen display. *Biomaterial Sci.* 2023 Jan 17;11(2):596-610. doi: 10.1039/d2bm01132h. PMID: 36476811; PMCID: PMC10775882.
- Li E, Brennan CK, **Ramirez A**, Tucker JA, Butkovich N, Meli VS, Ionkina AA, Nelson EL, Prescher JA, Wang SW. Macromolecular assembly of bioluminescent protein nanoparticles for enhanced imaging. *Mater. Today Bio.* 2022 Oct 8;17:100455. doi: 10.1016/j.mtbio.2022.100455. PMID: 36304975; PMCID: PMC9593766.
- Butkovich N\*, Li E\*, **Ramirez A\***, Burkhardt AM, Wang SW. Advancements in protein nanoparticle vaccine platforms to combat infectious disease. *Wiley Interdisciplinary Rev.*

*Nanomedicine and Nanobiotechnology*. 2021 May;13(3):e1681. doi: 10.1002/wnan.1681. Epub 2020 Nov 8. PMID: 33164326; PMCID: PMC8052270.

- Lopez T, Mustafa Z, Chen C, Lee KB, **Ramirez A**, Benitez C, Luo X, Ji RR, Ge X. Functional selection of protease inhibitory antibodies. *Proc. Natl. Acad. Sci. USA*. 2019 Aug 13;116(33):16314-16319. doi: 10.1073/pnas.1903330116. Epub 2019 Jul 30. PMID: 31363054; PMCID: PMC6697876.
- Lopez T, Chuan C, **Ramirez A**, Chen KE, Lorenson MY, Benitez C, Mustafa Z, Pham H, Sanchez R, Walker AM, Ge X. Epitope-specific affinity maturation improved stability of potent protease inhibitory antibodies. *Biotechnology and Bioengineering*. 2018 Nov;115(11):2673-2682. doi: 10.1002/bit.26814. Epub 2018 Sep 15. PMID: 30102763; PMCID: PMC6202216.
- Lopez T, **Ramirez A**, Benitez C, Mustafa Z, Pham H, Sanchez R, Ge X. Selectivity Conversion of Protease Inhibitory Antibodies. *Antib. Ther.* 2018 Oct 5;1(2):75–83. doi: 10.1093/abt/tby008. PMCID: PMC6206439.

\*Authors contributed equally to the work and are considered co-first authors.

#### PROVISIONAL PATENT

- Szu-Wen Wang, Lu Wang, David Huw Davies, and **Aaron Ramirez**. Injectable Hydrogel For Sustained Delivery Of An Antigen, And Uses Thereof. US Provisional Patent Application No. 63/536,695.

#### CONFERENCES & PRESENTATIONS

- **Aaron Ramirez**, Jiin Felgner, Aarti Jain, Sharon Jan, Tyler J. Albin, Alexander J. Badten, Anthony E. Gregory, Rie Nakajima, Algimantas Jasinskas, Philip L. Felgner, Amanda M. Burkhardt, D. Huw Davies, Szu-Wen Wang, Engineering nanoparticles functionalized with an immunodominant *Coxiella burnetii* antigen to generate a Q fever vaccine, 21<sup>st</sup> Annual UC Irvine Immunology Fair/conference, 2023
- **Aaron Ramirez**, Jiin Felgner, Aarti Jain, Sharon Jan, Tyler J. Albin, Alexander J. Badten, Anthony E. Gregory, Rie Nakajima, Algimantas Jasinskas, Philip L. Felgner, Amanda M. Burkhardt, D. Huw Davies, Szu-Wen Wang, Engineering protein nanoparticles functionalized with an immunodominant *Coxiella burnetii* antigen to generate a Q fever vaccine, Keystone Next Generation Nanomedicine conference, 2023
- **Aaron Ramirez**, Jiin Felgner, Aarti Jain, Sharon Jan, Tyler J. Albin, Alexander J. Badten, Philip L. Felgner, D. Huw Davies, Szu-Wen Wang, Decoration of protein antigens on protein nanoparticles for Q fever vaccine development, UC Irvine CBE Symposium/conference, 2023
- **Aaron Ramirez**, Jiin Felgner, Aarti Jain, Sharon Jan, Tyler Albin, Alex Badten, Huw Davies, Szu Wang, Engineering protein nanoparticles conjugated with antigens towards a Q-fever vaccine, ACS conference, 2022
- Presenter at Defense Threat Reduction Agency (DTRA) Single Dose consortium meetings, 2019-2020

## ABSTRACT OF THE DISSERTATION

Engineering Protein-Based Nanoparticles for Infectious Disease Vaccine Development

By

Aaron Ramirez

Doctor of Philosophy in Chemical and Biomolecular Engineering

University of California, Irvine, 2024

Professor Szu-Wen Wang, Chair

Vaccines have employed many designs to eradicate numerous infectious diseases. Influenza, the respiratory specific virus that causes flu, is a pathogen that readily mutates every year to avoid immune system detection. Due to this characteristic, new vaccine development is required each year and the demand for a universal flu vaccine has become very relevant. *Coxiella burnetii*, the causative agent of Q fever and a potential bioterrorism agent with no approved vaccine, is a bacterial pathogen that infects and resides internally in host cells. For this reason, a T lymphocyte response, in addition to an adequate antibody response, is likely necessary for eradication of the pathogen. Our previous studies, utilizing the E2 protein nanoparticle (E2) in a viral-mimetic strategy for cancer immunotherapy, resulted in formulations that elicited strong T cell responses against tumors. Our current studies aim to integrate immunodominant protein and peptide antigens of influenza and *C. burnetii* onto the surface of E2, to develop improved prophylactic vaccine formulations against these infectious diseases.

We explored the modularity, scope, and effectiveness of loading protein antigens onto protein nanoparticles (NPs). Multiple approaches for conjugation of the immunodominant *C. burnetii* protein antigen CBU1910 to the E2 nanoparticle were investigated including direct genetic fusion, a newly-synthesized high-affinity tris-NTA-Ni conjugation to polyhistidine-tagged CBU1910, and the SpyTag/SpyCatcher (ST/SC) system. Application of the ST/SC approach



yielded the most stable nanoparticles that could simultaneously co-deliver the protein antigen CBU1910 and adjuvant CpG1826 (CpG) on one nanoparticle. Evaluating the prophylactic immune responses elicited by these formulations showed that displaying antigen on nanoparticles significantly increased antigen-specific antibody responses than soluble antigen and delivering adjuvant CpG in nanoparticles increased its immune response skewing potency. In addition, E2 nanoparticles formulated with T cell epitope antigen peptides from CBU1910 generated elevated T cell responses to the whole CBU1910 protein. Integration of protein antigen hemagglutinin (HA) from H1N1 influenza with tris-NTA-Ni also revealed a synergistic effect from the combination of H1 display on the E2 NP and soluble adjuvant that generated broader homo- and heterosubtypic cross-reactivity, which is valuable when developing a universal flu vaccine.

Many NP-based vaccines build upon a pathogen-mimetic strategy to achieve sizes and structures comparable to that of viral or bacterial pathogens with antigens and adjuvants. However, the addition of a second, different adjuvant to the same protein NP scaffold has yet to be explored. We engineered NPs capable of co-delivering two adjuvants (i.e., flagellin and CpG) with protein antigen hemagglutinin from the potentially pandemic H5N1 avian influenza virus on a single NP. Displaying antigen and adjuvant elicited greater antigen-antibody responses and broader homosubtypic cross-reactivity. Skewing of the immune responses could be modulated by adjuvant type and NP attachment. Animals immunized with E2-based NPs and subsequently challenged with H5N1 influenza showed 100% survival. In all, these investigations highlight that NP-based delivery of antigen and adjuvants can effectively modulate the strength, breadth, and bias of an immune response against infectious disease.

## CHAPTER 1

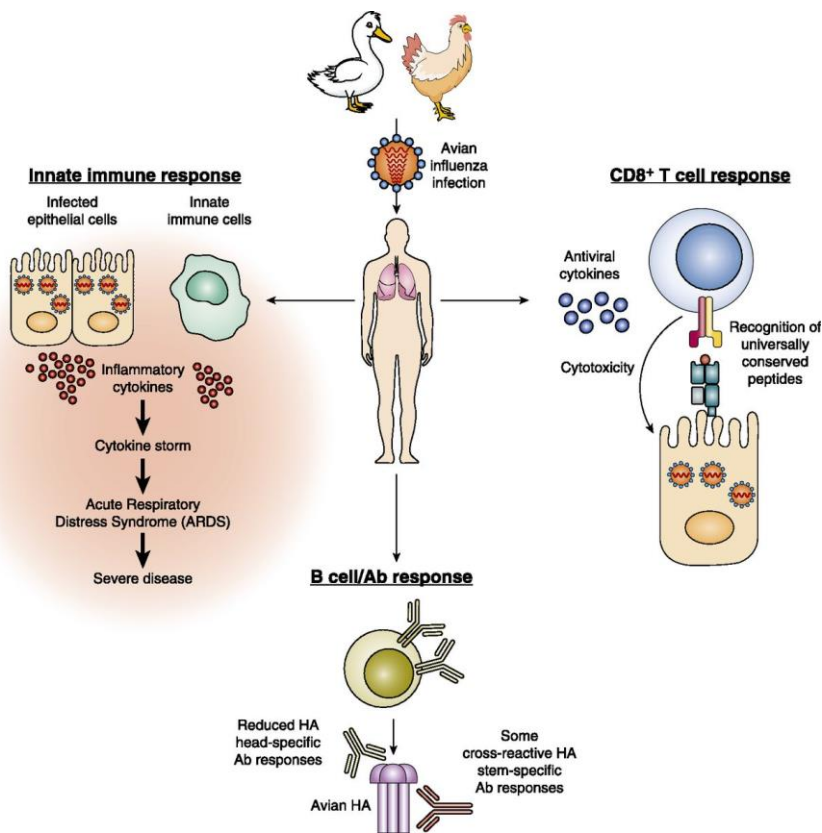
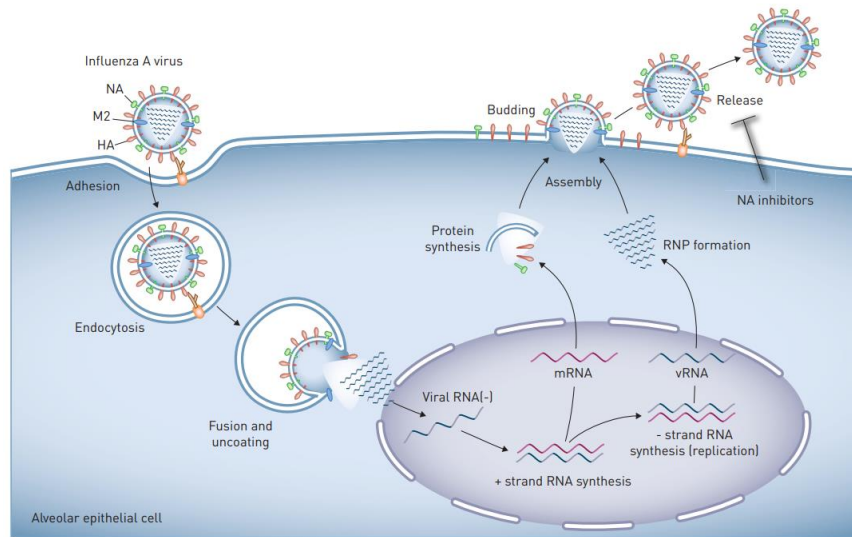
### BACKGROUND: INFECTIOUS DISEASE IMMUNITY, PROTEIN NANOPARTICLE DELIVERY PLATFORMS, IMMUNE SYSTEM ADJUVANTS

Portions of this chapter have been modified and published as: Butkovich, N.\* , Li, E.\* , Ramirez, A.\* , *et al.*, Advancements in protein nanoparticle vaccine platforms to combat infectious disease. *Wiley Interdisciplinary Reviews-Nanomedicine and Nanobiotechnology*, 2021. 13(3):e1681. \*Co-first authors

## 1.1. Influenza and the Immune System

Influenza, the respiratory specific virus that causes flu, is a pathogen that readily mutates every year to avoid immune system detection (Figure 1.1).<sup>1</sup> Due to this characteristic, new vaccine development is required each year and the demand for a universal flu vaccine has become relevant.<sup>2-4</sup> Hemagglutinin (HA) is the highly expressed, immunodominant protein of influenza. HA is a highly glycosylated, homotrimeric protein consisting of two distinct regions: a highly variable head region (HA1) that is readily used to characterize the specific influenza strain/subtype (i.e., group 1 or 2 influenza) and a more conserved stem region (HA2). The head region contains an  $\alpha$ -sialic acid-binding site that attaches to sialic acids found on host cells to initiate viral entry into the cell.<sup>5</sup> Both HA1 and HA2 contain regions directly involved in the fusion of the viral membrane with the host cell membrane.<sup>6</sup>

Due to its error-prone RNA polymerase, influenza is able to rapidly change its HA surface epitopes in order to escape antibody responses.<sup>7</sup> It has been shown, however, that certain regions of HA are far less prone to mutations than others, likely because they play functional roles in viral entry or are important for the structural integrity of the protein. These regions are primarily located in the stem, deep within the protein, or in areas blocked by glycans.<sup>8-11</sup> The fact that these regions are highly conserved between flu strains and subtypes makes them prime targets for eliciting cross-protective immunity. However, these regions are generally inaccessible to B cell receptors and serum antibodies, making them unsatisfactory for eliciting antibody responses. It has therefore been suggested that T cells may play a role in the development of cross-protective flu vaccines, as T cell epitopes are not limited to exposed surface regions like B cell epitopes.<sup>12</sup> Diagrams describing influenza's pathogenesis and the immune responses elicited after infection can be found in Figure 1.1. We expect that our E2 platform may be able to help direct the humoral- and cell-mediated immune response against the influenza antigen, HA.

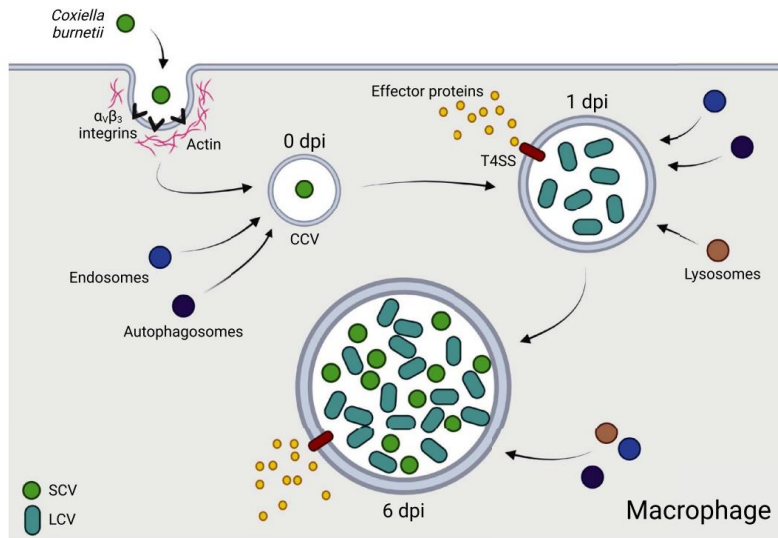


**Figure 1.1. Diagrams of influenza pathogenesis and general immune responses elicited by influenza infection.** (top) Illustration of the replication of influenza A viruses in lung epithelial cells which are the primary cell target of influenza. Influenza uses HA to bind and fuse to the membrane of target cells. Subsequently, the virus releases its RNA payload into the nucleus of the cell, and protein synthesis of influenza proteins occurs. Once the proteins are produced, the viral components bud off from the cell membrane releasing new virus. Diagram taken from Herold et al.<sup>1</sup> (bottom) The innate and adaptive immune responses to avian influenza virus infection. Both B cell and T cell responses are needed. Diagram taken from Koutsakos, et al.<sup>13</sup>

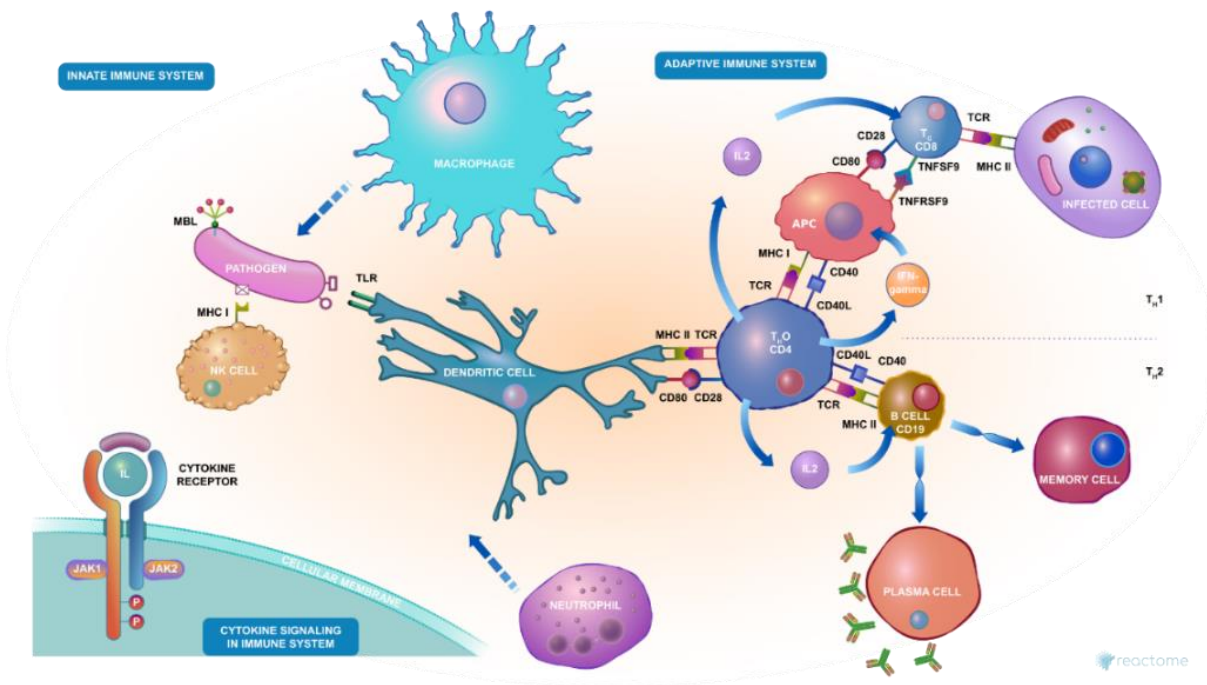
## 1.2. *Coxiella burnetii* and the Immune System

A vaccine for the life-threatening disease Q fever is currently not widely available and has not received FDA approval due to the potential for severe side effects.<sup>14-16</sup> *Coxiella burnetii* is the gram-negative intracellular bacterium that causes Q fever.<sup>17-19</sup> *C. burnetii* is considered a ubiquitous zoonotic pathogen that resides most commonly in livestock (i.e., cattle and sheep).<sup>17,19,20</sup> It has been classified by the U.S. Center of Disease Control and Prevention as a potential bioterrorism weapon due to its airborne transmission, highly infectious nature, and extreme resistance to environmental conditions.<sup>14,17,19,21</sup> In most cases, infection causes low mortality, but significant morbidity.<sup>17,22</sup>

Unlike typical bacterial pathogens, *C. burnetii* exhibits a tropism for professional immune system phagocytes (i.e., macrophage). *C. burnetii* actively directs phagocytosis and the maturation of phagolysosome-like compartments to reside within host cells in its favorable low pH environment enabling its long-term survival and persistence (Figure 1.2).<sup>17,23,24</sup> For this reason, a T lymphocyte response, in addition to an adequate antibody response, is likely necessary for eradication of the pathogen.<sup>25,26</sup> A general schematic of the immune response elicited towards infectious pathogens is found in Figure 1.3. Proteomics and antigen-specific serological assays have identified CBU1910 as the immunodominant protein of *C. burnetii*.<sup>22,27-33</sup> For this reason, CBU1910 was chosen as the antigen for this project. Unlike cancers, which generally bear peptide neoantigens that are utilized in a cancer vaccine to produce T cell responses, infectious disease vaccines typically require the use of whole protein antigens to elicit both antibody and T cell responses.<sup>34,35</sup> Protein antigens contain numerous immunogenic epitopes in natural conformations, allowing for stronger antibody responses and broader adaptive immune responses (both T cell and B cell).<sup>34-36</sup>



**Figure 1.2. Depiction of *C. burnetii* intracellular infection of macrophage immune cells.** *C. burnetii* enters the cell via  $\alpha\beta$  integrins where subsequent recruitment of endosomes and lysosomes allow for the formation of a low pH compartment where the pathogen resides and matures. Diagram taken from Osbron, et al.<sup>37</sup>



**Figure 1.3. Diagram of the general immune response that is elicited by an infectious pathogen (i.e., bacteria, viruses, fungi, and parasite).** As depicted, a complex adaptive immune response involves immune cells that work in symphony to produce both humoral immunity (B cell maturation and antibody production) and cellular immunity (CD4+ helper T cell activation which reinforce B cell responses and CD8+ cytotoxic T cell activation which kill infected cells). Diagram taken from Singh, et al.<sup>38</sup>

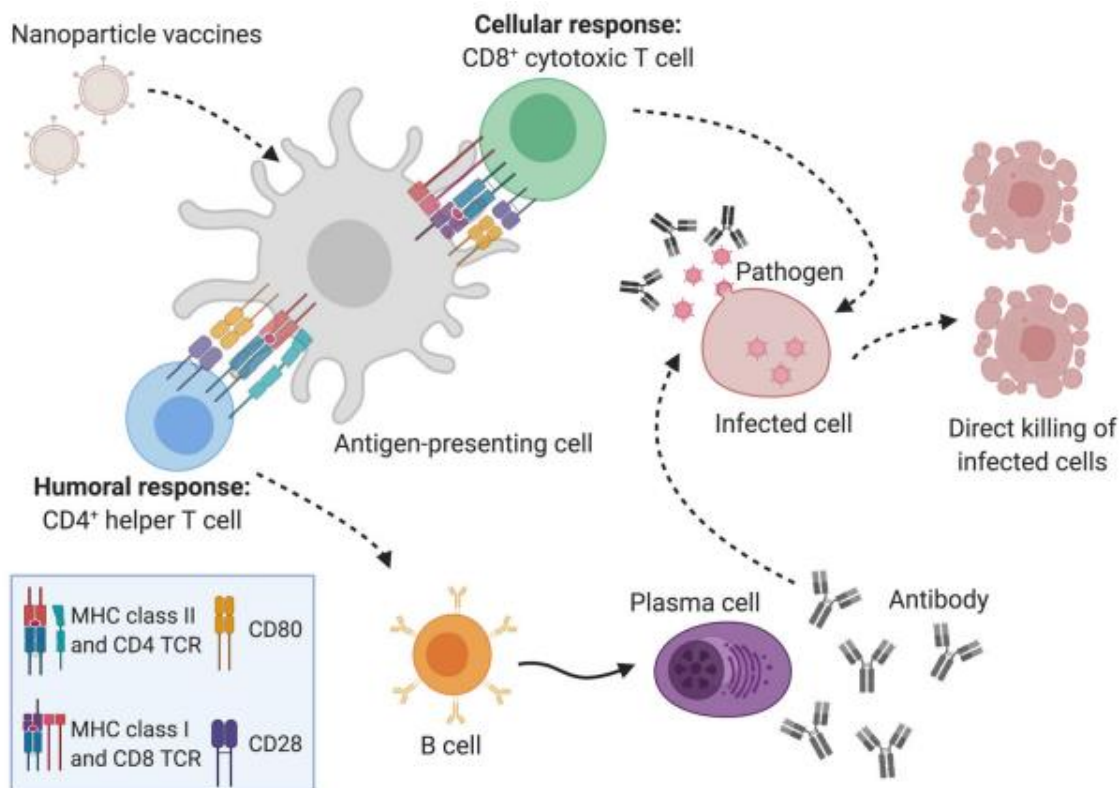
### 1.3. Nanoparticles for Infectious Disease Vaccine Platforms

Inactivated and live-attenuated vaccines can exhibit a number of problems, including low immunogenicity, hypersensitivities, and pathogenic reversion via mutation, that make them impractical for use under certain conditions.<sup>39-41</sup> Additionally, whole virus vaccines often need to be grown under BSL3 conditions which poses safety concerns, and their preparation can make controlling dosages of antigen and adjuvant challenging.<sup>42,43</sup> For these reasons, vaccinologists have turned toward the use of subunit vaccines. While early subunit vaccines overcame some of the aforementioned issues, these vaccines tended to have poor immunogenicity caused by factors such as rapid draining kinetics, monovalency of vaccine antigens, and differential pharmacokinetics of vaccine components.<sup>44-46</sup> Nanoparticle-based vaccine delivery systems are a promising solution, combining the safety and tunability of subunit vaccines with the strong immunogenicity of whole pathogen vaccines. In particular, a library of protein nanoparticles like that of our E2 nanocapsule have been applied to a multitude of infectious disease models and have exhibited robust humoral and cellular immune responses.<sup>47</sup> A representative diagram of the mechanism by which protein nanoparticle-based vaccines elicit an adaptive immune response is shown in Figure 1.4.

The improved immunogenicity of nanoparticle vaccines over their subunit counterparts has been repeatedly demonstrated.<sup>48-50</sup> This phenomenon is primarily due to two unique properties of nanoparticles: their increased size and the repetitive pattern in which antigens are displayed on their surface. Experimental and computational studies have indicated that dendritic cells preferentially take up nanoparticles smaller than 500 nm with an optimal uptake size of ~50 nm,<sup>51-53</sup> and diameters larger than 20 nm have increased retention times within lymph nodes.<sup>54-56</sup> Previous studies of nanoparticle scaffolds with controlled antigen valencies have also suggested that B cells are more efficiently activated by 5 or more repeated epitopes, allowing for improved B cell receptor crosslinking and subsequent activation.<sup>54-56</sup> Therefore, nanoparticle-based vaccines designed within these parameters are expected to elicit superior immune responses.

Nanoparticles have received attention in tumor<sup>57-61</sup> and autoimmunity<sup>62-65</sup> models due to the strong cytotoxic T lymphocyte (CTL) and regulatory T cell responses, respectively, that they can elicit. The success of nanoparticles in these applications is due, in part, to the relative ease of conjugating small peptides to the nanoparticle (compared to whole proteins). However, peptide antigens are generally not effective for eliciting adequate B cell-mediated antibody responses (which are often required for infectious disease eradication) because B cells epitopes, unlike T cell epitopes, require specific 3D conformations that are generally not conserved by peptide fragments.<sup>66-68</sup> Therefore, there is motivation to attach full-length proteins antigens onto nanoparticles, rather than rely on peptide attachment alone. One strategy to integrate full-length protein antigens to nanoparticles is genetically fusing the antigen to a protein that naturally self-assembles into a virus-like particle (VLP).<sup>69-72</sup> While this method has shown promise, genetic fusion frequently leads to protein misfolding or expression issues. For this reason, numerous methods have been explored to covalently (i.e., SpyTag/SpyCatcher bioconjugation system)<sup>73-77</sup> and noncovalently (i.e., high affinity Ni-NTA/His-Tag conjugation)<sup>78,79</sup> attach full proteins to various nanoparticle platforms post-assembly.



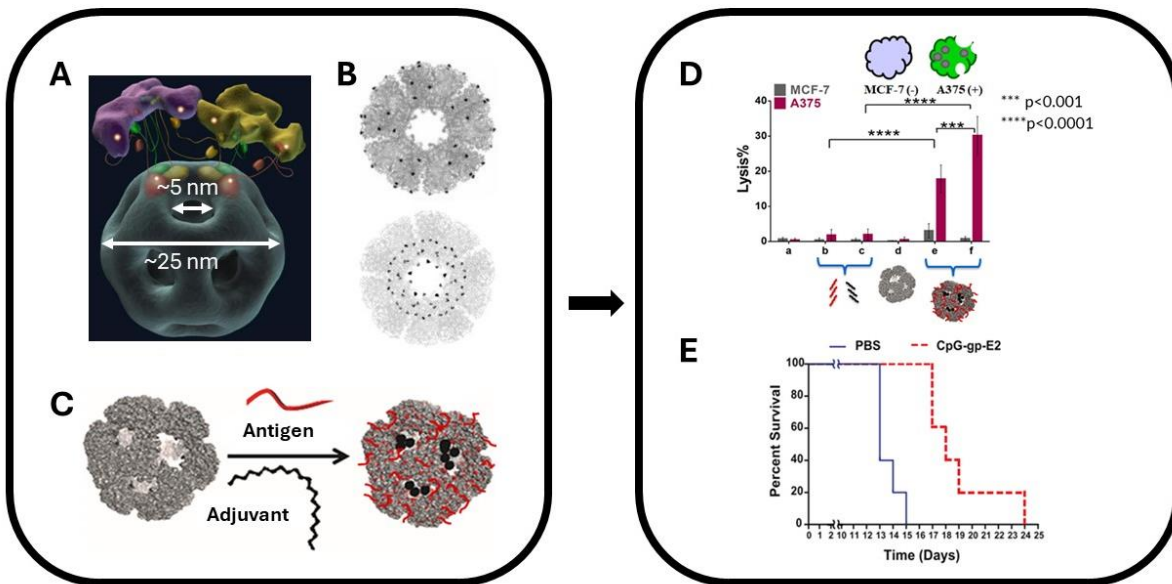


**Figure 1.4. Representative diagram of the immune response elicited by nanoparticle vaccines.** Nanoparticles loaded with antigens, and potentially adjuvants, are up-taken by antigen presenting cells (APCs) which process antigens and display them on their surface to activate T cells. T cells then can reinforce humoral antibody responses and/or produce cellular cytotoxic responses that eliminate infected cells. This interaction between the nanoparticle vaccines and the immune system results in immunological memory and protection against future infections. Diagram taken from Butkovich, Li, Ramirez, *et al.*<sup>47</sup>

#### 1.4. Pyruvate Dehydrogenase E2 and its Use as a Platform for Inducing Immune Responses

The protein nanocapsule utilized in this research is derived from the E2 subunit (E2) of the multienzyme complex, pyruvate dehydrogenase, sourced from the thermophilic bacteria, *Geobacillus stearothermophilus*.<sup>80,81</sup> E2 is a 60-subunit, self-assembling 25-nm dodecahedral scaffold with high thermal stability that can be genetically engineered for precise chemical conjugation sites at the external surface and internal cavity (Figure 1.5).<sup>80,82-86</sup> Our prior studies in developing cancer vaccines via a virus-mimetic strategy have demonstrated the utility of this scaffold for both adjuvant and peptide antigen delivery (Figure 1.5). This has resulted in a strong CTL response against tumor cells, significant delays in tumor growth, and increases in survival

time (Figure 1.5).<sup>61,87-90</sup> However, application of this strategy for protection against infectious disease pathogens had not yet been investigated. Utilizing E2's unique size, functional adaptability, and innate capability to elicit an antigen-specific immune response, in this work, we implemented a virus mimetic strategy to develop potential prophylactic vaccines for infectious disease.



**Figure 1.5. Diagram showing characteristics of E2 platform and subsequent anti-cancer immune responses elicited by E2 formulations. (A)** Depiction of E1(purple)-E2(blue)-E3(yellow) complex and E2 size.<sup>82</sup> **(B)** Crystal structure representation of E2 with mutations done to its external surface (**top**) and its internal cavity (**bottom**).<sup>83</sup> **(C)** Diagram of peptide antigen and adjuvant, CpG, attachment to E2 particles that would be used as a cancer vaccine.<sup>87</sup> **(D)** Co-delivery of antigen and adjuvant in nanoparticle yields higher specific tumor cell lysis.<sup>90</sup> **(E)** Immunization with CpG-gp100-E2 nanoparticle significantly delays tumor growth and extends survival time in mice.<sup>89</sup>

### 1.5. Toll-like Receptor (TLR) Agonists as Immune System Adjuvants

Toll-like receptors are membrane-based proteins that play a key role in innate immunity by recognizing pathogen-associated molecular patterns (PAMPs), such as bacterial membrane components and viral RNA (Figure 1.6).<sup>91-93</sup> The majority of TLRs can be categorized as cell surface-based (i.e., TLR2/1, TLR2/6, TLR4, and TLR5) or endosomal-based (i.e., TLR3, TLR7,

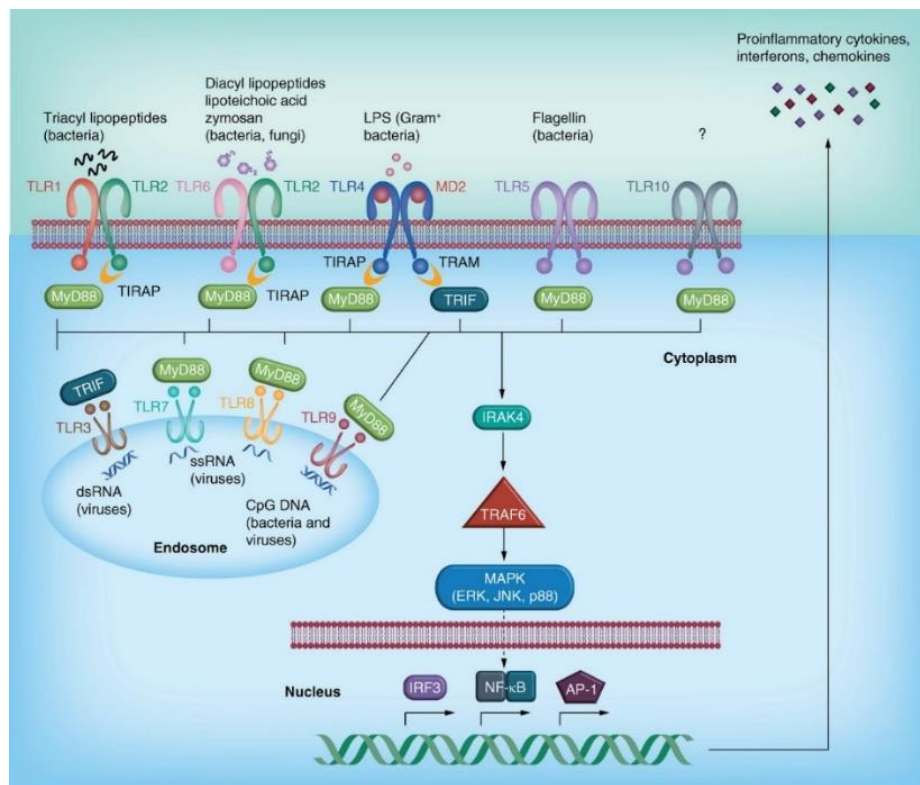
TLR8, and TLR9). TLRs activate very particular intracellular pathways that help the immune system prime for specific types of pathogens based the agonist.

Endosomal TLRs such as TLR3, TLR9, and TLR7/8 recognize CpG, Poly I:C, and ssRNA respectively, and have shown to activate dendritic cell differentiation, B cell antibody production, and Th1 bias IgG subclass shifting.<sup>94-96</sup> Conjugations of endosomal TLR agonists CpG and ssRNA have been demonstrated in nanoparticles and have been confirmed to induce pDC and mDC mediated immune responses.<sup>97</sup> TLR4 uniquely signals proinflammatory responses through both the NFkB and IRF3 pathways and has been shown to elicit Th1 responses.<sup>91,96</sup> LPS is the main agonist for TLR4 but is not FDA-approved due to its toxicity.<sup>98,99</sup> Other TLR4 agonists including monophosphoryl lipid A (MPLA) and CRX-527 are less toxic than LPS but suffer from low water solubility and typically require complicated sugar-based chemistries for conjugation.<sup>100-103</sup> TLR2 forms a heterodimer with TLR1 or TLR6, where TLR2/1 recognizes triacylated lipoproteins and TLR2/6 recognizes diacylated lipoproteins. Examples of TLR2 agonists include heat killed bacteria and microbial cell-wall components of which are large polymers that do not have straight forward methods for conjugation.<sup>104</sup> Synthetic TLR2 agonists (i.e., Pam3CSK4, Pam2CSK4, and FSL-1) have shown potential for conjugation to subunit vaccines due to their smaller size (ranging from 0.3-2 kDa), bioorthogonal chemistry, and water solubility.<sup>104-110</sup>

Flagellin is the only agonist for TLR5.<sup>111,112</sup> Flagellin has been shown to produce varied Th1/Th2 responses and is a potent T cell antigen.<sup>113,114</sup> Previous work using flagellin and hemagglutinin on a virus-like particle (VLP) produced enhanced levels of IgG2a/2b antibody responses, cytokine secreting T-cell responses, and survival protection against heterosubtypic flu challenge.<sup>114,115</sup> Flagellin from three bacterial species have been studied as vaccine adjuvants (*Bacillus subtilis* (~32 kDa), *Pseudomonas aeruginosa* (~52 kDa), and *Salmonella typhimurium*, (~55 kDa)).<sup>115,116</sup> The most popular and studied of the three is *S. typhimurium* flagellin. This flagellin is encoded by the FliC gene, does not require glycosylation for adjuvant activity, and has been expressed and purified in *E. coli*, making it a prime candidate for conjugation to protein

nanoparticles.<sup>117-119</sup> Flagellin can be recombinantly engineered to allow for attachment to nanoparticles (via bioconjugation systems like SpyTag/SpyCatcher), which we demonstrate in this work.

Combinations of TLR agonists have been shown to improve immune responses.<sup>120,121</sup> Particular studies administering TLR4 and TLR7 agonists or TLR2/6 and TLR9 agonists have shown that combining TLR agonists will synergistically increase immune responses, such as antigen-specific neutralizing antibodies, when compared to immunization with a single TLR ligand.<sup>101,122</sup> However, in these studies, the antigen and adjuvants were not attached and co-delivered on a single vehicle. Thus, the effects of co-delivering each component onto one platform that mimics the natural association of TLR agonists from pathogens to TLRs of immune cells has not been completely investigated.



**Figure 1.6. Signal pathways of TLRs after activation with agonists.** Diagram taken from Baxeavanis, et al.<sup>91</sup> depicting TLRs and the subsequent intracellular pathways activated after TLR agonist activation.

## 1.6. Project Goals and Specific Aims of Each Chapter

Our overall goal was to use the E2 protein nanoparticles as a platform to deliver protein antigens and immunostimulatory adjuvants for the induction of prophylactic immune responses against infectious diseases. The particular Specific Aims of each chapters are listed below.

**Specific Aim 1 (Chapter 2): Examine the modularity and effectiveness of loading protein antigens onto E2 nanoparticles with an influenza disease model.** By applying a tNTA-Ni linker strategy, we will determine the feasibility of attaching the immunodominant protein antigen hemagglutinin (HA, H1) to the E2 nanoparticle and evaluate the subsequent immune responses elicited after immunization in mice. Higher antigen-specific antibody responses are expected with HA loaded onto E2 nanoparticles compared to the free antigen. Neutralizing antibodies and influenza strain cross-reactive antibodies are most coveted in vaccine development.

**Specific Aim 2 (Chapter 3): Examine different methods to conjugate full length protein antigen onto a protein nanoparticle, using the *C. burnetii* antigen CBU1910 as the model for evaluating prophylactic immune responses.** A higher antigen-specific antibody response and T cell activity (via IFN- $\gamma$  secretion) is expected for mice immunized with CBU1910 loaded onto E2 and CpG-E2 nanoparticles compared to the free antigen. *In vivo* studies will provide information of the E2 nanoparticle's innate adjuvating capability due to its unique size and structure.

Examine if T cell epitope antigen peptides from *C. burnetii* can be formulated onto E2 nanoparticles to potentially skew the immune response towards a cell-mediated T cell response. A higher antigen-specific T cell response (via IFN- $\gamma$  secretion) is expected for mice immunized with the T cell epitope peptides loaded onto CpG-E2 nanoparticles compared to the free antigen. We hypothesize that using specific epitopes that have shown T cell skewing activity an immune

response towards the whole protein antigen containing these epitopes may be focused as a cell mediated response.

**Specific Aim 3 (Chapter 4): Examine the unique antigen-specific immune responses elicited by co-delivering multiple TLR agonists and an antigen on one E2 nanoparticle.**

Using the repertoire of E2-infectious disease antigen (protein or peptide) nanoparticles that we constructed, we assessed the feasibility of attaching a second adjuvant onto our platform. Utilizing the SpyTag/SpyCatcher bioconjugation strategy the feasibility of conjugating the TLR5 agonist flagellin, TLR9 agonist CpG, and the influenza protein antigen H5 hemagglutinin onto E2 nanoparticles will be determined. Once attached onto E2 nanoparticles, confirmation of TLR agonist activity, characterization of the effects on immune cell activity, and the investigation of the prophylactic immune responses elicited will be investigated using *in vitro* assays and *in vivo* studies.

**Chapter 5: A brief summary followed by future directions on developing the E2 platform.**

## 1.7. References

1. Herold, S.; Becker, C.; Ridge, K. M.; Budinger, G. R. S., Influenza virus-induced lung injury: pathogenesis and implications for treatment. *European Respiratory Journal* **2015**, *45* (5), 1463-1478.
2. Houser, K.; Subbarao, K., Influenza Vaccines: Challenges and Solutions. *Cell Host & Microbe* **2015**, *17* (3), 295-300.
3. Wei, C. J.; Crank, M. C.; Shiver, J.; Graham, B. S.; Mascola, J. R.; Nabel, G. J., Next-generation influenza vaccines: opportunities and challenges. *Nature Reviews Drug Discovery* **2020**, *19* (4), 239-252.
4. Krammer, F.; Smith, G. J. D.; Fouchier, R. A. M.; Peiris, M.; Kedzierska, K.; Doherty, P. C.; Palese, P.; Shaw, M. L.; Treanor, J.; Webster, R. G.; Garcia-Sastre, A., Influenza. *Nature Reviews Disease Primers* **2018**, *4*.
5. Wiley, D. C.; Skehel, J. J., The Structure And Function Of The Hemagglutinin Membrane Glycoprotein Of Influenza-Virus. *Annual Review of Biochemistry* **1987**, *56*, 365-394.
6. Stegmann, T., Membrane fusion mechanisms: The influenza hemagglutinin paradigm and its implications for intracellular fusion. *Traffic* **2000**, *1* (8), 598-604.
7. Drake, J. W., Rates Of Spontaneous Mutation Among RNA Viruses. *Proc. Natl. Acad. Sci. U. S. A.* **1993**, *90* (9), 4171-4175.
8. Skehel, J. J.; Waterfield, M. D., Studies On Primary Structure Of Influenza-Virus Hemagglutinin. *Proc. Natl. Acad. Sci. U. S. A.* **1975**, *72* (1), 93-97.
9. Nobusawa, E.; Aoyama, T.; Kato, H.; Suzuki, Y.; Tateno, Y.; Nakajima, K., Comparison Of Complete Amino-Acid-Sequences And Receptor-Binding Properties Among 13 Serotypes Of Hemagglutinins Of Influenza A-Viruses. *Virology* **1991**, *182* (2), 475-485.
10. Kirkpatrick, E.; Qiu, X. T.; Wilson, P. C.; Bahl, J.; Krammer, F., The influenza virus hemagglutinin head evolves faster than the stalk domain. *Sci Rep* **2018**, *8*.
11. Lee, J. M.; Huddleston, J.; Doud, M. B.; Hooper, K. A.; Wu, N. C.; Bedford, T.; Bloom, J. D., Deep mutational scanning of hemagglutinin helps predict evolutionary fates of human H3N2 influenza variants. *Proc. Natl. Acad. Sci. U. S. A.* **2018**, *115* (35), EB276-EB285.
12. Schmidt, A.; Lapuente, D., T Cell Immunity against Influenza: The Long Way from Animal Models Towards a Real-Life Universal Flu Vaccine. *Viruses-Basel* **2021**, *13* (2).
13. Koutsakos, M.; Kedzierska, K.; Subbarao, K., Immune Responses to Avian Influenza Viruses. *Journal of Immunology* **2019**, *202* (2), 382-391.
14. Q Fever. Centers for Disease Control and Prevention. <https://www.cdc.gov/qfever/index.html> (accessed June 2019).
15. Ruiz, S.; Wolfe, D. N., Vaccination against Q fever for biodefense and public health indications. *Frontiers in Microbiology* **2014**, *5* (726).
16. Marmion, B. P.; Ormsbee, R. A.; Kyrkou, M.; Wright, J.; Worswick, D. A.; Izzo, A. A.; Esterman, A.; Feery, B.; Shapiro, R. A., Vaccine prophylaxis of abattoir-associated Q fever: eight years' experience in Australian abattoirs. *Epidemiology and Infection* **1990**, *104* (2), 275-287.
17. van Schaik, E. J.; Chen, C.; Mertens, K.; Weber, M. M.; Samuel, J. E., Molecular pathogenesis of the obligate intracellular bacterium *Coxiella burnetii*. *Nat. Rev. Microbiol.* **2013**, *11* (8), 561-573.
18. Qiu, J. Z.; Luo, Z. Q., Legionella and Coxiella effectors: strength in diversity and activity. *Nat. Rev. Microbiol.* **2017**, *15* (10), 591-605.
19. Eldin, C.; Melenotte, C.; Mediannikov, O.; Ghigo, E.; Million, M.; Edouard, S.; Mege, J. L.; Maurin, M.; Raoult, D., From Q Fever to *Coxiella burnetii* Infection: a Paradigm Change. *Clinical Microbiology Reviews* **2017**, *30* (1), 115-190.

20. Agerholm, J. S., Coxiella burnetii associated reproductive disorders in domestic animals- a critical review. *Acta Veterinaria Scandinavica* **2013**, *55*.
21. Anderson, A.; Bijlmer, H.; Fournier, P. E.; Graves, S.; Hartzell, J.; Kersh, G. J.; Limonard, G.; Marrie, T. J.; Massung, R. F.; McQuiston, J. H.; Nicholson, W. L.; Paddock, C. D.; Sexton, D. J., Diagnosis and Management of Q Fever - United States, 2013 Recommendations from CDC and the Q Fever Working Group. *MMWR Recommendations and Reports* **2013**, *62* (3), 1-28.
22. Hendrix, L. R.; Samuel, J. E.; Mallavia, L. P., Identification and cloning of a 27-kDa Coxiella burnetii immunoreactive protein. *Annals of the New York Academy of Sciences* **1990**, *590*, 534-540.
23. Kazar, J., Coxiella burnetii infection. In *Rickettsioses: From Genome to Proteome, Pathobiology, and Rickettsiae as an International Threat*, Hechemy, K. E.; Oteo, J. A.; Raoult, D. A.; Silverman, D. J.; Blanco, J. R., Eds. 2005; Vol. 1063, pp 105-114.
24. Oswald G. Baca, Y.-P. L., Hemant Kumar, Survival of the Q fever agent Coxiella burnetii in the phagolysosome. *Trends in Microbiology* **1994**, *2* (12), 476-480.
25. Read, A. J.; Erickson, S.; Harmsen, A. G., Role of CD4(+) and CD8(+) T Cells in Clearance of Primary Pulmonary Infection with Coxiella burnetii. *Infection and Immunity* **2010**, *78* (7), 3019-3026.
26. Scholzen, A.; Richard, G.; Moise, L.; Baeten, L. A.; Reeves, P. M.; Martin, W. D.; Brauns, T. A.; Boyle, C. M.; Raju Paul, S.; Bucala, R.; Bowen, R. A.; Garritsen, A.; De Groot, A. S.; Sluder, A. E.; Poznansky, M. C., Promiscuous Coxiella burnetii CD4 Epitope Clusters Associated With Human Recall Responses Are Candidates for a Novel T-Cell Targeted Multi-Epitope Q Fever Vaccine. *Frontiers in Immunology* **2019**, *10* (207).
27. Vigil, A.; Ortega, R.; Nakajima-Sasaki, R.; Pablo, J.; Molina, D. M.; Chao, C.-C.; Chen, H.-W.; Ching, W.-M.; Felgner, P. L., Genome-wide profiling of humoral immune response to Coxiella burnetii infection by protein microarray. *PROTEOMICS* **2010**, *10* (12), 2259-2269.
28. Beare, P. A.; Chen, C.; Bouman, T.; Pablo, J.; Unal, B.; Cockrell, D. C.; Brown, W. C.; Barbian, K. D.; Porcella, S. F.; Samuel, J. E.; Felgner, P. L.; Heinzen, R. A., Candidate Antigens for Q Fever Serodiagnosis Revealed by Immunoscreening of a Coxiella burnetii Protein Microarray. *Clinical and Vaccine Immunology* **2008**, *15* (12), 1771-1779.
29. Thompson, H. A.; Suhan, M. L., Genetics of Coxiella burnetii. *FEMS Microbiology Letters* **1996**, *145* (2), 139-146.
30. To, H.; Hotta, A.; Zhang, G. Q.; Van Nguyen, S.; Ogawa, M.; Yamaguchi, T.; Fukushi, H.; Amano, K.; Hirai, K., Antigenic characteristics of polypeptides of Coxiella burnetii isolates. *Microbiology and Immunology* **1998**, *42* (2), 81-85.
31. Zhang, G. Q.; To, H.; Russell, K. E.; Hendrix, L. R.; Yamaguchi, T.; Fukushi, H.; Hirai, K.; Samuel, J. E., Identification and characterization of an immunodominant 28-kilodalton Coxiella burnetii outer membrane protein specific to isolates associated with acute disease. *Infection and Immunity* **2005**, *73* (3), 1561-1567.
32. Deringer, J. R.; Chen, C.; Samuel, J. E.; Brown, W. C., Immunoreactive Coxiella burnetii Nine Mile proteins separated by 2D electrophoresis and identified by tandem mass spectrometry. *Microbiology* **2011**, *157*, 526-542.
33. Stellfeld, M.; Gerlach, C.; Richter, I. G.; Miethe, P.; Fahlbusch, D.; Polley, B.; Sting, R.; Pfeffer, M.; Neubauer, H.; Mertens-Scholz, K., Evaluation of the Diagnostic Potential of Recombinant Coxiella burnetii Com1 in an ELISA for the Diagnosis of Q Fever in Sheep, Goats and Cattle. *Microorganisms* **2020**, *8* (8).
34. Katz, D. H.; Benacerraf, B., The Regulatory Influence of Activated T Cells on B Cell Responses to Antigen. *Advances in Immunology* **1972**, *15*, 1-94.



35. Saylor, K.; Gillam, F.; Lohneis, T.; Zhang, C. M., Designs of Antigen Structure and Composition for Improved Protein-Based Vaccine Efficacy. *Frontiers in Immunology* **2020**, *11*.
36. Guo, C. Q.; Manjili, M. H.; Subjeck, J. R.; Sarkar, D.; Fisher, P. B.; Wang, X. Y., Therapeutic Cancer Vaccines: Past, Present, and Future. In *Advances in Cancer Research, Vol 119*, Tew, K. D.; Fisher, P. B., Eds. 2013; Vol. 119, pp 421-475.
37. Osbron, C. A.; Goodman, A. G., To die or not to die: Programmed cell death responses and their interactions with *Coxiella burnetii* infection. *Molecular Microbiology* **2022**, *117* (4), 717-736.
38. Singh, N.; Suthar, B.; Mehta, A.; Pandey, A., Immune Response Towards COVID-19: A Review on Host Body. *Journal of Infectious Diseases and Diagnosis* **2020**, *5* (1).
39. Acosta, P. L.; Caballero, M. T.; Polack, F. P., Brief History and Characterization of Enhanced Respiratory Syncytial Virus Disease. *Clinical and Vaccine Immunology* **2016**, *23* (3), 189-195.
40. Fratzke, A. P.; Gregory, A. E.; van Schaik, E. J.; Samuel, J. E., *Coxiella burnetii* Whole Cell Vaccine Produces a Th1 Delayed-Type Hypersensitivity Response in a Novel Sensitized Mouse Model. *Frontiers in Immunology* **2021**, *12*.
41. Hanley, K. A., The double-edged sword: How evolution can make or break a live-attenuated virus vaccine. *Evolution* **2011**, *4* (4), 635-643.
42. Sanders, B.; Koldijk, M.; Schuitemaker, H., Inactivated Viral Vaccines. *Vaccine Analysis: Strategies, Principles, and Control* **2014**, 45-80.
43. Minor, P. D., Live attenuated vaccines: Historical successes and current challenges. *Virology* **2015**, *479*, 379-392.
44. Moyle, P. M.; Toth, I., Modern Subunit Vaccines: Development, Components, and Research Opportunities. *Chemmedchem* **2013**, *8* (3), 360-376.
45. Tam, H. H.; Melo, M. B.; Kang, M.; Pelet, J. M.; Ruda, V. M.; Foley, M. H.; Hu, J. K.; Kumari, S.; Crampton, J.; Baldeon, A. D.; Sanders, R. W.; Moore, J. P.; Crotty, S.; Langer, R.; Anderson, D. G.; Chakraborty, A. K.; Irvine, D. J., Sustained antigen availability during germinal center initiation enhances antibody responses to vaccination. *Proc. Natl. Acad. Sci. U. S. A.* **2016**, *113* (43), E6639-E6648.
46. Nguyen, B.; Tolia, N. H., Protein-based antigen presentation platforms for nanoparticle vaccines. *npj Vaccines* **2021**, *6* (1), 11.
47. Butkovich, N.; Li, E. Y.; Ramirez, A.; Burkhardt, A. M.; Wang, S. W., Advancements in protein nanoparticle vaccine platforms to combat infectious disease. *Wiley Interdisciplinary Reviews-Nanomedicine and Nanobiotechnology* **2021**, *13* (3).
48. Liu, Y. V.; Massare, M. J.; Barnard, D. L.; Kort, T.; Nathan, M.; Wang, L.; Smith, G., Chimeric severe acute respiratory syndrome coronavirus (SARS-CoV) S glycoprotein and influenza matrix 1 efficiently form virus-like particles (VLPs) that protect mice against challenge with SARS-CoV. *Vaccine* **2011**, *29* (38), 6606-6613.
49. Jardine, J.; Julien, J. P.; Menis, S.; Ota, T.; Kalyuzhniy, O.; McGuire, A.; Sok, D.; Huang, P. S.; MacPherson, S.; Jones, M.; Nieuwsma, T.; Mathison, J.; Baker, D.; Ward, A. B.; Burton, D. R.; Stamatatos, L.; Nemazee, D.; Wilson, I. A.; Schief, W. R., Rational HIV Immunogen Design to Target Specific Germline B Cell Receptors. *Science* **2013**, *340* (6133), 711-716.
50. Brune, K. D.; Leneghan, D. B.; Brian, I. J.; Ishizuka, A. S.; Bachmann, M. F.; Draper, S. J.; Biswas, S.; Howarth, M., Plug-and-Display: decoration of Virus-Like Particles via isopeptide bonds for modular immunization. *Sci Rep* **2016**, *6*.
51. Fifis, T.; Gamvrellis, A.; Crimeen-Irwin, B.; Pietersz, G. A.; Li, J.; Mottram, P. L.; McKenzie, I. F. C.; Plebanski, M., Size-dependent immunogenicity: Therapeutic and protective properties of nano-vaccines against tumors. *Journal of Immunology* **2004**, *173* (5), 3148-3154.

52. Foged, C.; Brodin, B.; Frokjaer, S.; Sundblad, A., Particle size and surface charge affect particle uptake by human dendritic cells in an in vitro model. *International Journal of Pharmaceutics* **2005**, *298* (2), 315-322.
53. Chaudhuri, A.; Battaglia, G.; Golestanian, R., The effect of interactions on the cellular uptake of nanoparticles. *Physical Biology* **2011**, *8* (4).
54. Jegerlehner, A.; Storni, T.; Lipowsky, G.; Schmid, M.; Pumpens, P.; Bachmann, M. F., Regulation of IgG antibody responses by epitope density and CD21-mediated costimulation. *European Journal of Immunology* **2002**, *32* (11), 3305-3314.
55. Kato, Y.; Abbott, R. K.; Freeman, B. L.; Haupt, S.; Groschel, B.; Silva, M.; Menis, S.; Irvine, D. J.; Schief, W. R.; Crotty, S., Multifaceted Effects of Antigen Valency on B Cell Response Composition and Differentiation In Vivo. *Immunity* **2020**, *53* (3), 548-563.
56. Veneziano, R.; Moyer, T. J.; Stone, M. B.; Wamhoff, E. C.; Read, B. J.; Mukherjee, S.; Shepherd, T. R.; Das, J.; Schief, W. R.; Irvine, D. J.; Bathe, M., Role of nanoscale antigen organization on B-cell activation probed using DNA origami. *Nat. Nanotechnol.* **2020**, *15* (8), 716-723.
57. Almeida, J. P. M.; Lin, A. Y.; Figueroa, E. R.; Foster, A. E.; Drezek, R. A., In vivo Gold Nanoparticle Delivery of Peptide Vaccine Induces Anti-Tumor Immune Response in Prophylactic and Therapeutic Tumor Models. *Small* **2015**, *11* (12), 1453-1459.
58. Lee, B. R.; Ko, H. K.; Ryu, J. H.; Ahn, K. Y.; Lee, Y. H.; Oh, S. J.; Na, J. H.; Kim, T. W.; Byun, Y.; Kwon, I. C.; Kim, K.; Lee, J., Engineered Human Ferritin Nanoparticles for Direct Delivery of Tumor Antigens to Lymph Node and Cancer Immunotherapy. *Sci Rep* **2016**, *6*.
59. Shevtsov, M.; Multhoff, G., Heat Shock Protein-Peptide and HSP-Based Immunotherapies for the Treatment of Cancer. *Frontiers in Immunology* **2016**, *7*.
60. Caldeira, J. C.; Perrine, M.; Pericle, F.; Cavallo, F., Virus-Like Particles as an Immunogenic Platform for Cancer Vaccines. *Viruses-Basel* **2020**, *12* (5).
61. Neek, M.; Tucker, J. A.; Butkovich, N.; Nelson, E. L.; Wang, S. W., An Antigen-Delivery Protein Nanoparticle Combined with Anti-PD-1 Checkpoint Inhibitor Has Curative Efficacy in an Aggressive Melanoma Model. *Adv. Therap.* **2020**, *3* (12), 10.
62. Tsai, S. E.; Shamel, A.; Yamanouchi, J.; Clemente-Casares, X.; Wang, J. G.; Serra, P.; Yang, Y.; Medarova, Z.; Moore, A.; Santamaria, P., Reversal of Autoimmunity by Boosting Memory-like Autoregulatory T Cells. *Immunity* **2010**, *32* (4), 568-580.
63. Yeste, A.; Nadeau, M.; Burns, E. J.; Weiner, H. L.; Quintana, F. J., Nanoparticle-mediated codelivery of myelin antigen and a tolerogenic small molecule suppresses experimental autoimmune encephalomyelitis. *Proc. Natl. Acad. Sci. U. S. A.* **2012**, *109* (28), 11270-11275.
64. LaMothe, R. A.; Kolte, P. N.; Vo, T.; Ferrari, J. D.; Gelsinger, T. C.; Wong, J.; Chan, V. T.; Ahmed, S.; Srinivasan, A.; Deitemeyer, P.; Maldonado, R. A.; Kishimoto, T. K., Tolerogenic Nanoparticles Induce Antigen-Specific Regulatory T Cells and Provide Therapeutic Efficacy and Transferrable Tolerance against Experimental Autoimmune Encephalomyelitis. *Frontiers in Immunology* **2018**, *9*.
65. Cappellano, G.; Comi, C.; Chiochetti, A.; Dianzani, U., Exploiting PLGA-Based Biocompatible Nanoparticles for Next-Generation Tolerogenic Vaccines against Autoimmune Disease. *International Journal of Molecular Sciences* **2019**, *20* (1).
66. Ahmad, T.; Eweida, A.; Sheweita, S., B-cell epitope mapping for the design of vaccines and effective diagnostics. *Trials in Vaccinology* **2016**, *5*, 71-83.
67. Irving, M. B.; Craig, L.; Menendez, A.; Gangadhar, B. P.; Montero, M.; van Houten, N. E.; Scott, J. K., Exploring peptide mimics for the production of antibodies against discontinuous protein epitopes. *Molecular Immunology* **2010**, *47* (5), 1137-1148.
68. Li, W. D.; Joshi, M. D.; Singhania, S.; Ramsey, K. H.; Murthy, A. K., Peptide Vaccine: Progress and Challenges. *Vaccines* **2014**, *2* (3), 515-536.

69. Ross, T. M.; Mahmood, K.; Crevar, C. J.; Schneider-Ohrum, K.; Heaton, P. M.; Bright, R. A., A Trivalent Virus-Like Particle Vaccine Elicits Protective Immune Responses against Seasonal Influenza Strains in Mice and Ferrets. *Plos One* **2009**, *4* (6).
70. Palladini, A.; Thrane, S.; Janitzek, C. M.; Pihl, J.; Clemmensen, S. B.; de Jongh, W. A.; Clausen, T. M.; Nicoletti, G.; Landuzzi, L.; Penichet, M. L.; Balboni, T.; Ianzano, M. L.; Giusti, V.; Theander, T. G.; Nielsen, M. A.; Salanti, A.; Lollini, P. L.; Nanni, P.; Sander, A. F., Virus-like particle display of HER2 induces potent anti-cancer responses. *Oncolimmunology* **2018**, *7* (3), 12.
71. Allen, J. D.; Jang, H.; DiNapoli, J.; Kleanthous, H.; Ross, T. M., Elicitation of Protective Antibodies against 20 Years of Future H3N2 Cocirculating Influenza Virus Variants in Ferrets Preimmune to Historical H3N2 Influenza Viruses. *J. Virol.* **2019**, *93* (3).
72. Serradell, M. C.; Rupil, L. L.; Martino, R. A.; Prucca, C. G.; Carranza, P. G.; Saura, A.; Fernandez, E. A.; Gargantini, P. R.; Tenaglia, A. H.; Petiti, J. P.; Tonelli, R. R.; Reinoso-Vizcaino, N.; Echenique, J.; Berod, L.; Piaggio, E.; Bellier, B.; Sparwasser, T.; Klatzmann, D.; Lujan, H. D., Efficient oral vaccination by bioengineering virus-like particles with protozoan surface proteins. *Nat. Commun.* **2019**, *10*.
73. Scaria, P. V.; Chen, B.; Rowe, C. G.; Jones, D. S.; Barnafo, E.; Fischer, E. R.; Anderson, C.; MacDonald, N. J.; Lambert, L.; Rausch, K. M.; Narum, D. L.; Duffy, P. E., Protein-protein conjugate nanoparticles for malaria antigen delivery and enhanced immunogenicity. *Plos One* **2017**, *12* (12).
74. Ma, W. W.; Saccardo, A.; Roccatano, D.; Aboagye-Mensah, D.; Alkaseem, M.; Jewkes, M.; Di Nezza, F.; Baron, M.; Soloviev, M.; Ferrari, E., Modular assembly of proteins on nanoparticles. *Nat. Commun.* **2018**, *9*.
75. Lu, L. T.; Duong, V. T.; Shalash, A. O.; Skwarczynski, M.; Toth, I., Chemical Conjugation Strategies for the Development of Protein-Based Subunit Nanovaccines. *Vaccines* **2021**, *9* (6).
76. Zakeri, B.; Fierer, J. O.; Celik, E.; Chittock, E. C.; Schwarz-Linek, U.; Moy, V. T.; Howarth, M., Peptide tag forming a rapid covalent bond to a protein, through engineering a bacterial adhesin. *Proc. Natl. Acad. Sci. U. S. A.* **2012**, *109* (12), E690-E697.
77. Brune, K. D.; Leneghan, D. B.; Brian, I. J.; Ishizuka, A. S.; Bachmann, M. F.; Draper, S. J.; Biswas, S.; Howarth, M., Plug-and-Display: decoration of Virus-Like Particles via isopeptide bonds for modular immunization. *Sci Rep* **2016**, *6*, 13.
78. Wadhwa, S.; Jain, A.; Woodward, J. G.; Mumper, R. J., Lipid nanocapsule as vaccine carriers for his-tagged proteins: Evaluation of antigen-specific immune responses to HIV I His-Gag p41 and systemic inflammatory responses. *European Journal of Pharmaceutics and Biopharmaceutics* **2012**, *80* (2), 315-322.
79. Chiba, S.; Frey, S. J.; Halfmann, P. J.; Kuroda, M.; Maemura, T.; Yang, J. E.; Wright, E. R.; Kawaoka, Y.; Kane, R. S., Multivalent nanoparticle-based vaccines protect hamsters against SARS-CoV-2 after a single immunization. *Commun. Biol.* **2021**, *4* (1), 9.
80. Izard, T.; ÅEvarsson, A.; Allen, M. D.; Westphal, A. H.; Perham, R. N.; de Kok, A.; Hol, W. G. J., Principles of quasi-equivalence and Euclidean geometry govern the assembly of cubic and dodecahedral cores of pyruvate dehydrogenase complexes. *Proc. Natl. Acad. Sci. U. S. A.* **1999**, *96* (4), 1240-1245.
81. Domingo, G. J.; Orru, S.; Perham, R. N., Multiple display of peptides and proteins on a macromolecular scaffold derived from a multienzyme complex. *J. Mol. Biol.* **2001**, *305* (2), 259-267.
82. Milne, J. L. S.; Wu, X. W.; Borgnia, M. J.; Lengyel, J. S.; Brooks, B. R.; Shi, D.; Perham, R. N.; Subramaniam, S., Molecular structure of a 9-MDa icosahedral pyruvate dehydrogenase subcomplex containing the E2 and E3 enzymes using cryoelectron microscopy. *J. Biol. Chem.* **2006**, *281* (7), 4364-4370.

83. Dalmau, M.; Lim, S.; Chen, H. C.; Ruiz, C.; Wang, S.-W., Thermostability and molecular encapsulation within an engineered caged protein scaffold. *Biotechnology and Bioengineering* **2008**, *101* (4), 654-664.
84. Ren, D. M.; Kratz, F.; Wang, S. W., Protein Nanocapsules Containing Doxorubicin as a pH-Responsive Delivery System. *Small* **2011**, *7* (8), 1051-1060.
85. Ren, D. M.; Dalmau, M.; Randall, A.; Shindel, M. M.; Baldi, P.; Wang, S. W., Biomimetic Design of Protein Nanomaterials for Hydrophobic Molecular Transport. *Adv. Funct. Mater.* **2012**, *22* (15), 3170-3180.
86. Ren, D. M.; Kratz, F.; Wang, S. W., Engineered drug-protein nanoparticle complexes for folate receptor targeting. *Biochem. Eng. J.* **2014**, *89*, 33-41.
87. Molino, N. M.; Anderson, A. K. L.; Nelson, E. L.; Wang, S.-W., Biomimetic Protein Nanoparticles Facilitate Enhanced Dendritic Cell Activation and Cross-Presentation. *ACS Nano* **2013**, *7* (11), 9743-9752.
88. Molino, N. M.; Bilotkach, K.; Fraser, D. A.; Ren, D.; Wang, S.-W., Complement Activation and Cell Uptake Responses Toward Polymer-Functionalized Protein Nanocapsules. *Biomacromolecules* **2012**, *13* (4), 974-981.
89. Molino, N. M.; Neek, M.; Tucker, J. A.; Nelson, E. L.; Wang, S.-W., Viral-mimicking protein nanoparticle vaccine for eliciting anti-tumor responses. *Biomaterials* **2016**, *86*, 83-91.
90. Neek, M.; Tucker, J. A.; Kim, T. I.; Molino, N. M.; Nelson, E. L.; Wang, S.-W., Co-delivery of human cancer-testis antigens with adjuvant in protein nanoparticles induces higher cell-mediated immune responses. *Biomaterials* **2018**, *156*, 194-203.
91. Baxevanis, C. N.; Voutsas, I. F.; Tsitsilonis, O. E., Toll-like receptor agonists: current status and future perspective on their utility as adjuvants in improving anticancer vaccination strategies. *Immunotherapy* **2013**, *5* (5), 497-511.
92. Zhao, S.; Zhang, Y. F.; Zhang, Q. Y.; Wang, F.; Zhang, D. K., Toll-like receptors and prostate cancer. *Frontiers in Immunology* **2014**, *5*.
93. Hennessy, E. J.; Parker, A. E.; O'Neill, L. A. J., Targeting Toll-like receptors: emerging therapeutics? *Nature Reviews Drug Discovery* **2010**, *9* (4), 293-307.
94. Hua, Z. L.; Hou, B. D., TLR signaling in B-cell development and activation. *Cellular & Molecular Immunology* **2013**, *10* (2), 103-106.
95. Visciano, M. L.; Tagliamonte, M.; Tornesello, M. L.; Buonaguro, F. M.; Buonaguro, L., Effects of adjuvants on IgG subclasses elicited by virus-like Particles. *J. Transl. Med.* **2012**, *10*, 8.
96. Pulendran, B.; Arunachalam, P. S.; O'Hagan, D. T., Emerging concepts in the science of vaccine adjuvants. *Nature Reviews Drug Discovery* **2021**, *20* (6), 454-475.
97. Butkovich, N.; Tucker, J. A.; Ramirez, A.; Li, E. Y.; Meli, V. S.; Nelson, E. L.; Wang, S. W., Nanoparticle vaccines can be designed to induce pDC support of mDCs for increased antigen display. *Biomaterials Science* **2022**, *11* (2), 596-610.
98. Zariri, A.; van der Ley, P., Biosynthetically engineered lipopolysaccharide as vaccine adjuvant. *Expert Review of Vaccines* **2015**, *14* (6), 861-876.
99. Wassenaar, T. M.; Zimmermann, K., Lipopolysaccharides in Food, Food Supplements, and Probiotics: Should We be Worried? *European Journal of Microbiology and Immunology* **2018**, *8* (3), 63-69.
100. Rhee, E. G.; Kelley, R. P.; Agarwal, I.; Lynch, D. M.; La Porte, A.; Simmons, N. L.; Clark, S. L.; Barouch, D. H., TLR4 Ligands Augment Antigen-Specific CD8(+) T Lymphocyte Responses Elicited by a Viral Vaccine Vector. *J. Virol.* **2010**, *84* (19), 10413-10419.
101. Kasturi, S. P.; Skountzou, I.; Albrecht, R. A.; Koutsonanos, D.; Hua, T.; Nakaya, H. I.; Ravindran, R.; Stewart, S.; Alam, M.; Kwissa, M.; Villinger, F.; Murthy, N.; Steel, J.; Jacob, J.; Hogan, R. J.; Garcia-Sastre, A.; Compans, R.; Pulendran, B., Programming

- the magnitude and persistence of antibody responses with innate immunity. *Nature* **2011**, *470* (7335), 543–547.
102. Wang, L. Z.; Feng, S. J.; Wang, S. B.; Li, H.; Guo, Z. W.; Gu, G. F., Synthesis and Immunological Comparison of Differently Linked Lipoarabinomannan Oligosaccharide-Monophosphoryl Lipid A Conjugates as Antituberculosis Vaccines. *Journal of Organic Chemistry* **2017**, *82* (23), 12085-12096.
  103. Reintjens, N. R. M.; Tondini, E.; de Jong, A. R.; Meeuwenoord, N. J.; Chiodo, F.; Peterse, E.; Overkleeft, H. S.; Filippov, D. V.; van der Marel, G. A.; Ossendorp, F.; Codee, J. D. C., Self-Adjuvanting Cancer Vaccines from Conjugation-Ready Lipid A Analogues and Synthetic Long Peptides. *Journal of Medicinal Chemistry* **2020**, *63* (20), 11691-11706.
  104. Oliveira-Nascimento, L.; Massari, P.; Wetzler, L. M., The role of TLR2 in infection and immunity. *Frontiers in Immunology* **2012**, *3*.
  105. Cheng, K.; Gao, M.; Godfroy, J. I.; Brown, P. N.; Kastelowitz, N.; Yin, H., Specific activation of the TLR1-TLR2 heterodimer by small-molecule agonists. *Science Advances* **2015**, *1* (3).
  106. Guan, Y.; Omueti-Ayoade, K.; Mutha, S. K.; Hergenrother, P. J.; Tapping, R. I., Identification of Novel Synthetic Toll-like Receptor 2 Agonists by High Throughput Screening. *J. Biol. Chem.* **2010**, *285* (31), 23755-23762.
  107. Shibata, K.; Hasebe, A.; Into, T.; Yamada, M.; Watanabe, T., The N-terminal lipopeptide of a 44-kDa membrane-bound lipoprotein of *Mycoplasma salivarium* is responsible for the expression of intercellular adhesion molecule-1 on the cell surface of normal human gingival fibroblasts. *Journal of Immunology* **2000**, *165* (11), 6538-6544.
  108. Takeuchi, O.; Kawai, T.; Muhlradt, P. F.; Morr, M.; Radolf, J. D.; Zychlinsky, A.; Takeda, K.; Akira, S., Discrimination of bacterial lipoproteins by Toll-like receptor 6. *International Immunology* **2001**, *13* (7), 933-940.
  109. Pavot, V.; Rochereau, N.; Resseguier, J.; Gutjahr, A.; Genin, C.; Tiraby, G.; Perouzel, E.; Lioux, T.; Vernejoul, F.; Verrier, B.; Paul, S., Cutting Edge: New Chimeric NOD2/TLR2 Adjuvant Drastically Increases Vaccine Immunogenicity. *Journal of Immunology* **2014**, *193* (12), 5781-5785.
  110. Buwitt-Beckmann, U.; Heine, H.; Wiesmuller, K. H.; Jung, G.; Brock, R.; Akira, S.; Ulmer, A. J., Toll-like receptor 6-independent signaling by diacylated lipopeptides. *European Journal of Immunology* **2005**, *35* (1), 282-289.
  111. Smith, K. D.; Andersen-Nissen, E.; Hayashi, F.; Strobe, K.; Bergman, M. A.; Barrett, S. L. R.; Cookson, B. T.; Aderem, A., Toll-like receptor 5 recognizes a conserved site on flagellin required for protofilament formation and bacterial motility. *Nature Immunology* **2003**, *4* (12), 1247-1253.
  112. Forstneric, V.; Ivicak-Kocjan, K.; Plaper, T.; Jerala, R.; Bencina, M., The role of the C-terminal D0 domain of flagellin in activation of Toll like receptor 5. *Plos Pathogens* **2017**, *13* (8).
  113. McSorley, S. J.; Ehst, B. D.; Yu, Y. M.; Gewirtz, A. T., Bacterial flagellin is an effective adjuvant for CD4(+) T cells in vivo. *Journal of Immunology* **2002**, *169* (7), 3914-3919.
  114. Wang, B. Z.; Quan, F. S.; Kang, S. M.; Bozja, J.; Skountzou, I.; Compans, R. W., Incorporation of Membrane-Anchored Flagellin into Influenza Virus-Like Particles Enhances the Breadth of Immune Responses. *J. Virol.* **2008**, *82* (23), 11813-11823.
  115. Kang, S. M.; Kim, M. C.; Compans, R. W., Virus-like particles as universal influenza vaccines. *Expert Review of Vaccines* **2012**, *11* (8), 995-1007.
  116. Skountzou, I.; Martin, M. D.; Wang, B. Z.; Ye, L.; Koutsouanos, D.; Weldon, W.; Jacob, J.; Compans, R. W., Salmonella flagellins are potent adjuvants for intranasally administered whole inactivated influenza vaccine. *Vaccine* **2010**, *28* (24), 4103-4112.

117. Merino, S.; Tomas, J. M., Gram-Negative Flagella Glycosylation. *International Journal of Molecular Sciences* **2014**, *15* (2), 2840-2857.
118. Makvandi, M.; Teimoori, A.; Nahad, M. P.; Khodadadi, A.; Cheshmeh, M. G. D.; Zandi, M., Expression of Salmonella typhimurium and Escherichia coli flagellin protein and its functional characterization as an adjuvant. *Microbial Pathogenesis* **2018**, *118*, 87-90.
119. Biedma, M. E.; Cayet, D.; Tabareau, J.; Rossi, A. H.; Ivicak-Kocjan, K.; Moreno, G.; Errea, A.; Soulard, D.; Parisi, G.; Jerala, R.; Berguer, P.; Rumbo, M.; Sirard, J. C., Recombinant flagellins with deletions in domains D1, D2, and D3: Characterization as novel immunoadjuvants. *Vaccine* **2019**, *37* (4), 652-663.
120. Mifsud, E. J.; Tan, A. C. L.; Jackson, D. C., TLR agonists as modulators of the innate immune response and their potential as agents against infectious disease. *Frontiers in Immunology* **2014**, *5*, 1-10.
121. Albin, T. J.; Tom, J. K.; Manna, S.; Gilkes, A. P.; Stetkevich, S. A.; Katz, B. B.; Supnet, M.; Felgner, J.; Jain, A.; Nakajima, R.; Jasinskas, A.; Zlotnik, A.; Pearlman, E.; Davies, D. H.; Felgner, P. L.; Burkhardt, A. M.; Esser-Kahn, A. P., Linked Toll-Like Receptor Triagonists Stimulate Distinct, Combination-Dependent Innate Immune Responses. *Acs Central Science* **2019**, *5* (7), 1137-1145.
122. Duggan, J. M.; You, D. H.; Cleaver, J. O.; Larson, D. T.; Garza, R. J.; Pruneda, F. A. G.; Tuvim, M. J.; Zhang, J. X.; Dickey, B. F.; Evans, S. E., Synergistic Interactions of TLR2/6 and TLR9 Induce a High Level of Resistance to Lung Infection in Mice. *Journal of Immunology* **2011**, *186* (10), 5916-5926.

## CHAPTER 2

# PROTEIN NANOPARTICLE-MEDIATED DELIVERY OF RECOMBINANT INFLUENZA HEMAGGLUTININ ENHANCES IMMUNOGENICITY AND BREADTH OF THE ANTIBODY RESPONSE

This chapter has been modified and published as: Badten, A.J.\*, Ramirez, A.\*, et al., Protein Nanoparticle-Mediated Delivery of Recombinant Influenza Hemagglutinin Enhances Immunogenicity and Breadth of the Antibody Response. *ACS Infectious Diseases*, 2023. **9**(2): p. 239-252. \*Co-first authors

## **2.1. Abstract**

The vast majority of seasonal influenza vaccines administered each year are derived from virus propagated in eggs using technology that has changed little since the 1930s. The immunogenicity, durability, and breadth of response would likely benefit from a recombinant nanoparticle-based approach. Although the E2 protein nanoparticle (NP) platform has been previously shown to promote effective cell-mediated responses to peptide epitopes, it has not yet been reported to deliver whole protein antigens. In this study, we synthesized a novel maleimido tris-NTA linker to couple protein hemagglutinin (HA) from H1N1 influenza virus to the E2 NP, and we evaluated the HA-specific antibody responses using protein microarrays. We found that recombinant H1 protein alone is immunogenic in mice, but requires two boosts for IgG to be detected, and is strongly IgG1 (Th2) polarized. When conjugated to E2 NPs, IgG2c is produced leading to a more balanced Th1/Th2 response. Inclusion of the Toll-like receptor 4 agonist monophosphoryl lipid A (MPLA) significantly enhances the immunogenicity of H1-E2 NPs while retaining the Th1/Th2 balance. Interestingly, broader homo- and hetero-subtypic cross-reactivity is also observed for conjugated H1-E2 with MPLA, compared to unconjugated H1 with or without MPLA. These results highlight the potential of a NP-based delivery of HA for tuning the immunogenicity, breadth, and Th1/Th2 balance generated by recombinant HA-based vaccination. Furthermore, the modularity of this protein-protein conjugation strategy may have utility for future vaccine development against other human pathogens.

## **2.2. Introduction**

Recombinant protein vaccines are inherently safer than live-attenuated vaccines since they pose no risk of reversion to a virulent phenotype and can be used in immunocompromised individuals. Recombinant proteins also obviate the need for propagation of the pathogen, which may introduce mutations (as is the case for influenza virus propagated in hen eggs<sup>1-5</sup>), or pose safety concerns if the pathogen needs to be grown at high containment (BSL3 or 4). It is also



challenging to control amounts of antigen with live vaccines, which can give rise to toxicity concerns, immunodominance of nonprotective antigens, or immune subversion caused by immunomodulatory materials.<sup>6,7</sup> However, recombinant proteins tend to have weaker immunogenicity than live attenuated vaccines, caused by factors such as rapid draining kinetics, monovalency of vaccine antigens, reduced capacity to stimulate innate immunity through pattern recognition receptors (PRRs), and differential pharmacokinetics of vaccine components.<sup>8-10</sup> This generally requires such vaccines to be administered with immunoenhancing substances (collectively termed 'adjuvants') such as emulsions and pattern recognition receptor (PRR) agonists, and typically in multiple (booster) doses to achieve adequate immunity.<sup>11</sup>

NP-based vaccine delivery systems are a promising solution, combining the safety and tunability of subunit vaccines with the strong immunogenicity of particulate antigen.<sup>12-15</sup> This phenomenon is primarily due to two unique properties of nanoparticles: their increased size relative to soluble antigen, and the repetitive pattern in which antigens are displayed on their surface. Experimental and computational studies have indicated that dendritic cells preferentially take up nanoparticles smaller than 500 nm with an optimal uptake size of ~25-50 nm.<sup>16-20</sup> Diameters larger than 25 nm also have increased retention times within draining lymph nodes.<sup>16-20</sup> Previous studies of nanoparticle (NP) scaffolds with controlled antigen valencies have also suggested that the antibody-producing B cells of the adaptive immune system are more efficiently activated by 5 or more repeated epitopes, via improved B cell receptor crosslinking and subsequent activation.<sup>21-23</sup>

NPs have received attention in tumor<sup>24-29</sup> and autoimmune disease<sup>30-33</sup> models due to their capacity to elicit strong cytotoxic T lymphocyte (CTL) and regulatory T cell responses (T-reg), respectively, to peptide epitopes. However, B cell epitopes require specific 3D conformations that are generally not represented by peptide fragments.<sup>34-36</sup> Therefore, there is a need to attach full-length proteins antigens onto NPs. One strategy to accomplish this is genetically fusing the antigen to a protein that naturally self-assembles into a virus-like particle (VLP).<sup>37-41</sup> However,

genetic fusion frequently leads to protein misfolding or expression issues.<sup>42,43</sup> For this reason, alternative methods have been explored to attach full-length proteins to various NP platforms post-assembly, both covalently<sup>44-46</sup> and noncovalently<sup>47,48</sup>.

In this work, we apply Ni(II)-chelated nitrilotriacetic acid (NTA), which has an affinity for polyhistidine-tagged proteins<sup>49-51</sup>, as a method for attachment of influenza hemagglutinin (HA) to a NP assembled from the E2 subunit of pyruvate dehydrogenase (PDH) (see below). To overcome the relatively low binding affinity of Ni-NTA to hexahistidine ( $K_D$  of ~13 mM<sup>52,53</sup>), we used a cyclic tris-NTA, which elicits 3-4 orders of magnitude higher affinities to His<sub>6</sub> tags than monovalent Ni-NTA, with a  $K_D$  of ~2-20 nM.<sup>53,54</sup> To accomplish this, a maleimide functional group was added to tris-NTA to conjugate to the cysteine residues on our E2 NP scaffold. Although the presence of a repetitive structural array of antigens and uniform antigen decoration is reported to enhance B-cell activation and antibody responses, there are currently limited options in the toolbox of short chemical linkers for attaching protein antigens to the surface of a nanoparticle while maintaining the same geometric orientation.<sup>10,55</sup> Therefore, the synthesis and development of a tris-NTA linker could more broadly enable relatively straightforward, modular assembly of NP-based vaccines using any polyhistidine-tagged antigen.

E2 is a subunit of the *Geobacillus stearothermophilus* PDH complex that self-assembles into a 60-mer hollow spherical protein cage of ~25 nm diameter<sup>56,57</sup> and can be functionalized with non-native molecules on its external and internal surfaces.<sup>58-60</sup> We have previously shown that this platform can efficiently activate dendritic cells<sup>61</sup>, and elicit CD8 T cell responses in tumor vaccination models when using CD8 epitope peptide antigens.<sup>28,62,63</sup> Here, we predicted that attaching a protein antigen to our E2 nanoparticle using a novel tris-NTA linker would yield a favorable size (relative to soluble antigen) that allows for B cell receptor cross-linking<sup>22,64</sup> and antibody production. To test this, we have conjugated an antigen protein to the surface of E2 for the first time, specifically the 523-amino acid influenza HA protein (subtype H1 from A/California/7/2009), and show that it engenders a quantitatively enhanced antibody response to

H1 compared to H1 + E2 administered separately. We also show that administration of H1-E2 NPs in an adjuvant comprising toll-like receptor-4 (TLR4) agonist (monophosphoryl lipid A; MPLA) enhances the magnitude and breadth of the response over non-adjuvanted formulations.

## 2.3. Methods

### 2.3.1. Materials

Chemical reagents were purchased from Fisher Scientific, Sigma Aldrich, Acros Organics, Iris Biotech, or TCI Pharmaceuticals unless otherwise noted. Phosphate buffer used for reactions in this study comprised of 50 mM KH<sub>2</sub>PO<sub>4</sub> and 100 mM NaCl at a pH 7.4. Phosphate buffered saline (PBS) used for *in vivo* studies was purchased from Gibco. HEPES buffers used in this study included 20 mM HEPES with 100 mM NaCl or 360 mM NaCl at a pH 7.3. Aqueous stock solutions of NiCl<sub>2</sub> were made at 500 mM. Stock solutions of mal-tNTA were made at 4 mg/ml in DMF. All HA proteins used in this investigation, including H1 for conjugating to E2 (variant A/California/07/2009, H1N1) and HA variants used in the protein arrays, were purchased from Sino Biological.

### 2.3.2. Synthesis of maleimido cyclic tris-NTA (*mal-tNTA*)

To generate mal-tNTA (5), the synthesis was performed following the route described in Scheme 2.1. The synthesis of t-butyl protected tris-NTA-NH (4) was first performed as previously described<sup>53</sup> and these steps, with minor modifications, are detailed in Appendix A.1.1. To produce t-butyl protected tris-NTA from (4), maleimido-propionic acid (27 mg, 0.16 mmol) and N,N,N',N'-Tetramethyl-O-(1H-benzotriazol-1-yl)uronium hexafluorophosphate (HBTU, 61 mg, 0.16 mmol) were dissolved in DMF (9.5 mL) and N,N-Diisopropylethylamine (DIPEA, 0.5 mL). After five minutes, t-butyl protected-tris-NTA-NH (151 mg, 0.11 mmol) was added and the reaction was stirred overnight. The solvent was evaporated, and the product purified by flash chromatography. Column conditions were: 40 g silica gel column; mobile phase A: hexanes; mobile phase B: ethyl

acetate. This was run at a gradient condition of mobile phase B: 0-4 min 0% B, 4-12 min 100% B ramp, 12-20 min 100% B. The product eluted at 13 min. The fractions containing product were collected, the solvent removed by rotary evaporation, and dried over high vacuum. The product was recovered and analyzed by ESI-MS (110 mg, 66% yield). ESI was performed on a Waters LCT ESI MS with flow injection at 0.1mL/min in 100% MeOH. Predicted [M+Na]<sup>+</sup>: 1613.9 m/z Observed [M+Na]<sup>+</sup>: 1612.9 m/z.

t-butyl protected tris-NTA-mal (109 mg, 0.069 mmol) was then dissolved in 95% TFA in water (5 mL) and stirred for 2 h. The TFA was removed by rotary evaporation and the residue added to 40 mL of cold diethyl ether to precipitate the product. The mixture was centrifuged to recover the product pellet. The pellet was dissolved in 50% water/ACN, sterile filtered through a nylon 0.22 μm filter, and lyophilized. The product (5) was weighed and analyzed by LC-MS in water/acetonitrile with 0.1% formic acid (53 mg, 71% yield). LC-MS was performed on a Waters LC-MS with QDA detector with Hclass UPLC with a water/acetonitrile 0.1% formic acid solvent system. Predicted [M+H]<sup>+</sup>: 1087.4 m/z Observed [M+H]<sup>+</sup>: 1087.8 m/z.

### 2.3.3 E2 nanoparticle expression and purification

Expression and purification of the E2 protein nanoparticle were performed as previously described.<sup>57,65</sup> In this study, the E2 mutant E279C was used and will be abbreviated "E2". This mutant has the native glutamic acid at position 279, which resides on the exterior surface of the nanoparticle, replaced with a cysteine residue enabling the conjugation of the mal-Ni-NTA (and subsequently, HA antigen) on the thiol.<sup>65</sup> Briefly, BL21(DE3) *E. coli* cells containing the plasmid with the E279C gene were grown in LB media with ampicillin, and protein expression was induced with IPTG. Soluble cell lysates were applied to a HiPrep Q Sepharose anion exchange column (GE Healthcare) followed by a Superose 6 size exclusion column (GE Healthcare) for purification, with 1 mM dithiothreitol (DTT) added to all lysis, purification, and storage buffers to reduce disulfide bonds and prevent protein cross-linking of the cysteines. The hydrodynamic diameter of

the purified protein nanoparticles was analyzed by dynamic light scattering (DLS; Zetasizer Nano-ZS ZEN3600, Malvern). Electrospray ionization mass spectrometry (Xevo G2-XS Qtof) and SDS-PAGE confirmed molecular weight and purity. Final protein preparations were stored in 50 mM potassium phosphate at pH 7.4 with 100 mM NaCl and 1 mM DTT at 4 °C for short-term and -80 °C for long-term storage. Lipopolysaccharide was removed using Triton X-114 (Sigma), residual surfactant was removed with detergent removal spin columns (Pierce), and low endotoxin levels were confirmed with an LAL ToxinSensor kit (Genscript).<sup>61</sup> Protein concentrations were quantified by bicinchoninic acid (BCA) (Pierce, Thermo Fisher Scientific).

#### *2.3.4. Conjugation of protein antigen to protein nanoparticle*

The overall strategy for conjugating the hemagglutinin (HA) antigen to E2 is shown in Figure 2.1. The attachment is mediated by a hexahistidine/Ni-NTA interaction, with the histidine tag on HA and tNTA on E2.

*Conjugation of mal-tNTA to E2.* To remove DTT from purified E2, the E2 nanoparticles were passed through a 0.5 mL 40 kDa molecular weight cutoff Zeba spin desalting column (Thermo Fisher Scientific) to exchange with HEPES buffer (20 mM HEPES, 100mM NaCl, pH 7.3) according to manufacturer instructions. An 8.5X molar excess of TCEP (Thermo Fisher Scientific) was added and incubated with the E2 (30-45 mins at room temperature), followed by addition and incubation with a 10X molar excess of mal-tNTA (1-2 hours at room temperature, then at 4°C overnight) (Final DMF concentration did not exceeded 10% (v/v)). A buffer exchange was performed with a desalting column using 20 mM HEPES, 100 mM NaCl to remove unreacted mal-tNTA, DMF, and TCEP. Conjugation efficiency of the mal-tNTA to E2 and characterization were performed via SDS-PAGE and ESI-MS (Xevo G2-XS QTof). Protein concentration and hydrodynamic diameters and protein concentrations were measured via BCA and DLS, respectively.

Attachment of His<sub>6</sub>-Tagged Hemagglutinin (HA) to E2 nanoparticle. A 10X molar excess of NiCl<sub>2</sub> in aqueous solution was added to the tNTA-E2 and incubated for 2 hours at room temperature with gentle shaking. Unchelated NiCl<sub>2</sub> was removed and buffer exchange (20 mM HEPES, 360 mM NaCl, pH 7.3) was performed by a spin desalting column. A C-terminally His<sub>6</sub>-tagged HA monomer lacking a transmembrane domain and cytoplasmic tail from A/California/07/2009 (H1N1) (SinoBiological Inc.; reconstituted at 1 mg/mL in water; GenBank protein accession # ACP41105.1) was added to Ni-tNTA-E2 at a 0.3:1 ratio of H1:E2 monomer and incubated at room temperature with gentle shaking for 2 hours. The mixture was filtered with a 0.22 μm PVDF membrane and separated with a Superose™ 6 analytical size exclusion column (SEC) column on ÄKTA FPLC (Cytiva/GE Healthcare) to remove unbound H1. Fractions were evaluated with an SDS-PAGE gel and stained with a Pierce Silver Stain Kit (Thermo Fisher Scientific) to identify the fractions containing H1 attached to E2 nanoparticles (H1-E2) vs. unbound H1. Conjugation efficiency of H1 to E2 was estimated using the SEC chromatographs that showed unbound H1 (peak 2) and conjugated H1-E2 (peak 1) (Figure 2.2B). In brief, we calculated the concentration of unreacted H1 from the area under the curve (AUC) using the volume and  $A = \epsilon bC$  (where  $A$  = absorbance,  $\epsilon$  = molar extinction coefficient of H1,  $b$  = path length, and  $C$  = molar concentration of unreacted H1). The extinction coefficient of H1 was estimated using ExPASy ProtParam (88,240 M<sup>-1</sup>cm<sup>-1</sup>).<sup>66</sup> Mole balances of H1 and E2 related the total amount of H1 and E2 input into the conjugation reaction (respectively) with the amounts after reaction, which enabled the determination of ratio of H1 bound per E2 nanoparticle ( $n = 9$  independent conjugation batches).

### 2.3.5. Transmission electron microscopy

Five microliters of the nanoparticles at approximately 0.015 mg/ml were applied to glow-discharged carbon-coated grids and negatively stained with a saturated ammonium molybdate

solution. The sample grids were examined with a JEM-2100F transmission electron microscope (JEOL) equipped with a OneView CCD (Gatan).

### *2.3.6. Protein modeling*

ChimeraX was used to model E2 nanoparticle (PDB code: 1b5s) and H1 monomer (PDB code: 3ztn), estimate protein dimensions, and generate protein graphics.<sup>67,68</sup> Protein dimensions were measured using ChimeraX's "distance" command and RCSB Protein Data Bank's (PDB's) distance tool. Two amino acids on opposite sides of the H1 stem region were selected, and their distance was recorded. Multiple pairs of amino acids were analyzed and an average distance for the width of H1 was calculated. A similar procedure was done to determine the distance between cysteines on the E2 NP.

### *2.3.7. Immunizations with H1-E2 nanoparticles*

All animal studies were carried out in accordance with protocols approved by the Institute for Animal Care and Use Committee (IACUC) at the University of California, Irvine and by the Animal Care and Use Review Office (ACURO) of the U.S. Army Medical Research and Materiel Command (USAMRMC). Six groups (N=5 per group) of 6–8-week-old C57Bl/6 female mice (Charles River) were administered 100  $\mu$ l vaccine formulations in phosphate buffered saline (PBS, Gibco) (Figure 2.3A) via the subcutaneous route (base of the tail) according to the schedule shown in Figure 2.3B. We examined the effects of immunizing with H1 bound and unbound to the E2 nanoparticle, with and without the TLR4 agonist, monophosphoryl lipid A (MPLA) (Avanti Polar Lipids, Inc). PBS and H1 in PBS served as control groups. H1 and E2 nanoparticle were administered at 2 and 4  $\mu$ g/dose, respectively. Since MPLA has limited solubility in aqueous solution, MPLA was integrated into DOPG liposomes (an inert co-lipid) at 1:5 molar ratio. Mice were primed via the s.c. route (base of tail) and boosted with identical formulations via the same route on days 14 and 49. Mice were weighed daily for approximately 2 weeks after each injection

and monitored for any changes in behavior or appearance. On days 0, 10, 28, 42, and 56 blood was collected via cheek vein bleed. Blood was collected via cardiac puncture on day 70, the experimental end point.

### *2.3.8. Antibody profiling by influenza protein microarray*

The construction and probing methodology of the influenza protein microarray used for the study has been reported previously.<sup>69</sup> Briefly, over 200 recombinant influenza HAs spanning 18 subtypes, expressed in human or insect cells as either HA0 or HA1 molecules with a C-terminal His-tag, were purchased from Sino Biological Inc. and printed as described.<sup>69</sup> The array content and data are shown in Appendix B.6. Plasma samples were incubated with rehydrated arrays at 4°C overnight and washed in Tris-buffered saline (TBS) containing 0.05% Tween 20 (T-TBS). Bound IgG was detected using biotinylated anti-mouse IgG (Jackson ImmunoResearch; Cat No. 115-068-071) and visualized after washing using streptavidin-conjugated Qdot-800 (Life technologies; Cat. No. Q10173MP). For IgG subtyping, anti-mouse IgG1-Alexa Fluor647 or IgG2c-Alexa Fluor555 (Southern Biotech; Cat. Nos. 1073-31 and 1077-32) were used. After washing and drying, images were acquired using the ArrayCAM imaging system (Grace Bio-Labs Inc., Bend, OR).

### *2.3.9. Statistical analyses*

Data describing nanoparticle characterization (e.g., hydrodynamic diameter, antigen/nanoparticle ratios, mass spectrometry molecular weights) are presented as mean  $\pm$  standard deviation (SD) of at least three independent experiments ( $n \geq 3$ ), unless otherwise noted. Protein microarray data from immunized mice sera was compiled in dot plots of signal intensities for each antigen (mean  $\pm$  SD for each vaccine group) generated in Prism version 9.3.1 (GraphPad, La Jolla, CA, USA). One-way ANOVAs were performed using a Kruskal-Wallis



multiple comparison test (Dunn's multiple-comparison) in Prism; a P value of <0.05 was considered statistically significant.

## **2.4. Results and Discussion**

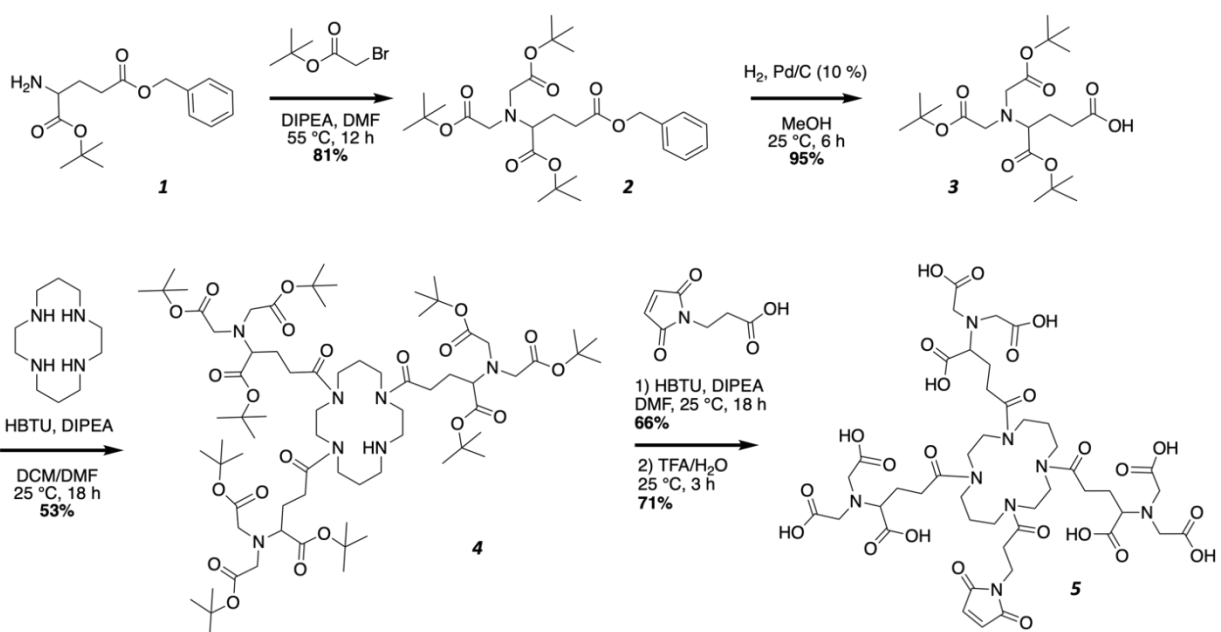
Seasonal influenza, caused by influenza A and B viruses, results in 290,000-650,000 deaths annually worldwide.<sup>70</sup> In this study, we selected influenza A virus (IAV) as our pathogen model to develop an E2 nanoparticle (NP) vaccine, due to its relevance to human health, the detailed understanding of influenza vaccinology, and the availability of many influenza proteins with His-tags suitable for Ni-NTA conjugation chemistry.<sup>71,72</sup> Attachment of virions to the host cell is mediated by binding of hemagglutinin (HA) present on the virion surface to cell-surface sialic acid residues. HA is also the immunodominant target of virus-neutralizing antibodies and a lead vaccine antigen. Of the 18 known IAV hemagglutinin subtypes (H1-H18), only H1 and H3 are currently found circulating in humans, and we have chosen to focus on H1 in these studies due to its importance in seasonal influenza in humans.

Structurally, HA is expressed in the viral membrane as a highly glycosylated homotrimer with each monomer consisting of a single polypeptide demarcated into two distinct regions by a cleavage site: HA1, which contains the highly variable head region and part of the more conserved stem region, and HA2, which encodes the remainder of the stem (See Appendix A.2.1). Here we speculated that our E2 NP, which is of a size (~25 nm) particularly suited to antigen presenting cell (APC) uptake, and its ability to present multiple HA proteins in a regular, repetitive pattern, would lead to the elicitation of superior immunity compared to a free antigen control.

### *2.4.1. Synthesis of maleimido cyclic tris-NTA (mal-tNTA)*

To perform the conjugation of the protein antigen to the E2 NP, we generated a maleimido cyclic tris-NTA (mal-tNTA) as described in Materials and Methods. By the synthetic route shown in Scheme 2.1, hundreds of milligrams of mal-tNTA were readily produced, enabling antigen

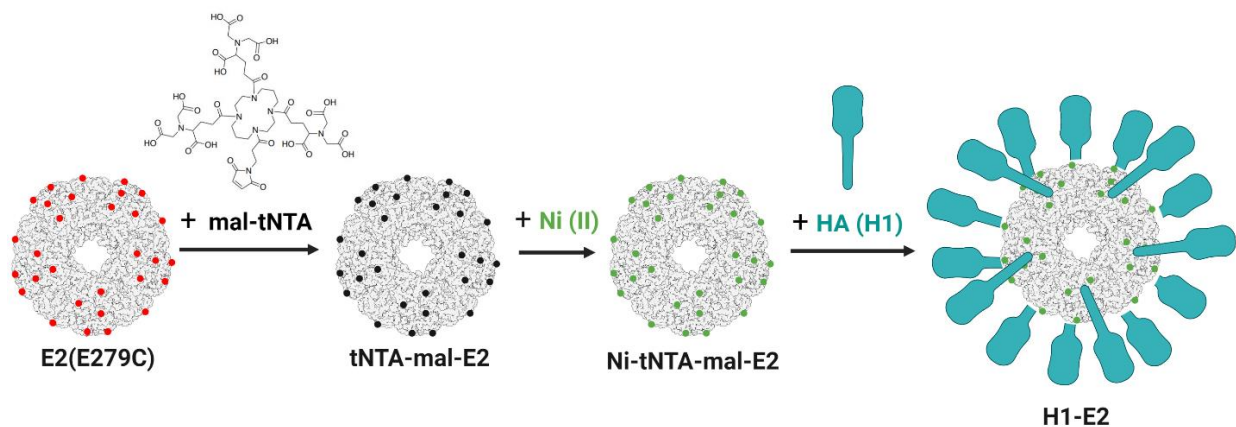
conjugation to the NPs. LC-MS was used to confirm the identity of mal-tNTA (See Appendix B.1). Mal-tNTA is significant as a new linker for joining His-tagged proteins to thiol-functionalized materials, such as cysteine-containing proteins, enabling modular assembly of different protein NPs and antigens. Previous uses of tNTA on NPs involved the use of tNTA linkers with lipid tails that allowed for embedding into liposomes, but here we show a covalent method of attaching tNTA onto protein NPs via maleimide.<sup>73-75</sup> The tris-NTA linker has previously been applied to delay the release of antigens and deliver genome-editing proteins from liposome NPs *in vitro*, though *in vivo* studies have not corroborated these findings.<sup>73-75</sup> Nonetheless, *in vivo* studies utilizing tris-NTA to bind protein antigens to liposome NPs have shown elevated antibody responses compared to unbound protein antigen and efficacy in a tumor model.<sup>73,76</sup>



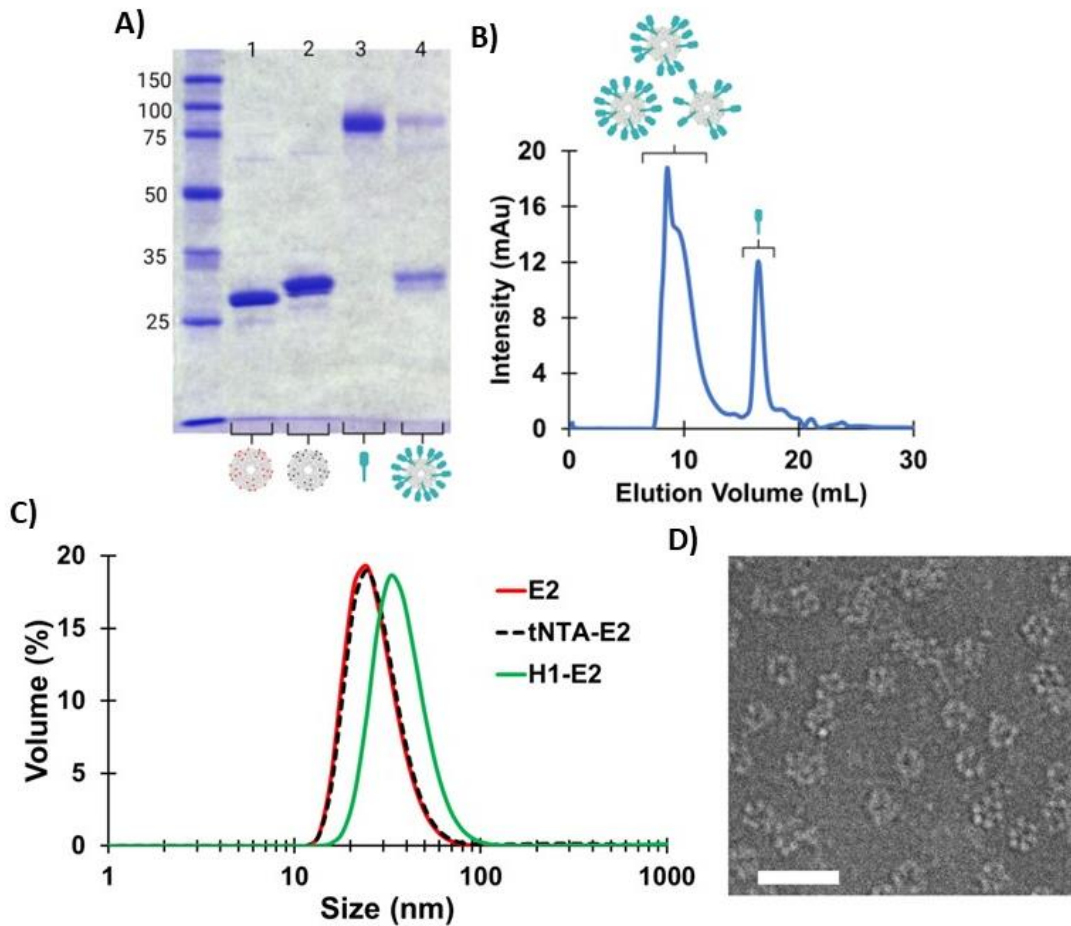
**Scheme 2.1. Synthesis route of mal-tNTA.** 1=H-L-Glu(Bzl)-OtBu<sup>+</sup>HCl, 2=di-*t*-butyl acetate-L-Glu(Bzl)-OtBu, 3=di-*t*-butylacetate-L-Glu-OtBu, 4=*t*-butyl protected tris-NTA-NH, 5=tris-NTA-mal (mal-tNTA).

#### 2.4.2. Surface display and attachment of His-tagged influenza hemagglutinin protein to E2 nanoparticle

*Attachment of mal-tNTA to E2.* HA was successfully attached on the surface of the E2 NP as shown in Figure 2.1 and Figure 2.2. The conjugation of mal-tNTA to E2 was supported by the ~1kDa band shift on SDS-PAGE (Figure 2.2A) and confirmed by mass spectrometry (See Appendix B.2). The theoretical molecular weights of E2 (E279C mutant) and mal-tNTA conjugated to E2 are 28091 and 29179 Da, respectively. Experimentally, we obtained molecular weights of  $28091 \pm 0$  Da for E2 (E279C; n=3) and  $29177 \pm 0.5$  Da for mal-tNTA-E2 (n=3), both of which closely match predicted values. Both SDS-PAGE and MS data show that the conjugation yield was >90%. The resulting mal-tNTA-E2 nanoparticles also structurally remained intact, resulting in a single peak at an average hydrodynamic diameter of  $28.8 \pm 2.2$  nm, which is similar to the size of E2-alone ( $27.3 \pm 1.1$  nm; Figure 2.2C); thus, particles appeared to be physically stable, and no aggregation issues were observed after mal-tNTA conjugation.



**Figure 2.1. Hemagglutinin (HA, subtype H1) protein attachment to E2 using mal-tNTA.** The E2 mutant, E279C, is a 60-subunit protein nanoparticle assembly which contains 60 cysteines on the surface (red points). Maleimide-tNTA is conjugated to these external cysteines (black points), and Ni (II) is loaded onto tNTA via chelation (green points). A polyhistidine tag on the H1 antigen associates with the Ni-chelated tNTAs to form a coordination bond, resulting in a nanoparticle displaying H1 on the surface.



**Figure 2.2. Characterization of tNTA-E2 and H1-E2 nanoparticles.** (A) SDS-PAGE showing E2 (E279C) alone (lane 1), tNTA-E2 (lane 2), H1 alone (lane 3), and H1-E2 (lane 4). (B) A representative chromatogram of the size exclusion chromatography (SEC) performed to separate unreacted HA. Each collected fraction was analyzed with SDS-PAGE (See Appendix B.4) and confirmed H1-bound E2 in the first SEC peak and unbound H1 in the second peak. (C) Hydrodynamic diameters for E2, tNTA-E2, and H1-E2, and average sizes were  $27.3 \pm 1.1$  nm,  $28.8 \pm 2.2$  nm, and  $38.2 \pm 1.7$  nm, respectively. (D) Representative TEM image of H1-E2 nanoparticles. Scale bar = 50 nm.

*Attachment of H1 to E2.* Our model HA antigen, H1 from A/California/7/2009 (Sino Biological), was His-tagged at the C-terminus, expressed in HEK293T cells, and lacked the transmembrane domain and cytoplasmic tail in native hemagglutinin. The protein also lacks an engineered trimerization domain, and size exclusion chromatography (SEC) comparing the elution profiles of this soluble H1 shows elution profiles consistent with previously-reported

monomers of H1<sup>77,78</sup> and other HA subtypes (H3, H5)<sup>77-80</sup>, rather than their trimers (See Appendix B.3). Although HA trimers may present quaternary epitopes not found in monomers and thereby elicit antibodies from a broader repertoire of B cell clones<sup>81,82</sup>, we aim to construct H1-E2 using HA monomers to facilitate synthesis, which is an important consideration for future nanoparticle vaccine scale-up. Moreover, we have also published IgG cross-reactivity profiles against different drift variants for mice that were administered monomeric or trimeric H5; we found that these datasets are highly correlated ( $R^2 = 0.92$ ), suggesting the immunogenicity of monomeric HA is broadly overlapping with trimeric HA.<sup>83</sup>

To attach the His-tagged H1 to E2, we chelated tNTA-E2 with Ni(II) and incubated with the His<sub>6</sub>-tagged H1. The H1-E2 product was then separated from unbound H1 by size exclusion chromatography (SEC), resulting in protein elution within two distinct peaks (Figures 2.2A,B). SDS-PAGE analysis of each of the fractions from the SEC showed that, as expected based on size, the first peak contained E2 nanoparticles with attached H1 and the second peak was free, unbound H1 (See Appendix B.4). It should be noted that the tNTA-H1 interaction with the hexahistidine is a coordination, not a covalent, bond and therefore leads to the appearance of separate H1, E2, and tNTA-E2 subunit bands on the SDS-PAGE denaturing gel (Figure 2.2A, lane 4; See Appendix B.4). The H1:E2 binding ratio was calculated from the SEC chromatograms based on the area under the curve as described in Materials and Methods. The average ratio of H1 bound per E2 nanoparticle was determined to be  $13.1 \pm 1.0$  and was consistent with estimations based on SDS-PAGE band intensities. This protein assembly yielded an intact H1-E2 particle with an average hydrodynamic diameter of approximately  $38.2 \pm 1.7$  nm (Figure 2.2C), ~9-10 nm larger than the sizes for E2 alone (E279C variant) and tNTA-E2 (Figure 2.2C). This H1-E2 size is within the range of the ideal size range for lymph node retention times and dendritic cell uptake.<sup>16-20,64</sup> DLS data also did not show evidence of protein aggregation after H1 attachment to the nanoparticle. Transmission electron microscopy of H1-E2 further confirms the

intact monodispersed nature of the nanoparticles reported by DLS and the assembly of particles consistent with a hollow dodecahedral cage structure (Figure 2.2D).

3D protein modeling using ChimeraX shows that on the surface of a 60-mer E2 nanoparticle, the location of the cysteines at position 279 is clustered in a trimeric configuration, with neighboring cysteines estimated to be only ~3 nm apart (See Appendix A.2.2). Based on modeling, monomeric HA is estimated to have a diameter of ~3.0 nm. Therefore, it is likely that steric hindrance between HA monomers limits the number of proteins that could associate with the tNTA-functionalized cysteines. Although the resulting average attachment ratio is below the theoretical maximum, this value is close to the observed conjugation of another model protein, green fluorescent protein (GFP), to E2 nanoparticles using the same tNTA/His-tag strategy (See Appendix A.1.2; See Appendix B.5). In examining the attachment of GFP to E2 using this tNTA approach, a molar excess of GFP was reacted with E2 which resulted in ~9 GFP attached to the surface of E2. We speculate that the theoretical maximum number of 60 H1 on a nanoparticle may not be necessary for a vaccine formulation, since B cell receptor cross-linking has an ideal antigen spacing of 5-10 nm<sup>8,20,71</sup>, which is above the distance of neighboring cysteines on this platform (See Appendix A.2.2).

#### *2.4.3. Immunogenicity of H1 is enhanced by conjugation to E2, with or without MPLA*

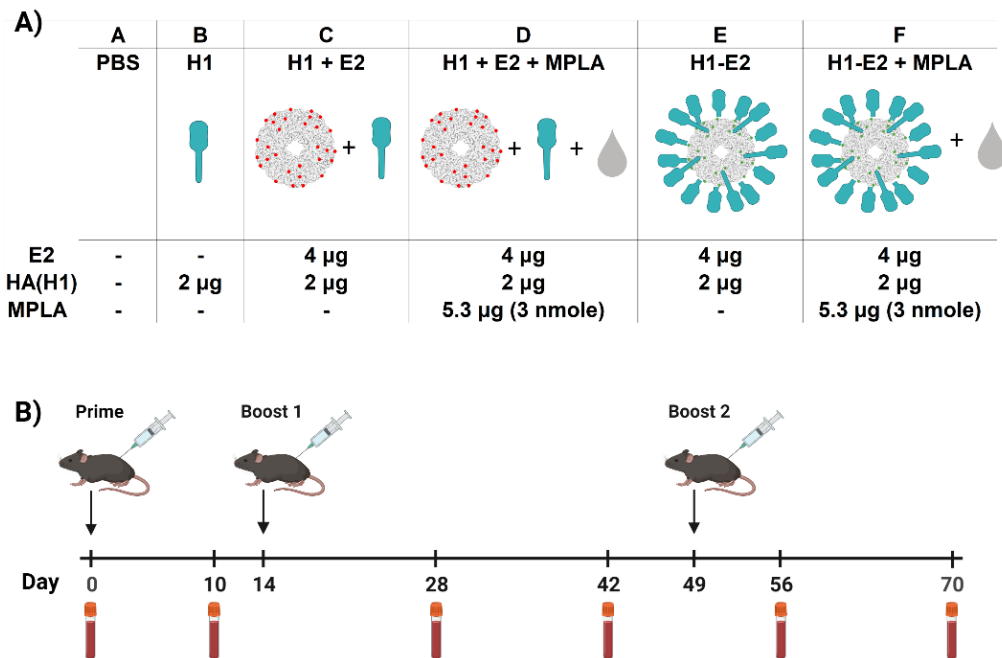
We then examined the immunogenicity of our H1-E2 nanoparticles in mice *in vivo*, following the vaccine groups and immunization schedule summarized in Figure 2.3. Plasma samples collected at regular intervals were probed for IgG breadth using HA protein microarrays (Figures 2.4 and See Appendix B.6). IgG reactivity toward full-length (HA0) proteins are shown in Figure 2.4A. PBS controls (Group A) failed to produce H1-specific IgG at any time point, as expected. H1 (Group B) was antigenic in the absence of an adjuvant, although required two boosts to generate a broad response across different H1 variants. Conjugation of H1 to E2 NPs (H1-E2, Group E) did not enhance immunogenicity unless also administered with MPLA (Group

F). Inclusion of MPLA to the H1-E2 conjugate also dramatically accelerated the response such that IgG was detected on day 10 (after a single dose), with a significant increase in magnitude after the first boost, and a further increase after the second boost. MPLA also enhanced the magnitude of the response to unconjugated H1 (Group D) although signals were lower than when conjugated (Group F). Interestingly, Group C, which received unconjugated H1 and E2 without MPLA, never induced H1-specific antibodies at any point during the study. Since H1 alone was able to induce IgG, there appears to be a suppressive function of E2 when admixed with H1. This suppressive effect does not appear to be unique to H1, as it was also observed when mice were immunized with a different protein antigen (CBU1910 from *Coxiella burnetii*) mixed with E2; however, the suppression that is observed for CBU1910 appears to be at a lower extent (See Appendix B.7). The reasons for this are currently unclear but seem to be overcome by the inclusion of MPLA (as can be seen in Group D). At no point in the study did any animals exhibit noticeable adverse reactions, including weight loss to any of the formulations (data not shown).

IgG reactivity toward HA1 fragments is shown in Figure 2.4B. HA1 contains the variable head domain and part of the conserved stem domain. Thus, cross-reactivity for HA1 is more stringent than for the whole HA0 protein since HA1 contains fewer conserved amino acids found in the stem. Overall, the dynamics of the response are similar to that seen against the full-length HA0, although the magnitude of signals for HA1 fragments is lower, consistent with lower sequence identity between HA1 fragments and the immunizing H1 variant. Moreover, the accelerated (d10) response seen against full length HA0 in Group F was not seen against the HA1 fragment, suggesting IgG against the stem (not encoded in HA1) arise first.

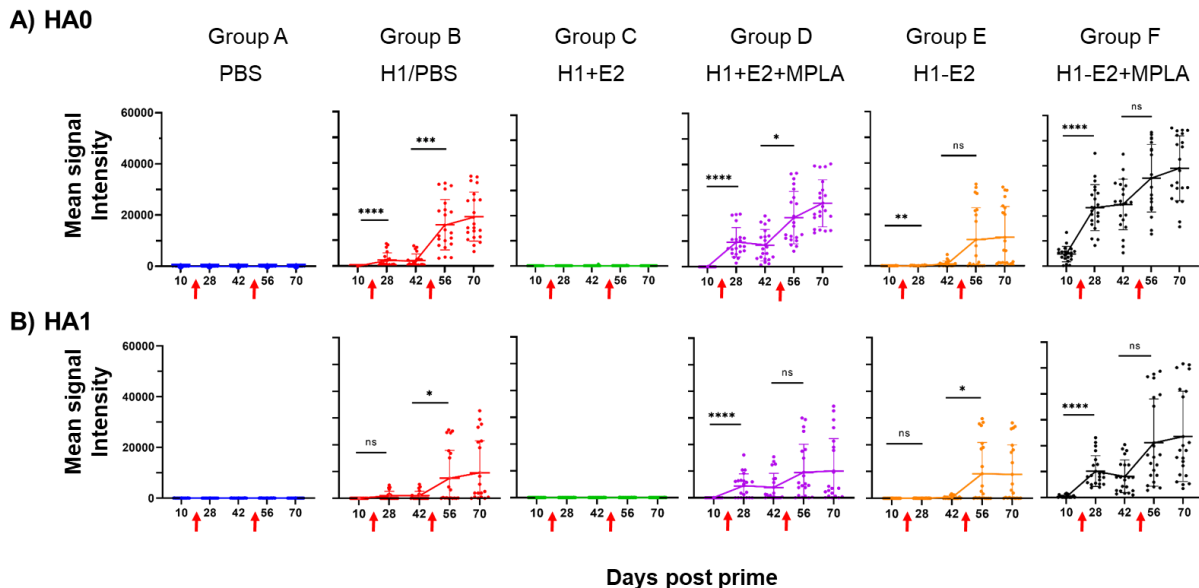
The early (d10) appearance of H1-specific IgG in Group F suggests conjugation of antigen to the NP enhances class switching of H1-specific B cells. Since neither unconjugated H1 with MPLA (Group D), nor conjugated H1-E2 without MPLA (Groups D and E, respectively) show IgG at d10, the data from Group F indicates physical linkage H1 to E2 and MPLA are synergistic in the acceleration of the response. This may be owing to the increased size of the H1-E2 complex

compared to unconjugated H1, which may lead to improved lymph node retention required for class switching and affinity maturation.<sup>64,84,85</sup> In addition, the display of H1 on the E2 NP in a repeating manner is conducive for B cell receptor (BCR) crosslinking, which is a requirement for B cell activation.<sup>86</sup> BCR crosslinking has also recently been shown to play a role in germinal center induction within lymph nodes, a necessary step for achieving affinity maturation and class switching of B cells.<sup>87</sup> Lastly, because the particulate nature of the H1-E2 nanoparticle makes it more likely to be taken up by APCs, we speculate that these cells may have higher levels of H1-derived peptide/MHC complexes on their surface leading to enhanced T cell activation.<sup>88,89</sup> Of note, activated CD4 “helper” T cells can then contribute to T cell-dependent maturation of B cells to elicit higher IgG titers. It is suspected that one, or a combination of the above mechanisms, are contributing to the accelerated and increased magnitude of signals observed in Group F.



**Figure 2.3. Vaccine groups and immunization schedule.** (A) Table summarizing the vaccine groups and dose amounts per injection. Group A) PBS control; Group B) Hemagglutinin (H1); Group C) E2 nanoparticle and H1 (unconjugated); Group D) E2 nanoparticle and H1 (unconjugated), with MPLA (TLR4 agonist); Group E) H1-E2 (conjugated); Group F) H1-E2 (conjugated) with MPLA. (B) Timeline of immunizations and plasma collection.





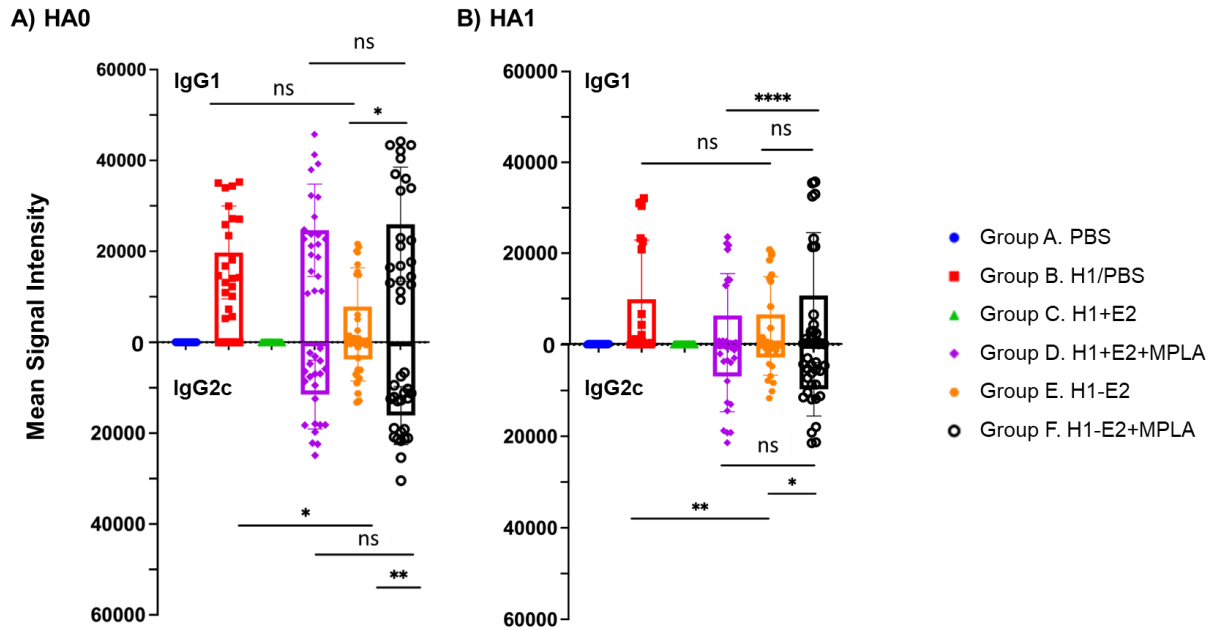
**Figure 2.4. H1-specific IgG profiling by protein microarray.** Six groups of 5 B6 mice (Groups A to F) were administered different formulations as indicated and boosted on d14 and d49 (red arrows). Array data are shown as dot plots of IgG signal intensities at different time points post-prime against H1 variants displayed on an influenza virus HA protein microarray; each dot represents an individual H1 variant (mean of 5 mice) with lines connecting the means ( $\pm$  SD error bars). **(A)** HA0, full-length H1 (N=21 variants); **(B)** HA1 fragment of H1 (N=21 variants). Variants of HA0 and HA1 were utilized and reflect those listed in Appendix A.2.3. One-way ANOVA (non-parametric) comparisons using a Kruskal-Wallis test were made between both pre- and post-boost time points: \*\*\*\*  $p < 0.0001$ , \*\*\*  $p < 0.001$ , \*\*  $p < 0.01$ , \*  $p < 0.05$ . Abbreviations: PBS, phosphate buffered saline; H1+E2, unconjugated H1 and E2 NPs; H1-E2, conjugated H1 and E2 NPs, MPLA, monophosphoryl lipid A.

#### 2.4.4. H1-E2 nanoparticle immunizations elicited a IgG1/IgG2c balanced antibody response

Endpoint plasma (d70) was also probed for H1-specific IgG1 and IgG2c using isotype-specific secondary antibodies (Figure 2.5). Group B (unadjuvanted H1) defaults to a strongly IgG1-polarized response. In contrast, Group D (unconjugated E2 + H1 with MPLA) and Group F (conjugated H1-E2 with MPLA) elicited a balanced IgG1 and IgG2c response, with Group F eliciting marginally higher IgG2c signals than group D. Group E (H1-E2 without MPLA) also induced a balanced response, although the magnitude of the signals was significantly lower than in the absence of MPLA.

IgG1/IgG2 subtyping is frequently used as a surrogate marker for Th2 and Th1 functionality, respectively.<sup>90-92</sup> In previous studies we showed the capacity of E2 NP to elicit anti-tumor immunity when conjugated with tumor peptide antigens and administered with CpG (a TLR9 agonist) as adjuvant.<sup>28,62,63</sup> The Th1-skewing property of CpG is well-known.<sup>93</sup> In the present study, the H1-E2 conjugate in the absence of MPLA (Group E) was able to elicit modest IgG2c, while H1 alone could not, which suggests that the E2 NP itself may have some inherent Th1-biasing properties. This is a novel finding and is significant as many FDA-approved human vaccines adjuvanted with alum (aluminum hydroxide salts), are biased towards stimulating Th2 immunity. Although neutralizing antibody responses have conventionally been the focus of evaluating influenza vaccine efficacy, it is now clear that Th1 and cell-mediated responses are also important for protection against influenza.<sup>94,95</sup>

Unlike B cells, which are confined to recognizing structural, often highly variable, antigens on the surface of viruses, T cell epitopes can be found also within non-structural antigens expressed in infected cells, and which in many cases are highly conserved between variants. This makes them attractive T cell vaccine antigens, particularly for pathogens such as influenza which has the capacity to undergo antigenic drift. CD8 T cells, which act by killing infected cells that present pathogen-associated peptide epitopes on MHCI, have long been demonstrated to have the capacity to react against heterosubtypic influenza strains<sup>96,97</sup> and their role in controlling symptomatic infection is well-documented.<sup>98,99</sup> Although the design of E2 nanoparticle-based cancer vaccines with tumor associated antigens has been demonstrated to elicit a CD8 cytotoxic response<sup>62,63</sup>, the utility of E2 for inducing CD8 to whole protein antigen is still under investigation. Our data does show, however, the ability of our E2 NP to skew IgG responses towards IgG2c, suggesting a stronger Th1 CD4 cell-mediated response, which may have benefits in the context of influenza vaccine design.<sup>100,101</sup>



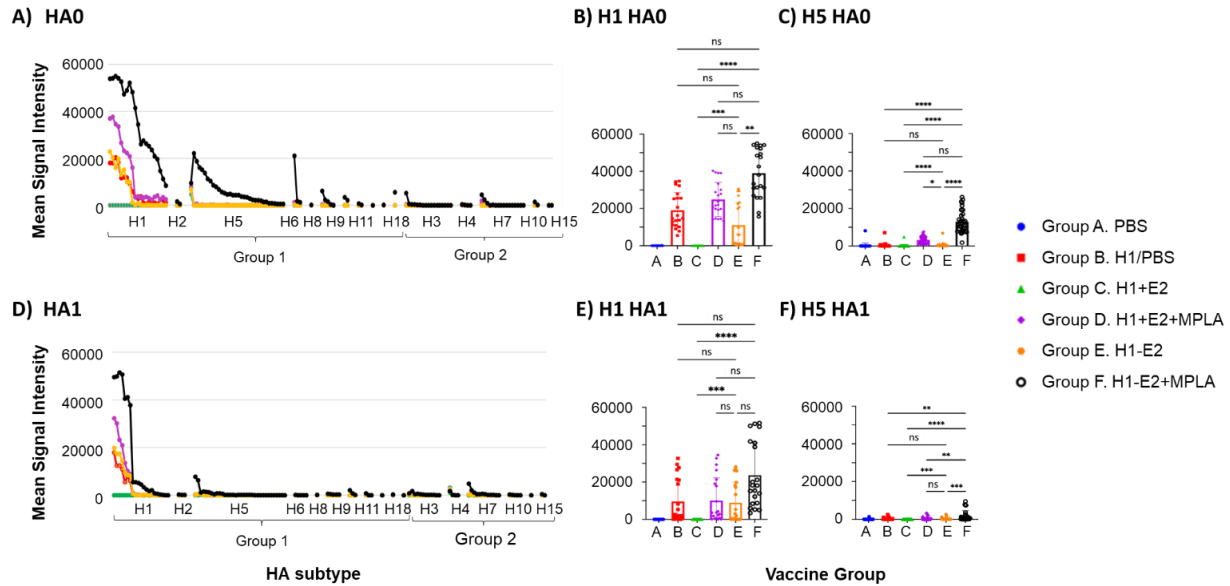
**Figure 2.5. Attachment of H1 to E2 (H1-E2) modulates the immune response to H1 towards a more balanced IgG1/IgG2c antibody response.** Box and whisker plots with each dot representing an individual H1 variant (means  $\pm$  SD of  $n=5$  mice) after probing d70 samples on HA protein microarrays followed by IgG1 and IgG2c-specific secondary antibodies. **(A)** HA0, full-length H1, **(B)** HA1 fragment of H1. 21 variants of HA0 and 21 variants of HA1 were utilized and reflect the H1 variants listed in Appendix A.2.3. One-way ANOVA (non-parametric) comparisons using a Kruskal-Wallis test for means of the data was performed between groups as shown, \*\*\*\*  $p < 0.0001$ , \*\*\*  $p < 0.001$ , \*\*  $p < 0.01$ , \*  $p < 0.05$ . Abbreviations: PBS, phosphate buffered saline; H1+E2, unconjugated H1 and E2 NPs; H1-E2, conjugated H1 and E2 NPs, MPLA, monophosphoryl lipid A.

#### 2.4.5. H1-E2 conjugated NPs elicited broader homosubtypic and heterosubtypic cross-reactivity than unconjugated H1

Subtype cross-reactivity on the array is a potential correlate of the breadth of the response induced by a vaccine. The head region of HA, encoded in HA1, is the most variable region found between influenza variants and contains epitopes recognized by neutralizing antibodies. Mutations within neutralizing antibody epitopes (located predominantly in the immunodominant head of HA) lead to immune selection of variants able to escape antibody neutralization and the emergence of novel variants.<sup>102</sup> More conserved regions, located in both the HA1 and HA2 domains, that play functional roles in receptor binding and membrane fusion, respectively, are

widely considered as prime targets for eliciting broad or cross-protective immunity. However, such vulnerabilities are often masked by glycans<sup>103-106</sup> and may be inaccessible to antibody or subdominant in the response, making them unsatisfactory targets for vaccination. Here we demonstrate that loading H1 on E2 NPs enhances antibody responses towards both of head and stem regions of different influenza subtypes. Shown in Figure 2.6 are IgG profiles for day 70 plasma (See Appendix B.6). The plots in Figure 2.6A show the signals for each vaccine group (mean of 5 mice) against all HA0 (full-length) HAs printed on the array, spanning HA subtypes 1 through 18 (horizontal axis), organized by phylogenetic group. The data for individual full length (HA0) H1 and H5 variants, are also shown in the box plots in Figures 2.6B and 6C, respectively. H1 and H5 both belong to phylogenetic group 1 and have ~63% amino acid sequence identity. While vaccine Groups B, D, E, and F were all able to elicit homosubtypic cross-reactivity (i.e., to the H1 variants) only Group F (H1-E2 conjugate with MPLA) elicited detectable heterosubtypic responses for H5 and other Group 1 subtypes. Overall, Group F elicited both the highest homosubtypic and heterosubtypic antibody signals.

The plots in Figure 2.6D show the mean signals for each vaccine group for all HA1 fragments on the array. The HA1 fragment contains the variable head domain of HA and part of the stem. Overall, the same vaccine formulations that induced a homosubtypic cross-reactive response to the full-length (HA0) H1 molecule, also induced a homosubtypic cross-reactive response to the H1 HA1 fragment, although the breadth was narrower. Similarly, Group F, which was the only group able to induce significant heterosubtypic cross-reactivity for full length H5, also induced a modest response to H5 HA1 fragments, although again the breadth was reduced. The data for individual HA1 fragments of H1 (homosubtypic cross-reactivity) and H5 (heterosubtypic cross-reactivity) are shown in the box plots in Figures 2.6E and 2.6F, respectively. These representations of the data emphasize that the breadth of both homo- and heterosubtypic responses are broader for the full length HA0 compared to the HA1 fragment.



**Figure 2.6. Attachment of H1 to E2 nanoparticle (H1-E2) engenders homosubtypic and heterosubtypic cross-reactivity that is enhanced by MPLA.** (A) and (D), day 70 plasma IgG profiles against full-length (HA0) and HA1 fragments, respectively, as measured by protein microarray. Each spot corresponds to an individual arrayed protein (mean of 5 mice). The arrayed proteins (horizontal axis) are arranged by phylogenetic group and ranked by descending signal intensity. (B) and (C) are box plots of H1 and H5 full-length (HA0) array data. (E) and (F) are box plots of H1 and H5 HA1 fragment array data. Each plot showing one-way ANOVA (non-parametric) comparisons using a Kruskal-Wallis test for means as indicated; \*\*\*\*  $p < 0.0001$ , \*\*\*  $p < 0.001$ , \*\*  $p < 0.01$ , \*  $p < 0.05$ .

This relatively broader response to full length (HA0) compared to HA1 fragment by protein microarray (Figure 2.6) has been seen in other studies where the breadth of the response induced by adjuvanted HA was examined using the microarray platform.<sup>83,107</sup> One possibility is the stem is immunodominant over the head, at least when recombinant HA protein is delivered in adjuvant. This contrasts with the response to natural infection where the head is usually immunodominant.<sup>108</sup> We speculate the membrane distal head is readily accessible to antibody on the virion surface, whereas the stem might be relatively less accessible to antibody, accounting for the immunodominance of the head during natural infection. In contrast, administration of recombinant HA protein in adjuvant may allow the stem to be more available for antibody recognition. Regardless of the precise mechanism, this is significant because, in contrast to the variable head domain, the stem is a relatively well-conserved and a vaccine strategy able to drive

the response toward the conserved stem may offer a path to a more broadly protective vaccine compared to current vaccine approaches.<sup>109</sup> We are also aware it is possible the immunodominance of the stem in this study may be because HA1 adopts a more authentic conformation in the array platform when assembled in the full-length (HA0) molecule rather than as an HA1 fragment. Monoclonal antibodies (mAbs) that are usually used to probe for correct conformation of HA typically recognize the stem rather than the head; conversely, HA1-binding mAbs (e.g., those that inhibit virus-mediated hemagglutination) generally bind to linear epitopes and are not conformation dependent. Nevertheless, we did identify two conformation-sensitive mAbs that bind H1 HA1 on the array that lost reactivity against denatured antigen,<sup>107</sup> supporting the notion that HA1 is correctly folded on the array. However, further studies to establish whether administration of recombinant HA in adjuvant helps overcome immunodominance of the head are warranted.

Homosubtypic cross-reactivity of antibodies generated by the H1 (A/California/7/2009) vaccine and other H1 drift variants is mediated by B cell clones that recognize antigenically similar epitopes. Although not defined here, these epitopes will map to conserved amino acids shared by multiple variants and are typically regions of the HA protein required for structural stability, receptor-mediated attachment, or membrane fusion.<sup>110</sup> Homosubtypic cross-reactivity elicited by the H1-E2 vaccine reported here is significant, as it may offer a path to providing protection against drift variants. Current seasonal influenza vaccines, manufactured predominantly from inactivated influenza virus and detergent extracted to enrich for the membrane HA and NA molecules, elicit antibodies that are highly specific to the immunizing variant. Consequently, seasonal vaccines need to be revised each year in response to antigenic drift, i.e., the process by which the circulating viruses (currently H1N1 and H3N2) accumulate mutations within the neutralizing epitopes under selective pressure from antibodies. Although the breadth of the response can be broadened using adjuvants<sup>107</sup> these are not routinely used for seasonal influenza.

Seasonal influenza vaccines provide negligible heterosubtypic cross-reactivity. Here we show that among the formulations tested, the conjugated H1-E2 with MPLA induced cross-reactivity for H5. Avian influenza H5N1 is endemic in wild birds and frequently causes outbreaks in domestic poultry; it is also well-known known for causing zoonotic infections of humans.<sup>111</sup> Indeed, the risk of pandemics caused by H5N1 has prompted the stockpiling of H5N1-based vaccines as part of the US Government's Pandemic Influenza Vaccine Stockpiling Program. A vaccine able to provide broader protection, achieved through the use of improved delivery systems such as adjuvants and/or nanoparticles, would reduce the need to annual reformulations and may lead to vaccines against both seasonal and pandemic influenzas, or ideally across all subtypes (so-called 'universal' influenza vaccines).

## **2.5. Conclusions**

A model antigen (H1 hemagglutinin from influenza) has been successfully conjugated to the E2 NP using a new tris-NTA chemical linker that utilizes polyhistidine tags engineered into recombinant proteins. Unlike many conventional protein-protein linkers, this strategy enables the attachment of protein antigens onto the surface of a vaccine nanoparticle platform in a defined orientation, which can potentially increase B-cell activation. We tested the antibody responses after administration with vaccine nanoparticles that were fabricated using this approach. In immunogenicity studies in mice where H1-E2 was compared to unconjugated H1, the conjugate elicited a more balanced IgG1/IgG2c response to H1, compared to the strongly polarized IgG1 response seen against H1 alone, showing the E2 particle may have an inherent Th1-biasing property. Administration of the H1-E2 conjugate with MPLA significantly accelerated the response (with IgG appearing on d10) but not when administered with unconjugated H1, nor when H1-E2 conjugate was administered in the absence of MPLA, suggesting NP-mediated delivery of antigen and MPLA signaling synergize to accelerate the response. While several formulations tested engendered homosubtypic cross-reactivity, only the conjugated H1-E2 NP with MPLA induced

significant heterosubtypic cross-reactivity, a favorable characteristic for vaccine designs that may protect against drift variants. Our tris-NTA/His-tag conjugation strategy is applicable to other protein antigens and should broaden the utility of the E2 NP as a delivery vehicle for other human pathogens.

## **2.6. Acknowledgements**

This work was supported by the Defense Threat Reduction Agency (HDTRA11810035 and HDTRA11810036), the National Institutes of Health (R01EB027797), and the National Science Foundation (Graduate Research Fellowship to A.R.). We thank Drs. Felix Grun and Benjamin Katz at the UCI Mass Spectrometry Facility. The authors acknowledge the use of facilities and instrumentation at the UC Irvine Materials Research Institute (IMRI), which is supported in part by the National Science Foundation through the UC Irvine Materials Research Science and Engineering Center (DMR-2011967).



## 2.7. References

1. Park, Y. W.; Kim, Y. H.; Jung, H. U.; Jeong, O. S.; Hong, E. J.; Kim, H.; Lee, J. I., Comparison of antigenic mutation during egg and cell passage cultivation of H3N2 influenza virus. *Clinical and Experimental Vaccine Research* **2020**, *9* (1), 56-63.
2. Wu, N. C.; Zost, S. J.; Thompson, A. J.; Oyen, D.; Nycholat, C. M.; McBride, R.; Paulson, J. C.; Hensley, S. E.; Wilson, I. A., A structural explanation for the low effectiveness of the seasonal influenza H3N2 vaccine. *PLOS Pathogens* **2017**, *13* (10).
3. Wang, W.; Alvarado-Facundo, E.; Vassell, R.; Collins, L.; Colombo, R. E.; Ganesan, A.; Geaney, C.; Hrnčir, D.; Lalani, T.; Markelz, A. E.; Maves, R. C.; McClenathan, B.; Mende, K.; Richard, S. A.; Schofield, C.; Seshadri, S.; Spooner, C.; Utz, G. C.; Warkentien, T. E.; Levine, M.; Coles, C. L.; Burgess, T. H.; Eichelberger, M.; Weiss, C. D., Comparison of A(H3N2) Neutralizing Antibody Responses Elicited by 2018-2019 Season Quadrivalent Influenza Vaccines Derived from Eggs, Cells, and Recombinant Hemagglutinin. *Clinical Infectious Diseases* **2021**, *73* (11), E4312-E4320.
4. Garretson, T. A.; Petrie, J. G.; Martin, E. T.; Monto, A. S.; Hensley, S. E., Identification of human vaccinees that possess antibodies targeting the egg-adapted hemagglutinin receptor binding site of an H1N1 influenza vaccine strain. *Vaccine* **2018**, *36* (28), 4095-4101.
5. Zost, S. J.; Parkhouse, K.; Gumina, M. E.; Kim, K.; Perez, S. D.; Wilson, P. C.; Treanor, J. J.; Sant, A. J.; Cobey, S.; Hensley, S. E., Contemporary H3N2 influenza viruses have a glycosylation site that alters binding of antibodies elicited by egg-adapted vaccine strains. *Proc. Natl. Acad. Sci. U. S. A.* **2017**, *114* (47), 12578-12583.
6. Sanders, B.; Koldijk, M.; Schuitemaker, H., Inactivated Viral Vaccines. *Vaccine Analysis: Strategies, Principles, and Control* **2014**, 45-80.
7. Minor, P. D., Live attenuated vaccines: Historical successes and current challenges. *Virology* **2015**, *479*, 379-392.
8. Moyle, P. M.; Toth, I., Modern Subunit Vaccines: Development, Components, and Research Opportunities. *Chemmedchem* **2013**, *8* (3), 360-376.
9. Tam, H. H.; Melo, M. B.; Kang, M.; Pelet, J. M.; Ruda, V. M.; Foley, M. H.; Hu, J. K.; Kumari, S.; Crampton, J.; Baldeon, A. D.; Sanders, R. W.; Moore, J. P.; Crotty, S.; Langer, R.; Anderson, D. G.; Chakraborty, A. K.; Irvine, D. J., Sustained antigen availability during germinal center initiation enhances antibody responses to vaccination. *Proc. Natl. Acad. Sci. U. S. A.* **2016**, *113* (43), E6639-E6648.
10. Nguyen, B.; Tolia, N. H., Protein-based antigen presentation platforms for nanoparticle vaccines. *npj Vaccines* **2021**, *6* (1), 11.
11. Nanishi, E.; Dowling, D. J.; Levy, O., Toward precision adjuvants: optimizing science and safety. *Current Opinion in Pediatrics* **2020**, *32* (1), 125-138.
12. Liu, Y. V.; Massare, M. J.; Barnard, D. L.; Kort, T.; Nathan, M.; Wang, L.; Smith, G., Chimeric severe acute respiratory syndrome coronavirus (SARS-CoV) S glycoprotein and influenza matrix 1 efficiently form virus-like particles (VLPs) that protect mice against challenge with SARS-CoV. *Vaccine* **2011**, *29* (38), 6606-6613.
13. Jardine, J.; Julien, J. P.; Menis, S.; Ota, T.; Kalyuzhniy, O.; McGuire, A.; Sok, D.; Huang, P. S.; MacPherson, S.; Jones, M.; Nieuwma, T.; Mathison, J.; Baker, D.; Ward, A. B.; Burton, D. R.; Stamatatos, L.; Nemazee, D.; Wilson, I. A.; Schief, W. R., Rational HIV Immunogen Design to Target Specific Germline B Cell Receptors. *Science* **2013**, *340* (6133), 711-716.
14. Brune, K. D.; Leneghan, D. B.; Brian, I. J.; Ishizuka, A. S.; Bachmann, M. F.; Draper, S. J.; Biswas, S.; Howarth, M., Plug-and-Display: decoration of Virus-Like Particles via isopeptide bonds for modular immunization. *Sci Rep* **2016**, *6*.

15. Lee, K. L.; Twyman, R. M.; Fiering, S.; Steinmetz, N. F., Virus-based nanoparticles as platform technologies for modern vaccines. *Wiley Interdisciplinary Reviews-Nanomedicine and Nanobiotechnology* **2016**, *8* (4), 554-578.
16. Fifis, T.; Gamvrellis, A.; Crimeen-Irwin, B.; Pietersz, G. A.; Li, J.; Mottram, P. L.; McKenzie, I. F. C.; Plebanski, M., Size-dependent immunogenicity: Therapeutic and protective properties of nano-vaccines against tumors. *Journal of Immunology* **2004**, *173* (5), 3148-3154.
17. Foged, C.; Brodin, B.; Frokjaer, S.; Sundblad, A., Particle size and surface charge affect particle uptake by human dendritic cells in an in vitro model. *International Journal of Pharmaceutics* **2005**, *298* (2), 315-322.
18. Chaudhuri, A.; Battaglia, G.; Golestanian, R., The effect of interactions on the cellular uptake of nanoparticles. *Physical Biology* **2011**, *8* (4).
19. Reddy, S. T.; Rehor, A.; Schmoekel, H. G.; Hubbell, J. A.; Swartz, M. A., In vivo targeting of dendritic cells in lymph nodes with poly(propylene sulfide) nanoparticles. *Journal of Controlled Release* **2006**, *112* (1), 26-34.
20. Bachmann, M. F.; Jennings, G. T., Vaccine delivery: a matter of size, geometry, kinetics and molecular patterns. *Nature Reviews Immunology* **2010**, *10* (11), 787-796.
21. Jegerlehner, A.; Storni, T.; Lipowsky, G.; Schmid, M.; Pumpens, P.; Bachmann, M. F., Regulation of IgG antibody responses by epitope density and CD21-mediated costimulation. *European Journal of Immunology* **2002**, *32* (11), 3305-3314.
22. Kato, Y.; Abbott, R. K.; Freeman, B. L.; Haupt, S.; Groschel, B.; Silva, M.; Menis, S.; Irvine, D. J.; Schief, W. R.; Crotty, S., Multifaceted Effects of Antigen Valency on B Cell Response Composition and Differentiation In Vivo. *Immunity* **2020**, *53* (3), 548-563.
23. Veneziano, R.; Moyer, T. J.; Stone, M. B.; Wamhoff, E. C.; Read, B. J.; Mukherjee, S.; Shepherd, T. R.; Das, J.; Schief, W. R.; Irvine, D. J.; Bathe, M., Role of nanoscale antigen organization on B-cell activation probed using DNA origami. *Nat. Nanotechnol.* **2020**, *15* (8), 716-723.
24. Almeida, J. P. M.; Lin, A. Y.; Figueroa, E. R.; Foster, A. E.; Drezek, R. A., In vivo Gold Nanoparticle Delivery of Peptide Vaccine Induces Anti-Tumor Immune Response in Prophylactic and Therapeutic Tumor Models. *Small* **2015**, *11* (12), 1453-1459.
25. Lee, B. R.; Ko, H. K.; Ryu, J. H.; Ahn, K. Y.; Lee, Y. H.; Oh, S. J.; Na, J. H.; Kim, T. W.; Byun, Y.; Kwon, I. C.; Kim, K.; Lee, J., Engineered Human Ferritin Nanoparticles for Direct Delivery of Tumor Antigens to Lymph Node and Cancer Immunotherapy. *Sci Rep* **2016**, *6*.
26. Shevtsov, M.; Multhoff, G., Heat Shock Protein-Peptide and HSP-Based Immunotherapies for the Treatment of Cancer. *Frontiers in Immunology* **2016**, *7*.
27. Caldeira, J. C.; Perrine, M.; Pericle, F.; Cavallo, F., Virus-Like Particles as an Immunogenic Platform for Cancer Vaccines. *Viruses-Basel* **2020**, *12* (5).
28. Neek, M.; Tucker, J. A.; Butkovich, N.; Nelson, E. L.; Wang, S. W., An Antigen-Delivery Protein Nanoparticle Combined with Anti-PD-1 Checkpoint Inhibitor Has Curative Efficacy in an Aggressive Melanoma Model. *Adv. Therap.* **2020**, *3* (12), 10.
29. Neek, M.; Kim, T. I.; Wang, S. W., Protein-based nanoparticles in cancer vaccine development. *Nanomed.-Nanotechnol. Biol. Med.* **2019**, *15* (1), 164-174.
30. Tsai, S. E.; Shameli, A.; Yamanouchi, J.; Clemente-Casares, X.; Wang, J. G.; Serra, P.; Yang, Y.; Medarova, Z.; Moore, A.; Santamaria, P., Reversal of Autoimmunity by Boosting Memory-like Autoregulatory T Cells. *Immunity* **2010**, *32* (4), 568-580.
31. Yeste, A.; Nadeau, M.; Burns, E. J.; Weiner, H. L.; Quintana, F. J., Nanoparticle-mediated codelivery of myelin antigen and a tolerogenic small molecule suppresses experimental autoimmune encephalomyelitis. *Proc. Natl. Acad. Sci. U. S. A.* **2012**, *109* (28), 11270-11275.

32. LaMothe, R. A.; Kolte, P. N.; Vo, T.; Ferrari, J. D.; Gelsinger, T. C.; Wong, J.; Chan, V. T.; Ahmed, S.; Srinivasan, A.; Deitemeyer, P.; Maldonado, R. A.; Kishimoto, T. K., Tolerogenic Nanoparticles Induce Antigen-Specific Regulatory T Cells and Provide Therapeutic Efficacy and Transferrable Tolerance against Experimental Autoimmune Encephalomyelitis. *Frontiers in Immunology* **2018**, *9*.
33. Cappellano, G.; Comi, C.; Chiocchetti, A.; Dianzani, U., Exploiting PLGA-Based Biocompatible Nanoparticles for Next-Generation Tolerogenic Vaccines against Autoimmune Disease. *International Journal of Molecular Sciences* **2019**, *20* (1).
34. Ahmad, T.; Eweida, A.; Sheweita, S., B-cell epitope mapping for the design of vaccines and effective diagnostics. *Trials in Vaccinology* **2016**, *5*, 71-83.
35. Irving, M. B.; Craig, L.; Menendez, A.; Gangadhar, B. P.; Montero, M.; van Houten, N. E.; Scott, J. K., Exploring peptide mimics for the production of antibodies against discontinuous protein epitopes. *Molecular Immunology* **2010**, *47* (5), 1137-1148.
36. Li, W. D.; Joshi, M. D.; Singhania, S.; Ramsey, K. H.; Murthy, A. K., Peptide Vaccine: Progress and Challenges. *Vaccines* **2014**, *2* (3), 515-536.
37. Ross, T. M.; Mahmood, K.; Crevar, C. J.; Schneider-Ohrum, K.; Heaton, P. M.; Bright, R. A., A Trivalent Virus-Like Particle Vaccine Elicits Protective Immune Responses against Seasonal Influenza Strains in Mice and Ferrets. *PLOS One* **2009**, *4* (6).
38. Palladini, A.; Thrane, S.; Janitzek, C. M.; Pihl, J.; Clemmensen, S. B.; de Jongh, W. A.; Clausen, T. M.; Nicoletti, G.; Landuzzi, L.; Penichet, M. L.; Balboni, T.; Ianzano, M. L.; Giusti, V.; Theander, T. G.; Nielsen, M. A.; Salanti, A.; Lollini, P. L.; Nanni, P.; Sander, A. F., Virus-like particle display of HER2 induces potent anti-cancer responses. *Oncotmunology* **2018**, *7* (3), 12.
39. Allen, J. D.; Jang, H.; DiNapoli, J.; Kleanthous, H.; Ross, T. M., Elicitation of Protective Antibodies against 20 Years of Future H3N2 Cocirculating Influenza Virus Variants in Ferrets Preimmune to Historical H3N2 Influenza Viruses. *J. Virol.* **2019**, *93* (3).
40. Serradell, M. C.; Rupil, L. L.; Martino, R. A.; Prucca, C. G.; Carranza, P. G.; Saura, A.; Fernandez, E. A.; Gargantini, P. R.; Tenaglia, A. H.; Petiti, J. P.; Tonelli, R. R.; Reinoso-Vizcaino, N.; Echenique, J.; Berod, L.; Piaggio, E.; Bellier, B.; Sparwasser, T.; Klatzmann, D.; Lujan, H. D., Efficient oral vaccination by bioengineering virus-like particles with protozoan surface proteins. *Nat. Commun.* **2019**, *10*.
41. Butkovich, N.; Li, E. Y.; Ramirez, A.; Burkhardt, A. M.; Wang, S. W., Advancements in protein nanoparticle vaccine platforms to combat infectious disease. *Wiley Interdisciplinary Reviews-Nanomedicine and Nanobiotechnology* **2021**, *13* (3).
42. Challener, C. A., Fusion Proteins Pose Manufacturability Challenges. *Biopharm International* **2017**, *30* (5), 30-+.
43. Yang, H. Q.; Liu, L.; Xu, F., The promises and challenges of fusion constructs in protein biochemistry and enzymology. *Applied Microbiology and Biotechnology* **2016**, *100* (19), 8273-8281.
44. Scaria, P. V.; Chen, B.; Rowe, C. G.; Jones, D. S.; Barnafo, E.; Fischer, E. R.; Anderson, C.; MacDonald, N. J.; Lambert, L.; Rausch, K. M.; Narum, D. L.; Duffy, P. E., Protein-protein conjugate nanoparticles for malaria antigen delivery and enhanced immunogenicity. *PLOS One* **2017**, *12* (12).
45. Ma, W. W.; Saccardo, A.; Roccatano, D.; Aboagye-Mensah, D.; Alkaseem, M.; Jewkes, M.; Di Nezza, F.; Baron, M.; Soloviev, M.; Ferrari, E., Modular assembly of proteins on nanoparticles. *Nat. Commun.* **2018**, *9*.
46. Lu, L. T.; Duong, V. T.; Shalash, A. O.; Skwarczynski, M.; Toth, I., Chemical Conjugation Strategies for the Development of Protein-Based Subunit Nanovaccines. *Vaccines* **2021**, *9* (6).
47. Wadhwa, S.; Jain, A.; Woodward, J. G.; Mumper, R. J., Lipid nanocapsule as vaccine carriers for his-tagged proteins: Evaluation of antigen-specific immune responses to HIV

- I His-Gag p41 and systemic inflammatory responses. *European Journal of Pharmaceutics and Biopharmaceutics* **2012**, *80* (2), 315-322.
48. Chiba, S.; Frey, S. J.; Halfmann, P. J.; Kuroda, M.; Maemura, T.; Yang, J. E.; Wright, E. R.; Kawaoka, Y.; Kane, R. S., Multivalent nanoparticle-based vaccines protect hamsters against SARS-CoV-2 after a single immunization. *Commun. Biol.* **2021**, *4* (1), 9.
  49. Porath, J.; Carlsson, J.; Olsson, I.; Belfrage, G., Metal Chelate Affinity Chromatography, A New Approach To Protein Fractionation. *Nature* **1975**, *258* (5536), 598-599.
  50. Hochuli, E.; Dobeli, H.; Schacher, A., New Metal Chelate Adsorbent Selective For Proteins And Peptides Containing Neighboring Histidine-Residues. *Journal of Chromatography* **1987**, *411*, 177-184.
  51. Crowe, J.; Döbeli, H.; Gentz, R.; Hochuli, E.; Stüber, D.; Henco, K., 6xHis-Ni-NTA chromatography as a superior technique in recombinant protein expression/purification. *Methods Mol Bio.* **1994**, *31*, 371-387.
  52. Soh, N., Selective chemical labeling of proteins with small fluorescent molecules based on metal-chelation methodology. *Sensors* **2008**, *8* (2), 1004-1024.
  53. Lata, S.; Reichel, A.; Brock, R.; Tampe, R.; Piehler, J., High-affinity adaptors for switchable recognition of histidine-tagged proteins. *J. Am. Chem. Soc.* **2005**, *127* (29), 10205-10215.
  54. Gatterdam, K.; Joest, E. F.; Gatterdam, V.; Tampe, R., The Scaffold Design of Trivalent Chelator Heads Dictates Affinity and Stability for Labeling His-tagged Proteins in vitro and in Cells. *Angew. Chem.-Int. Edit.* **2018**, *57* (38), 12395-12399.
  55. Irvine, D. J.; Read, B. J., Shaping humoral immunity to vaccines through antigen-displaying nanoparticles. *Current Opinion in Immunology* **2020**, *65*, 1-6.
  56. Izzard, T.; Ævarsson, A.; Allen, M. D.; Westphal, A. H.; Perham, R. N.; de Kok, A.; Hol, W. G. J., Principles of quasi-equivalence and Euclidean geometry govern the assembly of cubic and dodecahedral cores of pyruvate dehydrogenase complexes. *Proc. Natl. Acad. Sci. U. S. A.* **1999**, *96* (4), 1240-1245.
  57. Dalmau, M.; Lim, S.; Chen, H. C.; Ruiz, C.; Wang, S.-W., Thermostability and molecular encapsulation within an engineered caged protein scaffold. *Biotechnology and Bioengineering* **2008**, *101* (4), 654-664.
  58. Ren, D. M.; Kratz, F.; Wang, S. W., Engineered drug-protein nanoparticle complexes for folate receptor targeting. *Biochem. Eng. J.* **2014**, *89*, 33-41.
  59. Ren, D. M.; Kratz, F.; Wang, S. W., Protein Nanocapsules Containing Doxorubicin as a pH-Responsive Delivery System. *Small* **2011**, *7* (8), 1051-1060.
  60. Molino, N. M.; Neek, M.; Tucker, J. A.; Nelson, E. L.; Wang, S.-W., Display of DNA on Nanoparticles for Targeting Antigen Presenting Cells. *ACS Biomater. Sci. Eng.* **2017**, *3* (4), 496-501.
  61. Molino, N. M.; Anderson, A. K. L.; Nelson, E. L.; Wang, S. W., Biomimetic Protein Nanoparticles Facilitate Enhanced Dendritic Cell Activation and Cross-Presentation. *ACS Nano* **2013**, *7* (11), 9743-9752.
  62. Molino, N. M.; Neek, M.; Tucker, J. A.; Nelson, E. L.; Wang, S. W., Viral-mimicking protein nanoparticle vaccine for eliciting anti-tumor responses. *Biomaterials* **2016**, *86*, 83-91.
  63. Neek, M.; Tucker, J. A.; Kim, T. I.; Molino, N. M.; Nelson, E. L.; Wang, S.-W., Co-delivery of human cancer-testis antigens with adjuvant in protein nanoparticles induces higher cell-mediated immune responses. *Biomaterials* **2018**, *156*, 194-203.
  64. Zhang, Y. N.; Lazarovits, J.; Poon, W.; Ouyang, B.; Nguyen, L. N. M.; Kingston, B. R.; Chan, W. C. W., Nanoparticle Size Influences Antigen Retention and Presentation in Lymph Node Follicles for Humoral Immunity. *Nano Letters* **2019**, *19* (10), 7226-7235.

65. Molino, N. M.; Bilotkach, K.; Fraser, D. A.; Ren, D.; Wang, S.-W., Complement Activation and Cell Uptake Responses Toward Polymer-Functionalized Protein Nanocapsules. *Biomacromolecules* **2012**, *13* (4), 974-981.
66. Gasteiger, E.; Hoogland, C.; Gattiker, A.; Duvaud, S. e.; Wilkins, M. R.; Appel, R. D.; Bairoch, A., Protein Identification and Analysis Tools on the ExPASy Server. In *The Proteomics Protocols Handbook. Springer Protocols Handbooks.*, Humana Press: 2005.
67. Goddard, T. D.; Huang, C. C.; Meng, E. C.; Pettersen, E. F.; Couch, G. S.; Morris, J. H.; Ferrin, T. E., UCSF ChimeraX: Meeting modern challenges in visualization and analysis. *Protein Science* **2018**, *27* (1), 14-25.
68. Pettersen, E. F.; Goddard, T. D.; Huang, C. R. C.; Meng, E. E. C.; Couch, G. S.; Croll, T. I.; Morris, J. H.; Ferrin, T. E., UCSF ChimeraX: Structure visualization for researchers, educators, and developers. *Protein Science* **2021**, *30* (1), 70-82.
69. Nakajima, R.; Supnet, M.; Jasinskas, A.; Jain, A.; Taghavian, O.; Obiero, J.; Milton, D. K.; Chen, W. H.; Grantham, M.; Webby, R.; Krammer, F.; Carter, D.; Felgner, P. L.; Davies, D. H., Protein Microarray Analysis of the Specificity and Cross-Reactivity of Influenza Virus Hemagglutinin-Specific Antibodies. *Mosphere* **2018**, *3* (6).
70. World-Health-Organization Global Influenza Programme - Burden of disease. (accessed 2022).
71. Houser, K.; Subbarao, K., Influenza Vaccines: Challenges and Solutions. *Cell Host & Microbe* **2015**, *17* (3), 295-300.
72. Wei, C. J.; Crank, M. C.; Shiver, J.; Graham, B. S.; Mascola, J. R.; Nabel, G. J., Next-generation influenza vaccines: opportunities and challenges. *Nature Reviews Drug Discovery* **2020**, *19* (4), 239-252.
73. Watson, D. S.; Platt, V. M.; Cao, L. M.; Venditto, V. J.; Szoka, F. C., Antibody Response to Polyhistidine-Tagged Peptide and Protein Antigens Attached to Liposomes via Lipid-Linked Nitrilotriacetic Acid in Mice. *Clinical and Vaccine Immunology* **2011**, *18* (2), 289-297.
74. Platt, V.; Huang, Z. H.; Cao, L. M.; Tiffany, M.; Riviere, K.; Szoka, F. C., Influence of Multivalent Nitrilotriacetic Acid Lipid-Ligand Affinity on the Circulation Half-Life in Mice of a Liposome-Attached His(6)-Protein. *Bioconjugate Chem.* **2010**, *21* (5), 892-902.
75. Li, Y. M.; Li, A. C.; Xu, Q. B., Intracellular Delivery of His-Tagged Genome-Editing Proteins Enabled by Nitrilotriacetic Acid-Containing Lipidoid Nanoparticles. *Adv. Healthc. Mater.* **2019**, *8* (6).
76. van Broekhoven, C. L.; Altin, J. G., The novel chelator lipid 3(nitrilotriacetic acid)-ditetradecylamine (NTA(3)-DTDA) promotes stable binding of His-tagged proteins to liposomal membranes: Potent anti-tumor responses induced by simultaneously targeting antigen, cytokine and costimulatory signals to T cells. *Biochimica Et Biophysica Acta-Biomembranes* **2005**, *1716* (2), 104-116.
77. Milder, F. J.; Jongeneelen, M.; Ritschel, T.; Bouchier, P.; Bisschop, I. J. M.; de Man, M.; Veldman, D.; Le, L.; Kaufmann, B.; Bakkers, M. J. G.; Juraszek, J.; Brandenburg, B.; Langedijk, J. P. M., Universal stabilization of the influenza hemagglutinin by structure-based redesign of the pH switch regions. *Proc. Natl. Acad. Sci. U. S. A.* **2022**, *119* (6).
78. McMillan, C. L. D.; Cheung, S. T. M.; Modhiran, N.; Barnes, J.; Amarilla, A. A.; Bielefeldt-Ohmann, H.; Lee, L. Y. Y.; Guilfoyle, K.; van Amerongen, G.; Stittelaar, K.; Jakon, V.; Lebas, C.; Reading, P.; Short, K. R.; Young, P. R.; Watterson, D.; Chappell, K. J., Development of molecular clamp stabilized hemagglutinin vaccines for Influenza A viruses. *npj Vaccines* **2021**, *6* (1).
79. Maciola, A. K.; Pietrzak, M. A.; Kosson, P.; Czarnocki-Cieciura, M.; Smietanka, K.; Minta, Z.; Kopera, E., The Length of N-Glycans of Recombinant H5N1 Hemagglutinin Influences the Oligomerization and Immunogenicity of Vaccine Antigen. *Frontiers in Immunology* **2017**, *8*.

80. Pietrzak, M.; Maciola, A.; Zdanowski, K.; Protas-Klukowska, A. M.; Olszewska, M.; Smietanka, K.; Minta, Z.; Szewczyk, B.; Kopera, E., An avian influenza H5N1 virus vaccine candidate based on the extracellular domain produced in yeast system as subviral particles protects chickens from lethal challenge. *Antiviral Research* **2016**, *133*, 242-249.
81. Aartse, A.; Eggink, D.; Claireaux, M.; van Leeuwen, S.; Mooij, P.; Bogers, W. M.; Sanders, R. W.; Koopman, G.; van Gils, M. J., Influenza A Virus Hemagglutinin Trimer, Head and Stem Proteins Identify and Quantify Different Hemagglutinin-Specific B Cell Subsets in Humans. *Vaccines* **2021**, *9* (7).
82. Copeland, C. S.; Doms, R. W.; Bolzau, E. M.; Webster, R. G.; Helenius, A., Assembly Of Influenza Hemagglutinin Trimers And Its Role In Intracellular-Transport. *Journal of Cell Biology* **1986**, *103* (4), 1179-1191.
83. Hernandez-Davies, J. E.; Dollinger, E. P.; Pone, E. J.; Felgner, J.; Liang, L.; Strohmeier, S.; Jan, S.; Albin, T. J.; Jain, A.; Nakajima, R.; Jasinskas, A.; Krammer, F.; Esser-Kahn, A.; Felgner, P. L.; Nie, Q.; Davies, D. H., Magnitude and breadth of antibody cross-reactivity induced by recombinant influenza hemagglutinin trimer vaccine is enhanced by combination adjuvants. *Sci Rep* **2022**, *12* (1), 9198.
84. Reddy, S. T.; van der Vlies, A. J.; Simeoni, E.; Angeli, V.; Randolph, G. J.; O'Neill, C. P.; Lee, L. K.; Swartz, M. A.; Hubbell, J. A., Exploiting lymphatic transport and complement activation in nanoparticle vaccines. *Nature Biotechnology* **2007**, *25* (10), 1159-1164.
85. Manolova, V.; Flace, A.; Bauer, M.; Schwarz, K.; Saudan, P.; Bachmann, M. F., Nanoparticles target distinct dendritic cell populations according to their size. *European Journal of Immunology* **2008**, *38* (5), 1404-1413.
86. Vos, Q.; Lees, A.; Wu, Z. Q.; Snapper, C. M.; Mond, J. J., B-cell activation by T-cell-independent type 2 antigens as an integral part of the humoral immune response to pathogenic microorganisms. *Immunological Reviews* **2000**, *176*, 154-170.
87. Turner, J. S.; Ke, F.; Grigorova, I. L., B Cell Receptor Crosslinking Augments Germinal Center B Cell Selection when T Cell Help Is Limiting. *Cell Reports* **2018**, *25* (6), 1395-+.
88. Viola, A.; Lanzavecchia, A., T cell activation determined by T cell receptor number and tunable thresholds. *Science* **1996**, *273* (5271), 104-106.
89. Kimachi, K.; Croft, M.; Grey, H. M., The minimal number of antigen-major histocompatibility complex class II complexes required for activation of naive and primed T cells. *European Journal of Immunology* **1997**, *27* (12), 3310-3317.
90. Mountford, A. P.; Fisher, A.; Wilson, R. A., The Profile Of IgG1 And IgG2a Antibody-Responses In Mice Exposed To Schistosoma-Mansoni. *Parasite Immunology* **1994**, *16* (10), 521-527.
91. Visciano, M. L.; Tagliamonte, M.; Tornesello, M. L.; Buonaguro, F. M.; Buonaguro, L., Effects of adjuvants on IgG subclasses elicited by virus-like Particles. *J. Transl. Med.* **2012**, *10*, 8.
92. Rostamian, M.; Sohrabi, S.; Kavosifard, H.; Niknam, H. M., Lower levels of IgG1 in comparison with IgG2a are associated with protective immunity against Leishmania tropica infection in BALB/c mice. *Journal of Microbiology Immunology and Infection* **2017**, *50* (2), 160-166.
93. Shi, S. T.; Zhu, H. R.; Xia, X. Y.; Liang, Z. H.; Ma, X. H.; Sun, B. B., Vaccine adjuvants: Understanding the structure and mechanism of adjuvant activity. *Vaccine* **2019**, *37* (24), 3167-3178.
94. Schotsaert, M.; Saelens, X.; Leroux-Roels, G., Influenza vaccines: T-cell responses deserve more attention. *Expert Review of Vaccines* **2012**, *11* (8), 949-962.

95. Sridhar, S.; Begom, S.; Bermingham, A.; Hoschler, K.; Adamson, W.; Carman, W.; Bean, T.; Barclay, W.; Deeks, J. J.; Lalvani, A., Cellular immune correlates of protection against symptomatic pandemic influenza. *Nature Medicine* **2013**, *19* (10), 1305-+.
96. Braciale, T., Immunologic recognition of influenza virus-infected cells. I. Generation of a virus-strain specific and a cross-reactive subpopulation of cytotoxic T cells in the response to type A influenza viruses of different subtypes. *Cellular Immunology* **1977**, *33* (2), 423-436.
97. Lu, L. Y.; Askonas, B. A., Cross-Reactivity For Different Type-A Influenza-Viruses Of A Cloned T-Killer Cell-Line. *Nature* **1980**, *288* (5787), 164-165.
98. Yap, K. L.; Ada, G. L.; McKenzie, I. F. C., Transfer Of Specific Cytotoxic T-Lymphocytes Protects Mice Inoculated With Influenza-Virus. *Nature* **1978**, *273* (5659), 238-239.
99. Bender, B. S.; Croghan, T.; Zhang, L. P.; Small, P. A., Transgenic Mice Lacking Class-I Major Histocompatibility Complex-Restricted T-Cells Have Delayed Viral Clearance And Increased Mortality After Influenza-Virus Challenge. *Journal of Experimental Medicine* **1992**, *175* (4), 1143-1145.
100. Miyauchi, K.; Sugimoto-Ishige, A.; Harada, Y.; Adachi, Y.; Usami, Y.; Kaji, T.; Inoue, K.; Hasegawa, H.; Watanabe, T.; Hijikata, A.; Fukuyama, S.; Maemura, T.; Okada-Hatakeyama, M.; Ohara, O.; Kawaoka, Y.; Takahashi, Y.; Takemori, T.; Kubo, M., Protective neutralizing influenza antibody response in the absence of T follicular helper cells. *Nature Immunology* **2016**, *17* (12), 1447-1458.
101. Gu, X.; Li, P.; Liu, H.; Li, N.; Li, S.; Sakuma, T., The effect of influenza virus A on th1/th2 balance and alveolar fluid clearance in pregnant rats. *Experimental Lung Research* **2011**, *37* (7), 445-451.
102. Drake, J. W., Rates Of Spontaneous Mutation Among RNA Viruses. *Proc. Natl. Acad. Sci. U. S. A.* **1993**, *90* (9), 4171-4175.
103. Skehel, J. J.; Waterfield, M. D., Studies On Primary Structure Of Influenza-Virus Hemagglutinin. *Proc. Natl. Acad. Sci. U. S. A.* **1975**, *72* (1), 93-97.
104. Nobusawa, E.; Aoyama, T.; Kato, H.; Suzuki, Y.; Tateno, Y.; Nakajima, K., Comparison Of Complete Amino-Acid-Sequences And Receptor-Binding Properties Among 13 Serotypes Of Hemagglutinins Of Influenza A-Viruses. *Virology* **1991**, *182* (2), 475-485.
105. Kirkpatrick, E.; Qiu, X. T.; Wilson, P. C.; Bahl, J.; Krammer, F., The influenza virus hemagglutinin head evolves faster than the stalk domain. *Sci Rep* **2018**, *8*.
106. Lee, J. M.; Huddleston, J.; Doud, M. B.; Hooper, K. A.; Wu, N. C.; Bedford, T.; Bloom, J. D., Deep mutational scanning of hemagglutinin helps predict evolutionary fates of human H3N2 influenza variants. *Proc. Natl. Acad. Sci. U. S. A.* **2018**, *115* (35), EB276-EB285.
107. Hernandez-Davies, J. E.; Felgner, J.; Strohmeier, S.; Pone, E. J.; Jain, A.; Jan, S.; Nakajima, R.; Jasinskas, A.; Strahsburger, E.; Krammer, F.; Felgner, P. L.; Davies, D. H., Administration of Multivalent Influenza Virus Recombinant Hemagglutinin Vaccine in Combination-Adjuvant Elicits Broad Reactivity Beyond the Vaccine Components. *Frontiers in Immunology* **2021**, *12*, 18.
108. Zost, S. J.; Wu, N. C.; Hensley, S. E.; Wilson, I. A., Immunodominance and Antigenic Variation of Influenza Virus Hemagglutinin: Implications for Design of Universal Vaccine Immunogens. *Journal of Infectious Diseases* **2019**, *219*, S38-S45.
109. Fukuyama, H.; Shinnakasu, R.; Kurosaki, T., Influenza vaccination strategies targeting the hemagglutinin stem region. *Immunological Reviews* **2020**, *296* (1), 132-141.
110. Wu, N. C.; Wilson, I. A., Structural Biology of Influenza Hemagglutinin: An Amaranthine Adventure. *Viruses-Basel* **2020**, *12* (9).
111. Wan, X. F., Lessons from Emergence of A/Goose/Guangdong/1996-Like H5N1 Highly Pathogenic Avian Influenza Viruses and Recent Influenza Surveillance Efforts in Southern China. *Zoonoses and Public Health* **2012**, *59*, 32-42.

## CHAPTER 3

# ENGINEERING PROTEIN NANOPARTICLES FUNCTIONALIZED WITH AN IMMUNODOMINANT *COXIELLA BURNETII* ANTIGEN TO GENERATE A Q FEVER VACCINE

This chapter has been modified and published as: Ramirez, A., *et al.*, Engineering Protein Nanoparticles Functionalized with an Immunodominant *Coxiella burnetii* Antigen to Generate a Q Fever Vaccine. *Bioconjugate Chemistry*, 2023. **34**(9): p. 1653-1666.



### 3.1. Abstract

*Coxiella burnetii* is the causative agent of Q fever, for which there is yet to be an FDA-approved vaccine. This bacterial pathogen has both extra- and intracellular stages in its life cycle, and therefore both a cell-mediated (i.e., T lymphocyte) and humoral (i.e., antibody) immune response are necessary for effective eradication of this pathogen. However, most proposed vaccines elicit strong responses to only one mechanism of adaptive immunity, and some can cause either reactogenicity or lack sufficient immunogenicity. In this work, we aim to apply a nanoparticle-based platform towards producing both antibody and T cell immune responses against *C. burnetii*. We investigated three approaches for conjugation of the immunodominant outer membrane protein antigen (CBU1910) to the E2 nanoparticle to obtain a consistent antigen orientation: direct genetic fusion, high affinity tris-NTA-Ni conjugation to polyhistidine-tagged CBU1910, and the SpyTag/SpyCatcher (ST/SC) system. Overall, we found that the ST/SC approach yielded nanoparticles loaded with the highest number of antigens while maintaining stability, enabling formulations that could simultaneously co-deliver the protein antigen (CBU1910) and adjuvant (CpG1826) on one nanoparticle (CBU1910-CpG-E2). Using protein microarray analyses, we found that after immunization, antigen-bound nanoparticle formulations elicited significantly higher antigen-specific IgG responses than soluble CBU1910 alone and produced more balanced IgG1/IgG2c ratios. Although T cell recall assays from these protein antigen formulations did not show significant increases in antigen-specific IFN- $\gamma$  production compared to soluble CBU1910 alone, nanoparticles conjugated with a CD4 peptide epitope from CBU1910 generated elevated T cell responses in mice to both the CBU1910 peptide epitope and whole CBU1910 protein. These investigations highlight the feasibility of conjugating antigens to nanoparticles for tuning and improving both humoral and cell-mediated adaptive immunity against *C. burnetii*.

### 3.2. Introduction

*Coxiella burnetii* is the Gram-negative intracellular bacterium that causes the life-threatening disease Q fever<sup>1-3</sup>, and has been classified by the US Center for Disease Control and Prevention as a potential bioterrorism agent due to its airborne transmission, highly infectious nature, and extreme resistance to environmental conditions.<sup>1,3-5</sup> Q fever has an almost global distribution and can be found in a wide variety of animal reservoirs, with ruminants the most common.<sup>6</sup> Human infections are often acquired from inhalation of contaminated aerosols resulting in an acute febrile illness, which can progress to pneumonia and hepatitis.<sup>7</sup> In approximately 5% of cases, patients develop a potentially fatal chronic disease resulting in endocarditis, osteomyelitis, and chronic fatigue.<sup>8</sup> In chronic forms of Q fever, that may arise weeks or years post-infection, long-term combination therapies are required to prevent death. Between 2007-2010, the largest known outbreak of Q fever occurred in the Netherlands resulting in >4000 cases.<sup>9</sup> Of those identified as having chronic Q fever, mortality was 15.8%.<sup>10</sup>

Despite its pathogenic potential, an FDA-approved vaccine for this infectious agent is not yet available. A formalin-inactivated whole cell vaccine was previously licensed in Australia but was not approved in the US, and was discontinued due to the costs of production and required associated screening to prevent severe side effects in patients with previous exposure.<sup>4,11,12</sup> Unlike typical bacterial pathogens, *C. burnetii* exhibits a tropism for professional immune system phagocytes (i.e., macrophages) and actively directs its own phagocytosis in order to reside within the terminal phagolysosomes of host cells in a favorable low pH environment, enabling its long-term survival and persistence.<sup>1,13,14</sup> For this reason, a T lymphocyte response, in addition to an adequate antibody response, is considered necessary for eradication of the pathogen.<sup>15-17</sup> In this investigation, we examine the ability of designing and synthesizing a *C. burnetii* vaccine using a protein nanoparticle (NP) platform to elicit both strong B and T cell responses. Although the advantages of NPs in vaccine development have been well-demonstrated<sup>18,19</sup>, the design of antigen-conjugated nanoparticles for a Q fever vaccine has not yet been reported.

The protein NP utilized in this research is derived from the E2 subunit (E2) of the multienzyme complex, pyruvate dehydrogenase, sourced from *Geobacillus stearothermophilus*.<sup>20,21</sup> E2 is a 60-subunit, self-assembling ~25-nm dodecahedral scaffold with high stability that can be genetically engineered for precise chemical conjugation sites at the external surface and internal cavity.<sup>20,22-26</sup> Our prior studies in developing cancer vaccines via a virus-mimetic strategy have demonstrated the utility of this scaffold for both adjuvant and antigen delivery.<sup>27-31</sup> However, application of this E2-based strategy for protection against bacterial pathogens has not yet been investigated. In this work, we utilize E2's unique size, functional adaptability, and innate capability to elicit an antigen-specific immune response towards developing a prophylactic *C. burnetii* vaccine.

Proteomics and antigen-specific serological assays have identified the outer membrane protein CBU1910 as an immunodominant protein antigen of *C. burnetii*.<sup>32-39</sup> For this reason, CBU1910 was chosen as the antigen for this prophylactic vaccine formulation. Unlike cancers, which can utilize peptide neoantigens in a vaccine to produce the desired anti-epitope T cell responses, infectious disease vaccines typically require the use of whole protein antigens to elicit both antibody and T cell responses.<sup>40,41</sup> Protein antigens contain numerous immunogenic epitopes in native structural conformations, allowing for stronger antibody responses and broader adaptive immune responses.<sup>40-42</sup> Although immunogenic peptide epitopes of *C. burnetii* have been identified and characterized for their potential use in vaccine development, application of these peptides in vaccines has not yet shown significant efficacy.<sup>16,43-46</sup> More recently, vaccine formulations using *C. burnetii* protein antigens and tri-agonist adjuvants showed significant levels of protection for challenged animals, but to a lesser extent than the whole cell vaccine (which is not FDA approved).<sup>47</sup> Thus, there is still a need for the development of a safer efficacious prophylactic vaccine for *C. burnetii*.

In this study, we investigated the integration of *C. burnetii* antigens onto the surface of the E2 NP. It is known that B cell activation and antibody responses are enhanced by a repetitive

structural array on virus-like particles<sup>18,48,49</sup>; however, there are currently limited options for conjugating protein antigens onto a NP surface while maintaining this consistent geometric orientation. Here, we examined three bioconjugation strategies that would enable a desired consistent antigen configuration: (1) direct recombinant fusion, (2) high affinity tris-NTA-Ni conjugation to polyhistidine-tagged (His-tag) antigen, and (3) the SpyTag(ST)/SpyCatcher(SC) system (Figure 3.1). Direct genetic fusion of protein antigens onto virus-like particles has shown some success with particular platforms and therefore was explored with the E2 protein nanoparticle; however, expression and correct folding into a soluble protein assembly needs to be empirically tested.<sup>18,50-52</sup> The introduction of polyhistidine tags on recombinant proteins to bind to Ni-NTA-based matrices is a well-established protein purification methodology<sup>53-55</sup>, and we previously applied this complexation-based approach in nanoparticle-mediated delivery of influenza hemagglutinin antigen<sup>56</sup>; here, we used it as the basis for loading polyhistidine-tagged (His-tag) CBU1910 antigen onto E2 NPs. To attach protein antigens, covalently and modularly, onto the surface of E2 NPs, the versatile protein-protein conjugation method, SpyTag/SpyCatcher, was implemented.<sup>57-62</sup> The adaptive immune response (i.e., antibody and T cell responses) to the most favorable NP construct was then examined to determine the prophylactic potential of the vaccine formulation.

### **3.3. Methods**

#### **3.3.1. Materials**

All buffer and cloning reagents were purchased from Fisher Scientific, unless otherwise noted. All cloning enzymes were purchased from New England Biolabs (NEB), unless otherwise noted. DH5 $\alpha$  and BL21(DE3) *E. coli* were used for general cloning and expression studies, respectively. DNA minipreps and gel extractions were performed with QIAprep Spin Miniprep Kit (Qiagen) and GeneJET Gel Extraction Kit (Thermo Fisher Scientific), respectively. DNA primers were synthesized and ordered from Integrated DNA Technologies (IDT). CloneJET PCR cloning

kit (Thermo Fisher Scientific) was used for all polymerase chain reactions (PCRs). Plasmid pET11a was used as the expression vector for all protein constructs.

### 3.3.2. Construction of CBU1910-E2 fusion protein mutants

Previously established E2 mutants E2\_152 and E2\_158 were used to engineer CBU1910-E2 fusion constructs.<sup>63,64</sup> D381C is an E2 mutation that introduces 60 cysteines to the internal cavity of the nanoparticle allowing for internal conjugation.<sup>23,27</sup> To introduce the D381C mutation to E2\_158 and E2\_152 via site directed mutagenesis (SDM)<sup>65,66</sup> the forward primer: 5'-/5Phos/GCCGATCGTTCGTTGCGGTGAAATCGTTGC-3' and reverse primer: 5'-/5Phos/TTTTTCGGCTATACGACCAATACCCAG-3' were used. To introduce the DNA cut sites required for ligation to the N-terminus of E2 mutants, an Nde1 and Nhe1 cut site were introduced to the N-terminus DNA coding region and C-terminus DNA coding region, respectively, of CBU1910 using the forward primer: 5'-CATATGCACCATCACCATCACCATCCGCAGCAAGTCAAAGACATTTCAG-3' and reverse primer: 5'-GCTAGCTTAGCCGCCGTTTCCGG-3'. The plasmid encoding the CBU1910 protein (with its signal peptide deleted and portion of N-terminus truncated) was previously synthesized by GenScript Biotech<sup>47,67</sup> and was used as the DNA template for all genetic engineering of the protein antigen.

A standard Phusion High-Fidelity DNA polymerase protocol was used for PCRs. These reactions were performed in a thermal cycler using a 30 s denaturation step at 98 °C, followed by 30 cycles of 15 s at 98 °C, 15 s at 58 °C (E2 D381C mutation) or 53 °C (CBU1910), and 7 min (E2 D381C mutation) or 45 s (CBU1910) at 72 °C, with a final step of 10 min at 72 °C. The CBU1910 gene was then ligated via the Nde1/Nhe1 sites of a pET11a vector that contained the E2 gene between Nhe1/BamH1. Sequencing was performed by GeneWiz/Azenta, and DNA and protein sequences are given in Appendix A.2.5.

### 3.3.3. Expression of CBU1910-E2 fusion protein mutants

The CBU1910-E2 fusion protein was expressed in a similar fashion to previous mutants described.<sup>27,29,30</sup> Expression studies were performed for each mutant and controls. Proteins were expressed in BL21(DE3) *E. coli* via 1 mM IPTG induction. After induction for 3 h at 37 °C, cells were pelleted and stored at -80 °C. Cells were thawed and lysed by vortexing with glass beads. Soluble and insoluble lysates were centrifuged at 18000 x g for 15 min and analyzed using SDS-PAGE for molecular weight and soluble:insoluble ratios.

### 3.3.4. Conjugation of mal-tNTA to E2 (E279C)

E2 (E279C) is an E2 mutant that displays 60 cysteines on its surface that can be used for thiol-based functionalization.<sup>28</sup> We have reported the generation of tNTA-E2 nanoparticles previously.<sup>56</sup> Purified E2 (E279C) in 20 mM HEPES + 100 mM NaCl (pH 7.3) was incubated with an 8.5x molar excess of TCEP (Thermo Fisher Scientific; dissolved in MilliQ water). A 10x molar excess of maleimido cyclic tris-NTA (mal-tNTA) (diluted to 4 mg/mL in DMF) was added to the E2 and incubated at room temperature for 2 hours and then at 4°C overnight. Unreacted mal-tNTA, DMF, and TCEP were removed using Zeba spin desalting columns in 20 mM HEPES + 100 mM NaCl. Conjugation efficiency and characterization were determined using SDS-PAGE and mass spectrometry (Xevo G2-XS QToF) (See Appendix B.2). The hydrodynamic diameter of purified constructs was analyzed by dynamic light scattering (DLS) (Malvern Zetasizer Nano ZS).

### 3.3.5. Attachment of His<sub>6</sub>-Tagged CBU1910 to E2-tNTA

Attachment of CBU1910-(His)<sub>6</sub> to tNTA-E2 nanoparticles followed similar procedures established using other protein-(His)<sub>n</sub> antigens.<sup>56</sup> Briefly, a 10x molar excess of NiCl<sub>2</sub> was incubated with tNTA-E2 for 2 hours at room temperature and subsequently purified from unchelated Ni using Zeba spin desalting columns into 20mM HEPES + 360mM NaCl buffer pH 7.3. To test optimal conjugation, varying molar ratios of (His)<sub>6</sub>-tagged CBU1910 (previously

synthesized<sup>47</sup>) were added to the Ni-tNTA-E2 and incubated at room temperature for 2 hours. The Ni-tNTA-E2 + CBU1910-(His)<sub>6</sub> reaction required optimization to yield unaggregated/precipitated constructs, the details of which are described in Appendix B.9. After conjugation, solutions were purified with size exclusion chromatography (SEC) using a Superose™ 6 Increase 10/300 GL column (Cytiva) on a FPLC (AKTA, Cytiva). Fractions from the SEC were run on a SDS-PAGE gel and stained with a Pierce™ Silver Stain Kit (Thermo Fisher Scientific) to determine the presence of CBU1910-E2, E2, and CBU1910, and conjugation efficiencies were estimated by evaluating band intensities with standards. Fractions containing CBU1910-E2 were combined and concentrated with a centrifuge concentrator (Vivaspin 6, 10,000 MWCO). Protein concentration was measured via a bicinchoninic acid assay kit (Pierce). Nanoparticle size was assessed via dynamic light scattering (DLS).

### 3.3.6. Construction of SpyTag-E2 mutants and SpyCatcher-CBU1910 fusion protein

Previously established mutants E2(D381C) and E2<sub>152</sub> were used to engineer SpyTag-E2 platforms. To introduce the D381C mutation to E2<sub>152</sub> via site directed mutagenesis (SDM) the forward primer: 5'-/5Phos/GCCGATCGTTGCGGTGAAATCGTTGC-3' and reverse primer: 5'-/5Phos/TTTTCGGCTATACGACCAATACCCAG-3' were used. Introduction of the SpyTag to E2(D381C) and E2<sub>152</sub> was done using the forward primers: 5'-CATATGGCCCACATCGTTATGGTGGATGCCTACAAGCCAACTAAAGGTTTCAGGAACAGCAGGTGGTGGGTCAGGTTCCCTGTCTGTTCCCTGGTCCCGC -3' and 5'-CATATGGCCCACATCGTTATGGTGGATGCCTACAAGCCAACTAAAGCTAGCACCGGCAAAAA TGGTCG -3', respectively. E2 mutants used the same reverse primer: 5'-GGATCCTTAAGCTTCCATCAGCAGCAGTTCCGG-3'.

The plasmid encoding the truncated CBU1910 protein was previously synthesized by GenScript Biotech.<sup>47,67</sup> The plasmid containing the SpyCatcher gene (pDEST14-SpyCatcher) was obtained from Addgene. To introduce the endonuclease sites and GS-rich spacer on CBU1910

for fusion to SpyCatcher, the forward primer was 5'-GCTAGCGGTTTCAGGAACAGCAGGTGGTGGGTCAGGTTCCCCGCAGCAAGTCAAAGACATT C-3' and reverse primer was 5'-GGATCCTTATTTTTCGACACGGTCAATTTCTTTTTGCAGG-3'. To introduce the endonuclease sites on SpyCatcher, the forward primer 5'-CATATGTCGTACTACCATCACCATCACCATCACG-3' and reverse primer 5'-GCTAGCAATATGAGCGTCACCTTTAGTTGCTTTGCC -3' were used. A standard Phusion High-Fidelity DNA polymerase protocol was used for PCRs. These reactions were performed in a thermal cycler using a 30 s denaturation step at 98 °C, followed by 30 cycles of 15 s at 98 °C, 15 s at 56 °C (SpyTag introduced to E2) or 55 °C (SpyCatcher) or 52 °C (CBU1910), and 45 s (SpyTag introduced to E2) or 40 s (SpyCatcher) or 45 s (CBU1910) at 72 °C, with a final step of 10 min at 72 °C. Sequencing was performed by GeneWiz/Azenta, and DNA and protein sequences are given in Appendix A.2.5.

### *3.3.7. Expression, purification, and characterization of SpyTag-E2 particles*

The new E2 protein mutants were prepared similarly to previously described mutants.<sup>27,29,30</sup> Expression analysis of the ST-E2 mutants is described in Appendix A.1.3. Mutant ST-E2(D381C) was ultimately chosen for scale up expression. Briefly, a 1L culture supplemented with 100 ug/ml of ampicillin was inoculated with an overnight culture at 37 °C until an OD of 0.7-0.9 at which time it was induced by 1 mM IPTG and further incubated for 3 h at 37 °C. Cells were pelleted and stored at -80 °C overnight before breaking. Cells were lysed using a lysing buffer containing 3mM PMSF and French Press (Thermo Fisher Scientific). Soluble cell lysates are heat shocked at 70 °C and ultracentrifuged to remove thermolabile containments. Subsequently, the lysates were purified using a HiPrep Q Sepharose anion exchange column (GE Healthcare) followed by a Superose 6 prep grade (GE Healthcare) size exclusion column. The purified proteins were characterized by DLS (Zetasizer Nano ZS, Malvern), mass spectrometry (Xevo G2-XS QTof)



and SDS-PAGE, and bicinchoninic acid assay (BCA) for size, molecular weight and purity, and protein concentration, respectively.

The residual *E. coli* expression derived lipopolysaccharide (LPS) was removed following a previously described method.<sup>27</sup> Briefly, Triton X-114 (Sigma) was added to the purified protein at 1% (v/v), chilled to 4 °C, vortexed vigorously, and heated to 37 °C. The mixture was then centrifuged at 18,000 xg and 37 °C for 1 min, and the protein-containing aqueous phase was separated from the detergent phase. This total process was repeated 9 times. Residual Triton was removed with detergent removal spin columns (Pierce). LPS levels were tested to be below 0.1 EU per microgram of E2 protein (LAL ToxinSensor gel clot assay, Genscript).

### 3.3.8. Expression, purification, and characterization of SpyCatcher-CBU1910

The SpyCatcher-CBU1910 fusion protein was expressed in a similar fashion to the E2 particles. Proteins were expressed in *E. coli* via 1 mM IPTG induction. After induction for 3 h at 37 °C, cells were pelleted and stored at -80 °C before breaking. Cells were lysed via French Press and soluble protein was purified using a HisPur Ni-NTA resin batch protocol (Thermo Fisher Scientific). Briefly, soluble cell lysates were mixed with equal parts equilibration buffer and applied to a HisPur Ni-NTA affinity spin column using a packing ratio of 1.5 ml resin per 10 ml of lysate slurry. The lysate was allowed to incubate with the resin for 1 h at 4 °C. Wash buffers and elution buffer containing 75 mM and 150 mM imidazole, and 250 mM imidazole, respectively, were used to attain pure SC-CBU1910. Pure protein fractions were collected and dialyzed into PBS to remove imidazole using a 6-8 kDa MWCO dialysis tubing. The purified protein was characterized by mass spectrometry (Xevo G2-XS QTof) and SDS-PAGE, and BCA for molecular weight and purity, and protein concentration, respectively.

Residual *E. coli* expression derived LPS was removed in similar fashion to the E2 protein. Residual Triton was removed with detergent removal spin columns (Pierce) or SM2 detergent

removal beads (Bio-Rad). LPS levels were below 0.1 EU per microgram of SC-CBU1910 protein (LAL ToxinSensor gel clot assay, Genscript).

### 3.3.9. CpG and SpyCatcher conjugation onto SpyTag-E2 particles

The oligodeoxynucleotide TLR9 ligand CpG 1826 (5'-tccatgacgttcctgacgtt-3') (CpG) was synthesized with a phosphorothioated backbone and 5' benzaldehyde modification by Integrated DNA Technologies (IDT). CpG was conjugated to the internal cavity of the E2 nanoparticle as described previously.<sup>27</sup> In brief, the internal cavity cysteines of E2 were reduced with TCEP (Pierce) for 30 min followed by incubation with the N-( $\beta$ -maleimidopropionic acid) hydrazide (BMPH) linker (Pierce) for 2 h at room temperature (RT). Unreacted linker was removed using 40 kDa cutoff Zeba spin desalting columns (Pierce). The aldehyde-modified CpG was subsequently added and incubated overnight at RT. Unreacted CpG was removed by desalting spin columns. Conjugation was estimated by SDS-PAGE and measured by band intensity analysis.<sup>27</sup>

Directly incubating SpyCatcher-CBU1910 and SpyTag-E2 particles allowed for spontaneous isopeptide bond formation and conjugation. SC-CBU1910 proteins were incubated with ST-E2 particles at a ~0.5:1 (SC-CBU1910:ST-E2 monomer) molar ratio, supplemented with 0.080-0.0875% (w/v) Sarkosyl (SLS), for 20h at room temperature. SDS-PAGE densitometry analysis with protein standards was used to quantify protein loading onto the particles. DLS and transmission electron microscopy (TEM) were used to measure the size, assembly, and monodispersity of the particles. Transmission electron micrographs of 2% uranyl acetate-stained nanoparticles on Cu 200 or 300 mesh carbon coated grids were obtained on a JEM-2100F (JEOL) with a Gatan OneView camera (Gatan).

Further details describing the optimization trials required to determine the final formulation condition can be found in Appendix A.1.4.

### 3.3.10. Mice and Immunizations

All animal studies were carried out in accordance with protocols approved by the Institutional Animal Care and Use Committee (IACUC) at the University of California, Irvine. Briefly, 6–8-week-old female C57BL/6 mice (n=5) were immunized subcutaneously at the left flank on Day 0 and followed by a booster on Day 14. Injections were 30  $\mu$ l per mouse and contained definite amounts of CBU1910, E2, and CpG, based on the formulations investigated. In groups that used the adjuvant, IVAX, an equal volume of IVAX to formulation was supplemented (i.e., 30  $\mu$ l E2 formulation + 30  $\mu$ l IVAX). IVAX contains Addavax (InvivoGen), 1 nmole of CpG 1018, and 3 nmole of MPLA. Seven days after the last immunization, mice were sacrificed, blood was collected via cardiac puncture, and spleens were isolated.

For peptide (CBU1910p) formulations the same prime boost immunization schedule was followed as described above. Each dosage of peptide formulation contained 10  $\mu$ g of CBU1910p and 5  $\mu$ g of CpG 1826 (when indicated).

### 3.3.11. Protein Microarrays

Protein microarrays were fabricated as previously described.<sup>68</sup> Briefly, CBU1910 protein was diluted to a concentration of 0.1 mg/ml and printed onto nitrocellulose-coated glass Oncyte® Avid slides (Grace Bio-Labs) using an Omni Grid 100 microarray printer (Genomic Solutions). For probing, mouse plasma samples were diluted 1:100 in protein array blocking buffer supplemented with 10 mg/ml *E. coli* lysate (GenScript) and His-tag containing peptide HHHHHHHHHHGGGG (Biomatik) to a concentration of 0.1mg/ml to block anti-polyhistidine antibodies. Arrays were rehydrated with blocking buffer prior to addition of pre-incubated sera. Arrays were incubated overnight at 4°C with gentle agitation. After overnight incubation, the slides were washed with Tris-buffered saline (TBS) containing 0.05% Tween 20 (T-TBS) and incubated with biotinylated-SP-conjugated goat antimouse IgG, IgG1, or IgG2c (Jackson ImmunoResearch). Arrays were washed with T-TBS and incubated with streptavidin conjugated Qdot-800 (ThermoFisher). Arrays

were washed three times with T-TBS followed by TBS, dipped in water, and dried by centrifugation. Images were acquired using the ArrayCAM imaging system (Grace Bio-Labs). Spot and background intensities were measured using an annotated grid (.gal) file. IgG1 and IgG2c antibody subtype proportions were calculated using respective signal intensities:  $\text{IgG1}/(\text{IgG1}+\text{IgG2c})$  and  $\text{IgG2c}/(\text{IgG1}+\text{IgG2c})$ , respectively.<sup>47</sup>

### 3.3.12. *T cell recall assays*

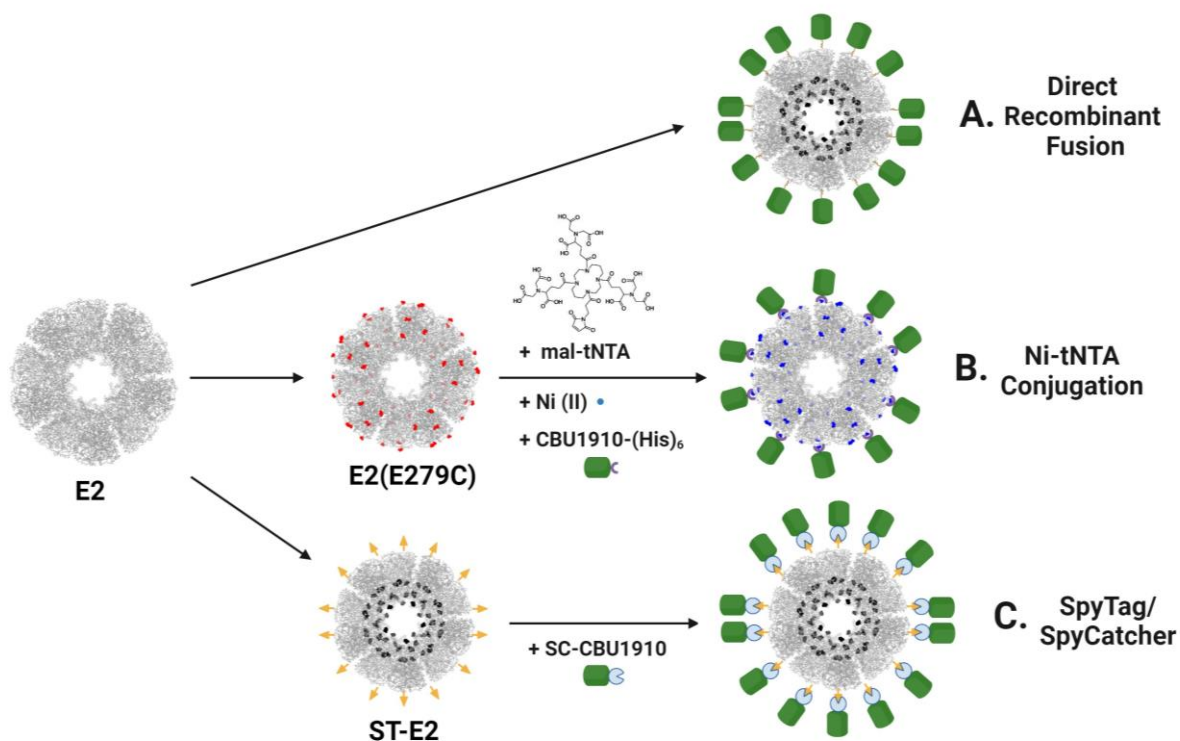
Recall assays were performed using IFN- $\gamma$  ELISpot format and spleens collected on day 21 essentially as previously described.<sup>69</sup> Antigens used for recall were *C. burnetii* CBU1910 and OVA as an irrelevant control antigen. Assays were performed in Roswell Park Memorial Institute (RPMI) 1640, containing  $5 \times 10^{-5}$  M  $\beta$ -mercaptoethanol, 100 IU/mL penicillin, 100  $\mu\text{g}/\text{mL}$  streptomycin, and 10% heat-inactivated fetal bovine serum (complete medium). Briefly, erythrocyte-depleted splenocytes were incubated at  $5 \times 10^5$  cells per well in 96-well ELISpot plates, coated previously with IFN- $\gamma$  capture antibody and blocked in complete medium, containing titrations of antigen ranging from 2.5-10  $\mu\text{g}/\text{ml}$ . Mice were assayed separately. Concanavalin A was included as a viability control.

### 3.3.13. *Statistical analysis*

For nanoparticle characterization, including hydrodynamic diameter measurements, molecular weights determined by mass spectrometry, and antigen/nanoparticle ratios, data are presented as mean  $\pm$  standard deviation (SD) of at least three independent experiments ( $n \geq 3$ ), unless otherwise noted. Statistical analysis of immunization data was carried out using GraphPad Prism. Data are presented as mean  $\pm$  standard error of the mean (SEM) from at least five independent individuals ( $n \geq 5$ ). Statistical analysis was determined by a one-way ANOVA or two-

way ANOVA over all groups followed by a Bonferroni multiple comparison test, unless otherwise noted. P-values less than 0.05 were considered significant.

### 3.4. Results and Discussion



**Figure 3.1. Overview of protein antigen-nanoparticle conjugation strategies. (A)** Direct recombinant fusion of CBU1910 (green) onto E2 nanoparticles (grey). **(B)** Maleimide-tNTA-Ni linker chemistry on E2 nanoparticles (NPs) that contain surface cysteines (with E279C mutation, red). His-tagged CBU1910 antigens are conjugated to the NP surface. **(C)** Assembly with SpyTag/SpyCatcher system to conjugate ST-E2 and SC-CBU1910.

### 3.4.1. Three approaches were investigated for loading *C. burnetii* protein antigen onto E2 nanoparticles.

We examined three strategies to attach the CBU1910 protein antigen to protein nanoparticles, as summarized in Figure 3.1 and described below. Appendix A.2.4 lists the description of each of the components and the corresponding abbreviations used in this work.

#### 3.4.1.1. Direct recombinant fusion of CBU1910 onto E2 nanoparticles

To investigate this loading strategy, CBU1910 was genetically fused to the N-terminus of a truncated E2 monomer. The wild-type form of the core E2 nanoparticle (dihydrolipoyl transacetylase) includes, on its N-terminus, a lipoyl domain and a peripheral subunit-binding domain, which enables association with the E1 and E3 proteins in the complex.<sup>20,22,70</sup> In our studies, we distill this protein down to its structural dodecahedral core for application as a nanoparticle scaffold<sup>23-26,28</sup>; however, based on the native structure, we hypothesized that other proteins with independent binding domains could be genetically fused to its N-terminus. We created two E2 mutants with different N-terminus linker lengths and 60 internal cavity cysteines [E2\_152(D381C) and E2\_158(D381C)]. Relative to the truncated E2(D381C) mutant used previously<sup>23,27,29-31</sup>, the E2\_152 and E2\_158 mutants have an additional 20 and 14 amino acids of the wild-type protein sequence, respectively, added to their N-termini.<sup>63,64</sup> Introduction of 60 internal cavity cysteines allows for adjuvant conjugation.<sup>27,71</sup>

The CBU1910 protein was recombinantly fused to E2 (See Appendix A.2.5), and the fusion proteins were expressed in *E. coli* (See Appendix B.8). CBU1910 protein antigen fused to an E2 monomer was strongly expressed. However, these fusion proteins aggregated as inclusion bodies and were only present in the insoluble fraction, even under different expression conditions (e.g., lower temperatures, different induction conditions) (See Appendix B.8). In contrast, the individual proteins (E2 monomers alone, CBU1910 alone) showed fractions which were soluble (See Appendix B.8); with solubility linked to correct folding and nanoparticle assembly in prior studies.<sup>23</sup>

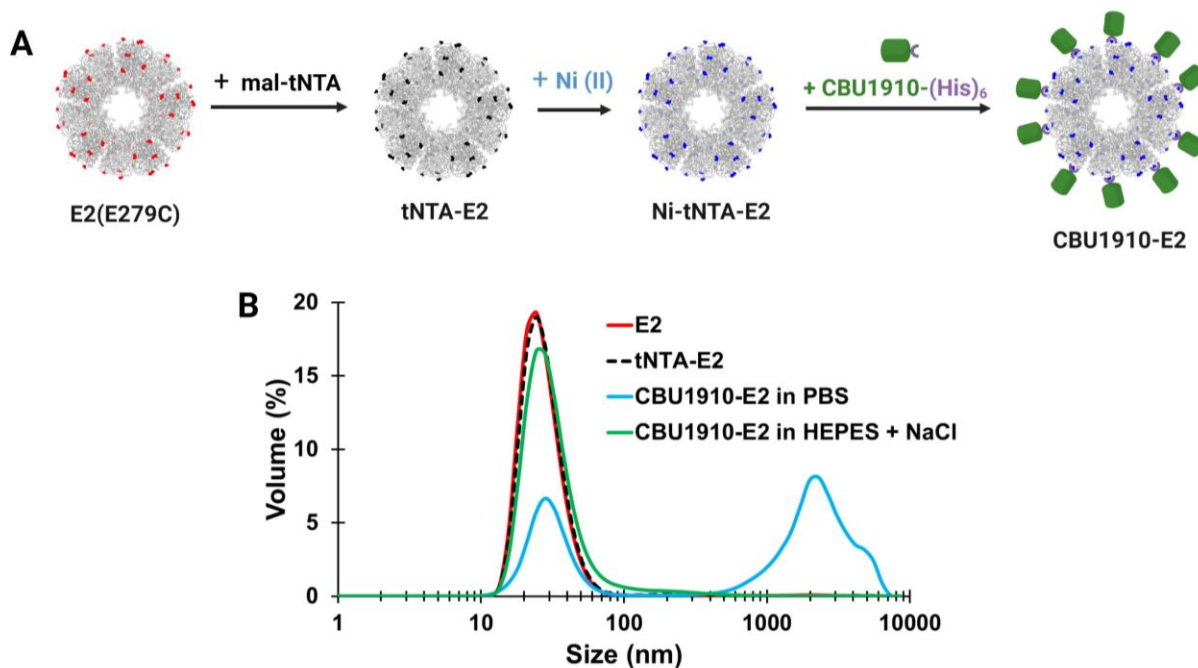
Under the conditions tested, the fused proteins (CBU1910-E2) could not be expressed as a soluble protein, suggesting misfolding and/or misassembly of the complex. For this reason, the two subsequent loading strategies focused on generating the two proteins separately, followed by conjugation together.

#### 3.4.1.2. Using a tris-NTA-Ni linker to conjugate CBU1910 onto E2 nanoparticles

To conjugate CBU1910 onto the surface of the E2 protein NP, we used an affinity strategy that we had developed for conjugating green fluorescent protein (GFP) and influenza hemagglutinin (HA).<sup>56</sup> An E2 NP displaying 60 cysteines on its surface (E279C)<sup>28</sup> allows for conjugation of a synthesized maleimide-tris-NTA (mal-tNTA) linker<sup>56</sup>, which enables a His-tagged protein to couple to the NP. This protocol was performed for CBU1910 as shown in Figure 3.2A. Unlike GFP and HA conjugation, which remained soluble and physically stable over an extended period, conjugation of CBU1910-(His)<sub>6</sub> to E2 yielded a mixture of single nanoparticles and aggregates of nanoparticles. Optimization of conjugation conditions (e.g., buffers, salts, surfactants) to yield non-aggregated nanoparticles was required, and these conditions are summarized in Appendix B.9. HEPES buffer at pH 7.3 with 360 mM NaCl was found to stabilize nanoparticles and was used for subsequent purification and characterization steps. Free CBU1910-(His)<sub>6</sub> was separated from E2-bound CBU1910 using size exclusion chromatography (SEC). Quantification of the number of E2-attached CBU1910 was determined to be  $6 \pm 3$  per E2 nanoparticle.

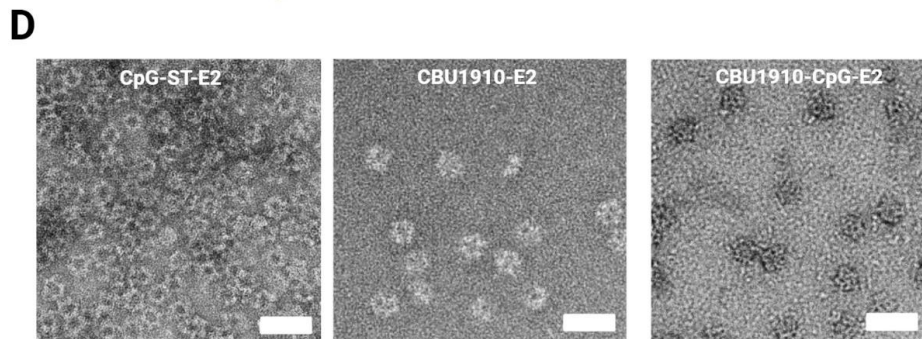
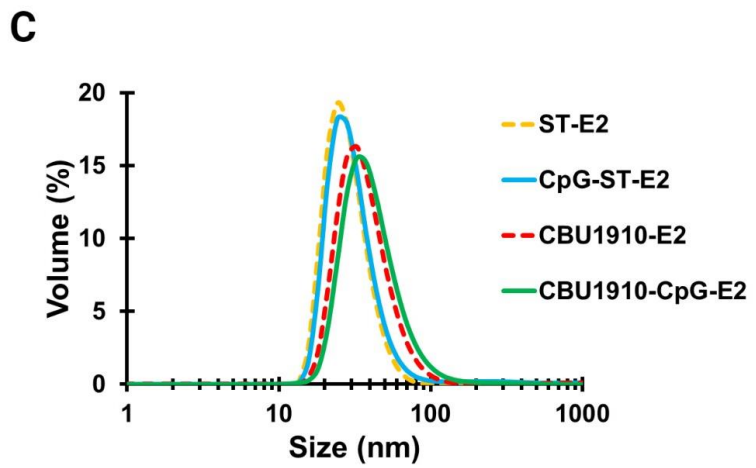
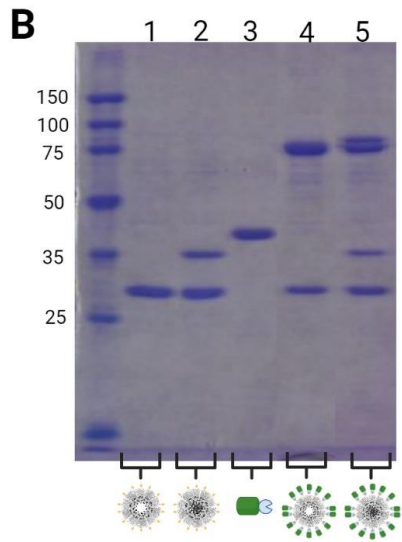
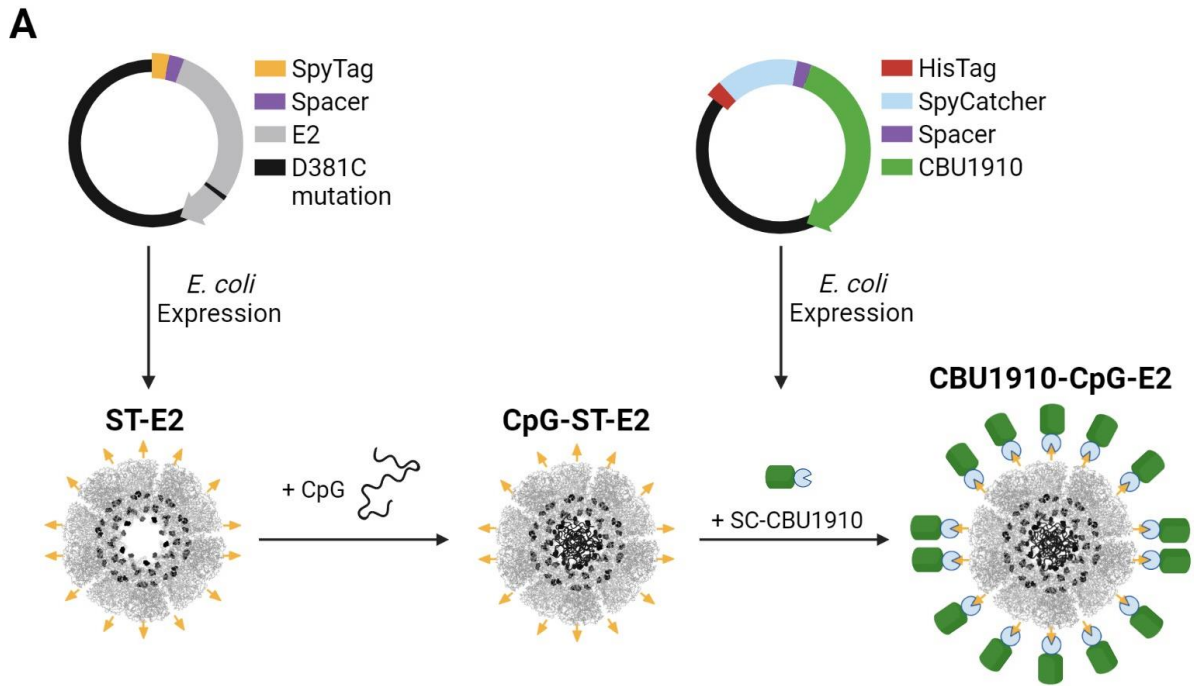
Hydrodynamic diameters for E2, tNTA-E2, and CBU1910-E2 NPs were  $27.3 \pm 1.1$  nm,  $28.8 \pm 2.2$  nm, and  $31.6 \pm 4.0$  nm, respectively, all of which fall in the size range shown to be beneficial for lymphatic system trafficking and antigen-presenting cell (i.e., dendritic cell and B cell) engagement (Figure 3.2B).<sup>18,72</sup> The small increase in diameter for CBU1910-E2 was consistent with the relatively low number of CBU1910 on the surface of the E2 nanoparticle. To dose an adequate amount of antigen for an *in vivo* vaccine study, a 10-fold increase in

concentration was required; however, concentrating the formulation to this extent led to significant protein aggregation. Although conjugation of the CBU1910 antigen to the protein nanoparticle using a tNTA linker showed promise, this strategy showed limitations for this specific antigen that included low conjugation capacity and inconsistent physical stability. We note that this result is different than attachment of HA to E2, which had yielded reliable conjugation and stable, monodisperse particles, suggesting that these effects are highly antigen-dependent. Furthermore, the use of the maleimide-tNTA for surface conjugation via cysteine residues limits the use of cysteines internally for conjugation of immune-stimulating adjuvants.<sup>27,29-31,71</sup>



**Figure 3.2. Conjugating CBU1910 onto E2 protein nanoparticles using a tris-NTA-Ni linker.** (A) Schematic showing loading CBU1910 of E2 nanoparticle via a tNTA-Ni linker. (B) Hydrodynamic diameters of E2 particles alone (E2), after linker conjugation (tNTA-E2), and CBU1910 loading on E2 (CBU1910-E2) in two different buffers. The NP component here is the E279C E2 mutant with cysteines displayed on the external surface.





**Figure 3.3. Conjugation of CBU1910 onto E2 nanoparticles using the SpyTag/SpyCatcher system.** (A) Schematics of (top) plasmids for ST-E2 and SC-CBU1910 and (bottom) structure of expressed E2 with 60 SpyTags (yellow) on surface and highlighted 60 cysteines (black) in cavity and SpyCatcher-CBU1910 (green) fusion proteins. CpG1826 and SC-CBU1910 are conjugated onto ST-E2 to form CBU1910-CpG-E2. (B) SDS-PAGE of nanoparticle components. Lanes: 1. ST-E2; 2. CpG-ST-E2; 3. SC-CBU1910; 4. CBU1910-E2; 5. CBU1910-CpG-E2. (C) Hydrodynamic diameters of E2 constructs after CpG and SC-CBU1910 conjugations. (D) Representative TEM images of nanoparticles CpG-ST-E2, CBU1910-E2, and CBU1910-CpG-E2. Scale bar = 50 nm.

#### 3.4.1.3. Using SpyTag(ST)/SpyCatcher(SC) to conjugate CBU1910 onto E2 nanoparticles

The SpyTag/SpyCatcher system<sup>57</sup> was used to attach CBU1910 to the E2 nanoparticle using the strategy outlined in Figure 3.3A. The advantages of this approach include its stable covalent interaction and the ability to separately express both the antigen and the nanoparticle proteins prior to conjugation, which can circumvent protein expression challenges. SpyTag (ST) was genetically attached to the E2 nanoparticle, and SpyCatcher (SC) was genetically fused with the protein antigen CBU1910. We reasoned that coupling SpyCatcher to the antigen minimizes the amount of exposed SC after conjugation to the NP, which is likely favorable for reducing anti-SC immune responses.

The ST peptide was genetically fused to the N-terminus of E2 with a spacer sequence (Figure 3.3 and See Appendix B.10). The E2 mutant D381C possessed 60 internal cavity cysteines, which would enable conjugation of adjuvant.<sup>27,71</sup> Because a high-resolution protein structure of CBU1910 has not yet been determined, we used the protein folding prediction tool AlphaFold2<sup>73</sup> to predict the structure of CBU1910 (See Appendix B.11). Based on this predicted structure of N-terminal truncated CBU1910 (to enable a soluble antigen)<sup>47,67</sup>, we decided to fuse SC to the N-terminus of CBU1910 (Figure 3.3; See Appendix B.11). This ensured that when conjugated to the E2 nanoparticle, CBU1910 would be oriented in the same direction as when it is displayed on *C. burnetii*, exposing more relevant B cell epitopes.

The attachment of ST and SC to E2 and CBU1910, respectively, did not appear to decrease expression levels or soluble protein amounts (See Appendix B.10). Therefore, we

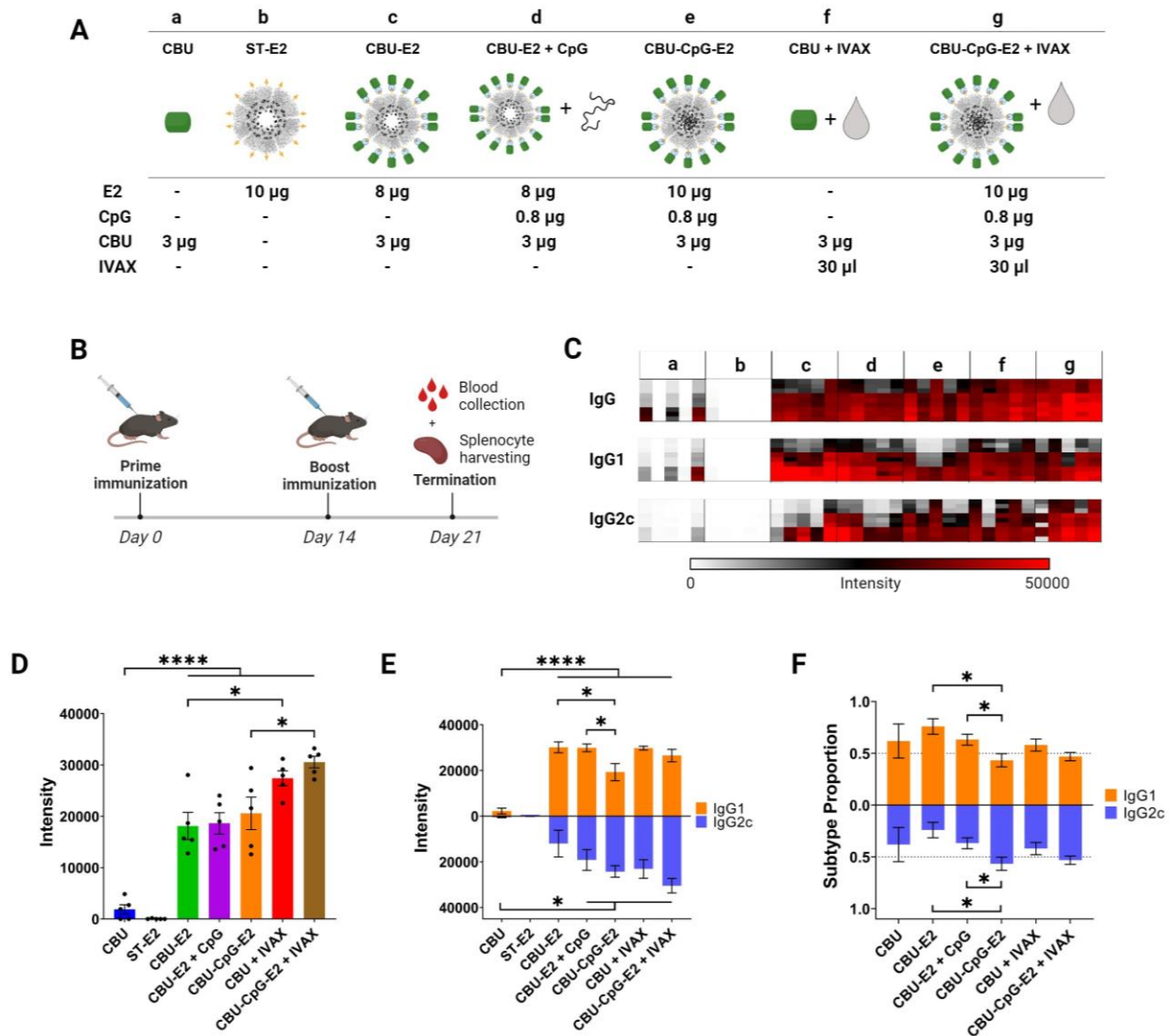
proceeded with purifying ST-E2(D381C) (henceforth referred to as ST-E2) and SC-CBU1910 for further characterization and studies. Both SDS-PAGE and mass spectrometry showed the expected molecular weight increase of ~2.2 kDa (ST and spacer) for ST-E2 monomers (See Appendix B.10). The ST-E2 NP assembly yielded a hydrodynamic diameter of  $29.2 \pm 0.5$  nm, which is slightly larger than the E2 diameter size of  $27.8 \pm 0.6$  nm (See Appendix B.10), as expected. This is approximately 1 nm larger, which is consistent with previous literature estimates of ST on virus like particles (VLPs).<sup>58</sup> For SC-CBU1910, we achieved a >95% purity and the average molecular weight of ~40.8 kDa, as determined by SDS-PAGE and mass spectrometry, which is consistent with SC fused to CBU1910 with a linker (See Appendix B.10).

The E2 protein NP platform, together with the ST/SC conjugation system, allows interior and exterior attachments designed for co-delivery of adjuvants and antigens, respectively. We conjugated the TLR9 agonist, CpG1826, to the interior of the ST-E2 NP platform via an acid-labile BMPH linker (Figure 3.3A).<sup>27</sup> Consistent with prior syntheses using E2, on SDS-PAGE the lower band on CpG-ST-E2 at ~30 kDa shows the unconjugated ST-E2 monomer, and the band at ~37 kDa supports the conjugation of one CpG molecule (~7 kDa) to a ST-E2 monomer (Figure 3.3B). Quantification indicated  $20.5 \pm 1.5$  CpG1826 molecules were encapsulated internally per 60-mer E2 NP, similar to previous E2 formulations.<sup>27</sup> The average hydrodynamic diameter of CpG-ST-E2 nanoparticles was  $31.8 \pm 1.4$  nm (Figure 3.3C).

Although it is well-documented that the isopeptide bond formation between SpyTag and SpyCatcher is robust and reliable<sup>57,58,74-76</sup>, conjugation of the SC-CBU1910 antigen onto the surface to ST-E2 required optimization to yield intact and monodisperse nanoparticles. As seen with other ST/SC VLP formulations, adjustments to reaction molar ratios, pH, ionic strength, and/or detergent concentrations were required to prevent precipitation/aggregation.<sup>58,77-80</sup> A tabulated list of the optimization conditions and solubilizing additives (i.e., surfactants, buffers, salts) can be found in Appendix B.12. From our investigation, we determined favorable reaction conditions to be a 1:0.5 molar ratio of ST-E2 (monomer):SC-CBU1910 at room temperature for

20 h with an addition of 0.08-0.0875% (w/v) SLS; this resulted in stable, monodisperse nanoparticles (Figure 3.3).

Size and antigen-to-nanoparticle ratios were then determined. When conjugated to SC-CBU1910, the ST-E2 monomer molecular weight increases by ~41 kDa to ~71 kDa. As expected, when SC-CBU1910 is conjugated to CpG-ST-E2, two conjugate bands appear; one band is CBU1910-E2 monomers (~71 kDa) and the other CBU1910-CpG-E2 monomers (~78 kDa; both CBU1910 antigen and CpG conjugated onto E2) (Figure 3.3B). Quantification estimated that  $29 \pm 2$  and  $24 \pm 2$  SC-CBU1910 were conjugated to each ST-E2 and CpG-ST-E2 nanoparticle, respectively, out of a maximum possible number of 30 per nanoparticle (based on 1:0.5 molar ratio, by monomer). CBU1910-E2 and CBU1910-CpG-E2 hydrodynamic diameters were  $37.9 \pm 1.9$  nm and  $43.6 \pm 5.1$  nm, respectively (Figure 3.3), with the size increase corresponding to the successful loading of antigens on the nanoparticles. Furthermore, TEM images confirmed intact monodisperse nanoparticles (Figure 3.3D). Because the ST/SC protein-protein conjugation system could be implemented to co-deliver protein antigen and adjuvant simultaneously, we used these stable nanoparticles (e.g., CBU-CpG-E2, CBU-E2) to evaluate their prophylactic vaccine potential.



**Figure 3.4. Antibody responses of protein antigen and nanoparticle formulations.** (A) Table describing each formulation and its individual components. IVAX = 30 µl Addavax emulsion + 1 nmole CpG1018 + 3 nmole MPLA. (B) Schematic of prime/boost immunization schedule. (C) Heat map of antigen-specific antibody profiling using protein micro arrays probed with plasma from day 21. CBU1910 was printed at three different concentrations of 0.1, 0.03, and 0.01 mg/ml (rows, bottom-to-top). Each column represents signal intensities of an individual mouse. (D) Total CBU1910-specific IgG in plasma on day 21. Quantification of data shown in panel C (0.03 mg/ml array spots only). Each dot represents an individual mouse. (E) CBU1910-specific IgG1 and IgG2c in plasma on day 21. Quantification of data shown in panel C (0.03 mg/ml array spots only). (F) Calculated proportions of antibody subtypes in plasma on day 21 (intensities of IgG1 or IgG2c relative to [IgG1 + IgG2c]<sup>47</sup>). The subtype proportions of negative control ST-E2 was not applicable because IgG1 and IgG2 levels were at negligible background levels. Data in panels D, E, F is presented as an average ± SEM of 5 mice per group (n = 5). Statistical significance was determined by one-way ANOVA followed by a Bonferroni multiple comparisons test. Two-tailed student t-tests were used in panel F. \*p < 0.05, \*\*p < 0.005, \*\*\*\*p < 0.0001. Abbreviations: CBU = CBU1910; CpG = CpG1826.

### 3.4.2. Attaching CBU1910 onto nanoparticles elicits significantly higher IgG responses than soluble CBU1910 alone

We investigated the antibody responses of different vaccine formulations containing CBU1910 protein antigen, CpG1826, E2, and oil-in-water emulsion adjuvant, IVAX, after prime and boost immunization in mice (Figures 3.4A, B). The NPs generated using the ST/SC approach were selected for evaluation of immune responses due to their higher physical stability and protein antigen loading characteristics, as described above. Sera of each animal were evaluated using antigen microarrays to determine the antibody production elicited by each formulation (Figure 3.4C). The most striking result was seen when displaying CBU1910 on E2 nanoparticles (CBU1910-E2), *i.e.*, in the absence of adjuvants, which elevated the CBU1910-specific total IgG response significantly relative to soluble CBU1910 alone (Figure 3.4D).

It has been previously described that nanoparticle size and antigen display topography can play a crucial role in B cell engagement.<sup>18,72</sup> Nanoparticles between ~20-50 nm in diameter with antigen valences greater than ~5 per nanoparticle and antigen spacing larger than ~25 nm are reported to obtain effective B cell engagement.<sup>18</sup> The CBU-E2 formulations used in this immunization study possess these characteristics and could be one explanation for obtaining >9 times increased IgG antibody response towards CBU by simply displaying the antigen on the nanoparticle platform (relative to unbound antigen). This also supports the premise that B cell activation can be augmented by the decoration of nanoparticles with repetitive epitopes; the repetitive geometry and spatial configuration of NP-attached antigens mimic natural pathogens such as viruses, which can yield strong innate adjuvating outcomes by improving uptake by antigen-presenting cells and enabling binding and simultaneous activation of multiple B cell receptors.<sup>18,81</sup>

### *3.4.3. Adjuvant, either co-administered in solution or encapsulated within the nanoparticle, increases anti-CBU1910 titers*

The IgG responses obtained with CpG-E2-based formulations were comparable to the positive control oil-in-water emulsion adjuvant, IVAX, a combination adjuvant consisting of AddaVax (a squalene-based adjuvant), monophosphoryl-lipid A (MPLA), and CpG1018, that has been shown to induce broadly reactive responses to influenza HA proteins<sup>68</sup> (Group **f**, Figure 3.4D). Our previous *in vitro* studies using CpG-E2 nanoparticles demonstrated that once taken up by a cell, encapsulated CpG can be released from the nanoparticle in an acidic environment and activate mouse bone marrow-derived dendritic cells.<sup>27</sup> Furthermore, encapsulated CpG was shown to activate these cells at significantly lower concentrations than unbound CpG, indicating the need for bioconjugation of CpG to the nanoparticle.<sup>27</sup> Other studies have also shown that alternative types of nanoparticles which simultaneously deliver both conjugated CpG and antigen can increase the immunogenicity and immune response mounted against the target antigen.<sup>29,30,82-84</sup> Thus, to deliver adjuvants more precisely to immune cells involved in adaptive immunity, such as dendritic cells, CpG was encapsulated within the nanoparticle in an approach that increases uptake efficiency of CpG and the dose of CpG that an individual cell receives upon endocytosing a nanoparticle versus free-floating CpG. The effects of CpG adjuvant and its delivery covalently encapsulated within the E2 NP (CBU-CpG-E2) or co-administered with the E2 NP by mixing only (CBU-E2 + CpG) showed comparable results on total IgG responses (Groups **c-e**, Figure 3.4D). Addition of IVAX to the CBU1910-CpG-E2 formulation further increased the overall anti-CBU1910 IgG response (Figure 3.4D, Group **g**).

### *3.4.4. E2 formulations that contained an adjuvant elicited more balanced IgG1/IgG2c antibody responses*

Antibody class switching to IgG1 and IgG2c are associated with the cytokine profiles released from Th2 and Th1 lymphocytes, respectively. Th2 responses are described by B cell

proliferation, antibody production, and induction of IgG1 antibodies.<sup>85,86</sup> Th1 responses are characterized by the activation of antigen-presenting cells, stimulation of T cells, and induction of IgG2c antibodies.<sup>85-87</sup> Thus, IgG1 and IgG2c production can be used as indicators of Th2 and Th1 responses, respectively. Profiles of the IgG1 and IgG2c antibody responses suggest modulation capabilities that depend on the adjuvant used and whether it was loaded in the E2 nanoparticle (Figure 3.4E, F). Soluble CBU1910 (Group **a**) elicited a very weak total IgG response that was slightly skewed towards IgG1 (Th2). Loading CBU1910 onto nanoparticles (CBU1910-E2, Group **c**) significantly increased total IgG (predominantly IgG1 (Th2)), with some measurable IgG2c (Th1) isotype switched antibodies, suggesting the E2 NP may have some inherent Th1 skewing properties in the absence of any TLR agonists. The addition of soluble CpG1826 to CBU1910-E2 particles (CBU1910-E2 + CpG1826; Group **d**) further increased the shift towards a Th1 response as expected, although few of these shifts were significantly different from CBU1910-E2 alone and did not significantly alter IgG1/IgG2c ratios. Uniquely, when CpG1826 was internally conjugated to the E2 vaccine particle (CBU1910-CpG1826-E2; Group **e**), the total IgG amount did not significantly change, but the nature of the response shifted towards a Th1 response, as indicated by a more balanced IgG1/IgG2c ratio, compared to soluble or no CpG adjuvant addition (Figure 3.4E, F). Our data show that nanoparticles loaded with CpG elicited a more balanced IgG1/IgG2c response. Addition of IVAX to the CBU1910-CpG-E2 nanoparticle slightly increased IgG1 and IgG2c responses without greatly affecting the subtype balance conferred by the E2 formulation itself.

#### *3.4.5. Immunization with C. burnetii antigen loaded onto E2 nanoparticles increased antigen-specific IFN- $\gamma$ secretion*

The more balanced IgG1/IgG2c antibody ratio elicited by CBU1910-CpG-E2 suggests that T cell responses towards the CBU1910 antigen are likely to be produced. However, when we examined the effector T cell response, we found that antigen-specific IFN- $\gamma$  responses (which



corresponds to an IgG2c/Th1 response) were low in mice that were administered CBU1910-CpG-E2 alone (Figure 3.5A and See Appendix B.13). The addition of IVAX to this formulation significantly increased IFN- $\gamma$  secretion. This observation was not expected, given the similar levels of antigen-specific IgG2c production after immunization with the CBU1910-CpG-E2 nanoparticle, both with and without IVAX. The unexpectedly low IFN- $\gamma$  response from formulations that induced IgG2c/Th1 responses compared to IVAX, such as the CBU1910-CpG-E2, may have resulted from cytokines other than IFN- $\gamma$  (including IL-2, IL-10 or TNF- $\alpha$ ) driving the IgG2c response, or a different temporal release of IFN- $\gamma$  (assayed after 18h of restimulation with antigen, only). Further experiments would be necessary to test these hypotheses. Another reason for this discrepancy could stem from the TLR4 agonist (MPLA) and TLR9 agonist (CpG1018) present in IVAX. It has been shown that simultaneous stimulation of cell-surface and endosomal TLR receptors can cause synergistic increases in the activating/inflammatory immune response and the soluble delivery of the adjuvants may cause a more systemic initial innate immune response.<sup>88,89</sup> This differs from the delivery of CpG via a nanoparticle, which avoids non-specific systemic immune system stimulation due to encapsulation and increases uptake by antigen presenting cells (i.e., dendritic cells).<sup>27</sup> Furthermore, previous studies that co-delivered peptide antigens and adjuvant for cancer vaccines resulted in dosages of ~2-5  $\mu$ g of CpG and ~2-5  $\mu$ g of T cell immunogenic peptide epitopes<sup>29-31</sup>; however, for this protein antigen vaccine, both the CpG and immunodominant T cell epitope dosage were nearly an order of magnitude less than typically dosed for the peptide formulations of the cancer studies.

To determine if an E2 formulation was capable of inducing a strong antigen-specific T cell response towards *C. burnetii*, we examined if a peptide antigen (rather than protein antigen) coupled to the E2 NP could increase the cell-mediated response. Peptide antigens were conjugated to the NP using a linker and characterized, as described in Appendix A.1.5 and Appendix B.14. Interestingly, we observed that immunizing with the CBU1910p-CpG-E2 formulation, an E2 nanoparticle loaded with the immunodominant CD4 T cell epitope peptide of



### 3.5. Conclusions

We investigated three methods of conjugating the *C. burnetii* immunodominant protein antigen, CBU1910, to a protein nanoparticle: genetic fusion, tris-NTA-Ni linker, and ST/SC. We determined that ST/SC yielded vaccine nanoparticles with the highest antigen loading, had capacity to internally encapsulate adjuvant, and could be formulated to yield stable, monodisperse particles. We engineered this platform, ST-E2(D381C), to allow for the simultaneous packing of Th1-skewing adjuvant, CpG, within the interior of the nanoparticle and displaying of protein antigen, CBU1910, on its surface. By displaying the antigen on the nanoparticle only, *i.e.*, in the absence of CpG adjuvant, significant increases in antigen-specific IgG antibodies were observed in immunized mice compared to soluble antigen alone. The addition of an encapsulated or co-administered adjuvant balanced the IgG1/IgG2c antibody profile, which suggests induction of both Th1 (associated with cellular immunity) and Th2 (associated with humoral immunity) responses.

Both antibodies and T cells have been shown to contribute towards host-mediated protection against *C. burnetii* infection. While antibodies play an important role during the early stages of extracellular infection, T cell activation is vital for clearance of intracellular bacteria.<sup>90</sup> Of particular significance are Th1 cells, identified by class switched B cells to produce IgG2c and IFN- $\gamma$  positive CD4 T cells. Th1 cells contribute towards immunity by polarizing macrophages towards an M1 phenotype that is less permissive for intracellular *C. burnetii*.<sup>91</sup> Th1 cells also support the activation of cytotoxic T cells that target infected cells and aid in the formation of protective granulomas that surround parasitized cells. Moreover, Th1 cells contribute to long-term immunity through the generation of memory responses. A balance between antibody mediated and Th1 mediated immunity is essential for effective protection against *C. burnetii*. To confirm the presence of cell-mediated immunity more directly, we show that vaccination with a CBU1910 CD4 epitope peptide conjugated to E2 elicits robust Th1 responses, as measured via T cell recall assay with IFN- $\gamma$  ELISpot. This peptide-conjugation strategy has clear potential to confer protection against a pathogen with both extra- and intra-cellular stages to its life cycle, such as *C. burnetii*,

which requires activation of both humoral and cellular arms of the immune system to grant protection.

### **3.6. Acknowledgements**

This work was supported by the Defense Threat Reduction Agency (DTRA) (Award HDTRA11810035, HDTRA11810036), the National Institutes of Health (R01EB027797), and a Graduate Research Fellowship from the National Science Foundation (NSF) to A.R. We acknowledge the use of transmission electron microscopy facilities and instrumentation at the UC Irvine Materials Research Institute (IMRI), which is supported in part by the National Science Foundation through the UC Irvine Materials Research Science and Engineering Center (DMR-2011967). We thank Drs. Felix Grun and Benjamin Katz at the UCI Mass Spectrometry Facility and Dr. Nicholas Molino for plasmids containing E2\_152 and E2\_158. Portions of Figures 3.1, 3.2, 3.3, 3.4, and Appendix B were created with BioRender.com. E2 protein structure was obtained from Protein Data Bank (PDB; 1b5s).

### 3.7. References

1. van Schaik, E. J.; Chen, C.; Mertens, K.; Weber, M. M.; Samuel, J. E., Molecular pathogenesis of the obligate intracellular bacterium *Coxiella burnetii*. *Nat. Rev. Microbiol.* **2013**, *11* (8), 561-573.
2. Qiu, J. Z.; Luo, Z. Q., Legionella and Coxiella effectors: strength in diversity and activity. *Nat. Rev. Microbiol.* **2017**, *15* (10), 591-605.
3. Eldin, C.; Melenotte, C.; Mediannikov, O.; Ghigo, E.; Million, M.; Edouard, S.; Mege, J. L.; Maurin, M.; Raoult, D., From Q Fever to *Coxiella burnetii* Infection: a Paradigm Change. *Clinical Microbiology Reviews* **2017**, *30* (1), 115-190.
4. Q Fever. Centers for Disease Control and Prevention. <https://www.cdc.gov/qfever/index.html> (accessed June 2019).
5. Anderson, A.; Bijlmer, H.; Fournier, P. E.; Graves, S.; Hartzell, J.; Kersh, G. J.; Limonard, G.; Marrie, T. J.; Massung, R. F.; McQuiston, J. H.; Nicholson, W. L.; Paddock, C. D.; Sexton, D. J., Diagnosis and Management of Q Fever - United States, 2013 Recommendations from CDC and the Q Fever Working Group. *MMWR Recommendations and Reports* **2013**, *62* (3), 1-28.
6. Maurin, M.; Raoult, D., Q fever. *Clinical Microbiology Reviews* **1999**, *12* (4), 518-553.
7. Marrie, T. J., Q Fever Pneumonia. *Infectious Disease Clinics of North America* **2010**, *24* (1), 27-41.
8. Million, M.; Thuny, F.; Richet, H.; Raoult, D., Long-term outcome of Q fever endocarditis: a 26-year personal survey. *Lancet Infectious Diseases* **2010**, *10* (8), 527-535.
9. van der Hoek, W.; Morroy, G.; Renders, N. H. M.; Wever, P. C.; Hermans, M. H. A.; Leenders, A.; Schneeberger, P. M., Epidemic Q Fever in Humans in the Netherlands. In *Coxiella Burnetii: Recent Advances and New Perspectives in Research of the Q Fever Bacterium*, Toman, R.; Heinzen, R. A.; Samuel, J. E.; Mege, J. L., Eds. 2012; Vol. 984, pp 329-364.
10. Kampschreur, L. M.; Delsing, C. E.; Groenwold, R. H. H.; Wegdam-Blans, M. C. A.; Bleeker-Rovers, C. P.; de Jager-Leclercq, M. G. L.; Hoepelman, A. I. M.; van Kasteren, M. E.; Buijs, J.; Renders, N. H. M.; Nabuurs-Franssen, M. H.; Oosterheert, J. J.; Wever, P. C., Chronic Q Fever in the Netherlands 5 Years after the Start of the Q Fever Epidemic: Results from the Dutch Chronic Q Fever Database. *Journal of Clinical Microbiology* **2014**, *52* (5), 1637-1643.
11. Ruiz, S.; Wolfe, D. N., Vaccination against Q fever for biodefense and public health indications. *Frontiers in Microbiology* **2014**, *5* (726).
12. Marmion, B. P.; Ormsbee, R. A.; Kyrkou, M.; Wright, J.; Worswick, D. A.; Izzo, A. A.; Esterman, A.; Feery, B.; Shapiro, R. A., Vaccine prophylaxis of abattoir-associated Q fever: eight years' experience in Australian abattoirs. *Epidemiology and Infection* **1990**, *104* (2), 275-287.
13. Kazar, J., *Coxiella burnetii* infection. In *Rickettsioses: From Genome to Proteome, Pathobiology, and Rickettsiae as an International Threat*, Hechemy, K. E.; Oteo, J. A.; Raoult, D. A.; Silverman, D. J.; Blanco, J. R., Eds. 2005; Vol. 1063, pp 105-114.
14. Oswald G. Baca, Y.-P. L., Hemant Kumar, Survival of the Q fever agent *Coxiella burnetii* in the phagolysosome. *Trends in Microbiology* **1994**, *2* (12), 476-480.
15. Read, A. J.; Erickson, S.; Harmsen, A. G., Role of CD4(+) and CD8(+) T Cells in Clearance of Primary Pulmonary Infection with *Coxiella burnetii*. *Infection and Immunity* **2010**, *78* (7), 3019-3026.
16. Scholzen, A.; Richard, G.; Moise, L.; Baeten, L. A.; Reeves, P. M.; Martin, W. D.; Brauns, T. A.; Boyle, C. M.; Raju Paul, S.; Bucala, R.; Bowen, R. A.; Garritsen, A.; De

- Groot, A. S.; Sluder, A. E.; Poznansky, M. C., Promiscuous Coxiella burnetii CD4 Epitope Clusters Associated With Human Recall Responses Are Candidates for a Novel T-Cell Targeted Multi-Epitope Q Fever Vaccine. *Frontiers in Immunology* **2019**, *10* (207).
17. Kersh, G. J.; Fitzpatrick, K. A.; Self, J. S.; Biggerstaff, B. J.; Massung, R. F., Long-Term Immune Responses to Coxiella burnetii after Vaccination. *Clinical and Vaccine Immunology* **2013**, *20* (2), 129-133.
  18. Nguyen, B.; Tolia, N. H., Protein-based antigen presentation platforms for nanoparticle vaccines. *npj Vaccines* **2021**, *6* (1), 11.
  19. Irvine, D. J.; Read, B. J., Shaping humoral immunity to vaccines through antigen-displaying nanoparticles. *Current Opinion in Immunology* **2020**, *65*, 1-6.
  20. Izard, T.; Årvarsson, A.; Allen, M. D.; Westphal, A. H.; Perham, R. N.; de Kok, A.; Hol, W. G. J., Principles of quasi-equivalence and Euclidean geometry govern the assembly of cubic and dodecahedral cores of pyruvate dehydrogenase complexes. *Proc. Natl. Acad. Sci. U. S. A.* **1999**, *96* (4), 1240-1245.
  21. Domingo, G. J.; Orru, S.; Perham, R. N., Multiple display of peptides and proteins on a macromolecular scaffold derived from a multienzyme complex. *J. Mol. Biol.* **2001**, *305* (2), 259-267.
  22. Milne, J. L. S.; Wu, X. W.; Borgnia, M. J.; Lengyel, J. S.; Brooks, B. R.; Shi, D.; Perham, R. N.; Subramaniam, S., Molecular structure of a 9-MDa icosahedral pyruvate dehydrogenase subcomplex containing the E2 and E3 enzymes using cryoelectron microscopy. *J. Biol. Chem.* **2006**, *281* (7), 4364-4370.
  23. Dalmau, M.; Lim, S.; Chen, H. C.; Ruiz, C.; Wang, S.-W., Thermostability and molecular encapsulation within an engineered caged protein scaffold. *Biotechnology and Bioengineering* **2008**, *101* (4), 654-664.
  24. Ren, D. M.; Kratz, F.; Wang, S. W., Protein Nanocapsules Containing Doxorubicin as a pH-Responsive Delivery System. *Small* **2011**, *7* (8), 1051-1060.
  25. Ren, D. M.; Dalmau, M.; Randall, A.; Shindel, M. M.; Baldi, P.; Wang, S. W., Biomimetic Design of Protein Nanomaterials for Hydrophobic Molecular Transport. *Adv. Funct. Mater.* **2012**, *22* (15), 3170-3180.
  26. Ren, D. M.; Kratz, F.; Wang, S. W., Engineered drug-protein nanoparticle complexes for folate receptor targeting. *Biochem. Eng. J.* **2014**, *89*, 33-41.
  27. Molino, N. M.; Anderson, A. K. L.; Nelson, E. L.; Wang, S.-W., Biomimetic Protein Nanoparticles Facilitate Enhanced Dendritic Cell Activation and Cross-Presentation. *ACS Nano* **2013**, *7* (11), 9743-9752.
  28. Molino, N. M.; Bilotkach, K.; Fraser, D. A.; Ren, D.; Wang, S.-W., Complement Activation and Cell Uptake Responses Toward Polymer-Functionalized Protein Nanocapsules. *Biomacromolecules* **2012**, *13* (4), 974-981.
  29. Molino, N. M.; Neek, M.; Tucker, J. A.; Nelson, E. L.; Wang, S.-W., Viral-mimicking protein nanoparticle vaccine for eliciting anti-tumor responses. *Biomaterials* **2016**, *86*, 83-91.
  30. Neek, M.; Tucker, J. A.; Kim, T. I.; Molino, N. M.; Nelson, E. L.; Wang, S.-W., Co-delivery of human cancer-testis antigens with adjuvant in protein nanoparticles induces higher cell-mediated immune responses. *Biomaterials* **2018**, *156*, 194-203.
  31. Neek, M.; Tucker, J. A.; Butkovich, N.; Nelson, E. L.; Wang, S. W., An Antigen-Delivery Protein Nanoparticle Combined with Anti-PD-1 Checkpoint Inhibitor Has Curative Efficacy in an Aggressive Melanoma Model. *Adv. Therap.* **2020**, *3* (12), 10.
  32. Hendrix, L. R.; Samuel, J. E.; Mallavia, L. P., Identification and cloning of a 27-kDa Coxiella burnetii immunoreactive protein. *Annals of the New York Academy of Sciences* **1990**, *590*, 534-540.
  33. Vigil, A.; Ortega, R.; Nakajima-Sasaki, R.; Pablo, J.; Molina, D. M.; Chao, C.-C.; Chen, H.-W.; Ching, W.-M.; Felgner, P. L., Genome-wide profiling of humoral immune

- response to *Coxiella burnetii* infection by protein microarray. *PROTEOMICS* **2010**, *10* (12), 2259-2269.
34. Beare, P. A.; Chen, C.; Bouman, T.; Pablo, J.; Unal, B.; Cockrell, D. C.; Brown, W. C.; Barbian, K. D.; Porcella, S. F.; Samuel, J. E.; Felgner, P. L.; Heinzen, R. A., Candidate Antigens for Q Fever Serodiagnosis Revealed by Immunoscreening of a *Coxiella burnetii* Protein Microarray. *Clinical and Vaccine Immunology* **2008**, *15* (12), 1771-1779.
  35. Thompson, H. A.; Suhan, M. L., Genetics of *Coxiella burnetii*. *FEMS Microbiology Letters* **1996**, *145* (2), 139-146.
  36. To, H.; Hotta, A.; Zhang, G. Q.; Van Nguyen, S.; Ogawa, M.; Yamaguchi, T.; Fukushi, H.; Amano, K.; Hirai, K., Antigenic characteristics of polypeptides of *Coxiella burnetii* isolates. *Microbiology and Immunology* **1998**, *42* (2), 81-85.
  37. Zhang, G. Q.; To, H.; Russell, K. E.; Hendrix, L. R.; Yamaguchi, T.; Fukushi, H.; Hirai, K.; Samuel, J. E., Identification and characterization of an immunodominant 28-kilodalton *Coxiella burnetii* outer membrane protein specific to isolates associated with acute disease. *Infection and Immunity* **2005**, *73* (3), 1561-1567.
  38. Deringer, J. R.; Chen, C.; Samuel, J. E.; Brown, W. C., Immunoreactive *Coxiella burnetii* Nine Mile proteins separated by 2D electrophoresis and identified by tandem mass spectrometry. *Microbiology* **2011**, *157*, 526-542.
  39. Stellfeld, M.; Gerlach, C.; Richter, I. G.; Miethe, P.; Fahlbusch, D.; Polley, B.; Sting, R.; Pfeiffer, M.; Neubauer, H.; Mertens-Scholz, K., Evaluation of the Diagnostic Potential of Recombinant *Coxiella burnetii* Com1 in an ELISA for the Diagnosis of Q Fever in Sheep, Goats and Cattle. *Microorganisms* **2020**, *8* (8).
  40. Katz, D. H.; Benacerraf, B., The Regulatory Influence of Activated T Cells on B Cell Responses to Antigen. *Advances in Immunology* **1972**, *15*, 1-94.
  41. Saylor, K.; Gillam, F.; Lohneis, T.; Zhang, C. M., Designs of Antigen Structure and Composition for Improved Protein-Based Vaccine Efficacy. *Frontiers in Immunology* **2020**, *11*.
  42. Guo, C. Q.; Manjili, M. H.; Subjeck, J. R.; Sarkar, D.; Fisher, P. B.; Wang, X. Y., Therapeutic Cancer Vaccines: Past, Present, and Future. In *Advances in Cancer Research, Vol 119*, Tew, K. D.; Fisher, P. B., Eds. 2013; Vol. 119, pp 421-475.
  43. Xiong, X.; Qi, Y.; Jiao, J.; Gong, W.; Duan, C.; Wen, B., Exploratory Study on Th1 Epitope-Induced Protective Immunity against *Coxiella burnetii* Infection. *PLOS ONE* **2014**, *9* (1), e87206.
  44. Xiong, X.; Jiao, J.; Gregory, A. E.; Wang, P.; Bi, Y.; Wang, X.; Jiang, Y.; Wen, B.; Portnoy, D. A.; Samuel, J. E.; Chen, C., Identification of *Coxiella burnetii* CD8+ epitopes and delivery by attenuated *Listeria monocytogenes* as a vaccine vector in a C57BL/6 mouse model. *J Infect Dis* **2016**, *215* (10), 1580-1589.
  45. Chen, C.; Dow, C.; Wang, P.; Sidney, J.; Read, A.; Harmsen, A.; Samuel, J. E.; Peters, B., Identification of CD4+ T Cell Epitopes in *C. burnetii* Antigens Targeted by Antibody Responses. *PLOS One* **2011**, *6* (3), e17712.
  46. Zhu, M. M.; Niu, B. W.; Liu, L. L.; Yang, H.; Qin, B. Y.; Peng, X. H.; Chen, L. X.; Liu, Y.; Wang, C.; Ren, X. N.; Xu, C. H.; Zhou, X. H.; Li, F., Development of a humanized HLA-A30 transgenic mouse model. *Animal Models and Experimental Medicine* **5** (4), 350-361.
  47. Gilkes, A. P.; Albin, T. J.; Manna, S.; Supnet, M.; Ruiz, S.; Tom, J.; Badten, A. J.; Jain, A.; Nakajima, R.; Felgner, J.; Davies, D. H.; Stetkevich, S. A.; Zlotnik, A.; Pearlman, E.; Nalca, A.; Felgner, P. L.; Esser-Kahn, A. P.; Burkhardt, A. M., Tuning Subunit Vaccines with Novel TLR Triagonist Adjuvants to Generate Protective Immune Responses against *Coxiella burnetii*. *Journal of Immunology* **2020**, *204* (3), 611-621.
  48. Bachmann, M. F.; Jennings, G. T., Vaccine delivery: a matter of size, geometry, kinetics and molecular patterns. *Nature Reviews Immunology* **2010**, *10* (11), 787-796.

49. Veneziano, R.; Moyer, T. J.; Stone, M. B.; Wamhoff, E. C.; Read, B. J.; Mukherjee, S.; Shepherd, T. R.; Das, J.; Schief, W. R.; Irvine, D. J.; Bathe, M., Role of nanoscale antigen organization on B-cell activation probed using DNA origami. *Nat. Nanotechnol.* **2020**, *15* (8), 716-723.
50. Boyoglu-Barnum, S.; Ellis, D.; Gillespie, R. A.; Hutchinson, G. B.; Park, Y. J.; Moin, S. M.; Acton, O. J.; Ravichandran, R.; Murphy, M.; Pettie, D.; Matheson, N.; Carter, L.; Creanga, A.; Watson, M. J.; Kephart, S.; Ataca, S.; Vaile, J. R.; Ueda, G.; Crank, M. C.; Stewart, L.; Lee, K. K.; Guttman, M.; Baker, D.; Mascola, J. R.; Veesler, D.; Graham, B. S.; King, N. P.; Kanekiyo, M., Quadrivalent influenza nanoparticle vaccines induce broad protection. *Nature* **2021**, *592* (7855), 623–628.
51. Le, D. T.; Muller, K. M., In Vitro Assembly of Virus-Like Particles and Their Applications. *Life-Basel* **2021**, *11* (4).
52. Zepeda-Cervantes, J.; Ramirez-Jarquín, J. O.; Vaca, L., Interaction Between Virus-Like Particles (VLPs) and Pattern Recognition Receptors (PRRs) From Dendritic Cells (DCs): Toward Better Engineering of VLPs. *Frontiers in Immunology* **2020**, *11*.
53. Bornhorst, J. A.; Falke, J. J., Purification of proteins using polyhistidine affinity tags. *Applications of Chimeric Genes and Hybrid Proteins, Pt A* **2000**, *326*, 245-254.
54. Furukawa, A.; Maenaka, K.; Nomura, T., Purification Using Affinity Tag Technology. In *Advanced Methods in Structural Biology*, Senda, T.; Maenaka, K., Eds. 2016; pp 67-81.
55. Loughran, S. T.; Bree, R. T.; Walls, D., Purification of Polyhistidine-Tagged Proteins. In *Protein Chromatography: Methods and Protocols, 2nd Edition*, Walls, D.; Loughran, S. T., Eds. 2017; Vol. 1485, pp 275-303.
56. Badten, A. J.; Ramirez, A.; Hernandez-Davies, J. E.; Albin, T. J.; Jain, A.; Nakajima, R.; Felgner, J.; Davies, D. H.; Wang, S. W., Protein Nanoparticle-Mediated Delivery of Recombinant Influenza Hemagglutinin Enhances Immunogenicity and Breadth of the Antibody Response. *ACS Infectious Diseases* **2023**, *9* (2), 239-252.
57. Zakeri, B.; Fierer, J. O.; Celik, E.; Chittock, E. C.; Schwarz-Linek, U.; Moy, V. T.; Howarth, M., Peptide tag forming a rapid covalent bond to a protein, through engineering a bacterial adhesin. *Proc. Natl. Acad. Sci. U. S. A.* **2012**, *109* (12), E690-E697.
58. Thrane, S.; Janitzek, C. M.; Matondo, S.; Resende, M.; Gustavsson, T.; de Jongh, W. A.; Clemmensen, S.; Roeffen, W.; van de Vegte-Bolmer, M.; van Gemert, G. J.; Sauerwein, R.; Schiller, J. T.; Nielsen, M. A.; Theander, T. G.; Salanti, A.; Sander, A. F., Bacterial superglue enables easy development of efficient virus-like particle based vaccines. *J. Nanobiotechnol.* **2016**, *14*, 16.
59. Anuar, I.; Banerjee, A.; Keeble, A. H.; Carella, A.; Nikov, G. I.; Howarth, M., Spy&Go purification of SpyTag-proteins using pseudo-SpyCatcher to access an oligomerization toolbox. *Nat. Commun.* **2019**, *10*, 13.
60. Keeble, A. H.; Howarth, M., Power to the protein: enhancing and combining activities using the Spy toolbox. *Chem. Sci.* **2020**, *11* (28), 7281-7291.
61. Sharma, J.; Shepardson, K.; Johns, L. L.; Wellham, J.; Avera, J.; Schwarz, B.; Rynda-Appl, A.; Douglas, T., A Self-Adjuvanted, Modular, Antigenic VLP for Rapid Response to Influenza Virus Variability. *ACS Appl. Mater. Interfaces* **2020**, *12* (16), 18211-18224.
62. Li, E. Y.; Brennan, C. K.; Ramirez, A.; Tucker, J. A.; Butkovich, N.; Meli, V. S.; Ionkina, A. A.; Nelson, E. L.; Prescher, J. A.; Wang, S. W., Macromolecular assembly of bioluminescent protein nanoparticles for enhanced imaging. *Materials Today Bio* **2022**, *17*.
63. Chen, Q.; Sun, Q.; Molino, N. M.; Wang, S. W.; Boder, E. T.; Chen, W., Sortase A-mediated multi-functionalization of protein nanoparticles. *Chem. Commun.* **2015**, *51* (60), 12107-12110.



64. Molino, N. Engineering Virus-Mimicking Protein Nanoparticles for Cancer Immunotherapy - PhD Thesis. UNIVERSITY OF CALIFORNIA, IRVINE, 2015.
65. Carrigan, P. E.; Baller, P.; Tuzmen, S., Site-Directed Mutagenesis. In *Disease Gene Identification: Methods and Protocols*, DiStefano, J. K., Ed. 2011; Vol. 700, pp 107-124.
66. Castorena-Torres, F.; Penuelas-Urquides, K.; de Leon, M. B., *Site-Directed Mutagenesis by Polymerase Chain Reaction*. 2016; p 159-173.
67. Fratzke, A. P.; Gregory, A. E.; van Schaik, E. J.; Samuel, J. E., Coxiella burnetii Whole Cell Vaccine Produces a Th1 Delayed-Type Hypersensitivity Response in a Novel Sensitized Mouse Model. *Frontiers in Immunology* **2021**, *12*.
68. Hernandez-Davies, J. E.; Felgner, J.; Strohmeier, S.; Pone, E. J.; Jain, A.; Jan, S.; Nakajima, R.; Jasinskas, A.; Strahsburger, E.; Krammer, F.; Felgner, P. L.; Davies, D. H., Administration of Multivalent Influenza Virus Recombinant Hemagglutinin Vaccine in Combination-Adjuvant Elicits Broad Reactivity Beyond the Vaccine Components. *Frontiers in Immunology* **2021**, *12*, 18.
69. Hernandez-Davies, J. E.; Dollinger, E. P.; Pone, E. J.; Felgner, J.; Liang, L.; Strohmeier, S.; Jan, S.; Albin, T. J.; Jain, A.; Nakajima, R.; Jasinskas, A.; Krammer, F.; Esser-Kahn, A.; Felgner, P. L.; Nie, Q.; Davies, D. H., Magnitude and breadth of antibody cross-reactivity induced by recombinant influenza hemagglutinin trimer vaccine is enhanced by combination adjuvants. *Sci Rep* **2022**, *12* (1), 9198.
70. Tuting, C.; Kyrilidis, F. L.; Muller, J.; Sorokina, M.; Skolidis, I.; Hamdi, F.; Sadian, Y.; Kastiritis, P. L., Cryo-EM snapshots of a native lysate provide structural insights into a metabolon-embedded transacetylase reaction. *Nat. Commun.* **2021**, *12* (1).
71. Butkovich, N.; Tucker, J. A.; Ramirez, A.; Li, E. Y.; Meli, V. S.; Nelson, E. L.; Wang, S. W., Nanoparticle vaccines can be designed to induce pDC support of mDCs for increased antigen display. *Biomaterials Science* **2022**, *11* (2), 596-610.
72. Lopez-Sagaseta, J.; Malito, E.; Rappuoli, R.; Bottomley, M. J., Self-assembling protein nanoparticles in the design of vaccines. *Computational and Structural Biotechnology Journal* **2016**, *14*, 58-68.
73. Tunyasuvunakool, K.; Adler, J.; Wu, Z.; Green, T.; Zielinski, M.; Zidek, A.; Bridgland, A.; Cowie, A.; Meyer, C.; Laydon, A.; Velankar, S.; Kleywegt, G. J.; Bateman, A.; Evans, R.; Pritzel, A.; Figurnov, M.; Ronneberger, O.; Bates, R.; Kohl, S. A. A.; Potapenko, A.; Ballard, A. J.; Romera-Paredes, B.; Nikolov, S.; Jain, R.; Clancy, E.; Reiman, D.; Petersen, S.; Senior, A. W.; Kavukcuoglu, K.; Birney, E.; Kohli, P.; Jumper, J.; Hassabis, D., Highly accurate protein structure prediction for the human proteome. *Nature* **2021**, *596* (7873), 590–596.
74. Li, L.; Fierer, J. O.; Rapoport, T. A.; Howarth, M., Structural Analysis and Optimization of the Covalent Association between SpyCatcher and a Peptide Tag. *J. Mol. Biol.* **2014**, *426* (2), 309-317.
75. Bruun, T. U. J.; Andersson, A. M. C.; Draper, S. J.; Howarth, M., Engineering a Rugged Nanoscaffold To Enhance Plug-and-Display Vaccination. *ACS Nano* **2018**, *12* (9), 8855-8866.
76. Tan, T. K.; Rijal, P.; Rahikainen, R.; Keeble, A. H.; Schimanski, L.; Hussain, S.; Harvey, R.; Hayes, J. W. P.; Edwards, J. C.; McLean, R. K.; Martini, V.; Pedrera, M.; Thakur, N.; Conceicao, C.; Dietrich, I.; Shelton, H.; Ludi, A.; Wilsden, G.; Browning, C.; Zagrajek, A. K.; Bialy, D.; Bhat, S.; Stevenson-Leggett, P.; Hollinghurst, P.; Tully, M.; Moffat, K.; Chiu, C.; Waters, R.; Gray, A.; Azhar, M.; Mioulet, V.; Newman, J.; Asfor, A. S.; Burman, A.; Crossley, S.; Hammond, J. A.; Tchilian, E.; Charleston, B.; Bailey, D.; Tuthill, T. J.; Graham, S. P.; Duyvesteyn, H. M. E.; Malinauskas, T.; Huo, J. D.; Tree, J. A.; Buttigieg, K. R.; Owens, R. J.; Carroll, M. W.; Daniels, R. S.; McCauley, J. W.; Stuart, D. I.; Huang, K. Y. A.; Howarth, M.; Townsend, A. R., A COVID-19 vaccine candidate using SpyCatcher multimerization of the SARS-CoV-2

- spike protein receptor-binding domain induces potent neutralising antibody responses. *Nat. Commun.* **2021**, *12* (1), 16.
77. Brune, K. D.; Leneghan, D. B.; Brian, I. J.; Ishizuka, A. S.; Bachmann, M. F.; Draper, S. J.; Biswas, S.; Howarth, M., Plug-and-Display: decoration of Virus-Like Particles via isopeptide bonds for modular immunization. *Sci Rep* **2016**, *6*, 13.
  78. Leneghan, D. B.; Miura, K.; Taylor, I. J.; Li, Y. Y.; Jin, J.; Brune, K. D.; Bachmann, M. F.; Howarth, M.; Long, C. A.; Biswas, S., Nanoassembly routes stimulate conflicting antibody quantity and quality for transmission-blocking malaria vaccines. *Sci Rep* **2017**, *7*, 14.
  79. Sungwa, M.; Susan, T.; Mikkil, J. C.; Adolph, K. R.; Boniface, M. S.; Grundtvig, T. T.; Ali, S.; Agertoug, N. M.; Frederik, S. A., A VAR2CSA: CSP conjugate capable of inducing dual specificity antibody responses. *Afr. Health Sci.* **2017**, *17* (2), 373-381.
  80. Cohen, A. A.; Yang, Z.; Gnanapragasam, P. N. P.; Ou, S. S.; Dam, K. M. A.; Wang, H. Q.; Bjorkman, P. J., Construction, characterization, and immunization of nanoparticles that display a diverse array of influenza HA trimers. *PLOS One* **2021**, *16* (3), e0247963.
  81. Kato, Y.; Abbott, R. K.; Freeman, B. L.; Haupt, S.; Groschel, B.; Silva, M.; Menis, S.; Irvine, D. J.; Schief, W. R.; Crotty, S., Multifaceted Effects of Antigen Valency on B Cell Response Composition and Differentiation In Vivo. *Immunity* **2020**, *53* (3), 548-563.
  82. Chatzikleantous, D.; Schmidt, S. T.; Buffi, G.; Paciello, I.; Cunliffe, R.; Carboni, F.; Romano, M. R.; O'Hagan, D. T.; D'Oro, U.; Woods, S.; Roberts, C. W.; Perrie, Y.; Adamo, R., Design of a novel vaccine nanotechnology-based delivery system comprising CpGODN-protein conjugate anchored to liposomes. *J Control Release* **2020**, *323*, 125-137.
  83. Li, Z. H.; Liu, Z.; Yin, M. L.; Yang, X. J.; Ren, J. S.; Qu, X. G., Combination Delivery of Antigens and CpG by Lanthanides-Based Core-Shell Nanoparticles for Enhanced Immune Response and Dual-Mode Imaging. *Adv. Healthc. Mater.* **2013**, *2* (10), 1309-1313.
  84. Lee, I. H.; Kwon, H. K.; An, S.; Kim, D.; Kim, S.; Yu, M. K.; Lee, J. H.; Lee, T. S.; Im, S. H.; Jon, S., Imageable Antigen-Presenting Gold Nanoparticle Vaccines for Effective Cancer Immunotherapy In Vivo. *Angew. Chem.-Int. Edit.* **2012**, *51* (35), 8800-8805.
  85. Stevens, T. L.; Bossie, A.; Sanders, V. M.; Fernandezbotran, R.; Coffman, R. L.; Mosmann, T. R.; Vitetta, E. S., Regulation of antibody isotype secretion by subsets of antigen-specific helper T cells. *Nature* **1988**, *334* (6179), 255-258.
  86. Carty, S. A.; Riese, M. J.; Koretzky, G. A., Chapter 21 - T-Cell Immunity. In *Hematology (Seventh Edition)*, Hoffman, R.; Benz, E. J.; Silberstein, L. E.; Heslop, H. E.; Weitz, J. I.; Anastasi, J.; Salama, M. E.; Abutalib, S. A., Eds. Elsevier: 2018; pp 221-239.
  87. Nazeri, S.; Zakeri, S.; Mehrizi, A. A.; Sardari, S.; Djadid, N. D., Measuring of IgG2c isotype instead of IgG2a in immunized C57BL/6 mice with Plasmodium vivax TRAP as a subunit vaccine candidate in order to correct interpretation of Th1 versus Th2 immune response. *Experimental Parasitology* **2020**, *216*.
  88. Kasturi, S. P.; Skountzou, I.; Albrecht, R. A.; Koutsonanos, D.; Hua, T.; Nakaya, H. I.; Ravindran, R.; Stewart, S.; Alam, M.; Kwissa, M.; Villinger, F.; Murthy, N.; Steel, J.; Jacob, J.; Hogan, R. J.; Garcia-Sastre, A.; Compans, R.; Pulendran, B., Programming the magnitude and persistence of antibody responses with innate immunity. *Nature* **2011**, *470* (7335), 543-547.
  89. Duggan, J. M.; You, D. H.; Cleaver, J. O.; Larson, D. T.; Garza, R. J.; Pruneda, F. A. G.; Tuvim, M. J.; Zhang, J. X.; Dickey, B. F.; Evans, S. E., Synergistic Interactions of TLR2/6 and TLR9 Induce a High Level of Resistance to Lung Infection in Mice. *Journal of Immunology* **2011**, *186* (10), 5916-5926.

90. Shannon, J. G.; Cockrell, D. C.; Takahashi, K.; Stahl, G. L.; Heinzen, R. A., Antibody-mediated immunity to the obligate intracellular bacterial pathogen *Coxiella burnetii* is Fc receptor- and complement-independent. *BMC Immunology* **2009**, *10*.
91. Fernandes, T. D.; Cunha, L. D.; Ribeiro, J. M.; Massis, L. M.; Lima, D. S.; Newton, H. J.; Zamboni, D. S., Murine Alveolar Macrophages Are Highly Susceptible to Replication of *Coxiella burnetii* Phase II In Vitro. *Infection and Immunity* **2016**, *84* (9), 2439-2448.

## **CHAPTER 4**

# **ENGINEERING PROTEIN NANOPARTICLES CO-DELIVERING MULTIPLE TOLL-LIKE RECEPTOR AGONISTS AND POTENTIAL PANDEMIC INFLUENZA HEMAGGLUTININ H5 TO ENHANCE VACCINE IMMUNOGENICITY AND EFFICACY**

#### 4.1. Abstract

Avian influenza H5N1 is endemic in wild birds, and a zoonotic infection that could be the next pandemic strain. The majority of seasonal and pandemic influenza vaccines are derived from inactivated or attenuated virus propagated in chicken eggs, while more advanced technologies, such as the use of recombinant proteins and adjuvants are under-utilized. Delivery vehicles, such as protein nanoparticles (NPs), for co-delivery of hemagglutinin (HA) antigen and toll-like receptor (TLR) agonists, have the potential to form the next generation of influenza vaccines. In this study, we apply the E2 protein NP platform and the SpyTag/SpyCatcher bioconjugation system to synthesize stable vaccines that simultaneously co-delivered influenza hemagglutinin (H5) antigen, TLR5 agonist flagellin (FliCc), and TLR9 agonist CpG 1826 (CpG), all on one particle (termed H5-FliCc-CpG-E2). *In vitro* assays showed that attachment of flagellin on NPs increased both the inflammatory cytokine production from macrophages and the flagellin's bioactivity by upwards of 30- and 20- fold, respectively. Serology of immunized mice, evaluated by protein microarrays, demonstrated that all the antigen-bound NP formulations elicited greater than 5 times higher IgG antibody responses and broader homosubtypic cross-reactivity than unconjugated antigen alone. IgG1/IgG2c skewing could be modulated by adjuvant type and NP attachment. Conjugation of flagellin to the NP caused significant IgG1 (Th2) skewing, attachment of CpG caused significant IgG2c (Th1) skewing, and simultaneous conjugation of both flagellin and CpG resulted in a balanced IgG1/IgG2c (Th2/Th1) response. Animals immunized with E2-based NP vaccines and subsequently challenged with H5N1 influenza showed 100% survival, and only animals that received adjuvanted NP formulations were also protected against morbidity. This investigation highlights that NP-based delivery of antigen and multiple adjuvants can effectively modulate the strength, breadth, and bias of an immune response against influenza viruses.

## 4.2. Introduction

Subunit vaccines such as recombinant protein vaccines have been shown to be safer than attenuated or inactivated vaccines. However, these recombinant proteins tend to suffer from weaker immunogenicity caused by rapid draining kinetics, reduced immunostimulatory adjuvant capacity, and variant pharmacokinetics of subunit vaccine components.<sup>1,2</sup> For this reason, the inclusion of pattern recognition receptor (PRR) agonists, such as pathogen associated molecular patterns (PAMPs), as immunoenhancing components have been explored with some success, but these molecules suffer from similar issues of differential and reduced pharmacokinetics when administered as soluble adjuvants.<sup>3</sup>

Nanoparticle (NP)-based delivery of vaccine antigen and adjuvant components have shown to be a promising solution by combining the safety and tunability of subunit vaccines with enhanced immunogenicity.<sup>4-6</sup> The increased size of NPs relative to soluble antigen or adjuvant, and the ability to repetitively display antigen or adjuvant give NP platforms intrinsic advantages over conventional subunit vaccines. Studies have shown that dendritic cells preferably take up NPs between 20-500 nm with an optimal uptake of about 20-50 nm.<sup>2,7-9</sup> NPs larger than 20 nm have been shown to exhibit longer retention times within draining lymph nodes.<sup>2,9,10</sup> Investigations have also described size and antigen display topography to play a crucial role in B cell engagement; NPs between ~20-50 nm in diameter with antigen valences greater than 5 have been reported to more effectively engage B cell receptor cross-linking and activation.<sup>2</sup> These size and antigen orientation effects collectively increase antigen-specific responses towards NP-based vaccines.

In light of this, many NP-based vaccines build upon a “pathogen-mimetic strategy” of achieving sizes and structure comparable to that of viral or bacterial pathogens and displaying both protein antigens and PAMP molecules. Our previous studies using the well-established E2 protein NP platform have shown its capability to co-deliver single endosomal toll-like receptor (TLR) agonists with target antigens within a ~25-45 nm particle size, for the development of

cancer and infectious disease vaccines.<sup>11-13</sup> However, the addition of a second, different TLR agonist to the same protein NP scaffold has yet to be explored, despite previous studies that have shown that combinations of agonists for endosomal-based (TLR3, 7, 8, 9) and cell-surface-based (TLR1, 2, 4, 5, 6) TLRs in vaccine formulations can elicit improved immune responses.<sup>14-16</sup> For that reason, in this study we engineer protein NPs capable of co-delivering endosomal and cell-surface TLR agonists with antigen on a single NP, and investigate the prophylactic immune responses elicited by these NPs.

To our knowledge, no study to date has used a NP to co-deliver two different TLR agonists and a target antigen conjugated on the same vaccine particle with consistent and uniform molecular orientation. For example, in the context of nanoparticulate structures, multiple TLR agonists have been co-delivered with protein/peptide antigens, but these have often been in emulsion-based formulations<sup>17-20</sup> or PLGA or lipid nanoparticles<sup>21-24</sup>, the syntheses of which do not allow for the consistent antigen surface display or orientation that is favorable for B cell receptor engagement. Furthermore, in emulsion-based formulations, adjuvants and antigens in the soluble phase of the emulsion are not attached to each other, so diffusion and simultaneous transport of individual components to immune cells after injection is not well-controlled. Others have examined protein-based NPs to co-deliver TLR agonists with antigen; this strategy improves molecular orientation, but these investigations have been limited to only one TLR agonist used<sup>25-28</sup> or two TLR agonists but only one was conjugated to the NP.<sup>29,30</sup>

To build upon this body of work and to test the advantages of multiple-component co-delivery on NPs, we have engineered E2 protein NPs that can conjugate and deliver two TLR agonists (flagellin [a TLR5 agonist] and CpG [a TLR9 agonist]) and influenza H5 antigen on a single NP, attached in a way that displays each component in its native-pathogenic orientation. The most well-studied flagellin is derived from *Salmonella typhimurium*, which does not require glycosylation for adjuvant activity and has been expressed and purified from *E. coli*.<sup>31-34</sup> Flagellin has been shown to elicit Th1 and Th2 immune responses,<sup>35-37</sup> and combining flagellin into H1

influenza vaccine formulations enhanced antibody and T cell responses.<sup>35,36</sup> In the majority of studies, flagellin is solubly co-administered with antigen; however, an alternative strategy genetically incorporated flagellin with a recombinant virus expressing influenza antigen.<sup>35-37</sup> The Th1-skewing TLR9 agonist, CpG 1826, is the second adjuvant conjugated to our current E2 NP vaccine formulations in this study. Our group has previously synthesized CpG-loaded E2 protein NPs and demonstrated their efficient dendritic cell activation capability *in vitro*, as well as potent CD8+ T cell responses in tumor vaccination models.<sup>11,38-40</sup> This protein scaffold can be engineered to encapsulate molecules in its hollow interior (e.g., CpG) and display guest proteins on its surface (e.g., flagellin, antigen).<sup>13,41</sup>

In recent years, the World Health Organization has acknowledged the growing pandemic risk of avian flu (H5N1).<sup>42,43</sup> For this reason, the immunodominant influenza hemagglutinin (HA) protein antigen (subtype H5 A/Vietnam/1194/2004) (H5) was utilized as the model antigen to investigate in this vaccine strategy. Due to the protein nature of flagellin and HA, both can be recombinantly engineered with the SpyTag/SpyCatcher bioconjugation system, allowing for their separate expression and subsequent conjugation to the E2 nanoparticle via spontaneous isopeptide bond formation.<sup>13,44</sup> In this work, we synthesized NPs displaying flagellin, CpG, and HA, investigated the bioactivity of flagellin when displayed on a NP *in vitro*, evaluated the antibodies elicited after immunization, and demonstrated the protection from viral challenge elicited by adjuvanted NPs. Development of a modular vaccine platform capable of improving and directing prophylactic immune responses by the precise delivery of multiple adjuvants and antigen on a NP could prove extremely favorable as a general vaccine approach.

### **4.3. Methods**

#### **4.3.1. Materials**

Chemical and cloning reagents were purchased from Fisher Scientific or New England Biolabs (NEB) unless otherwise noted. DH5 $\alpha$  and BL21(DE3) *E. coli* were used for general cloning



and expression studies, respectively. DNA minipreps and extractions were performed with the QIAprep Spin Miniprep Kit (Qiagen) and GeneJET Gel Extraction Kit (Thermo Fisher Scientific), respectively. DNA primers were synthesized and ordered from Integrated DNA Technologies (IDT). CloneJET PCR cloning kit (Thermo Fisher Scientific) was used for all polymerase chain reactions (PCRs). Plasmid pET11a was used as the expression vector for all protein constructs. HA variants used in the protein arrays were purchased from Sino Biological.<sup>45</sup>

#### 4.3.2. Construction of SpyCatcher-flagellins and SpyCatcher-hemagglutinin fusion proteins

The plasmids encoding the wild type flagellin (FliC) and the cysteine-stabilized flagellin (FliCc) were previously synthesized and generously gifted by Dr. James Swartz.<sup>32</sup> The plasmid containing the SpyCatcher gene (pDEST14-SpyCatcher) was obtained from Addgene. The plasmid containing the hemagglutinin subtype H5 gene was synthesized using RNA obtained from H5N1 virus A/Vietnam/1194/2004 (National Institute for Biological Standards & Controls, South Mimms, UK; catalog # NIBRG-14), which was used as a template for cDNA synthesis. In brief, 140uL allantois fluid from H5N1 (A/Vietnam/1194/2004 reassortant virus preparation) was processed using the QIAamp Viral RNA minikit (Qiagen). To synthesize cDNA of the H5 A/Vietnam/1194/2004 gene from RNA, the forward primer: 5'-TTTGCAATAGTCAGTCTTGTTAAAAGTG-3' and reverse primer: 5'-AATTCTGCATTGTAACGACCC-3' were used. cDNA of the H5 A/Vietnam/1194/2004 gene was then inserted into a pJET cloning vector using a CloneJET PCR cloning kit. To fabricate the well-studied N-terminus truncated form of SpyCatcher (referred to here as SC) the first 24 AA of the native SpyCatcher were deleted.<sup>46,47</sup> To accomplish this, forward primer #1 (introduce deletion and TEV cleavage site) 5'-GATTACGACATCCCAACGACCGAAAACCTGTATTTTCAGGGCGATAGTGCTACCCATATTAAATTCTCAAACG-3', forward primer #2 (introduce 6x-HisTag and endonuclease cut-site) 5'-CATATGTCGTACTACCATCACCATCACCATCACGATTACGACATCCCAACGACCG-3', and

reverse primer 5'-GCTAGCAATATGAGCGTCACCTTTAGTTGCTTTGCC-3' were used. To introduce the endonuclease sites and GS-rich spacer on both FliC and FliC<sub>c</sub> variants for fusion to SpyCatcher, the forward primer was 5'-ATATGCTAGCATGGGATCAGGGGGATCAGGTGGCAGCGGAGCACAAGTGATTAATACAAACAGCCTGTCGC-3' and 5'-ATATGCTAGCATGGGATCAGGGGGATCAGGTGGCAGCGGAATACAAGTGATTAATACAAACGCCTGTCGC-3', respectively, and the reverse primer was 5'-ATATGGATCCTTAACGCAGTAAAGAGAGGACGTTTTTGC-3'. To introduce the endonuclease sites and GS-rich spacer on H5 hemagglutinin for fusion to SpyCatcher, the forward primer was 5'-GCTAGCGGTTTCAGGAACAGCAGGTGGTGGGTCAGGTTCCGATCAGATTTGCATTGGTTACCATG-3' and the reverse primer was 5'-GGATCCTTATATTTGGTAAATTCCTATTGATTCCAATTTTAC-3'. The SC-H5 fusion protein gene was cloned into a pJET vector. A standard Phusion High-Fidelity DNA polymerase protocol was used for PCRs and sequences were confirmed by Azenta (See Appendix A.2.6). The protein was expressed by BioTimes Inc. in a mammalian CHO cell system.

#### 4.3.3. Expression, purification, and characterization of SpyCatcher-Flagellins and SpyCatcher-Hemagglutinin

The SpyCatcher-flagellins were prepared similarly to previously described SpyCatcher fusion proteins.<sup>13,48</sup> Proteins were expressed in *E. coli* as follows: after growing cells to an OD of 0.6-0.9 and induction with 1mM IPTG for 3 h at 37 °C, the cells were pelleted and stored at -80 °C before lysing. Cells were lysed via French press and soluble protein was purified using a HisPur Ni-NTA resin batch protocol (ThermoFisher Scientific). In brief, soluble cell lysates were mixed with equal parts equilibration buffer and applied to a HisPur Ni-NTA affinity spin column using a packing ratio of 1.5 mL of resin per 10 mL of lysate slurry. The lysate incubated with the

resin for 1 h at 4 °C. Wash buffers and elution buffer containing 75 and 150 mM imidazole, and 250 mM imidazole, respectively, were used to attain pure SC-flagellins. Pure protein fractions were collected, and buffer exchanged into PBS to remove imidazole using an Amicon Stirred Cell unit with a 10kDa MWCO Ultracel membrane. The purified protein was characterized by mass spectrometry (Xevo G2-XS QTof) and SDS-PAGE, and bicinchoninic acid assay (BCA) for molecular weight and purity, and protein concentration, respectively. LPS was removed following our protocol used for the E2 protein.<sup>13</sup> Briefly, Triton X-114 was added to the purified protein at 1% (v/v), chilled to 4 °C, vortexed, and heated to 37 °C. The mixture was then centrifuged at 18000 × g and 37 °C for 1 min, and the protein containing aqueous phase was separated from the detergent phase. This total process was repeated 9 times. Residual Triton was removed with detergent removal spin columns. LPS levels were below 0.1 EU per microgram of SC-flagellin protein, and was determined by an LAL ToxinSensor gel clot assay (Genscript).

Expression and purification of SpyCatcher-H5 was performed by BioTimes Inc. in a mammalian Chinese hamster ovary (CHO) cell system. The resulting fusion protein was purified to >90% using Ni-affinity chromatography and was concentrated to 1 mg/ml in PBS with an endotoxin level <0.1 EU per microgram of protein as determined by the LAL method.

#### *4.3.4. CpG and SpyCatcher conjugation onto SpyTag-E2 particles*

The TLR9 agonist CpG 1826 (5'-tccatgacgttctgacgtt-3') (CpG) was synthesized with a phosphorothioated backbone and 5' benzaldehyde modification by Integrated DNA Technologies (IDT). CpG was conjugated to the internal cavity of the ST-E2 nanoparticle as described previously.<sup>38</sup> In brief, the internal cavity cysteines of ST-E2 were reduced with TCEP for 30 min, followed by incubation with the N-(β-maleimidopropionic acid) hydrazide (BMPH) linker for 2 h at room temperature (RT). Unreacted linker was removed using 40 kDa cutoff Zeba spin desalting columns (Pierce). The aldehyde-modified CpG was subsequently added and incubated overnight

at RT. Unreacted CpG was removed by desalting spin columns. Conjugation was estimated by SDS-PAGE and measured by band intensity analysis.

Directly incubating SpyCatcher-flagellins and SpyCatcher-H5 with SpyTag-E2 particles allowed for spontaneous isopeptide bond formation and conjugation. SpyCatcher-flagellins were incubated with ST-E2 NPs at a 0.1:1 and 0.4:1 (SC-flagellin:ST-E2 monomer) molar ratio for 22 h at 4°C to synthesize low- and high-density NPs, respectively. To synthesize H5-loaded NPs, SpyCatcher-H5 was incubated with ST-E2 NPs at a 0.3:1 (SC-H5:ST-E2 monomer) molar ratio, supplemented with 500 mM NaCl, for 22 h at 4°C. SDS-PAGE densitometry analysis with protein standards was used to quantify protein loading onto the particles. Dynamic light scattering (DLS; Malvern Zetasizer Nano-ZS) and transmission electron microscopy (TEM) were used to measure the size, assembly, and monodispersity of the particles. Transmission electron micrographs, on Cu 200 mesh carbon coated grids (Electron Microscopy Sciences) with 2% uranyl acetate-stained nanoparticles, were obtained on a JEM-2100F (JEOL) instrument with a Gatan OneView camera (Gatan).

#### *4.3.5. In vitro characterization of flagellin bioactivity*

To characterize flagellin bioactivity, we used the HEK-Blue hTLR5 reporter cell line (Invivogen), which overexpresses human TLR 5 on its surface and contains an inducible secreted alkaline phosphatase (SEAP) gene. We followed the manufacturer's protocol using HEKblue detection media to evaluate activation. Briefly, in a 96-well tissue culture plate at ~25,000 cells per well, we added concentrations of flagellin ranging between 0.01-1000 ng/ml and incubated with HEK Blue detection media at 37 °C in a CO<sub>2</sub> incubator for 16 h. The enzymatic activity of SEAP was measured using a spectrophotometer plate reader (SpectraMax M2) by absorbance at 630 nm.

To access the activity of flagellin in a more immunologically-relevant cell, the macrophage cell line J774.1 (UCSF cell bank) was employed. Cells were plated at ~100,000 cell per well in 96

well plates and stimulated with 5 ng/ml flagellin for 24 h. The supernatant of cell culture was collected and the concentration of cytokines [CXCL1 (KC), TGF- $\beta$ 1 (Free Active Form), IL-18, IL-23, CCL22 (MDC), IL-10, IL-12p70, IL-6, TNF- $\alpha$ , G-CSF, CCL17 (TARC), IL-12p40, IL-1 $\beta$ ] were measured by a LEGENDplex™ Mouse Macrophage/Microglia Panel (13-plex) (BioLegend), following the manufacturer's instructions.

#### *4.3.6. Mice, immunizations, and challenge*

All animal work was approved by the UCI Institutional Animal Care and Use Committee (IACUC protocol #AUP-18-096) and by the Animal Care and Use Review Office (ACURO) of the U.S. Army Medical Research and Materiel Command (USAMRMC). The laboratory animal resources at UCI are Internationally accredited by the Association for Assessment and Accreditation of Laboratory Animal Care (AAALAC #000238). All virus handling was performed in USDA inspected and approved BSL2+/ABSL2+ facilities. Female C57Bl/6 mice were purchased from Charles River Inc., and housed in standard cages with enrichment. Briefly, 6-8 week old female C57Bl/6 mice (8 mice per group) were immunized with 50  $\mu$ l vaccine formulations via the subcutaneous route (left flank) according to the dosages and schedule shown in Figure 4.4A and 4B, respectively. The mice were weighed daily for approximately two weeks after each injection and monitored for any changes in behavior or appearance. On days 14, 28, and 42 blood was collected via cheek vein into heparinized tubes and plasma stored at -80 until required for use. On day 52 of the study, transiently anesthetized mice were administered  $10^4$  TCID<sub>50</sub>/ml in a volume of 50  $\mu$ l of virus (A/Vietnam/1194/2004 reassortant virus preparation NIBSC, NIBRG-14) via the intranasal route. Mice were monitored daily for behavior and body weight until the endpoint, defined when >20% of the original body weight was lost or 18 days, whichever occurred sooner. Additionally, on day 4 post challenge the lungs of three mice were harvested for viral lung titers by qPCR. Morbidity (transient weight loss or 'partial protection') was defined as maximum weight drop after viral challenge.

Lungs of infected mice (3 per group) were harvested 4 days post infection and lung viral titers were subsequently quantified using qPCR. Briefly, for total RNA extraction, lungs were weighed, mixed with 1 ml of Trizol (Thermo Fisher Scientific), and homogenized using a GentleMacs Tissue Homogenizer (Miltenyi Biotec) applying the RNA-01 program. Then, the total RNA was extracted using Phasemaker-TM tubes following the manufacturer's recommendation (Thermo Fisher Scientific). The RNA sample was stored at -70°C until its use for RT-qPCR. HA5 gene quantification by qPCR was performed based on the World Health Organization information for the molecular detection of influenza viruses, protocol 3 with slight modifications (February 2021). For HA5 gene amplification primers H5HA-205-227v2-For 5'-CGATCTAGATGGAGTGAAGCCTC-3', H5HA-326-302v2-Rev 5'-CCTTCTCCACTATGTAAGACCATTC-3', and the TaqMan probe H5-Probe-239-RVa2 5'-56-FAM-TGTAGTTGA-ZEN-GCTGGATGGCT-3IBkFQ-3' were used. As a positive amplification control the housekeeping gene glyceraldehyde-3-phosphate dehydrogenase (GAPDH) from *Mus musculus* was used by employing primers GADPH-Fw 5'-CAATGTGTCCGTCGTGGATCT-3', GADPH-Rv 5'-GTCCTCAGTGTAGCCCAAGAT-3', and the TaqMan probe GADPH probe 5'-SUN-CGTGCCGCC-ZEN-TGGAGAAACCTGCC-3IABkFQ-3'.<sup>49,50</sup> The quantitative RT-PCR was performed using the kit AgPath-ID™ One-Step RT-PCR Reagents (Thermo Fisher Scientific) following the manufacturer's recommendation. For quantification purposes, an HA5 standard curve was performed with a synthetic linear DNA that contains one copy of the target HA5 sequence. This DNA was serial diluted in base 10 between  $8.3 \times 10^7$  copies/reaction until 8.3 copies/reaction. The qPCR was performed as was described previously but replacing the total RNA sample volume for 5 µl of each standard serial dilution. This single standard curve was always performed with the same RT-qPCR reaction used for all RNA samples analyzed. From this standard curve the Ct value of each RNA sample was converted in HA5 copies/reaction. Finally, was estimated the total copies of HA5 per total RNA extraction and normalized with

respect to the total weight of lungs in milligrams. Thus, each outcome was expressed as gene copies of HA5 per milligram of lung.

#### *4.3.7. Protein Microarrays*

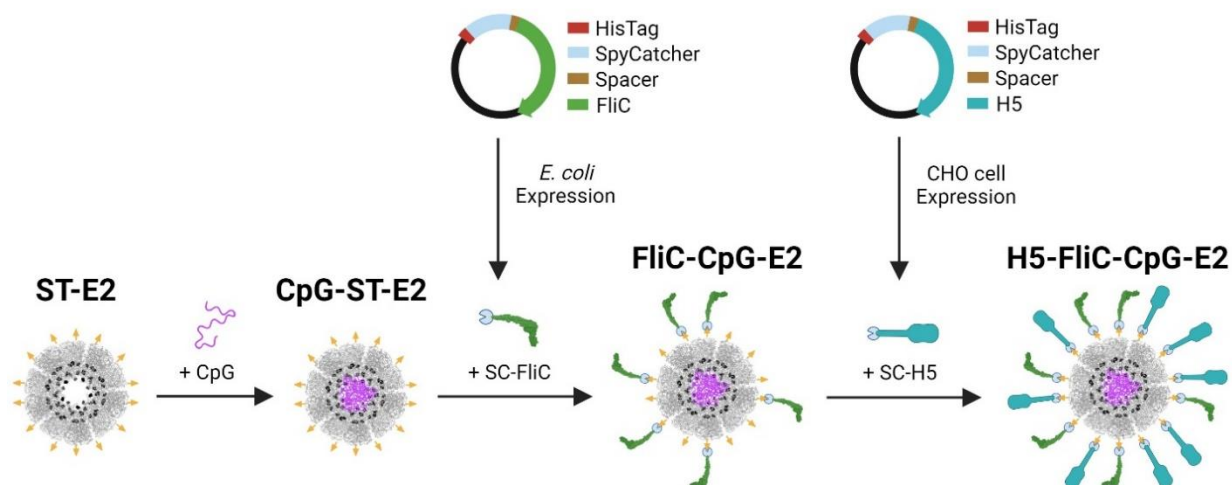
The construction and probing methodology of the influenza protein microarray used for the study has been previously reported.<sup>41,51</sup> Briefly, 28 variants of recombinant H5 subtype hemagglutinin, expressed in mammalian or insect cells, were purchased from Sino Biological Inc. and printed as described previously.<sup>41,51</sup> The array content and raw data are shown in Appendix A.2.7 and Appendix B.17. For probing, plasma samples were diluted 1:100 in protein array blocking buffer. A His-tag containing peptide HHHHHHHHGGGG was used to block anti-polyhistidine antibodies. Plasma samples were incubated with rehydrated arrays in blocking buffer at 4°C overnight and washed in tris-buffered saline (TBS) containing 0.05% Tween 20 (T-TBS) to remove the sera. Bound IgG, IgG1, and IgG2c were detected and visualized using anti-mouse IgG-Alexa Fluor 647, IgG1-Alexa Fluor 647, and IgG2c-Alexa Fluor 488 (Southern Biotech), respectively. The arrays were incubated with the anti-mouse detection antibody for 1 hour at RT. After washing with T-TBS to remove non-specific binding, arrays were air-dried. The fluorescence intensity of each spot was captured using a Tiny Imager Microarray Imaging System. Spot and background intensities were measured using an annotated grid (.gal) file and captured tiff files quantified using ScanArray express software (Perkin Elmer, Waltham, MA, USA). The background of arrays was subtracted from median spot intensity for each antigen and the data was normalized.

#### *4.3.8. Statistical Analyses*

Data describing nanoparticle characterization, including hydrodynamic diameter measurements, molecular weights determined by mass spectrometry, and antigen/nanoparticle ratios, are presented as the mean  $\pm$  standard deviation (SD) of at least three independent

experiments ( $n \geq 3$ ), unless otherwise noted. Statistical analysis of immunization data was carried out by using GraphPad Prism. Mouse data are presented as mean  $\pm$  standard error of the mean (SEM). Antibody and challenge data are gathered from at least 5 independent individuals ( $n \geq 5$ ). Lung titer data is gathered from 3 independent individuals ( $n = 3$ ). Statistical analysis was determined by a one-way ANOVA over all groups, followed by a Tukey multiple comparison test, unless otherwise noted. Mantel-Cox log-rank test was used for survival curve analysis. P-values  $<0.05$  were considered significant.

#### 4.4. Results and Discussion



**Figure 4.1. Schematic of nanoparticle synthesis with two adjuvants, CpG and flagellin (FliC), and the immunodominant influenza antigen hemagglutinin (H5).** CpG is first conjugated into the internal cavity of the SpyTag-E2 (ST-E2) NP. SpyCatcher-fused flagellin (SC-FliC) is then attached to the surface of CpG-ST-E2 NPs via ST/SC bond formation. Lastly, SpyCatcher-fused H5 hemagglutinin (SC-H5) is attached to the surface of FliC-CpG-E2 NPs via the remaining available SpyTags on the E2 NP surface.

##### 4.4.1. Conjugation of TLR agonists flagellin (FliC) and CpG1826 (CpG), and antigen (H5) onto a single E2 nanoparticle

Design of NPs and their individual adjuvant and antigen components. The SpyTag(ST)/SpyCatcher(SC) bioconjugation system was used to conjugate the TLR5 agonist



flagellin (FliC) and immunodominant influenza antigen hemagglutinin (H5), to the external surface of the E2 protein nanoparticle (Figure 4.1). Two forms of flagellin were investigated: wild-type flagellin (FliC) and cysteine-modified flagellin (FliCc).<sup>32</sup> Wild-type flagellin can be expressed in bacterial expression systems but suffers from C-terminus degradation.<sup>32</sup> The cysteine-modified flagellin mutant, FliCc, was previously designed to increase the stability of flagellin in solution via internal cross-links, but it demonstrated 5-10x lower TLR5-specific activity than FliC. In previous investigations, cysteine-modified flagellin showed improved bioactivity in a TLR reporter cell line when loaded on NPs using a click-chemistry. In our studies, we aim to build on these observations by applying flagellin using an alternative chemical conjugation strategy (SpyTag/SpyCatcher) and to examine the resulting bioactivity *in vitro* and *in vivo*.

The E2 NP with 60 STs displayed on its external surface and 60 internal-cavity cysteines for CpG attachment (ST-E2) was utilized in this synthesis strategy.<sup>13</sup> SpyCatcher was genetically fused to the N-terminus of the flagellin and H5 proteins. This ensured that when conjugated to the ST-E2 nanoparticle, flagellin and H5 would be oriented in the same direction as when they are natively presented on *S. typhimurium* and influenza, respectively, exposing relevant activation domains and B cell epitopes, respectively. Soluble protein expression of flagellin fused to SC was observed in *E. coli* (See Appendix B.15). After purification, we achieved >90% purity for SC-fused FliC (SC-FliC) and FliCc (SC-FliCc) and the predicted average molecular weights of ~65.2 kDa (See Appendix B.15; Figure 4.2A). SC fused to H5 (SC-H5) was expressed in a mammalian cell system, allowing for post-translational glycosylation as in natively-expressed H5,<sup>52,53</sup> which has been shown to be important in eliciting conformation-dependent immune responses.<sup>54,55</sup>

Attachment of TLR5 agonist (flagellin) to NP surface. The ST-E2 protein NP allows interior and exterior attachments designed for co-delivery of adjuvants and antigens. To examine the display of, and activation by, flagellin on NPs, we attached each variant of flagellin onto the particles at two different surface densities. Conjugation of FliC and FliCc onto the surface of ST-E2 yielded intact and monodisperse NPs (Figure 4.2; See Appendix B.15). As expected, when

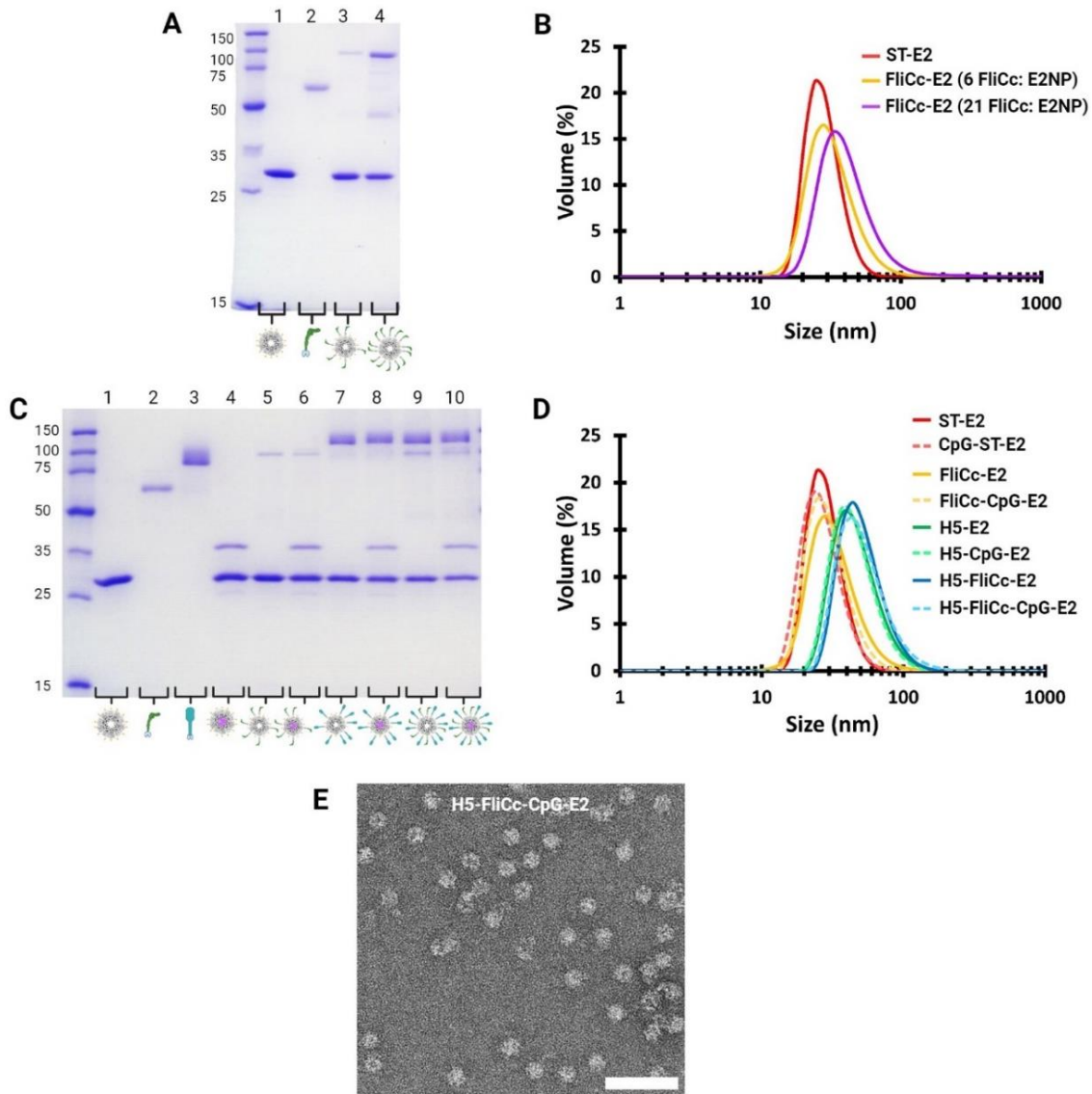
conjugated to either form of flagellin, the ST-E2 monomer molecular weight increases from ~30 kDa to ~95 kDa (Figure 4.2A; See Appendix B.15). Quantification revealed that  $5.9 \pm 1.1$  and  $21.2 \pm 0.8$  FliCc molecules per NP were conjugated for low-density and high-density NPs, respectively. The average hydrodynamic diameters of low-density and high-density loaded FliCc-E2 NPs were  $34 \pm 1.2$  nm and  $46.2 \pm 5.1$  nm, respectively, with the size increase corresponding to the additional number of flagellin per NP (Figure 4.2B). Similar ratios and size changes were also obtained for FliC molecules attached to E2 NPs (See Appendix B.15).

These NPs (low- and high-density FliCc-E2 and FliC-E2 NPs) were used to evaluate the effects of loading TLR5 agonist on NPs for TLR5 activation *in vitro*. Stability assays of the SC-fused flagellins (SC-FliC and SC-FliCc) showed that the cysteine-stabilized flagellin fusion protein (SC-FliCc) was more stable than the wild-type fusion protein (SC-FliC) (See Appendix B.15); we therefore used SC-FliCc for construction of NP vaccine formulations in subsequent *in vivo* studies.

Attachment of TLR9 agonist (CpG 1826) to NP interior. The TLR9 agonist, CpG 1826, was conjugated to the interior of the ST-E2 NP platform via an acid-labile linker (Figure 4.1).<sup>13,38</sup> The SDS-PAGE band at ~37 kDa supports the conjugation of one CpG molecule (~7 kDa) to a ST-E2 monomer, while the band at ~30 kDa reflects unconjugated ST-E2 monomer (Figure 4.2C). Sixty monomers self-assemble into CpG-ST-E2 nanoparticles, with an average hydrodynamic diameter of  $29.9 \pm 2$  nm (Figure 4.2D). Quantification indicated  $16.1 \pm 3.2$  CpG 1826 molecules were encapsulated internally per 60-mer ST-E2 NP, which was consistent with our previously reported studies.<sup>13,38</sup>

Attachment of antigen (influenza H5 hemagglutinin) to NP surface. Conjugation of SC-H5 antigen onto the surface of ST-E2 yielded intact and monodispersed nanoparticles after optimization. When conjugating the NP with H5 antigen, we aimed for a minimum loading of 6 antigens per NP because antigen valences greater than ~5 per NP are reported to be effective for optimal B cell receptor engagement and B cell activation.<sup>2</sup> Thus, based on models predicting steric hindrance at the high surface densities and the activation results discussed below (Figure

4.3), the low-density flagellin-E2 NP was used to enable higher SC-H5 conjugation numbers. Upon SC-H5 attachment, the ST-E2 monomer molecular weight increased by ~80-90 kDa, from ~30 kDa to ~110-120 kDa, consistent with the molecular weight of hemagglutinin conjugation (Figure 4.2C). We confirmed the simultaneous loading of nucleic acid (CpG) and two whole proteins (SC-FliC<sub>c</sub> and SC-H5) on a single NP (Figure 4.2C, lane 10), along with several intermediate combinations of adjuvant and antigen attachment (Figure 4.2C). Quantification estimated that  $19.6 \pm 2.5$  H5 were conjugated to each E2 nanoparticle. H5-E2 and H5-CpG-E2 hydrodynamic diameters were  $48.2 \pm 1.3$  nm and  $46.3 \pm 1.1$  nm, respectively (Figure 4.2D). Combining SC-FliC<sub>c</sub> and SC-H5 in the H5-FliC<sub>c</sub>-E2 and H5-FliC<sub>c</sub>-CpG-E2 NPs further increased the diameters to  $52.3 \pm 0.3$  nm and  $50.3 \pm 2.4$  nm, respectively (Figure 4.2D). TEM images confirmed intact monodisperse NPs of the complete dual-adjuvant with antigen particle (H5-FliC<sub>c</sub>-CpG-E2) (Figure 4.2E). These stable NPs were then used *in vivo* to evaluate the prophylactic vaccine potential of simultaneous delivery of antigen and adjuvants uniformly attached to a single delivery vehicle.



**Figure 4.2. Synthesis of ST-E2 nanoparticles conjugated with CpG, SC-FliC, and/or SC-H5.** (A) SDS-PAGE showing nanoparticles with ~6 and ~21 SC-FliC loaded on the external surface. Lanes: 1. ST-E2; 2. SC-FliC; 3. FliC-E2 (6 FliC: E2NP); 4. FliC-E2 (21 FliC: E2NP).  $MW_{ST-E2} = 30.2$  kDa,  $MW_{SC-FliC} = 65.2$  kDa,  $MW_{FliC-E2} = 95.4$  kDa. (B) Hydrodynamic diameters of FliC-E2 NPs with ~6 and ~21 SC-FliC per nanoparticle conjugated to the external surface. (C) SDS-PAGE of the H5-FliC-CpG-E2 nanoparticle vaccine showing conjugation of CpG, SC-FliC, and SC-H5 individually and combined on a single nanoparticle. Lanes: 1. ST-E2; 2. SC-FliC; 3. SC-H5; 4. CpG-ST-E2; 5. FliC-E2; 6. FliC-CpG-E2; 7. H5-E2; 8. H5-CpG-E2; 9. H5-FliC-E2; 10. H5-FliC-CpG-E2.  $MW_{ST-E2} = 30.2$  kDa,  $MW_{SC-FliC} = 65.2$  kDa,  $MW_{SC-H5} = 71.4$  kDa,  $MW_{CpG} = 6.6$  kDa,  $MW_{FliC-E2} = 95.4$  kDa,  $MW_{H5-E2} = 101.6$  kDa,  $MW_{CpG-ST-E2} = 36.8$  kDa,  $MW_{FliC-CpG-E2} = 102$  kDa,  $MW_{H5-CpG-E2} = 108.2$  kDa. SC-H5 protein migrates between approximately 80-90 kDa on SDS-PAGE due to glycosylation. SC-H5 conjugates run ~10-20 kDa higher than expected on SDS-PAGE due to glycosylation. (D) Hydrodynamic diameters of H5-E2 NPs showing physical stability and monodispersity of nanoparticles and shifts in size upon conjugation with adjuvants. (E) Representative TEM image of the H5-FliC-CpG-E2 nanoparticles. Scale bar = 100 nm.

#### *4.4.2. Attachment of flagellin onto nanoparticles increases flagellin bioactivity*

Flagellin variants (SC-FliC and SC-FliCc) were conjugated to ST-E2 NPs, and the resulting bioactivities were evaluated using a hTLR5 reporter cell line. SC-FliC alone (not loaded on NPs) was ~10 times more active than SC-FliCc alone, which is consistent with previously reported results (Figure 4.3A, B).<sup>32</sup> Attaching SC-FliC and SC-FliCc on NPs at a low-density of ~6 flagellin (per ST-E2 NP) significantly increased the activity of the flagellins, from average EC50s of ~30 and ~300 ng/ml (for unbound FliC and FliCc, respectively) to EC50s of ~8 and ~15 ng/ml (for FliC-E2 and FliCc-E2, respectively) (Figure 4.3A, B). At this low-density surface loading, SC-FliCc activity increased by more than an order of magnitude when NP-bound and the disparity between SC-FliC and SC-FliCc was reduced from ~10x to only ~2x. This phenomenon of loading immunomodulatory motifs onto NPs has been shown to have significant benefits for cell recognition, as increasing the valency and density of a motif can make receptor engagement more likely and activation stronger.<sup>2,56</sup>

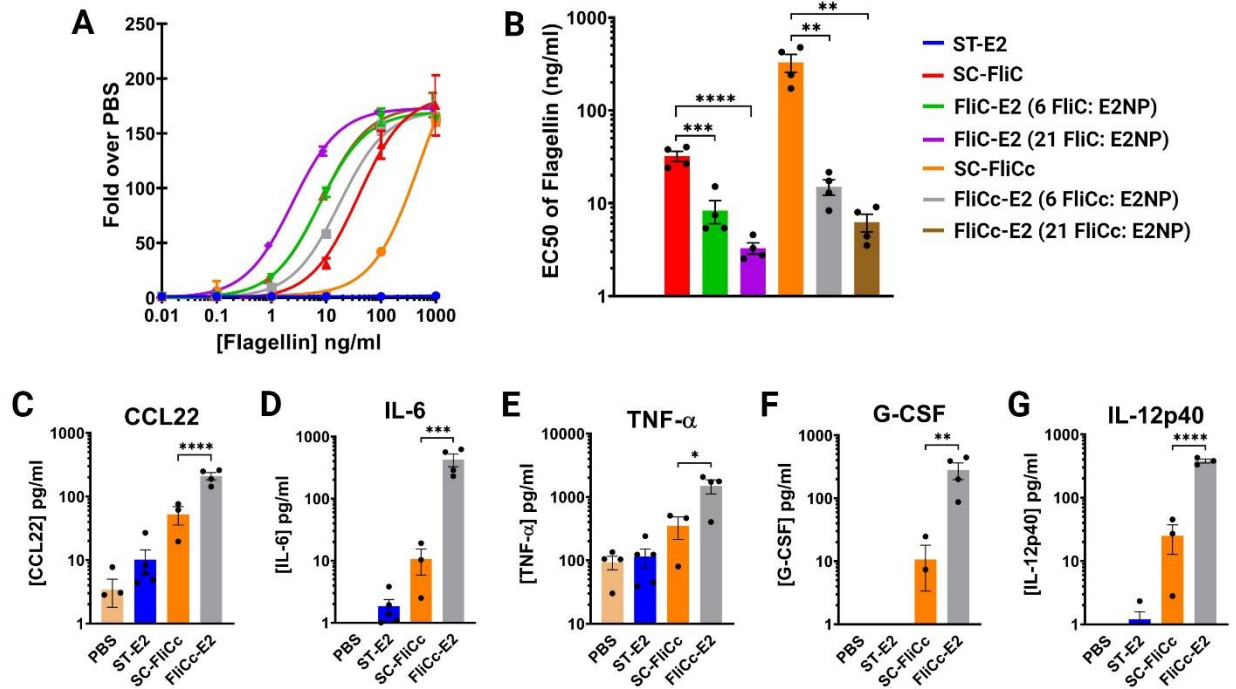
At high-density loading of ~21 flagellin per ST-E2 NP, activation increased further to EC50s of ~3 and ~6 ng/ml for SC-FliC and SC-FliCc, respectively, but was not significantly higher than the response to the low-density loaded NPs (Figure 4.3A, B). Like the low-density NPs, by loading flagellin on NPs, the discrepancy in bioactivity between SC-FliCc and SC-FliC was significantly reduced to an extent that SC-FliCc becomes nearly as active as SC-FliC. Given this result, together with the higher observed stability of SC-FliCc (See Appendix B.15), subsequent studies utilized SC-FliCc at the lower surface density.

#### *4.4.3. FliCc-E2 nanoparticles promote inflammatory cytokine release by macrophages*

To examine the effect of loading flagellin on NPs in a more immunologically-relevant cell type, we examined macrophage activation by incubating cells with flagellin (unbound SC-FliCc and low-density FliCc-E2 NPs) and quantifying secreted inflammatory cytokines. We consistently observed activation of five cytokines (CCL22, IL-6, TNF- $\alpha$ , G-CSF, and IL-12p40), which

overlapped with the cytokine production reported from previous studies utilizing this macrophage cell line for flagellin activation (IL-6, TNF- $\alpha$ , GCSF, and IL-1 $\beta$ ).<sup>57-59</sup> In our investigation, inflammatory cytokine secretion was significantly increased by conjugation of SC-FliCc to ST-E2 NPs, relative to SC-FliCc alone (Figure 4.3).

Interestingly, these observed cytokines are associated with both innate and adaptive immunity. Specifically, CCL22 production increased by ~4x, from an average of 53 pg/ml (for free SC-FliCc) to 210 pg/ml when SC-FliCc was attached to the NP (FliCc-E2; Figure 4.3C). CCL22 is attributed to adaptive immune responses as a chemoattractant for T cells and dendritic cells, and it is a regulator of Th2-type immune responses.<sup>60,61</sup> After conjugating SC-FliCc onto the NP, IL-6 production increased by 40x, from 10.6 pg/ml (free SC-FliCc) to 425 pg/ml (FliCc-E2). IL-6 is connected to both proinflammatory and anti-inflammatory immune responses, and it is often recognized as an acute phase response regulator and stimulator of adaptive immune responses.<sup>62</sup> TNF- $\alpha$ , a macrophage regulator and acute inflammation activator<sup>63,64</sup>, also increased from 350 pg/ml to 1490 pg/ml. G-CSF, an innate immune system cytokine that regulates neutrophil maturation,<sup>65,66</sup> increased by nearly 30x, from 10.7 pg/ml to 280 pg/ml for cells incubated with SC-FliCc and FliCc-E2, respectively. IL-12p40 production increased by more than 10x, from 25 pg/ml secreted by SC-FliCc alone to 380 pg/ml secreted when SC-FliCc was loaded on the NP. IL-12p40 is a cytokine that is part of both the innate and adaptive immune response as a macrophage chemoattractant and promoter of T cell differentiation and proliferation.<sup>67-69</sup> Notably, IL-1 $\beta$  levels were below detection in our activation studies. In all this unique cytokine profile is consistent with the many observations of flagellin eliciting Th1 and/or Th2 responses.<sup>30,70,71</sup>



**Figure 4.3. Conjugation of SC-FliCc onto ST-E2 NPs increases activation of TLR5 reporter cells and macrophages, relative to SC-FliCc alone.** (A) Representative experiment of the activation of HEK-blue hTLR5 cells after 16h incubation. Absorbance of each group was normalized to the absorbance of PBS-only incubation. EC50 was determined using a sigmoidal dose-response curve-fit of each group. (B) Average EC50 concentrations of flagellin from HEK-blue hTLR5 activation. Panels C-G: Cytokine secretion from J774.1 macrophage cells after 24 h incubation. (C) CCL22 (One PBS data point is between 0-1 pg/ml), (D) IL-6 (PBS data are between 0-1pg/ml), (E) TNF- $\alpha$ , (F) G-CSF (PBS and ST-E2 data are between 0-1 pg/ml. One data point of SC-FliCc is between 0-1 pg/ml), (G) IL-12p40 (PBS data are between 0-1 pg/ml. Three ST-E2 data points are between 0-1 pg/ml). Data in panel B is presented as an average  $\pm$  SEM of 4 independent experiments ( $n = 4$ ). Data in panel C-G is presented as an average  $\pm$  SEM of greater than or equal to 4 independent experiments ( $n \geq 4$ ). Statistical significance was determined by one-way ANOVA followed by a Tukey multiple comparisons test. \* $p < 0.05$ , \*\* $p < 0.005$ , \*\*\* $p < 0.0005$ , \*\*\*\* $p < 0.0001$ .

#### 4.4.4. Attaching H5 hemagglutinin onto nanoparticles elicits significantly higher IgG responses than soluble SC-H5 alone

We investigated the antibody response elicited by different vaccine formulations after a prime and boost immunization in C57Bl/6 mice (Figure 4.4A, B). The study included different combinations of adjuvant (flagellin, CpG), HA antigen (H5), and bound (or unbound) to the E2 NP, described in Figure 4.4A. Sera from each animal was probed against HA protein microarrays

displaying 28 variants of H5 (See Appendix B.17; See Appendix A.2.7) including the subtype H5 used in the vaccine formulations and immunizations (A/Vietnam/1194/2004). Immunizing with the SC-H5 antigen alone (no NP) elicited the lowest H5-specific IgG response after 42 days (Figure 4.4C). Strikingly, when SC-H5 was displayed on ST-E2 nanoparticles (H5-E2 NPs), with or without the TLR adjuvants, H5-specific IgG antibody response significantly increased relative to immunization with SC-H5 alone (Figure 4.4C). H5-E2 NPs elicit >5 times greater IgG antibody responses toward H5 by simply displaying the antigen on the NP scaffold. H5-E2 also elicited observably higher H5-specific IgG responses compared to the formulation with all antigen and adjuvant vaccine components present but unconjugated (SC-H5 + SC-FliC<sub>c</sub> + CpG + E2 [without ST]) (Figure 4.4C). This demonstrates that simply displaying antigen on a NP can produce adjuvating magnitudes similar to, or even higher than, having two highly specific PRR targets (flagellin and CpG) soluble in the formulation. It has been previously reported that NP size and repetitive antigen display can play a crucial role in B cell receptor engagement and B cell activation<sup>2,72,73</sup> Our data supports this premise that B cell activation can be augmented by the decoration of NPs with repetitive epitopes which mimic natural pathogens such as viruses, and can yield strong innate responses by increasing uptake from antigen-presenting cells and enabling binding and simultaneous activation of multiple B cell receptors.<sup>2,74</sup>

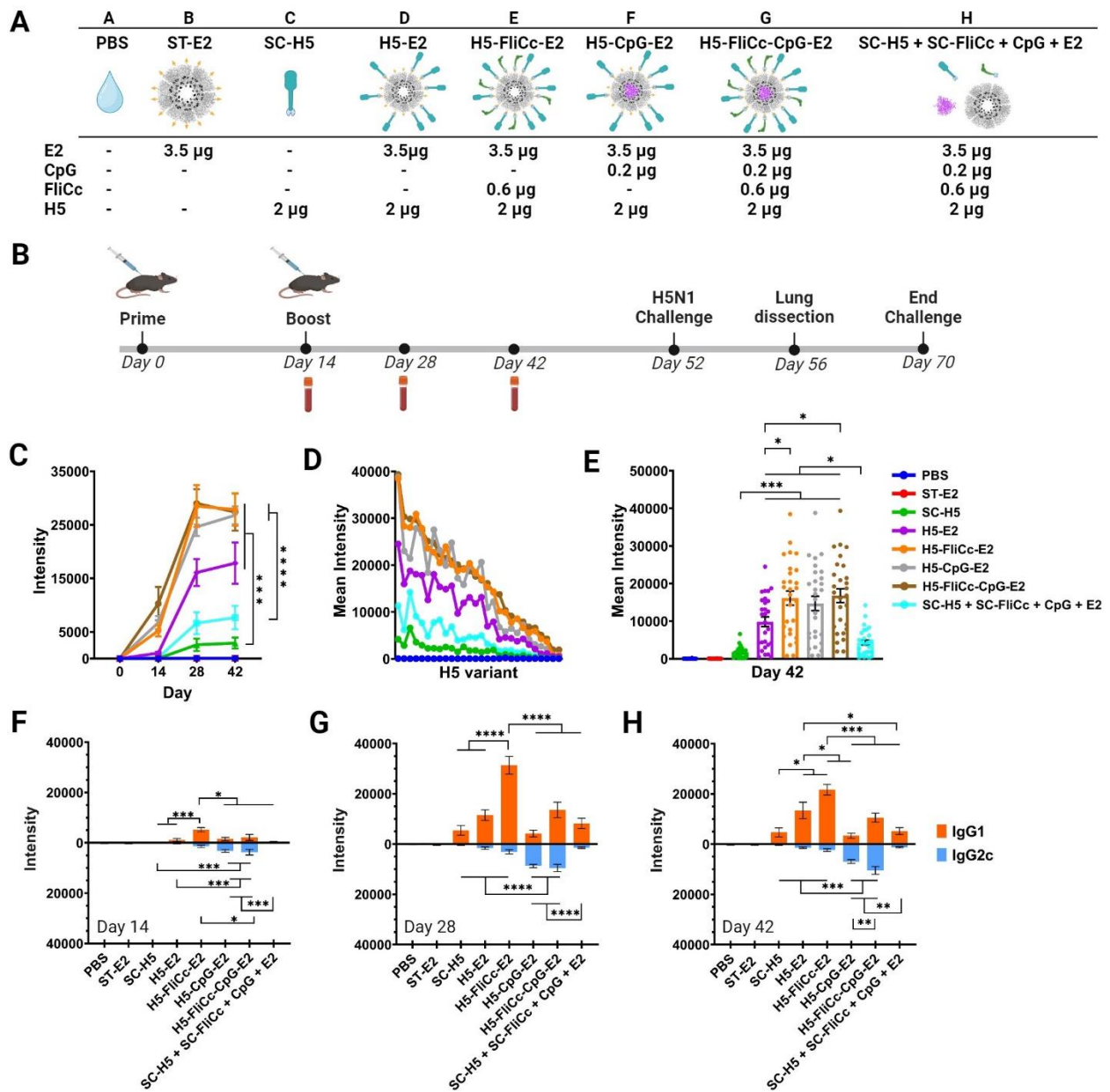
#### *4.4.5. One or two adjuvants attached to a nanoparticle elicits significantly higher IgG responses than two co-administered soluble adjuvants*

We examined the effects of attaching the adjuvants to the NP vaccines, compared to unconjugated adjuvants. Typically, approximately 1-100 µg CpG and approximately 0.5-10 µg flagellin have been used as soluble adjuvants for *in vivo* immunizations.<sup>11,31,37,39,75-78</sup> In each of our formulations, the dosage of CpG and flagellin was ~0.2 µg and ~0.6 µg, respectively, both of which lie at the low end of dosage amounts for typical immunization studies. The total IgG responses obtained with CpG-E2- and FliC<sub>c</sub>-E2-based formulations (H5-CpG-E2 and H5-FliC<sub>c</sub>-



E2, respectively) were relatively high and comparable to one another (Figure 4.4C). Unexpectedly, the combination of CpG and flagellin both loaded together onto one NP (H5-FliCc-CpG-E2) did not increase the total IgG response above the effects of a single adjuvant loaded onto the NP (H5-CpG-E2 or H5-FliCc-E2), despite being conjugated to agonists for two different TLR receptors. This may be in part due to both adjuvants primarily signaling through the MyD88 pathway to activate NFκB leading to the secretion of inflammatory cytokines.<sup>79</sup>

Interestingly, loading a single adjuvant onto a NP (H5-CpG-E2 or H5-FliCc-E2) or both adjuvants onto a NP (H5-FliCc-CpG-E2) elicited significantly stronger IgG responses than having the equivalent amounts of both soluble adjuvants dosed concurrently (SC-H5 + SC-FliCc + CpG + E2) (Figure 4.4C). Encapsulating CpG in a particle has been shown to activate antigen presenting cells at significantly lower concentrations than unbound CpG, indicating the advantage for CpG-NP conjugation for eliciting increased immune response.<sup>38</sup> Other studies have also shown that NPs capable of simultaneously delivering flagellin or CpG, together with antigen, can increase the immune response mounted against the target antigen.<sup>13,29,39</sup> In our formulations, CpG was encapsulated within a NP to increase uptake efficiency of CpG, and flagellin was displayed onto a NP to increase TLR5 receptor engagement of flagellin, both properties of which could increase the dose of CpG and flagellin that an individual cell receives upon interacting with the E2 NP (relative to unbound CpG or flagellin).



**Figure 4.4. Antibody response elicited by H5-FliCc-CpG-E2 dual-adjutant nanoparticle formulations.** (A) Table describing each formulation and its individual components. The mole amounts of each component are shown in Appendix B.16. SC-H5 is colored blue, SC-FliCc is green, CpG is magenta, and ST-E2 NP is grey. To avoid conjugation from occurring during immunization the E2 NP used in group H did not have SpyTag. (B) Immunization schedule and challenge timeline. (C) H5-specific IgG response in plasma on days 0, 14, 28, and 42. This response is specific to antigen used in the vaccination (H5 variant A/Vietnam 1194/ 2004). (D) Homosubtypic IgG response to 28 different variants of H5, from day 42 plasma. Each column of spots corresponds to the antibody response to a unique H5 antigen variant, with each spot being an average response from  $n=8$  mice. (E) Box plot of homosubtypic IgG response to H5 variants at day 42. Each spot corresponds to response to a different H5 variant ( $n=8$  mice). Plotted is average  $\pm$  SEM of 28 variants. (F) H5-specific IgG1/IgG2c response on day 14 (H5 variant A/Vietnam 1194/ 2004). (G) H5-specific IgG1/IgG2c response on day 28 (H5 variant A/Vietnam

1194/ 2004). (H) H5-specific IgG1/IgG2c response on day 42 (H5 variant A/Vietnam 1194/ 2004). Data in panel C is presented as an average  $\pm$  SEM of 8 individual mice ( $n = 8$ ). Statistical significance was determined by one-way ANOVA followed by a Tukey multiple comparisons test of day 42 data. Data in panel E is presented as an average  $\pm$  SEM of 28 individual signals ( $n = 28$ ). Statistical significance was determined by one-way ANOVA followed by a Tukey multiple comparisons test. Data in panels F, G, H is presented as an average  $\pm$  SEM of 8 individual mice ( $n = 8$ ). Statistical significance was determined by one-way ANOVA followed by a Tukey multiple comparisons test. \* $p < 0.05$ , \*\* $p < 0.005$ , \*\*\* $p < 0.0005$ , \*\*\*\* $p < 0.0001$ .

#### 4.4.6. E2-bound formulations elicited higher homosubtypic cross-reactivity amongst H5 variants (relative to unbound antigen or adjuvants)

The breadth of the antibody response elicited by the vaccine formulations was examined by quantifying subtype cross-reactivity on the protein microarrays. We demonstrate that attaching SC-H5 on ST-E2 NPs (i.e., H5-E2) enhances antibody breadth relative to unbound SC-H5. Shown in Figures 4.4D and 4.4E are IgG profiles for day 42 sera towards 28 variants of H5 (variants listed in Appendix A.2.7). The plot in Figure 4.4D shows response intensities for each vaccine group (mean of  $n=8$  mice) against all H5 hemagglutinins printed on the microarray, spanning H5 variants 1 through 28 (left to right on horizontal axis). The data for individual H5 variants are also shown in the box plots in Figure 4.4E. Displaying SC-H5 on ST-E2 NPs (H5-E2) not only significantly increased homosubtypic cross-reactivity relative to SC-H5 alone ( $p < 0.0005$ ) (Figure 4.4D, E), but also elicited significantly higher cross-reactivity than SC-H5 co-administered with unbound CpG and SC-FliCc (SC-H5 + SC-FliCc + CpG + E2) ( $p < 0.05$ ) (Figure 4.4D, E). All NP formulations with single or both adjuvants conjugated also elicited significantly higher homosubtypic cross-reactivities than the unconjugated dual adjuvant formulation (SC-H5 + SC-FliCc + CpG + E2) (Figure 4.4D, E). This demonstrates that although the same amount of adjuvant was administered *in vivo* in these studies, attachment to the E2 NP significantly increases their effect on the immune response at this dose.

The addition of CpG onto H5-E2 NPs (H5-CpG-E2) increases the average of its homosubtypic cross-reactivity compared to H5-E2 NPs alone; however, only when SC-FliCc is attached (H5-FliCc-E2 and H5-FliCc-CpG-E2) does its homosubtypic cross-reactivity significantly

increase above H5-E2 NPs alone ( $p < 0.05$ ) (Figure 4.4E). Homosubtypic cross-reactivity of antibodies generated by the H5 (A/Vietnam/1194/2004) vaccine is mediated by B cell clones that recognize shared epitopes across drift variants.<sup>80</sup> Homosubtypic cross-reactivity produced by the H5-E2 vaccine reported here is significant, as it may offer a path to providing protection against drift variants. Current seasonal influenza vaccines elicit antibodies that are highly specific to the immunizing variant;<sup>81-83</sup> consequently, seasonal vaccines need to be modified each year in response to antigenic drift. Avian influenza H5N1 is endemic in wild birds. It is also known for causing sporadic zoonotic infections in humans and therefore has potential to cause pandemics.<sup>42,43</sup> A vaccine able to provide broader protection than conventional inactivated or attenuated virus formulations, accomplished through the use of adjuvants and/or nanoparticles, would reduce the need for annual reformulations in the case of seasonal vaccines, and improved anticipatory protection against potentially emerging pandemic influenzas.

#### *4.4.7. IgG1 and IgG2c antibody responses can be modulated by adjuvant type and attachment on nanoparticle*

Sera on days 14, 28 and 42 were probed using microarrays for H5-specific IgG1 and IgG2c using isotype-specific secondary antibodies (Figure 4.4F, G, H). Antibody class switching to IgG1 and IgG2c is frequently used as a surrogate marker for Th2 and Th1 immune responses, respectively.<sup>13,84-86</sup> Profiles of the IgG1 and IgG2c antibody responses suggest modulation capabilities that depend on the adjuvant used and whether it was loaded on the E2 nanoparticle (Figure 4.4F, G, H). Signs of IgG1/IgG2c response skewing are observed as early as day 14 for E2 NP formulations after only a prime immunization, while SC-H5 antigen alone or soluble co-administration of SC-H5, SC-FliCc, CpG, and E2 did not elicit strong enough responses for detection (Figure 4.4F). By day 28, the IgG1/IgG2c responses of each formulation were heightened, with day 42 responses being comparable in magnitude while maintaining subclass skewing (Figure 4.4G, H).

To characterize the IgG1/IgG2c bias for each formulation, we focused on data from day 42. Soluble SC-H5 antigen elicited a weak total IgG response that was biased toward IgG1 (Th2) (Figure 4.4H). Loading SC-H5 onto NPs (H5-E2) significantly increased total IgG and retained the IgG1-bias that was observed for SC-H5 alone (Figure 4.4H). The addition of SC-FliCc conjugated to the H5-E2 NP (H5-FliCc-E2) further significantly increased IgG1 production without altering Th2 bias (Figure 4.4H). Flagellin has been utilized as an adjuvant in numerous vaccine formulations and has been shown to elicit Th1- and/or Th2-type responses.<sup>35-37,87,88</sup> The exact mechanisms for the reasons that flagellin elicits a Th1 or Th2 bias response are still being studied, but some have attributed these observations to be antigen-specific or dependent on certain cell-specific stimulations by flagellin.<sup>30,57,87-91</sup> In our hands, it appears that flagellin did not change the baseline Th2 bias elicited by SC-H5 alone and the H5-E2 NP. In contrast, when CpG was internally loaded into the ST-E2 NP (H5-CpG-E2), the total IgG response significantly increased (relative to SC-H5 antigen alone) and the response shifted toward Th1 bias, with significant decrease of IgG1 and significant increase of IgG2c, compared to H5-E2 NPs alone (Figure 4.4H). The Th1-skewing property of CpG is consistent with other studies.<sup>92-95</sup> In our previous studies, we also showed the capacity of E2 NPs to elicit CD8+ mediated anti-tumor immunity when conjugated with tumor peptide antigens and administered with CpG.<sup>11,12</sup>

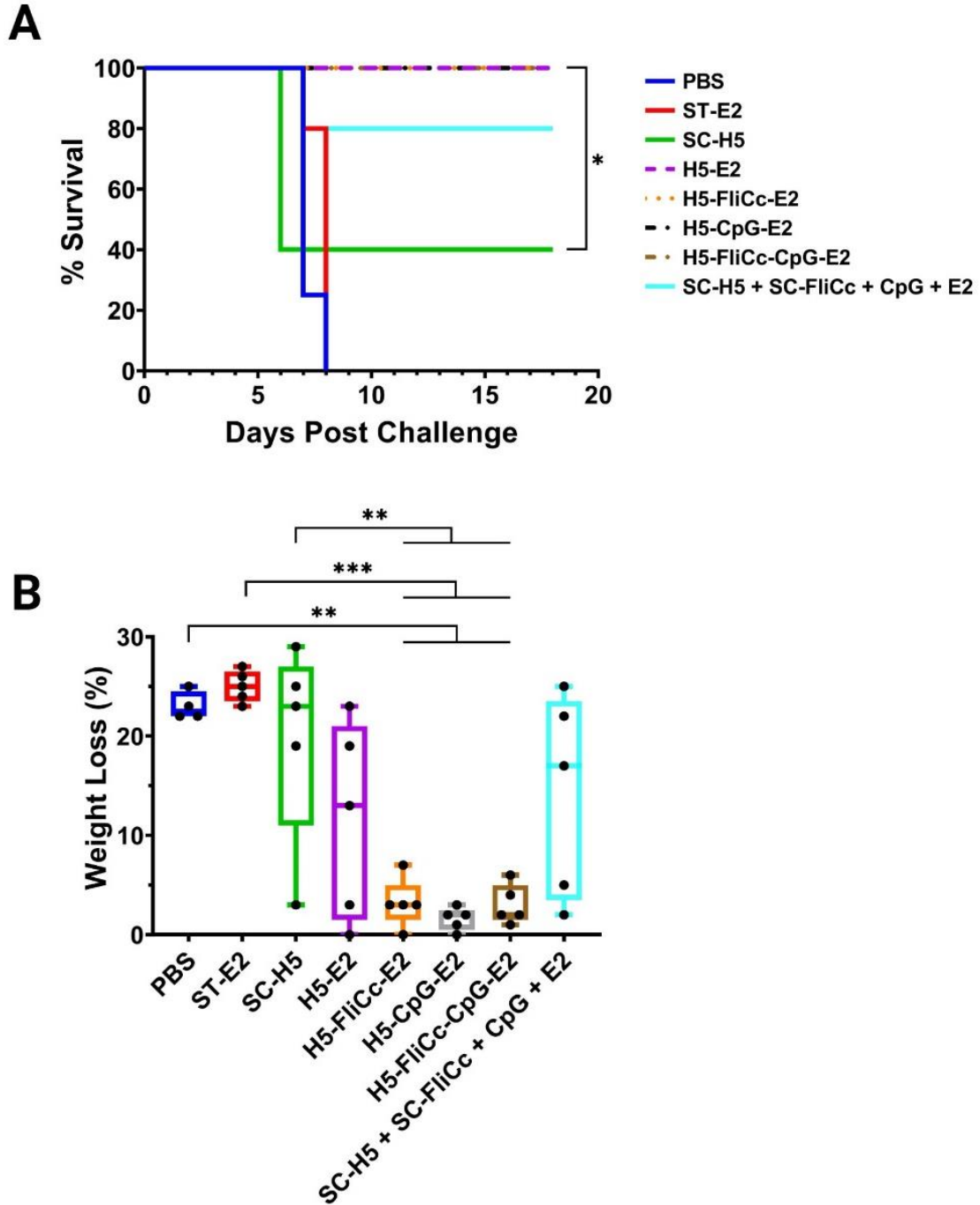
Given the Th2 and Th1 profiles observed from using SC-FliCc and CpG, respectively, it was expected that combining the two adjuvants together may give a more balanced Th2/Th1 response. Surprisingly, when soluble SC-H5 antigen and both adjuvants were co-administered without conjugation (SC-H5 + SC-FliCc + CpG + E2), the antibody response magnitude and immune response biases did not differ significantly from immunizing with SC-H5 antigen alone (Figure 4.4H). This could be that the adjuvant dosages administered here are too low to yield a response for the unconjugated soluble forms.<sup>11,31,37,39,75-78</sup> However, when all components of the vaccine formulation were conjugated to the ST-E2 NP (H5-FliCc-CpG-E2) a distinctive immune response was observed. Having both flagellin and CpG conjugated to the nanoparticle elicited a

balanced IgG1/IgG2c response (Figure 4.4H). Although antibody responses have conventionally been the focus of evaluating influenza vaccine efficacy, more recent studies have shown that cell-mediated responses are also valuable.<sup>96-98</sup> T cells can recognize epitopes that can be highly conserved between variants located within the structure of antigens. Our data shows the ability of our NP platform to skew IgG responses toward IgG2c, suggesting a stronger Th1 CD4 T cell-mediated response, which may have benefits in the context of influenza vaccine design.<sup>97,99</sup> The ability to precisely modulate the ratio of Th1/Th2 immune response by using a NP platform conjugated with different TLR agonists is novel and significant, as the majority of adjuvants used in FDA-approved human vaccines primarily stimulate one type of immunity; for example, the most popular adjuvant is alum, which primarily stimulates Th2-biased immunity.<sup>79,100</sup>

#### *4.4.8. E2 nanoparticle formulations protect mice from lethal H5N1 influenza challenge*

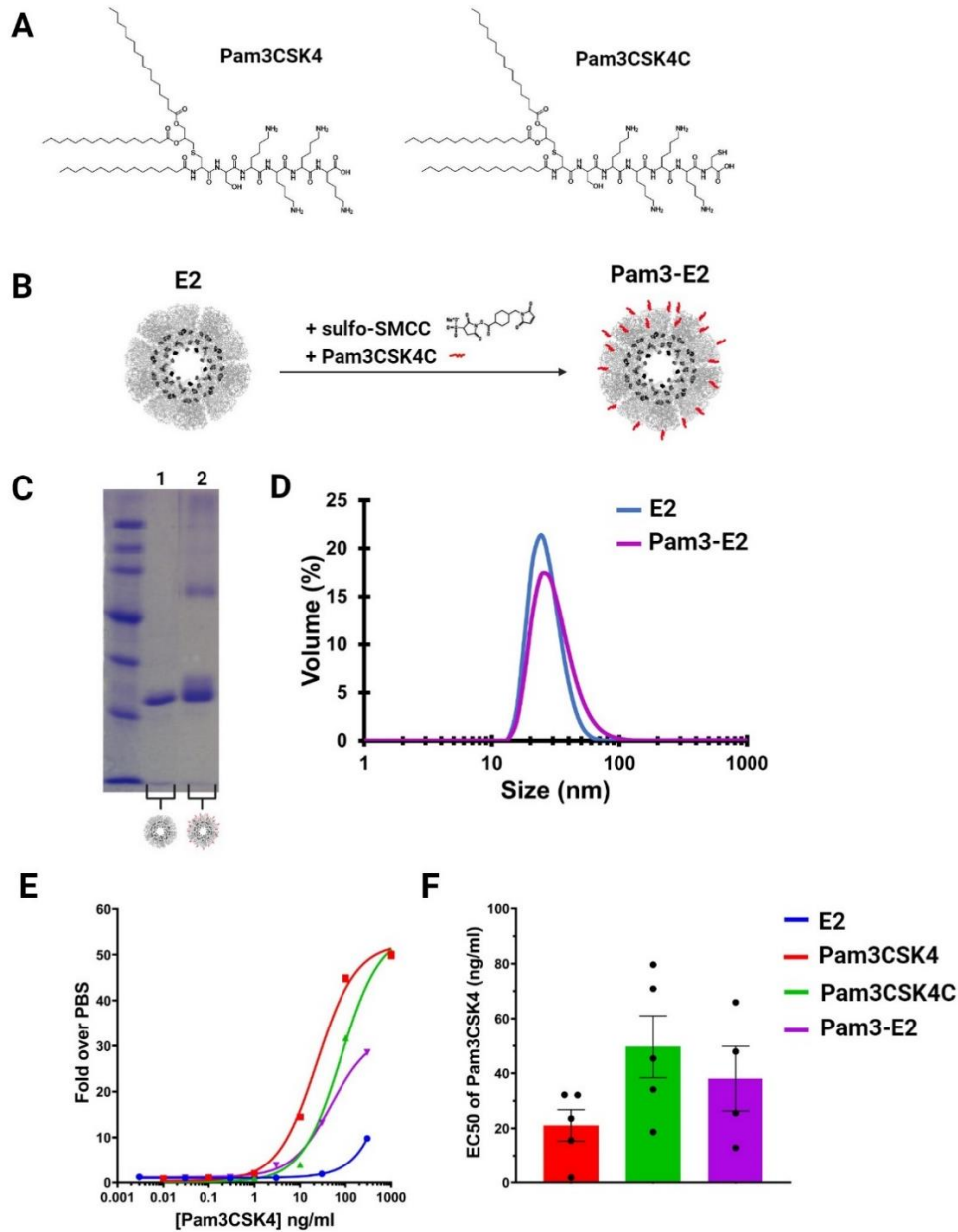
Thirty-eight days after the final immunization, mice (n=8 per group) were inoculated with a lethal dose of H5N1 virus expressing the A/Vietnam/1194/2004 H5 variant (Figure 4.4B). The mice were subsequently monitored for changes in weight, physical appearance, and behavior. Animals that lost greater than 20% of their original body weight were euthanized, and weight data of each individual mouse is shown in Appendix B.18. Four days after the start of the challenge, the lungs of three mice per group were harvested for viral lung titers. Mice administered PBS and the ST-E2 NP alone (no H5 antigen, no TLR agonists) succumbed to infection (Figure 4.5A). Mice immunized with the SC-H5 antigen alone showed 40% survival, and with the addition of soluble flagellin and CpG (SC-H5 + SC-FliC<sub>c</sub> + CpG + E2) showed 80% survival. All E2 NPs bound to antigen, including the unadjuvanted H5-E2 NP, demonstrated 100% survival from lethal H5 influenza challenge (Figure 4.5A). Despite having immune responses that skewed differently (Th1 or Th2), each E2 formulation was capable of protecting the mice. We postulate that although the T cell response (Th1 vs. Th2) from a vaccination may vary between different adjuvants, efficacy was accomplished predominantly by neutralizing antibodies.

Morbidity, manifested as transient weight loss (or 'partial protection') before regaining weight, helped reveal the nuances of the E2 formulations. Mice immunized with E2 NPs conjugated with adjuvant (i.e., H5-FliCc-E2, H5-CpG-E2, and H5-FliCc-CpG-E2) exhibited little to no signs of morbidity as seen by the minimal weight loss (Figure 4.5B). Viral lung titres showed a similar trend for NPs conjugated with adjuvant (See Appendix B.19). Nanoparticles without adjuvant (H5-E2), interestingly, performed similarly to that of the unconjugated complete formulation (SC-H5 + SC-FliCc + CpG + E2) with some mice exhibiting noticeable weight loss (Figure 4.5B). These observations demonstrated that to have 100% survival and minimal morbidity, formulations must have conjugated adjuvant (either singular or dual) on nanoparticles. The additive value to protection observed from the modular additions to the NP construction (i.e. from SC-H5 to H5-E2 to H5-FliCc-E2) demonstrates the control we have in modulating the immune response.



**Figure 4.5. Immunization with nanoparticles bound to H5 and TLR adjuvants protect mice from the lethal challenge of influenza and improve morbidity.** (A) Survival curves, after challenge with H5N1 influenza on day 52 of immunization. All groups with components conjugated to nanoparticles yielded 100% survival (i.e. H5-E2, H5-FliCc-E2, H5-CpG-E2, H5-FliCc-CpG-E2). (B) Morbidity plot showing maximal weight loss of each mouse after viral challenge. Data in each group reflects  $n \geq 4$  individual mice. Statistical significance was determined by one-way ANOVA followed by a Tukey multiple comparisons test. Mantel-Cox log-rank test used for survival curve analysis. \* $p < 0.05$ , \*\* $p < 0.005$ , \*\*\* $p < 0.0005$ .





**Figure 4.6. Synthesis of E2 nanoparticles conjugated with Pam3CSK4 and *in vitro* activation studies of HEK-blue reporter cells.** (A) Structure of Pam3CSK4 (left) and Pam3CSK4C (right). (B) Schematic of nanoparticle synthesis with Pam3SCK4. Pam3CSK4C will be abbreviated to Pam3 when conjugated to NP. (C) SDS-PAGE showing nanoparticles with Pam3CSK4, indicated by the smear above the monomer E2. Lanes: 1. E2; 2. Pam3-E2.  $MW_{E2} = 28.1$  kDa,  $MW_{Pam3} = 1.6$  kDa. (D) Hydrodynamic diameters of Pam3-E2 NPs. (E) Representative experiment of the activation of HEK-Blue hTLR2 cells after 12h incubation. Absorbance of each group was normalized to the absorbance of PBS-only incubation. EC50 was determined using a sigmoidal dose-response curve-fit of each group. (F) Average EC50 concentrations of Pam3CSK4 from HEK-Blue hTLR2 activation. Data in panel F is presented as an average  $\pm$  SEM of at least 4 independent experiments ( $n \geq 4$ ). Statistical significance was determined by one-way ANOVA followed by a Tukey multiple comparisons test. \* $p < 0.05$ , \*\* $p < 0.005$ , \*\*\* $p < 0.0005$ , \*\*\*\* $p < 0.0001$ .

#### 4.4.9. Constructing E2 nanoparticles displaying the TLR2/1 agonist Pam3CSK4

Given the interesting results gathered from conjugating the TLR5 agonist flagellin onto the E2 nanoparticle, we explored the integration of other cell-surface TLR agonists. Typical examples of TLR2/1 and 2/6 agonist include heat killed bacteria and microbial cell-wall components. Synthetic forms of these agonists include the triacylated and diacylated lipopeptide Pam3CSK4 and Pam2CSK4, respectively.<sup>101,102</sup> In most investigations, TLR2/1 and 2/6 agonists are co-administered solubly with the target antigen to elicit stronger immune responses. Studies have shown that these agonists can also be delivered via PLGA and lipid encapsulation to further bolster immunity.<sup>21</sup> However, due to the limited conjugation repertoire of TLR2/1 and 2/6 agonists, delivery on protein nanoparticles has yet to be explored in-depth. Recently, the synthesis the TLR2/1 agonist Pam3CSK4C (which contains an additional cysteine modification) was accomplished by the Yan-Mei Li Lab of Tsinghua University (Beijing, China) which allowed for conjugation to a cyclic dinucleotide for the synergistic activation of the TLR and STING signal pathways.<sup>103</sup> Therefore, using this newly synthesized Pam3CSK4C (generously gifted to us by the Li Lab), we implemented it with our E2 protein nanoparticle delivery platform.

##### 4.4.9.1. Conjugation of Pam3CSK4 onto the E2 protein nanoparticle

The linker sulfo-SMCC was used to conjugate the TLR2/1 agonist Pam3CSK4C to the E2 protein nanoparticle. The previously generated E2 NP with 60 internal cavity cysteines, E2 (D381C), was utilized in this conjugation strategy.<sup>38,104</sup> The addition of cysteine to the end of the Pam3CSK4 molecule to make Pam3CSK4C allows for conjugation through a maleimide:thiol chemistry to the surface of the E2 NP, similar to previously studied peptide conjugations to the E2 NP (Figure 4.6A, B).<sup>103</sup> Further details describing the conjugation methods can be found in the Appendix A.1.6.

Conjugation of Pam3CSK4C onto the surface of E2 required optimization to yield intact and monodispersed nanoparticles. It was observed that as Pam3CSK4C loading increased the

solubility of the construct decreased. This result could be attributed to the increase in hydrophobicity as more lipopeptide is displayed on the NP. The use of additives to increase solubility of higher-density Pam3-E2 NPs were explored in Appendix A.1.7 and tabulated in Appendix B.20. To reduce the concern about solubility in subsequent studies, a low-density display of Pam3CSK4C on the E2 NP was used moving forward. As seen previously when conjugation peptides via sulfo-SMCC linker on E2, conjugation of Pam3CSK4C on E2 is indicated by a smear above the molecular weight of E2 monomer on SDS-PAGE (Figure 4.6C). Quantification by SDS-PAGE revealed that  $14.7 \pm 5.4$  Pam3CSK4 molecules per E2 NP were conjugated for low-density NPs. The average hydrodynamic diameter of low-density loaded Pam3-E2 NPs was  $31.5 \pm 1.6$  nm (Figure 4.6D). These NPs were used to evaluate the effects of loading TLR2/1 agonist on NPs for TLR2/1 activation *in vitro*.

#### 4.4.9.2. Attachment of Pam3CSK4 onto nanoparticles does not improve Pam3CSK4 bioactivity

The bioactivity of Pam3CSK4 was investigated using the HEK-blue hTLR2 reporter cell line (See Appendix A.1.8). The EC50s of Pam3CSK4 and Pam3CSK4C alone were not significantly different from one another (Figure 4.6E, F). Loading immunomodulatory motifs onto NPs has been shown to benefit cell recognition, as increasing the valency and density of a motif can improve receptor engagement and enhance activation.<sup>2,56</sup> Unexpectedly, loading Pam3CSK4 on NPs did not significantly change the activity of the Pam3CSK4 (Figure 4.6E, F).

Several reasons could explain this unexpected observation. TLR2/1 engagement relies on the interaction between the triacylated groups of Pam3CSK4 and the binding pocket of formed from TLR2 and 6 joining. In addition, the four lysines on Pam3CSK4 help stabilize this receptor:ligand interaction. Given the large discrepancy between the size of the E2 NP and Pam3CSK4, conjugation onto the E2 NP may not display Pam3CSK4 in a flexible enough manner, and may cause steric hindrance, that disrupts the strict interaction required for TLR activation.

Using a PEG spacer between the NP and Pam3CSK4 may help to alleviate this issue by improving the accessibility of Pam3SCK4 for TLR engagement.

Another consideration is that increasing the amount of Pam3CSK4 displayed on the E2 NP could increase the dosage delivered to individual cells and improve activation; however, as mentioned, high-density Pam3-E2 NPs experienced severe problems of insolubility. Further optimization to find a stable high-density Pam3-E2 NP would be required to explore this. Another factor that should be accounted for is that due to the low-density loading of Pam3-E2 NPs concentrations of Pam3CSK4 high enough to elicit plateauing of the activation responses could not be reached (Figure 4.6E). This makes the curve-fit and, subsequently, the EC50 less reliable. However, based on the theoretical maximum activity elicited by Pam3CSK4 alone, the theoretical EC50 values for Pam3-E2 would only get larger and our conclusion of the platform not improving the Pam3CSK4 activity would still stand.

Testing the Pam3-E2 NPs with immunologically relevant cells, such as dendritic cells, should also be explored after formulation/solubility concerns are addressed. Bone marrow derived dendritic cells (BMDCs) can be cultured, incubated with NPs, and analyzed for activation markers. Loading Pam3-E2 NPs with the OVA peptide SIINFEKL can help us quantify activation of the BMDCs via SIINFEKL display on MHC molecules. Preliminary synthesis of SIINFEKL-Pam3-E2 NP indicates a feasible way of conjugating both SIINFEKL and Pam3CSK4 on one nanoparticle, but SDS-PAGE is not sensitive enough to accurately quantify the attachment of both molecules (See Appendix B.21). Other characterization techniques such as mass spectrometry or fluorescence spectrophotometry could be options to explore. Ultimately, due to questions concerning the physical instability of the Pam3-E2 NP, the potentially suboptimal orientation and density of Pam3CSK4 on the NP, and the lackluster reporter cell line *in vitro* assays, the Pam3-E2 NP was not implemented in the extensive way the flagellin-E2 NP was. Additional studies are required before moving forward with this NP construct.

#### 4.5. Conclusions

The co-delivery of a model protein antigen (H5 hemagglutinin) and two adjuvants, flagellin and CpG, on a single nanoparticle was successfully synthesized using the E2 protein nanoparticle scaffold and the SpyTag/SpyCatcher bioconjugation system. This strategy yielded stable monodispersed nanoparticles with H5 and flagellin displayed on its exterior and CpG loaded in its internal cavity. Displaying as little as ~6 flagellin molecules on the ST-E2 NP significantly increased the bioactivity of flagellin and increased the activation of immunologically relevant cells *in vitro* by upwards of an order of magnitude compared to unconjugated flagellin. SC-H5 alone is weakly immunogenic and elicits a Th2 bias response. Conjugation of SC-H5 onto ST-E2 NPs (H5-E2) significantly enhances magnitude and breadth of antibody response but does not change the underlying Th2 profile. Compared to unconjugated soluble adjuvants co-administered with antigen (SC-H5 + SC-FliCc + CpG + E2), conjugation of adjuvants onto H5-E2 NPs increased both antibody magnitude and breadth, showing that adjuvant conjugation to NP is necessary to maximize the adjuvant activity.

IgG1/IgG2c antibody subclassing could also be precisely modulated, dependent on the adjuvant and whether it was attached to the nanoparticle. Addition of TLR agonist flagellin elevated magnitude and breadth but does not affect Th2 profile, while addition of CpG also enhanced magnitude and breadth but polarized the response into a Th1 direction. Interestingly, when both flagellin and CpG were loaded on the NP vaccine, a more balanced IgG1/IgG2c response was observed, suggesting the generation of both Th1 (associated with cellular immunity) and Th2 (associated with humoral immunity) responses. Mice immunized with any E2 NP-based vaccine exhibited complete protection from H5N1 influenza challenge. Notably, only mice that received adjuvanted E2 NP vaccine showed minimal or no signs of sickness. Our successful engineering of a protein nanoparticle to precisely orient and attach antigen and multiple adjuvants enabled specific modulation of an immune response. This highlights the potential of nanoparticle-based delivery systems for the development of prophylactic vaccines,

which could offer broader protection, reduce the need for annual reformulations of seasonal vaccines, and improve anticipatory protection against emerging pandemic pathogens.

A nanoparticle conjugated with the TLR2/1 agonist Pam3CSK4C was synthesized and its immunostimulatory effects were tested *in vitro*. Low-density loaded Pam3-E2 NPs (~15 Pam3CSK4C per E2 NP) did not elicit stronger TLR2/1-mediated activation than soluble Pam3CSK4C. Synthesis of higher-density Pam3-E2 NPs experienced instability and insolubility; thus, further optimization of these NPs is required before continuing the characterization of their immunostimulatory effects *in vitro* and *in vivo*.

#### **4.6. Acknowledgements**

This work was supported by the Defense Threat Reduction Agency (DTRA) (HDTRA11810036), the National Institutes of Health (R01EB027797), and the National Science Foundation (Graduate Research Fellowship to A.R.). We acknowledge the use of facilities and instrumentation at the UC Irvine Materials Research Institute, which is supported in part by the National Science Foundation through the UC Irvine Materials Research Science and Engineering Center (DMR-2011967). The authors thank Dr. Felix Grun and Dr. Benjamin Katz at the UCI Mass Spectrometry Facility for helpful discussions; Jiin Felgner, Rie Nakajima, and Dr. Algimantas Jasinskas at the UCI Vaccine R&D Center for helpful discussions and assistance with protein arrays; and Enya Li for statistical analysis suggestions. We thank Dr. Yang-Mei Li and Tianyang Wang for providing the Pam3CSK4C used in experiments. Portions of Figures 4.1, 4.2, 4.3, 4.4, 4.5, 4.6, Appendix A, and Appendix B were created with BioRender.com. Flagellin and HA structure were obtained from Protein Data Bank codes 1UCU and 4BGW, respectively. The views expressed in this article are those of the authors and do not reflect the official policy or position of the U.S. Department of Defense, the U.S. Army, or NIH.

#### 4.7. References

1. Moyle, P. M.; Toth, I., Modern Subunit Vaccines: Development, Components, and Research Opportunities. *Chemmedchem* **2013**, *8* (3), 360-376.
2. Nguyen, B.; Tolia, N. H., Protein-based antigen presentation platforms for nanoparticle vaccines. *npj Vaccines* **2021**, *6* (1).
3. Nanishi, E.; Dowling, D. J.; Levy, O., Toward precision adjuvants: optimizing science and safety. *Current Opinion in Pediatrics* **2020**, *32* (1), 125-138.
4. Lee, K. L.; Twyman, R. M.; Fiering, S.; Steinmetz, N. F., Virus-based nanoparticles as platform technologies for modern vaccines. *Wiley Interdisciplinary Reviews-Nanomedicine and Nanobiotechnology* **2016**, *8* (4), 554-578.
5. Diaz-Arévalo, D.; Zeng, M. T., *Nanoparticle-based vaccines: opportunities and limitations*. *Nanopharmaceuticals: 2020*; p 135-150.
6. Butkovich, N.; Li, E.; Ramirez, A.; Burkhardt, A. M.; Wang, S. W., Advancements in protein nanoparticle vaccine platforms to combat infectious disease. *Wiley Interdiscip Rev Nanomed Nanobiotechnol* **2021**, *13* (3), e1681.
7. Fifis, T.; Gamvrellis, A.; Crimeen-Irwin, B.; Pietersz, G. A.; Li, J.; Mottram, P. L.; McKenzie, I. F. C.; Plebanski, M., Size-dependent immunogenicity: Therapeutic and protective properties of nano-vaccines against tumors. *Journal of Immunology* **2004**, *173* (5), 3148-3154.
8. Foged, C.; Brodin, B.; Frokjaer, S.; Sundblad, A., Particle size and surface charge affect particle uptake by human dendritic cells in an in vitro model. *International Journal of Pharmaceutics* **2005**, *298* (2), 315-322.
9. Reddy, S. T.; Rehor, A.; Schmoekel, H. G.; Hubbell, J. A.; Swartz, M. A., In vivo targeting of dendritic cells in lymph nodes with poly(propylene sulfide) nanoparticles. *Journal of Controlled Release* **2006**, *112* (1), 26-34.
10. Chaudhuri, A.; Battaglia, G.; Golestanian, R., The effect of interactions on the cellular uptake of nanoparticles. *Physical Biology* **2011**, *8* (4).
11. Molino, N. M.; Neek, M.; Tucker, J. A.; Nelson, E. L.; Wang, S. W., Viral-mimicking protein nanoparticle vaccine for eliciting anti-tumor responses. *Biomaterials* **2016**, *86*, 83-91.
12. Neek, M.; Tucker, J. A.; Butkovich, N.; Nelson, E. L.; Wang, S. W., An Antigen-Delivery Protein Nanoparticle Combined with Anti-PD-1 Checkpoint Inhibitor Has Curative Efficacy in an Aggressive Melanoma Model. *Adv. Therap.* **2020**, *3* (12).
13. Ramirez, A.; Felgner, J.; Jain, A.; Jan, S.; Albin, T. J.; Badten, A. J.; Gregory, A. E.; Nakajima, R.; Jasinskas, A.; Felgner, P. L.; Burkhardt, A. M.; Davies, D. H.; Wang, S. W., Engineering Protein Nanoparticles Functionalized with an Immunodominant *Coxiella burnetii* Antigen to Generate a Q Fever Vaccine. *Bioconjugate Chem.* **2023**, *34* (9), 1653-1666.
14. Kasturi, S. P.; Skountzou, I.; Albrecht, R. A.; Koutsonanos, D.; Hua, T.; Nakaya, H. I.; Ravindran, R.; Stewart, S.; Alam, M.; Kwissa, M.; Villinger, F.; Murthy, N.; Steel, J.; Jacob, J.; Hogan, R. J.; Garcia-Sastre, A.; Compans, R.; Pulendran, B., Programming the magnitude and persistence of antibody responses with innate immunity. *Nature* **2011**, *470* (7335), 543-547.
15. Duggan, J. M.; You, D. H.; Cleaver, J. O.; Larson, D. T.; Garza, R. J.; Pruneda, F. A. G.; Tuvim, M. J.; Zhang, J. X.; Dickey, B. F.; Evans, S. E., Synergistic Interactions of TLR2/6 and TLR9 Induce a High Level of Resistance to Lung Infection in Mice. *Journal of Immunology* **2011**, *186* (10), 5916-5926.
16. Albin, T. J.; Tom, J. K.; Manna, S.; Gilkes, A. P.; Stetkevich, S. A.; Katz, B. B.; Supnet, M.; Felgner, J.; Jain, A.; Nakajima, R.; Jasinskas, A.; Zlotnik, A.; Pearlman, E.; Davies, D. H.; Felgner, P. L.; Burkhardt, A. M.; Esser-Kahn, A. P., Linked Toll-Like

- Receptor Triagonists Stimulate Distinct, Combination-Dependent Innate Immune Responses. *Acs Central Science* **2019**, 5 (7), 1137-1145.
17. Kayesh, M. E. H.; Kohara, M.; Tsukiyama-Kohara, K., TLR agonists as vaccine adjuvants in the prevention of viral infections: an overview. *Frontiers in Microbiology* **2023**, 14.
  18. Melssen, M. M.; Petroni, G. R.; Chianese-Bullock, K. A.; Wages, N. A.; Grosh, W. W.; Varhegyi, N.; Smolkin, M. E.; Smith, K. T.; Galeassi, N. V.; Deacon, D. H.; Gaughan, E. M.; Slingluff, C. L., A multipeptide vaccine plus toll-like receptor agonists LPS or polyI:CLC in combination with incomplete Freund's adjuvant in melanoma patients. *Journal for Immunotherapy of Cancer* **2019**, 7.
  19. Orr, M. T.; Beebe, E. A.; Hudson, T. E.; Moon, J. J.; Fox, C. B.; Reed, S. G.; Coler, R. N., A Dual TLR Agonist Adjuvant Enhances the Immunogenicity and Protective Efficacy of the Tuberculosis Vaccine Antigen ID93. *PLOS One* **2014**, 9 (1).
  20. Lampe, A. T.; Puniya, B. L.; Pannier, A. K.; Helikar, T.; Brown, D. M., Combined TLR4 and TLR9 agonists induce distinct phenotypic changes in innate immunity in vitro and in vivo. *Cellular Immunology* **2020**, 355.
  21. Kaur, A.; Baldwin, J.; Brar, D.; Salunke, D. B.; Petrovsky, N., Toll-like receptor (TLR) agonists as a driving force behind next-generation vaccine adjuvants and cancer therapeutics. *Curr. Opin. Chem. Biol.* **2022**, 70.
  22. Madan-Lala, R.; Pradhan, P.; Roy, K., Combinatorial Delivery of Dual and Triple TLR Agonists via Polymeric Pathogen-like Particles Synergistically Enhances Innate and Adaptive Immune Responses. *Sci Rep* **2017**, 7.
  23. Abianeh, H. S.; Nazarian, S.; Sadeghi, D.; Razgi, A. S. H.; Samarin, M. Z., PLGA nanoparticles containing Intimin-Flagellin fusion protein for E. coli O157:H7 nano-vaccine. *Journal of Immunological Methods* **2023**, 520.
  24. Atalis, A.; Keenum, M. C.; Pandey, B.; Beach, A.; Pradhan, P.; Vantucci, C.; O'Farrell, L.; Noel, R.; Jain, R.; Hosten, J.; Smith, C.; Kramer, L.; Jimenez, A.; Ochoa, M. A.; Frey, D.; Roy, K., Nanoparticle-delivered TLR4 and RIG-I agonists enhance immune response to SARS-CoV-2 subunit vaccine. *Journal of Controlled Release* **2022**, 347, 476-488.
  25. Kaba, S. A.; Karch, C. P.; Seth, L.; Ferlez, K. M. B.; Storme, C. K.; Pesavento, D. M.; Laughlin, P. Y.; Bergmann-Leitner, E. S.; Burkhard, P.; Lanar, D. E., Self-assembling protein nanoparticles with built-in flagellin domains increases protective efficacy of a Plasmodium falciparum based vaccine. *Vaccine* **2018**, 36 (6), 906-914.
  26. Li, J. P.; Helal, Z. H.; Karch, C. P.; Mishra, N.; Girshick, T.; Garmendia, A.; Burkhard, P.; Khan, M. I., A self-adjuvanted nanoparticle based vaccine against infectious bronchitis virus. *PLOS One* **2018**, 13 (9).
  27. Pei, C. C.; Dong, H.; Teng, Z. D.; Wei, S. M.; Zhang, Y.; Yin, S. H.; Tang, J. L.; Sun, S. Q.; Guo, H. C., Self-Assembling Nanovaccine Fused with Flagellin Enhances Protective Effect against Foot-and-Mouth Disease Virus. *Vaccines* **2023**, 11 (11).
  28. Barnowski, C.; Kadzioch, N.; Damm, D.; Yan, H. M.; Temchura, V., Advantages and Limitations of Integrated Flagellin Adjuvants for HIV-Based Nanoparticle B-Cell Vaccines. *Pharmaceutics* **2019**, 11 (5).
  29. Zhao, Y. W.; Li, Z. F.; Voyer, J.; Li, Y. B.; Chen, X. Y., Flagellin/Virus-like Particle Hybrid Platform with High Immunogenicity, Safety, and Versatility for Vaccine Development. *ACS Appl. Mater. Interfaces* **2022**, 14 (19), 21872-21885.
  30. Hajam, I. A.; Dar, P. A.; Shahnawaz, I.; Jaume, J. C.; Lee, J. H., Bacterial flagellin-a potent immunomodulatory agent. *Experimental and Molecular Medicine* **2017**, 49.
  31. Skountzou, I.; Martin, M. D.; Wang, B. Z.; Ye, L.; Koutsonanos, D.; Weldon, W.; Jacob, J.; Compans, R. W., Salmonella flagellins are potent adjuvants for intranasally administered whole inactivated influenza vaccine. *Vaccine* **2010**, 28 (24), 4103-4112.



32. Lu, Y.; Swartz, J. R., Functional properties of flagellin as a stimulator of innate immunity. *Sci Rep* **2016**, *6*.
33. Makvandi, M.; Teimoori, A.; Nahad, M. P.; Khodadadi, A.; Cheshmeh, M. G. D.; Zandi, M., Expression of Salmonella typhimurium and Escherichia coli flagellin protein and its functional characterization as an adjuvant. *Microbial Pathogenesis* **2018**, *118*, 87-90.
34. de Zoete, M. R.; Keestra, A. M.; Wagenaar, J. A.; van Putten, J. P. M., Reconstitution of a Functional Toll-like Receptor 5 Binding Site in Campylobacter jejuni Flagellin. *J. Biol. Chem.* **2010**, *285* (16), 12149-12158.
35. Kang, S. M.; Kim, M. C.; Compans, R. W., Virus-like particles as universal influenza vaccines. *Expert Review of Vaccines* **2012**, *11* (8), 995-1007.
36. Wang, B. Z.; Quan, F. S.; Kang, S. M.; Bozja, J.; Skountzou, I.; Compans, R. W., Incorporation of Membrane-Anchored Flagellin into Influenza Virus-Like Particles Enhances the Breadth of Immune Responses. *J. Virol.* **2008**, *82* (23), 11813-11823.
37. McSorley, S. J.; Ehst, B. D.; Yu, Y. M.; Gewirtz, A. T., Bacterial flagellin is an effective adjuvant for CD4(+) T cells in vivo. *Journal of Immunology* **2002**, *169* (7), 3914-3919.
38. Molino, N. M.; Anderson, A. K. L.; Nelson, E. L.; Wang, S. W., Biomimetic Protein Nanoparticles Facilitate Enhanced Dendritic Cell Activation and Cross-Presentation. *ACS Nano* **2013**, *7* (11), 9743-9752.
39. Neek, M.; Tucker, J. A.; Kim, T. I.; Molino, N. M.; Nelson, E. L.; Wang, S. W., Co-delivery of human cancer-testis antigens with adjuvant in protein nanoparticles induces higher cell-mediated immune responses. *Biomaterials* **2018**, *156*, 194-203.
40. Butkovich, N.; Tucker, J. A.; Ramirez, A.; Li, E. Y.; Meli, V. S.; Nelson, E. L.; Wang, S. W., Nanoparticle vaccines can be designed to induce pDC support of mDCs for increased antigen display. *Biomaterials Science* **2022**, *11* (2), 596-610.
41. Badten, A. J.; Ramirez, A.; Hernandez-Davies, J. E.; Albin, T. J.; Jain, A.; Nakajima, R.; Felgner, J.; Davies, D. H.; Wang, S.-W., Protein Nanoparticle-Mediated Delivery of Recombinant Influenza Hemagglutinin Enhances Immunogenicity and Breadth of the Antibody Response. *ACS Infectious Diseases* **2023**, *9* (2), 239-252.
42. World-Health-Organization Ongoing avian influenza outbreaks in animals pose risk to humans. World-Health-Organization. <https://www.who.int/news/item/12-07-2023-ongoing-avian-influenza-outbreaks-in-animals-pose-risk-to-humans> (accessed 2023).
43. World-Health-Organization Influenza (Avian and other zoonotic). World-Health-Organization. [https://www.who.int/news-room/fact-sheets/detail/influenza-\(avian-and-other-zoonotic\)](https://www.who.int/news-room/fact-sheets/detail/influenza-(avian-and-other-zoonotic)) (accessed 2023).
44. Zakeri, B.; Fierer, J. O.; Celik, E.; Chittock, E. C.; Schwarz-Linek, U.; Moy, V. T.; Howarth, M., Peptide tag forming a rapid covalent bond to a protein, through engineering a bacterial adhesin. *Proc. Natl. Acad. Sci. U. S. A.* **2012**, *109* (12), E690-E697.
45. Hernandez-Davies, J. E.; Felgner, J.; Strohmeier, S.; Pone, E. J.; Jain, A.; Jan, S.; Nakajima, R.; Jasinskas, A.; Strahsburger, E.; Krammer, F.; Felgner, P. L.; Davies, D. H., Administration of Multivalent Influenza Virus Recombinant Hemagglutinin Vaccine in Combination-Adjuvant Elicits Broad Reactivity Beyond the Vaccine Components. *Frontiers in Immunology* **2021**, *12*.
46. Li, L.; Fierer, J. O.; Rapoport, T. A.; Howarth, M., Structural Analysis and Optimization of the Covalent Association between SpyCatcher and a Peptide Tag. *J. Mol. Biol.* **2014**, *426* (2), 309-317.
47. Liu, Z. D.; Zhou, H.; Wang, W. J.; Tan, W. J.; Fu, Y. X.; Zhu, M. Z., A novel method for synthetic vaccine construction based on protein assembly. *Sci Rep* **2014**, *4*, 8.
48. Li, E. Y.; Brennan, C. K.; Ramirez, A.; Tucker, J. A.; Butkovich, N.; Meli, V. S.; Ionkina, A. A.; Nelson, E. L.; Prescher, J. A.; Wang, S. W., Macromolecular assembly of bioluminescent protein nanoparticles for enhanced imaging. *Materials Today Bio* **2022**, *17*.

49. Jones, K.; Versteeg, L.; Damania, A.; Keegan, B.; Kendricks, A.; Pollet, J.; Cruz-Chan, J. V.; Gusovsky, F.; Hotez, P. J.; Bottazzi, M. E., Vaccine-Linked Chemotherapy Improves Benznidazole Efficacy for Acute Chagas Disease. *Infection and Immunity* **2018**, *86* (4).
50. Gangisetty, O.; Reddy, D. S., The optimization of TaqMan real-time RT-PCR assay for transcriptional profiling of GABA-A receptor subunit plasticity. *Journal of Neuroscience Methods* **2009**, *181* (1), 58-66.
51. Nakajima, R.; Supnet, M.; Jasinskas, A.; Jain, A.; Taghavian, O.; Obiero, J.; Milton, D. K.; Chen, W. H.; Grantham, M.; Webby, R.; Krammer, F.; Carter, D.; Felgner, P. L.; Davies, D. H., Protein Microarray Analysis of the Specificity and Cross-Reactivity of Influenza Virus Hemagglutinin-Specific Antibodies. *Mosphere* **2018**, *3* (6).
52. Liu, W. C.; Lin, Y. L.; Spearman, M.; Cheng, P. Y.; Butler, M.; Wu, S. C., Influenza Virus Hemagglutinin Glycoproteins with Different N-Glycan Patterns Activate Dendritic Cells In Vitro. *J. Virol.* **2016**, *90* (13), 6085-6096.
53. Pose, A. G.; Morell, N. O.; Matos, D. A.; Rodríguez, E. R.; Rodríguez, E. S.; Cordero, L. R.; Moltó, M. P. R.; Ramos, E. M. G.; Gutiérrez, A. Á.; Pérez, L. G.; Gómez, J. N.; Redondo, A. V.; Nordelo, C. B., Stable lentiviral transformation of CHO cells for the expression of the hemagglutinin H5 of avian influenza virus in suspension culture. *Biotechnology Reports* **2014**, *3*, 108-116.
54. Chang, D.; Zaia, J., Why Glycosylation Matters in Building a Better Flu Vaccine\*. *Molecular & Cellular Proteomics* **2019**, *18* (12), 2348-2358.
55. Tate, M. D.; Job, E. R.; Deng, Y. M.; Gunalan, V.; Maurer-Stroh, S.; Reading, P. C., Playing Hide and Seek: How Glycosylation of the Influenza Virus Hemagglutinin Can Modulate the Immune Response to Infection. *Viruses-Basel* **2014**, *6* (3), 1294-1316.
56. Lee, H.; Odom, T. W., Controlling ligand density on nanoparticles as a means to enhance biological activity. *Nanomedicine* **2015**, *10* (2), 177-180.
57. Shibata, T.; Takemura, N.; Motoi, Y.; Goto, Y.; Karuppuchamy, T.; Izawa, K.; Li, X. B.; Akashi-Takamura, S.; Tanimura, N.; Kunisawa, J.; Kiyono, H.; Akira, S.; Kitamura, T.; Kitaura, J.; Uematsu, S.; Miyake, K., PRAT4A-dependent expression of cell surface TLR5 on neutrophils, classical monocytes and dendritic cells. *International Immunology* **2012**, *24* (10), 613-623.
58. Simon, R.; Samuel, C. E., Interleukin-1 Beta Secretion is Activated Comparably by FliC and FliB Flagellins but Differentially by Wild-Type and DNA Adenine Methylase-Deficient Salmonella. *Journal of Interferon and Cytokine Research* **2008**, *28* (11), 661-666.
59. Carvalho, F. A.; Aitken, J. D.; Gewirtz, A. T.; Vijay-Kumar, M., TLR5 activation induces secretory interleukin-1 receptor antagonist (sIL-1Ra) and reduces inflammasome-associated tissue damage. *Mucosal Immunology* **2011**, *4* (1), 102-111.
60. Yamashita, U.; Kuroda, E., Regulation of macrophage-derived chemokine (MDC, CCL22) production. *Critical Reviews in Immunology* **2002**, *22* (2), 105-114.
61. Korobova, Z. R.; Arsentieva, N. A.; Totolian, A. A., Macrophage-Derived Chemokine MDC/CCL22: An Ambiguous Finding in COVID-19. *International Journal of Molecular Sciences* **2023**, *24* (17).
62. Tanaka, T.; Narazaki, M.; Kishimoto, T., IL-6 in Inflammation, Immunity, and Disease. *Cold Spring Harbor Perspectives in Biology* **2014**, *6* (10).
63. Idriss, H. T.; Naismith, J. H., TNF $\alpha$  and the TNF receptor superfamily:: Structure-function relationship(s). *Microscopy Research and Technique* **2000**, *50* (3), 184-195.
64. Wajant, H.; Siegmund, D., TNFR1 and TNFR2 in the Control of the Life and Death Balance of Macrophages. *Frontiers in Cell and Developmental Biology* **2019**, *7*.
65. Link, H., Current state and future opportunities in granulocyte colony-stimulating factor (G-CSF). *Supportive Care in Cancer* **2022**, *30* (9), 7067-7077.

66. Karagiannidis, I.; Van Vilet, E. D.; Abu Egal, E. S.; Phinney, B.; Jacenik, D.; Prossnitz, E. R.; Beswick, E. J., G-CSF and G-CSFR Induce a Pro-Tumorigenic Macrophage Phenotype to Promote Colon and Pancreas Tumor Growth. *Cancers* **2020**, *12* (10).
67. Cooper, A. M.; Khader, S. A., IL-12p40: an inherently agonistic cytokine. *Trends in Immunology* **2007**, *28* (1), 33-38.
68. Wang, X. B.; Wu, T.; Zhou, F.; Liu, S.; Zhou, R.; Zhu, S. Y.; Song, L.; Zhu, F.; Wang, G.; Xia, B., IL12p40 Regulates Functional Development of Human CD4+ T Cells Enlightenment by the Elevated Expressions of IL12p40 in Patients With Inflammatory Bowel Diseases. *Medicine* **2015**, *94* (10).
69. Ha, S. J.; Lee, C. H.; Lee, S. B.; Kim, C. M.; Jang, K. L.; Shin, H. S.; Sung, Y. C., A novel function of IL-12p40 as a chemotactic molecule for macrophages. *Journal of Immunology* **1999**, *163* (5), 2902-2908.
70. Labastida-Conde, R. G.; Ramírez-Pliego, O.; Peleteiro-Olmedo, M.; Lopez-Guerrero, D. V.; Badillo-Godinez, O. D.; Gutiérrez-Xicoténcatl, M. D.; Rosas-Salgado, G.; González-Fernández, A.; Esquivel-Guadarrama, F. R.; Santana, M. A., Flagellin is a Th1 polarizing factor for human CD4+ T cells and induces protection in a murine neonatal vaccination model of rotavirus infection. *Vaccine* **2018**, *36* (29), 4188-4197.
71. Murtaza, A.; Afzal, H.; Doan, T. D.; Ke, G. M.; Cheng, L. T., Flagellin Improves the Immune Response of an Infectious Bursal Disease Virus (IBDV) Subunit Vaccine. *Vaccines* **2022**, *10* (11).
72. Lopez-Sagaseta, J.; Malito, E.; Rappuoli, R.; Bottomley, M. J., Self-assembling protein nanoparticles in the design of vaccines. *Computational and Structural Biotechnology Journal* **2016**, *14*, 58-68.
73. Pone, E. J.; Hernandez-Davies, J. E.; Jan, S. R.; Silzel, E.; Felgner, P. L.; Davies, D. H., Multimericity Amplifies the Synergy of BCR and TLR4 for B Cell Activation and Antibody Class Switching. *Frontiers in Immunology* **2022**, *13*.
74. Kato, Y.; Abbott, R. K.; Freeman, B. L.; Haupt, S.; Groschel, B.; Silva, M.; Menis, S.; Irvine, D. J.; Schief, W. R.; Crotty, S., Multifaceted Effects of Antigen Valency on B Cell Response Composition and Differentiation In Vivo. *Immunity* **2020**, *53* (3), 548-563.e8.
75. Huleatt, J. W.; Jacobs, A. R.; Tang, J.; Desai, P.; Kopp, E. B.; Huang, Y.; Song, L. Z.; Nakaar, V.; Powell, T. J., Vaccination with recombinant fusion proteins incorporating Toll-like receptor ligands induces rapid cellular and humoral immunity. *Vaccine* **2007**, *25* (4), 763-775.
76. Biedma, M. E.; Cayet, D.; Tabareau, J.; Rossi, A. H.; Ivicak-Kocjan, K.; Moreno, G.; Errea, A.; Soulard, D.; Parisi, G.; Jerala, R.; Berguer, P.; Rumbo, M.; Sirard, J. C., Recombinant flagellins with deletions in domains D1, D2, and D3: Characterization as novel immunoadjuvants. *Vaccine* **2019**, *37* (4), 652-663.
77. Song, L.; Zhang, Y.; Yun, N. E.; Poussard, A. L.; Smith, J. N.; Smith, J. K.; Borisevich, V.; Linde, J. J.; Zacks, M. A.; Li, H.; Kavita, U.; Reiserova, L.; Liu, X.; Dumuren, K.; Balasubramanian, B.; Weaver, B.; Parent, J.; Umlauf, S.; Liu, G.; Huleatt, J.; Tussey, L.; Paessler, S., Superior efficacy of a recombinant flagellin:H5N1 HA globular head vaccine is determined by the placement of the globular head within flagellin. *Vaccine* **2009**, *27* (42), 5875-5884.
78. Jie, J.; Zhang, Y. X.; Zhou, H. Y.; Zhai, X. Y.; Zhang, N. N.; Yuan, H. Y.; Ni, W. H.; Tai, G. X., CpG ODN1826 as a Promising Mucin1-Maltose-Binding Protein Vaccine Adjuvant Induced DC Maturation and Enhanced Antitumor Immunity. *International Journal of Molecular Sciences* **2018**, *19* (3).
79. Pulendran, B.; Arunachalam, P. S.; O'Hagan, D. T., Emerging concepts in the science of vaccine adjuvants. *Nature Reviews Drug Discovery* **2021**, *20* (6), 454-475.
80. Guthmiller, J. J.; Utset, H. A.; Wilson, P. C., B Cell Responses against Influenza Viruses: Short-Lived Humoral Immunity against a Life-Long Threat. *Viruses-Basel* **2021**, *13* (6).

81. Soema, P. C.; Kompier, R.; Amorij, J. P.; Kersten, G. F. A., Current and next generation influenza vaccines: Formulation and production strategies. *European Journal of Pharmaceutics and Biopharmaceutics* **2015**, *94*, 251-263.
82. Ellebedy, A. H.; Krammer, F.; Li, G. M.; Miller, M. S.; Chiu, C.; Wrammert, J.; Chang, C. Y.; Davis, C. W.; McCausland, M.; Elbein, R.; Edupuganti, S.; Spearman, P.; Andrews, S. F.; Wilson, P. C.; García-Sastre, A.; Mulligan, M. J.; Mehta, A. K.; Palese, P.; Ahmed, R., Induction of broadly cross-reactive antibody responses to the influenza HA stem region following H5N1 vaccination in humans. *Proc. Natl. Acad. Sci. U. S. A.* **2014**, *111* (36), 13133-13138.
83. Wei, C. J.; Crank, M. C.; Shiver, J.; Graham, B. S.; Mascola, J. R.; Nabel, G. J., Next-generation influenza vaccines: opportunities and challenges. *Nat Rev Drug Discov* **2020**, *19* (4), 239-252.
84. Stevens, T. L.; Bossie, A.; Sanders, V. M.; Fernandezbotran, R.; Coffman, R. L.; Mosmann, T. R.; Vitetta, E. S., Regulation Of Antibody Isotype Secretion By Subsets Of Antigen-Specific Helper T-Cells. *Nature* **1988**, *334* (6179), 255-258.
85. Carty, S. A.; Riese, M. J.; Koretzky, G. A., Chapter 21 - T-Cell Immunity. In *Hematology (Seventh Edition)*, Hoffman, R.; Benz, E. J.; Silberstein, L. E.; Heslop, H. E.; Weitz, J. I.; Anastasi, J.; Salama, M. E.; Abutalib, S. A., Eds. Elsevier: 2018; pp 221-239.
86. Nazeri, S.; Zakeri, S.; Mehrizi, A. A.; Sardari, S.; Djadid, N. D., Measuring of IgG2c isotype instead of IgG2a in immunized C57BL/6 mice with Plasmodium vivax TRAP as a subunit vaccine candidate in order to correct interpretation of Th1 versus Th2 immune response. *Experimental Parasitology* **2020**, *216*.
87. Li, X.; Cao, Y.; Mou, M.; Li, J. L.; Huang, S. J.; Zhang, E. J.; Yan, H. M.; Yang, J. Y.; Zhong, M. H., Enhanced TLR5-dependent migration and activation of antigen-loaded airway dendritic cells by flagellin. *Journal of Leukocyte Biology* **2023**, *113* (6), 567-576.
88. Bates, J. T.; Uematsu, S.; Akira, S.; Mizel, S. B., Direct Stimulation of tlr5(+/+) CD11c(+) Cells Is Necessary for the Adjuvant Activity of Flagellin. *Journal of Immunology* **2009**, *182* (12), 7539-7547.
89. Janot, L.; Sirard, J. C.; Secher, T.; Noulin, N.; Fick, L.; Akira, S.; Uematsu, S.; Didierlaurent, A.; Hussell, T.; Ryffel, B.; Erard, F., Radioresistant cells expressing TLR5 control the respiratory epithelium's innate immune responses to flagellin. *European Journal of Immunology* **2009**, *39* (6), 1587-1596.
90. Letran, S. E.; Lee, S. J.; Atif, S. M.; Uematsu, S.; Akira, S.; McSorley, S. J., TLR5 functions as an endocytic receptor to enhance flagellin-specific adaptive immunity. *European Journal of Immunology* **2011**, *41* (1), 29-38.
91. Zhang, B. Y.; Chassaing, B.; Shi, Z. D.; Uchiyama, R.; Zhang, Z.; Denning, T. L.; Crawford, S. E.; Puijssers, A. J.; Iskarpatyoti, J. A.; Estes, M. K.; Dermody, T. S.; Ouyang, W. J.; Williams, I. R.; Vijay-Kumar, M.; Gewirtz, A. T., Prevention and cure of rotavirus infection via TLR5/NLRC4-mediated production of IL-22 and IL-18. *Science* **2014**, *346* (6211), 861-865.
92. Heeg, K.; Zimmermann, S., CpG DNA as a Th1 trigger. *International Archives of Allergy and Immunology* **2000**, *121* (2), 87-97.
93. Lin, L.; Gerth, A. J.; Peng, S. L., CpG DNA redirects class-switching towards "Th1-like" Ig isotype production via TLR9 and MyD88. *European Journal of Immunology* **2004**, *34* (5), 1483-1487.
94. Klinman, D. M.; Klaschik, S.; Sato, T.; Tross, D., CpG oligonucleotides as adjuvants for vaccines targeting infectious diseases. *Advanced Drug Delivery Reviews* **2009**, *61* (3), 248-255.
95. Zhou, J. Y.; Deng, G. M., The role of bacterial DNA containing CpG motifs in diseases. *Journal of Leukocyte Biology* **2021**, *109* (5), 991-998.

96. Schotsaert, M.; Saelens, X.; Leroux-Roels, G., Influenza vaccines: T-cell responses deserve more attention. *Expert Review of Vaccines* **2012**, *11* (8), 949-962.
97. Sridhar, S., Heterosubtypic T-Cell immunity to influenza in Humans: Challenges for Universal T-Cell influenza vaccines. *Frontiers in Immunology* **2016**, *7*.
98. Sridhar, S.; Begom, S.; Bermingham, A.; Hoschler, K.; Adamson, W.; Carman, W.; Bean, T.; Barclay, W.; Deeks, J. J.; Lalvani, A., Cellular immune correlates of protection against symptomatic pandemic influenza. *Nature Medicine* **2013**, *19* (10), 1305-+.
99. Miyauchi, K.; Sugimoto-Ishige, A.; Harada, Y.; Adachi, Y.; Usami, Y.; Kaji, T.; Inoue, K.; Hasegawa, H.; Watanabe, T.; Hijikata, A.; Fukuyama, S.; Maemura, T.; Okada-Hatakeyama, M.; Ohara, O.; Kawaoka, Y.; Takahashi, Y.; Takemori, T.; Kubo, M., Protective neutralizing influenza antibody response in the absence of T follicular helper cells. *Nature Immunology* **2016**, *17* (12), 1447-1458.
100. The-Centers-for-Disease-Control-and-Prevention-(CDC) Adjuvants and Vaccines. United States Department of Health and Human Services (HHS). <https://www.cdc.gov/vaccinesafety/concerns/adjuvants.html> (accessed 2022).
101. Cheng, K.; Gao, M.; Godfroy, J. I.; Brown, P. N.; Kastelowitz, N.; Yin, H., Specific activation of the TLR1-TLR2 heterodimer by small-molecule agonists. *Science Advances* **2015**, *1* (3).
102. Kang, J. Y.; Nan, X.; Jin, M. S.; Youn, S. J.; Ryu, Y. H.; Mah, S.; Han, S. H.; Lee, H.; Paik, S. G.; Lee, J. O., Recognition of Lipopeptide Patterns by Toll-like Receptor 2-Toll-like Receptor 6 Heterodimer. *Immunity* **2009**, *31* (6), 873-884.
103. Hu, H. G.; Wu, J. J.; Zhang, B. D.; Li, W. H.; Li, Y. M., Pam(3)CSK(4)-CDG(SF) Augments Antitumor Immunotherapy by Synergistically Activating TLR1/2 and STING. *Bioconjugate Chem.* **2020**, *31* (11), 2499-2503.
104. Dalmau, M.; Lim, S.; Chen, H. C.; Ruiz, C.; Wang, S. W., Thermostability and Molecular Encapsulation Within an Engineered Caged Protein Scaffold. *Biotechnology and Bioengineering* **2008**, *101* (4), 654-664.

## **CHAPTER 5**

### **CONCLUSIONS AND FUTURE DIRECTIONS**

## **5.1. Functionalizing E2 protein nanoparticles with whole protein antigens and immunostimulatory agonists**

### *5.1.1. Summary and Conclusions*

In this work we have demonstrated that whole protein antigens can be delivered on the E2 protein nanoparticle. Previously, the E2 nanoparticle platform was used for cancer vaccines. Here we applied the E2 nanoparticle for infectious disease vaccine development, specifically influenza and *Coxiella burnetii*. We investigated multiple approaches for whole protein antigen conjugation to the E2 nanoparticle including direct genetic fusion, high affinity tris-NTA-Ni conjugation, and the SpyTag/SpyCatcher. By synthesizing a new maleimide functionalized tris-NTA-Ni linker, the high affinity tris-NTA-Ni conjugation was used to conjugate proteins including the H1 influenza antigen hemagglutinin. By engineering the E2 nanoparticle and protein antigens with the SpyTag/SpyCatcher bioconjugation system, the immunodominant protein antigen from H5 influenza and *Coxiella burnetii* were successfully delivered with the E2 nanoparticle.

In addition, we designed and engineered the first known example of a vaccine formulation capable of delivering a protein antigen (i.e., H5 hemagglutinin) and two immunostimulatory adjuvants (i.e., flagellin and CpG) on a single protein nanoparticle. The modularity of our protein-protein conjugation strategies may have utility in future vaccine development against other human pathogens. Given our ability to modulate the type of immune response elicited by loading antigen and adjuvant on the nanoparticle, this strategy can be applied to other diseases that require specific immune response for elimination.

### *5.1.2. Future Directions*

We have shown that delivering H1 and H5 antigens on E2 nanoparticles elicits increased homosubtypic antibody responses compared to antigen alone. However, we observed modest increases to heterosubtypic immune responses when hemagglutinin antigen was delivered on the E2 nanoparticle. Conserved epitopes on hemagglutinin in both the HA1 and HA2 domains are

widely considered as prime targets for eliciting broad and cross-protective immunity. Given the desire to elicit stronger heterosubtypic cross-reactivity, the delivery of multiple different HAs (i.e., H1, H5, H7, etc.) on single particle or on multiple particles, which has been shown to promote cross-reactive immune responses against flu, should be investigated.<sup>1</sup> Delivery of mosaic nanoparticles with HAs that also simultaneously deliver adjuvants like CpG and/or FliC has not been investigated before and could result in elevated responses to the HA1 and HA2 domains and cross-reactive immune responses.

There are limited options in the toolbox of chemical linkers for attaching molecules onto the surfaces of protein nanoparticles. We have applied genetic mutations and the SpyTag/SpyCatcher system to precisely functionalize the external surface and inner core of the E2 nanoparticle allowing the conjugation of antigen and adjuvants. Previously, the lab had engineered variants of E2 with hydrophobic cores for the delivery hydrophobic molecules, and cysteine mutations for the conjugation of maleimide modified molecules.<sup>2,3</sup> Nonnatural amino acids have been used to allow click chemistry to be applied to proteins for the conjugation of molecules such as sugars, proteins, and lipids.<sup>4-6</sup> Integration of nonnatural amino acids into E2 could potentially expand the toolbox of the E2 nanoparticle platform. This route can open the door to potentially conjugating other immunostimulatory adjuvants (i.e., Pam3CSK4, MPLA, and muropeptides), and even cell-selectivity motifs that could help the nanoparticle vaccine target immunologically relevant cell types.<sup>4-8</sup> In addition, other approaches for whole protein conjugation, such as SnoopTag/SnoopCatcher and DogTag/DogCatcher, have been developed and have unique catalytic specificity from SpyTag/SpyCatcher. Thus, developing particles that have both SnoopTag, DogTag, and/or SpyTag could increase the modularity of the nanoparticle platform for the application of multiple components in the same reaction.<sup>9-12</sup> These conjugation systems uses a unique peptide tag and protein for spontaneous isopeptide formation, similar to the ST/SC system, meaning that it can be applied to the nanoparticle and protein antigen in a similar fashion.



We have applied one variant of SpyTag and two variants of SpyCatcher to the E2 nanoparticle platform. In attempts to reduce cell-stress during expression and reduce immunogenicity of SpyCatcher a N-terminus truncated mutant has been employed. Other newer generations of SpyTag and SpyCatcher have been developed to have faster and more efficient kinetics, and with additional reductions in immunogenicity.<sup>13,14</sup> Implementing the newer generations of ST/SC will further optimize E2 formulations using this conjugation strategy.

Lastly, we struggled to synthesize nanoparticles with high densities of Pam3CSK4 on the surface, as loading more than 10-20 Pam3CSK4 molecules on the E2 surface caused the nanoparticles to precipitate out of solution. Extensive investigation of the reaction conditions was completed with different buffers, ionic strengths, surfactants, and other additives. Evaluation of the precipitated NPs demonstrated high densities of Pam3CSK4 loaded on the NPs. It would be interesting to introduce a PEG spacer between the E2 and the hydrophobic Pam3CSK4 molecule via a heterobifunctional PEG linker to possibly increase the solubility of higher density Pam3CSK4 loaded nanoparticles.

## **5.2. Construction of E2 nanoparticle-based vaccines enhance prophylactic immune responses against infectious disease antigens**

### *5.2.1. Summary and Conclusions*

In this work, we demonstrated that loading H1, H5, and CBU1910 protein antigens on E2 nanoparticles results in elevated adaptive immunity including humoral and cellular responses. We showed that delivering a TLR4 agonist, MPLA, with H1 conjugated E2 nanoparticles (H1-E2) increased antigen-specific antibody responses, as well as homo- and hetero-subtypic immune responses. We also demonstrated that immunizing with E2 nanoparticles conjugated with H5 antigen, and the flagellin and/or CpG adjuvants (H5-FliC-CpG-E2, H5-FliC-E2, and H5-CpG-E2) lead to elevated antigen-specific immune responses and 100% protection from H5N1 influenza challenge. We also observed that after a single dose of the H1-E2 or H5-E2 nanoparticle

formulations, significant increases in antibody responses (compared to soluble antigens or soluble antigen with adjuvant) were observed as early as day 10. The conjugation of HA antigen to the E2 nanoparticle enhanced IgG class switching to IgG1 and IgG2c, which was also dependent on the adjuvant's type and its attachment to the E2 nanoparticle.

We synthesized nanoparticles capable of delivering the immunodominant *Coxiella burnetii* protein antigen CBU1910 and the Th1-skewing adjuvant CpG. Mice immunized with this vaccine elicited elevated CBU1910-specific IgG responses and promoted IgG2c class switching. Unpredictably, only modest T lymphocyte response was observed via IFN $\gamma$  ELISpot when lymphocytes were restimulated with CBU1910. An E2 nanoparticle formulation co-delivering CpG and a CD4 T cell epitope peptide, derived from CBU1910, induced strong IFN $\gamma$  ELISpot responses to both the immunized peptide antigen and the whole CBU1910 protein.

### 5.2.2. Future Directions

We have shown homosubtypic cross-reactivity to twenty-eight variants of H5. It is known that current seasonal influenza vaccines elicit antibodies that are highly specific to the immunizing variant, so a direct comparison of our E2 NP vaccines with the conventional influenza vaccine would be very interesting to see.

Despite having immune responses that skewed differently (Th1 or Th2), based on adjuvant used, each H5-E2 formulation protected the mice from virus challenge. Explaining how differently skewed immune responses protect is important to determine. Establishing if this protective effect is due to T cell-specific responses or neutralizing antibody responses would help guide future vaccine development using this protein nanoparticle platform which could potentially translate to nanoparticle delivery in general. *In vivo* and *ex vivo* assays examining the changes in cell populations (i.e., effector and memory CD4 T cells, CD8 T cells, and B cells) using flow cytometry could help evaluate the protective properties of E2 formulations.<sup>15-17</sup> In addition,

microneutralization assays of the sera of immunized animals can be evaluated to characterize the contributions of neutralizing antibodies.<sup>17,18</sup>

We evaluated H5 specific antibody response and showed the E2 NP vaccines significantly increases these responses over antigen alone. As with the H1 antigen, elicitation of the HA0- and HA1-specific responses for H5 would be important to determine the stem and head specific antibody response elicited by the E2 formulations. This would give us information of how to improve the heterosubtypic responses (i.e., use other adjuvants, change antigen and/or adjuvant dosage). In addition, checking neutralization titres and/or hemagglutinin assay titres developed by H5-E2 NPs would help further characterize the immune response elicited and help find a correlation between immune responses elicited and protection. When using H1-E2 NPs the breadth of cross-reactive responses was broader for full-length HA0 compared to HA1, potentially indicating a notable response to the highly conserved stem region of HA, which is advantageous for the development of a universal flu vaccine. To determine if this phenomenon is conserved for different antigens and adjuvants, investigating the HA0- and HA1-specific antibody response elicited by the H5-E2 nanoparticles could be done. Like the H1 hemagglutinin probing analysis, full-length H5 proteins (HA0s) and truncated head-region H5 proteins (HA1s) can be printed on protein microarrays and the sera of immunized animals can be subsequently analyzed for HA0- and HA1-specific binding.

Broader homo- and hetero- subtypic cross-reactivity was observed for H1-E2 nanoparticles co-administered with MPLA adjuvant. Only homosubtypic cross-reactivity was observed for H5-E2 nanoparticles. Understanding the reason why the H1-E2 nanoparticle formulation elicited higher heterosubtypic cross-reactivity, compared to the H5-NPs is important. H1 hemagglutinin been shown to be more immunogenic in humans than other hemagglutinin variants such as the avian H5 strain.<sup>19</sup> This could explain the reduced heterosubtypic cross-reactivity of H5-E2 vaccines. To investigate this directly, E2 vaccines with either H1 or H5 (co-delivered with the same adjuvant) can be evaluated *in vivo* side by side. In addition, cross-

reactivity could be adjuvant-dependent since each adjuvant stimulates a unique signal pathway to promote a distinctive inflammatory response. To assess this, HA-E2 nanoparticles can be co-delivered with different adjuvants (i.e., MPLA, CpG, flagellin) at different dosages and their cross-reactive antibody responses can be compared.

Both the H1-E2 and H5-E2 nanoparticle vaccines demonstrated elevated antibody responses as soon as day 10, over antigen alone. In addition, IgG1/IgG2c response skewing was also observed as early as day 14 for H5-E2 nanoparticle formulations after only a prime immunization. The search for a single-dose influenza vaccine has eluded researchers due the difficulty in mounting a strong enough response to establish neutralizing antibodies and memory. Given the promising result of the H5-E2 NP, evaluating the H5-E2 NP as a single dose vaccine by optimizing antigen and adjuvant dosage would be intriguing.

CD4 T cell responses have been shown to be important for influenza immune responses by T cell-dependent maturation of B cells to elicit higher IgG titers.<sup>20,21</sup> Given the T cell responses elicited by previously synthesized E2 nanoparticles for cancer and *C. burnetii* using peptide antigens, it would be interesting to investigate a combination therapy where E2 nanoparticles loaded with CD4 specific peptide epitopes from HA could be used in a vaccine and co-administered with whole protein HA-E2 NPs to potentially bolster the B cell dependent antibody responses. Potentially increasing the magnitude and breadth of the HA-specific antibody responses. CD8 T cells have been shown to react against heterosubtypic influenza strains and have been shown to help control symptomatic infection.<sup>22-24</sup> Thus, like the CD4 peptide strategy utilizing a CD8 peptide E2 nanoparticle in combination with a protein antigen E2 nanoparticle would be remarkably interesting to investigate.

Neutralizing antibodies have been conventionally used to evaluate influenza vaccine efficacy but were not focused on in my studies. Thus, adding this form of characterization, via microneutralization assays, to our repertoire could be immensely helpful in further screening our influenza vaccines.

The conjugation of HA antigen to the nanoparticle enhanced class switching of both H1 and H5 specific B cells causing IgG1 and IgG2c responses. It would be interesting if we could investigate class switching directly by potentially using organoids such as that of the Lisa Wagar lab here at UCI's immunology department who works with human tonsil organoids to investigate B cell maturation and influenzas.<sup>25,26</sup>

T cell responses from the CBU1910-E2 nanoparticle vaccine evaluated using ELISpot were at best modest, and this was surprising given the increased IgG2c response observed. We hypothesize that this may have resulted from cytokines other IFN $\gamma$  (including IL-2, IL-10, or TNF $\alpha$ ) driving the IgG2c response or a different temporal release of IFN $\gamma$  (ELISpot assayed after 18h of restimulation with antigen, only). Thus, cytokine analysis of supernatants after ELISpot and varying incubation times (6h, 18h, 24h) could help resolve the reason for low ELISpot results. Another reason for this response could have been due to the relatively low molar dose of immunodominant T cell epitopes and the low dose of CpG (attributed to dose being calculated based on micrograms of protein antigen and not peptide antigen), as we typically dose 5-10x more CpG when investigating our cancer vaccines which are designed to promote T cell responses. In addition, our cancer vaccines can display upwards of ~200 immunodominant T cell epitope peptides on a single E2 NP while, as a result of having a maximum number of ~26 CBU1910 protein antigens on the E2 NP and each CBU1910 protein only containing one or two of these immunodominant T cell epitopes,<sup>27,28</sup> the CBU1910-E2 vaccine displays measurably less T cell epitope peptides. When we immunized mice with an E2 nanoparticle delivering a CD4 T cell specific epitope and loaded with CpG, which increased the dose of antigen and adjuvant by an order of magnitude, elevated T cell responses were observed not only to the immunized peptide antigen but also the CBU1910 protein antigen. Thus, adjustment of the vaccine dosage, both antigen and adjuvant, can be assessed to determine if higher T cell responses result from the CBU1910-E2 formulation. Because *Coxiella burnetii* is an intracellular pathogen, CD8 T cell responses are also particularly important for its elimination. For this reason, development of a

nanoparticle vaccine using the immunodominant CD8 cell peptide epitope on CBU1910, should be investigated as an effective candidate for a *Coxiella burnetii* vaccine. In addition, combination of protein- and peptide-based NP vaccines which are optimized for B cell and T cell immune responses, respectively, can be investigated as a combination therapy. This combination strategy has clear potential to confer protection against a pathogen with both extra- and intra-cellular stages to its life cycle, such as *Coxiella burnetii*, which requires activation of both humoral and cellular arms of the immune system to grant protection.

As we have demonstrated, the doses of adjuvants when loaded onto our protein-based E2 nanoparticle vaccines is quite low compared to the conventional dosage of these adjuvants, yet we still see significantly elevated prophylactic immune responses. It would be extremely fascinating to assess the effects of increasing adjuvant dosage on the immune responses. We possibly could see further elevated immune responses and maybe even some immune responses like antigen-specific T lymphocytes and high heterosubtypic cross-reactivity which we did not see before.

For all our formulations with antigens H1, H5, and CBU1910, we have only investigated shorter term immune responses. A desired quality of a vaccine is to also elicit strong long-term immunity such as memory B cells and T cells, which we have yet to fully explore. Thus, investigations characterizing the population of memory cells could prove fruitful in determining the efficacy of a vaccine even before challenge. More so, Th2 responses are described by B cell proliferation and antibody production while Th1 responses are characterized by the activation of antigen-presenting cells and stimulation of T cells. Further characterization of these responses with flow cytometry to identify effector and memory B cell and T cell populations would help in understanding these mechanisms of immunity.

The use of viral vectors as vaccine delivery platforms (i.e. AAV) has shown to be effective for a multitude of diseases; however, the concern of platform specific immune response that would neutralize and nullify subsequent vaccinations using the same platform has been a question of

concern for their long-term viability.<sup>29</sup> Investigating this phenomenon for a non-viral protein platform, such as our E2 nanoparticle platform would be interesting to determine. We now have vaccines for *Coxiella burnetii* and influenza and can potentially assess this phenomenon. An investigation immunizing with the CBU1910-E2 or H5-E2 vaccine then after a period of time immunizing with the H5-E2 or CBU1910-E2 vaccine, respectively, and comparing the immune response with immunizing only with a single type of nanoparticle would be help answer this question for a non-viral platform.

We have made nanoparticles that deliver all the components needed to elicit a targeted immune response. It would be interesting if we can use the E2 nanoparticle platform as an adjuvant delivery platform to be used with other vaccines. E2 nanoparticles can more precisely deliver adjuvants to immunologically relevant cells (i.e., antigen presenting cells), than the soluble forms of the adjuvants. This makes the E2 nanoparticle platform a potentially powerful adjuvant delivery vehicle that can be used in combination with established vaccine formulations that require stronger adjuvant effects to elicit improved immune responses. Varying dosages of flagellin, CpG, and other conjugated adjuvants on the E2 NP can be evaluated to determine the dose dependent effect on the immune response when co-administering these adjuvant-E2 NPs with other established vaccines.

### **5.3. *In vitro* evaluation of co-delivering multiple adjuvants on a single E2 nanoparticle**

#### **5.3.1. *Summary and Conclusions***

The E2 nanoparticle platform was utilized as an adjuvant delivery vehicle for flagellin, CpG, and Pam3CSK4. We show that attaching flagellin onto nanoparticles increased its bioactivity *in vitro*. In addition, flagellin loaded E2 nanoparticles promoted inflammatory cytokine release by macrophage. When loaded onto E2 nanoparticles, Pam3CSK4's *in vitro* bioactivity unexpectedly decreased when compared to soluble Pam3CSK4 alone.

### 5.3.2. Future Directions

We hypothesize that the reason for the Pam3CSK4's decrease in bioactivity when displayed on the surface of the E2 NP could be due to steric hinderance caused by the E2 surface impeding the interaction between Pam3CSK4 and TLR2/1. We propose that introducing a flexible spacer, such as PEG, between the Pam3CSK4 and the E2 NP would allow for more efficient receptor engagement and facilitate better Pam3CSK4 activation.

Previous studies have shown that the combination of endosomal-based (TLR3, 7, 8, 9) with cell-surface-based (TLR1, 2, 4, 5, 6) TLR agonists in vaccines can elicit improved immune responses. Our lab has implemented endosomal TLR agonists including the TLR7 agonist ssRNA and TLR9 agonist CpG. In addition, the cell-surface TLR5 agonist flagellin and TLR2/1 agonist Pam3CSK4 have also been utilized in our E2 nanoparticle platform. ssRNA activation via TLR7 follows the IRF7 signal pathway to promote inflammatory responses. This is a different pathway from the typical NFκB pathway the most TLRs operate under.<sup>30</sup> Exploring the effects of co-delivering adjuvants on nanoparticles (i.e. CpG with flagellin, ssRNA with flagellin, CpG with Pam3CSK4, etc.) *in vitro* studies would help in understanding the cooperative interplay that occurs when cells are activated by these adjuvants. In addition, *in vitro* assays could act as an initial screen to determine which combinations of nanoparticle-loaded adjuvants would elicit desired immune responses before formulating nanoparticles for *in vivo* work.

The implementation of an adjuvant with unique signaling pathway in tandem with cell-surface-based adjuvants like FliC or Pam3CSK4 could help us further understand the immunomodulatory characteristics we observe *in vivo* for the E2 nanoparticle vaccine platform. Additionally, other immunostimulatory agonists such as MPLA, which signals through NFκB or IRF3, and muropeptides, which target innate immune receptors NOD1/2 in the cytosol,<sup>8</sup> could be explored once conjugations to the E2 nanoparticle are established. We showed that displaying flagellin on E2 nanoparticles triggered a dramatic increase in TLR5 activation and its subsequent signal cascade. Interestingly, flagellin has also been shown to trigger different immune responses



when interacting with inflammasome receptors in the cytosol of cells.<sup>31,32</sup> Using mucopeptides that can drive cytosolic entry via NOD1/2 receptors, FliC-E2 nanoparticles could be tuned further to elicit another precisely modulated immune response.

Reporter cell lines and a macrophage cell line were used to evaluate adjuvant activity of flagellin and Pam3CSK4 once loaded onto the E2 nanoparticle. Immunologically relevant cells, such as macrophage, dendritic cells, and epithelial cells, have differential expressions of each toll-like receptor altering their activation by each TLR agonist. More so, each immune cell has a unique occupation in the immune system which makes understanding the interaction to each cell type important when characterizing the adjuvant activity of the E2 NPs. Thus, expanding the repertoire of cell lines that can be used when assessing future adjuvant-loaded E2 nanoparticles is required. For example, Pam3CSK4-E2 and Pam3CSK4-CpG-E2 nanoparticles can be evaluated with BMDC or BMDM cells. The addition of OVA peptide antigen (SIINFEKL) to Pam3CSK4-E2 and Pam3CSK4-CpG-E2 NPs will allow for the evaluation of activation markers and MHCII peptide display by BMDCs. Using macrophage, activation markers and secreted cytokine analysis can be used to evaluate the NPs.

## 5.4. References

1. Cohen, A. A.; Yang, Z.; Gnanapragasam, P. N. P.; Ou, S. S.; Dam, K. M. A.; Wang, H. Q.; Bjorkman, P. J., Construction, characterization, and immunization of nanoparticles that display a diverse array of influenza HA trimers. *PLOS One* **2021**, *16* (3), e0247963.
2. Ren, D. M.; Kratz, F.; Wang, S. W., Protein Nanocapsules Containing Doxorubicin as a pH-Responsive Delivery System. *Small* **2011**, *7* (8), 1051-1060.
3. Molino, N. M.; Anderson, A. K. L.; Nelson, E. L.; Wang, S. W., Biomimetic Protein Nanoparticles Facilitate Enhanced Dendritic Cell Activation and Cross-Presentation. *ACS Nano* **2013**, *7* (11), 9743-9752.
4. Kim, C. H.; Axup, J. Y.; Schultz, P. G., Protein conjugation with genetically encoded unnatural amino acids. *Curr. Opin. Chem. Biol.* **2013**, *17* (3), 412-419.
5. Wang, Y.; Zhang, J. M.; Han, B. Y.; Tan, L. Z.; Cai, W. K.; Li, Y. X.; Su, Y. Y.; Yu, Y. T.; Wang, X.; Duan, X. J.; Wang, H. Y.; Shi, X. M.; Wang, J.; Yang, X.; Liu, T., Noncanonical amino acids as doubly bio-orthogonal handles for one-pot preparation of protein multiconjugates. *Nat. Commun.* **2023**, *14* (1).
6. Zhou, Q., Site-Specific Antibody Conjugation with Payloads beyond Cytotoxins. *Molecules* **2023**, *28* (3).
7. Yang, D. Y.; Luo, X.; Lian, Q. H.; Gao, L. Q.; Wang, C. X.; Qi, X. X.; Zhang, R.; Liu, Z. Q.; Liao, G. C., Fully synthetic Tn-based three-component cancer vaccine using covalently linked TLR4 ligand MPLA and iNKT cell agonist KRN-7000 as built-in adjuvant effectively protects mice from tumor development. *Acta Pharmaceutica Sinica B* **2022**, *12* (12), 4432-4445.
8. Bharadwaj, R.; Anonick, M. V.; Jaiswal, S.; Mashayekh, S.; Brown, A.; Wodzanowski, K. A.; Okuda, K.; Silverman, N.; Grimes, C. L., Synthesis and validation of click-modified NOD1/2 agonists. *Innate Immunity* **2023**, *29* (8), 186-200.
9. Veggiani, G.; Nakamura, T.; Brenner, M. D.; Gayet, R. V.; Yan, J.; Robinson, C. V.; Howarth, M., Programmable polyproteins built using twin peptide superglues. *Proc. Natl. Acad. Sci. U. S. A.* **2016**, *113* (5), 1202-1207.
10. Keeble, A. H.; Yadav, V. K.; Ferla, M. P.; Bauer, C. C.; Chuntharpursat-Bon, E.; Huang, J.; Bon, R. S.; Howarth, M., DogCatcher allows loop-friendly protein-protein ligation. *Cell Chemical Biology* **2022**, *29* (2), 339-+.
11. Brune, K. D.; Leneghan, D. B.; Brian, I. J.; Ishizuka, A. S.; Bachmann, M. F.; Draper, S. J.; Biswas, S.; Howarth, M., Plug-and-Display: decoration of Virus-Like Particles via isopeptide bonds for modular immunization. *Sci Rep* **2016**, *6*.
12. Hatlem, D.; Trunk, T.; Linke, D.; Leo, J. C., Catching a SPY: Using the SpyCatcher-SpyTag and Related Systems for Labeling and Localizing Bacterial Proteins. *International Journal of Molecular Sciences* **2019**, *20* (9).
13. Li, L.; Fierer, J. O.; Rapoport, T. A.; Howarth, M., Structural Analysis and Optimization of the Covalent Association between SpyCatcher and a Peptide Tag. *J. Mol. Biol.* **2014**, *426* (2), 309-317.
14. Rahikainen, R.; Rijal, P.; Tan, T. K.; Wu, H. J.; Andersson, A. M. C.; Barrett, J. R.; Bowden, T. A.; Draper, S. J.; Townsend, A. R.; Howarth, M., Overcoming Symmetry Mismatch in Vaccine Nanoassembly through Spontaneous Amidation. *Angew. Chem.-Int. Edit.* **2021**, *60* (1), 321-330.
15. Sant, A. J.; DiPiazza, A. T.; Nayak, J. L.; Rattan, A.; Richards, K. A., CD4 T cells in protection from influenza virus: Viral antigen specificity and functional potential. *Immunological Reviews* **2018**, *284* (1), 91-105.
16. Hernandez-Davies, J. E.; Felgner, J.; Strohmeier, S.; Pone, E. J.; Jain, A.; Jan, S.; Nakajima, R.; Jasinskas, A.; Strahsburger, E.; Krammer, F.; Felgner, P. L.; Davies, D. H., Administration of Multivalent Influenza Virus Recombinant Hemagglutinin Vaccine in

- Combination-Adjuvant Elicits Broad Reactivity Beyond the Vaccine Components. *Frontiers in Immunology* **2021**, *12*.
17. Hernandez-Davies, J. E.; Dollinger, E. P.; Pone, E. J.; Felgner, J.; Liang, L.; Strohmeier, S.; Jan, S.; Albin, T. J.; Jain, A.; Nakajima, R.; Jasinskas, A.; Krammer, F.; Esser-Kahn, A.; Felgner, P. L.; Nie, Q.; Davies, D. H., Magnitude and breadth of antibody cross-reactivity induced by recombinant influenza hemagglutinin trimer vaccine is enhanced by combination adjuvants. *Sci Rep* **2022**, *12* (1).
  18. Verschoor, C. P.; Singh, P.; Russell, M. L.; Bowdish, D. M. E.; Brewer, A.; Cyr, L.; Ward, B. J.; Loeb, M., Microneutralization Assay Titres Correlate with Protection against Seasonal Influenza H1N1 and H3N2 in Children. *PLOS One* **2015**, *10* (6).
  19. Couch, R. B.; Decker, W. K.; Utama, B.; Atmar, R. L.; Niño, D.; Feng, J. Q.; Halpert, M. M.; Air, G. M., Evaluations for In Vitro Correlates of Immunogenicity of Inactivated Influenza A H5, H7 and H9 Vaccines in Humans. *PLOS One* **2012**, *7* (12).
  20. Sridhar, S., Heterosubtypic T-Cell immunity to influenza in Humans: Challenges for Universal T-Cell influenza vaccines. *Frontiers in Immunology* **2016**, *7*.
  21. Sridhar, S.; Begom, S.; Bermingham, A.; Hoschler, K.; Adamson, W.; Carman, W.; Bean, T.; Barclay, W.; Deeks, J. J.; Lalvani, A., Cellular immune correlates of protection against symptomatic pandemic influenza. *Nature Medicine* **2013**, *19* (10), 1305-+.
  22. Braciale, T., Immunologic recognition of influenza virus-infected cells. I. Generation of a virus-strain specific and a cross-reactive subpopulation of cytotoxic T cells in the response to type A influenza viruses of different subtypes. *Cellular Immunology* **1977**, *33* (2), 423-436.
  23. Yap, K. L.; Ada, G. L.; McKenzie, I. F. C., Transfer Of Specific Cytotoxic T-Lymphocytes Protects Mice Inoculated With Influenza-Virus. *Nature* **1978**, *273* (5659), 238-239.
  24. Bender, B. S.; Croghan, T.; Zhang, L. P.; Small, P. A., Transgenic Mice Lacking Class-I Major Histocompatibility Complex-Restricted T-Cells Have Delayed Viral Clearance And Increased Mortality After Influenza-Virus Challenge. *Journal of Experimental Medicine* **1992**, *175* (4), 1143-1145.
  25. Wagar, L. E., Human immune organoids: a tool to study vaccine responses. *Nature Reviews Immunology* **2023**, *23* (11), 699-699.
  26. Kastenschmidt, J. M.; Sureshchandra, S.; Jain, A.; Hernandez-Davies, J. E.; de Assis, R.; Wagoner, Z. W.; Sorn, A. M.; Mitul, M. T.; Benchorin, A. I.; Levendosky, E.; Ahuja, G.; Zhong, Q.; Trask, D.; Boeckmann, J.; Nakajima, R.; Jasinskas, A.; Saligrama, N.; Davies, D. H.; Wagar, L. E., Influenza vaccine format mediates distinct cellular and antibody responses in human immune organoids. *Immunity* **2023**, *56* (8), 1910-+.
  27. Chen, C.; Dow, C.; Wang, P.; Sidney, J.; Read, A.; Harmsen, A.; Samuel, J. E.; Peters, B., Identification of CD4+ T Cell Epitopes in *C. burnetii* Antigens Targeted by Antibody Responses. *PLOS One* **2011**, *6* (3), e17712.
  28. Xiong, X.; Jiao, J.; Gregory, A. E.; Wang, P.; Bi, Y.; Wang, X.; Jiang, Y.; Wen, B.; Portnoy, D. A.; Samuel, J. E.; Chen, C., Identification of *Coxiella burnetii* CD8+ epitopes and delivery by attenuated *Listeria monocytogenes* as a vaccine vector in a C57BL/6 mouse model. *J Infect Dis* **2016**, *215* (10), 1580-1589.
  29. Butkovich, N.; Li, E.; Ramirez, A.; Burkhardt, A. M.; Wang, S. W., Advancements in protein nanoparticle vaccine platforms to combat infectious disease. *Wiley Interdiscip Rev Nanomed Nanobiotechnol* **2021**, *13* (3), e1681.
  30. Pulendran, B.; Arunachalam, P. S.; O'Hagan, D. T., Emerging concepts in the science of vaccine adjuvants. *Nature Reviews Drug Discovery* **2021**, *20* (6), 454-475.
  31. Miao, E. A.; Alpuche-Aranda, C. M.; Dors, M.; Clark, A. E.; Bader, M. W.; Miller, S. I.; Aderem, A., Cytoplasmic flagellin activates caspase-1 and secretion of interleukin 1 $\beta$  via Ipaf. *Nature Immunology* **2006**, *7* (6), 569-575.

32. Vijay-Kumar, M.; Carvalho, F. A.; Aitken, J. D.; Fifadara, N. H.; Gewirtz, A. T., TLR5 or NLRC4 is necessary and sufficient for promotion of humoral immunity by flagellin. *European Journal of Immunology* **2010**, *40* (12), 3528-3534.

## **APPENDIX A**

### **ADDITIONAL METHODS, DESCRIPTIONS, AND DNA AND PROTEIN SEQUENCES**

## A.1. Additional Methods and Detailed Protocols

### A.1.1. Synthesis of maleimide-tris-NTA (Relevant to section 2.3.2.)

**(N,N) di-*t*-butyl acetate-L-Glu(Bzl)-OtBu (2).** Reaction was performed similarly as previously reported.<sup>1</sup> *t*-butyl bromoacetate (3.558 mL, 4.681 g, 24 mmol) and DIPEA (5.3 mL, 3.877 g, 30 mmol) were added to a solution of H-L-Glu(Bzl)-OtBu hydrochloride (**1**) (1.979 g, 6 mmol) in DMF (50 mL). The reaction was purged with nitrogen gas and heated to 55 °C for 12 h with continuous stirring. The solvent was removed by rotary evaporation at 60 °C. Ethyl acetate (20 mL) was added to the reaction residue to obtain a slurry and was filtered and the liquid collected. The precipitate was washed 3X with hexane/ethyl acetate (3:1, 3X 40 mL) and the liquid collected. The combined filtrate and washes were concentrated by rotary evaporation. The product was purified by flash chromatography using hexane/ethyl acetate. Column Conditions: mobile phase A: hexanes, mobile phase B: ethyl acetate. Gradient: 0-3 min 0% B, 3-7 min ramp to 15% B, 7-15 min 100% B. Product eluted as a peak between 9.5-12 min. The fractions containing product were pooled, concentrated by rotary evaporation, dried over high vacuum, and weighed. The product was confirmed by NMR and TLC in cyclohexane/ethyl acetate ( $R_f = 0.6$ ) and was obtained in 81% yield (2.535 g, 4.866 mmol). <sup>1</sup>H NMR (500 MHz, CDCl<sub>3</sub>)  $\delta$  7.37-7.28 (m, 5H), 5.11 (s, 2H), 3.43 (s, 4H), 3.38 (dd, 1H), 2.73 – 2.56 (m, 2H), 2.04-2.87 (m, 2H), 1.45 (s, 9H), 1.43 (s, 18H). <sup>13</sup>C NMR (126 MHz, CDCl<sub>3</sub>)  $\delta$  173.6, 171.9, 170.6, 136.3, 128.6, 128.3, 128.2, 81.4, 80.8, 66.2, 64.5, 54.0, 30.7, 28.3, 28.2, 25.5.

**(N,N) di-*t*-butylacetate-L-Glu-OtBu (3).** Reaction was performed similarly as previously reported.<sup>1</sup> 10% Pd/C was added to a flame dried round bottom flask with a magnetic stir bar and purged with nitrogen gas. Methanol (110 mL) was added to the flask, followed by compound **1** (2.535 g) dissolved in methanol (10 mL). The solution was purged again with nitrogen gas. A hydrogen balloon was then added and the reaction ran for 6 h. The reaction solution was passed through a celite plug to remove Pd/C. The methanol was removed by rotary evaporation,

transferred to a pre-weighed vial, and dried under high vacuum. The product was weighed and characterized by NMR. The product was obtained in 95% yield (1.994 g, 4.621 mmol). <sup>1</sup>H NMR (500 MHz, CDCl<sub>3</sub>) δ 3.43 (s, 4H), 3.36 (dd, 1H), 2.63 (m, 2H), 1.95 (m, 2H), 1.45 (s, 9H), 1.43 (s, 18H). <sup>13</sup>C NMR (126 MHz, CDCl<sub>3</sub>) δ 177.6, 171.6, 170.7, 81.7, 81.27, 64.7, 54.1, 31.0, 28.3, 28.2, 25.5.

**t-butyl protected tris-NTA-NH (4).** Reaction was performed similarly as previously reported.<sup>1</sup> Compound **2** (3.495 g, 8.100 mmol) and HBTU (3.351 g, 8.837 mmol) were added to a flame dried round bottom flask and dissolved in DCM/DMF (1:1, 100 mL). DIPEA (10 mL) was added to the reaction mixture and the solution stirred for 5 min. Tetraazacyclodecane (0.487 g, 2.430 mmol) was added to the reaction mixture and the reaction stirred for 18 h. The solvent was removed by rotary evaporation at 50 °C. The reaction residue was dissolved in hexanes/ethyl acetate and purified by flash chromatography. Column conditions: mobile phase A: hexanes, mobile phase B: ethyl acetate. Gradient: 0-5 min 0% B, 5-15 min ramp to 100% B, 15-25 min 100% B. Product eluted as a broad peak at 15-22 min. The fractions containing product were combined, the solvent removed by rotary evaporation, and the product dried under high vacuum which was obtained in 53% yield (1.861 g, 1.292 mmol).

**t-butyl protected-tris-NTA-mal.** Maleimido-propionic acid (27 mg, 0.16 mmol) and HBTU (61 mg, 0.16 mmol) was dissolved in DMF (9.5 mL) and DIPEA (0.5 mL). After five minutes, t-butyl protected-tris-NTA-NH (151 mg, 0.11 mmol) was added and the reaction was stirred overnight. The solvent was removed by rotary evaporation and the product purified by flash chromatography. Column conditions: 40 g silica gel column, Mobile phase A: hexanes, mobile phase B: ethyl acetate. Gradient: percent mobile phase B: 0-4 min 0% B, 4-12 min 100% B ramp, 12-20 min 100% B. Product eluted at 13 min. The fractions containing product were collected, the solvent removed by rotary evaporation, and dried over high vacuum. The product was recovered and analyzed by ESI-MS (110 mg, 66% yield). ESI was performed on a Waters LCT ESI MS with

flow injection at 0.1mL/min in 100% MeOH. Predicted [M+Na]<sup>+</sup>: 1613.9 m/z Observed [M+Na]<sup>+</sup>: 1612.9 m/z.

**mal-tNTA (5).** t-butyl protected tris-NTA-mal (109 mg, 0.07 mmol) was dissolved in 95% TFA in water (5 mL) and stirred for 2 h. The TFA was removed by rotary evaporation and the residue added to 40 mL of cold diethyl ether to precipitate the product. The mixture was centrifuged to recover the product pellet. The pellet was dissolved in 50% water/ACN, sterile filtered through a nylon 0.22 μm filter, and lyophilized. The product (5) was weighed and analyzed by LC-MS in water/acetonitrile with 0.1% formic acid (53 mg, 71% yield). LC-MS was performed on a Waters LC-MS with QDA detector with Hclass UPLC with a water/acetonitrile 0.1% formic acid solvent system. Predicted [M+H]<sup>+</sup>: 1087.4 m/z Observed [M+H]<sup>+</sup>: 1087.8 m/z.

#### *A.1.2. Attachment of His<sub>6</sub>-Tagged GFP to tNTA-E2 (Relevant to section 2.4.2.)*

A 10X molar excess of aqueous NiCl<sub>2</sub> was first added to the tNTA-E2 and incubated for 2 hours at room temperature on a shaker. The sample was then run through a 0.5mL 40kDa molecular weight cutoff Zeba spin desalting column according to manufacturer's instructions to remove unchelated NiCl<sub>2</sub>. A 1:2.2 molar ratio (E2 monomer:GFP) of His<sub>6</sub>-tagged GFP was added to Ni-tNTA-E2 or tNTA-E2 and incubated at room temperature on a shaker for 2 hours. Reaction solutions were then run through a packed Sephacryl S-200 SEC column via gravity separation to remove unreacted reactants. Elution profiles and loading quantifications of GFP-(His)<sub>6</sub> were determined with spectrophotometry at 280 nm and fluorescence spectrometry of GFP (Ex: 488 nm and Em: 510 nm).

#### *A.1.3. Expression analysis of SpyTag-E2 particles (Relevant to section 3.3.7.)*

Expression studies were done for each ST-E2 mutant and controls. Proteins were expressed in BL21 (DE3) *E. coli* via 1 mM IPTG induction. After induction for 3 h at 37 °C, cells were pelleted and stored at -80 °C before breaking. Cells were lysed by vortexing with glass



beads. Soluble and insoluble lysates were centrifuged at 18000 x g for 15 min and analyzed using SDS-PAGE for molecular weight and soluble: insoluble ratios. Mutant ST-E2(D381C) was chosen for subsequent scale up expression.

*A.1.4. Reaction optimizations to synthesize final ST/SC CBU1910-E2 formulation (Relevant to section 3.3.9.)*

Investigated excipients included Sarkosyl (SLS) concentrations from 0.05-5.0% (w/v), 3-((3-cholamidopropyl) dimethylammonio)-1-propanesulfonate (CHAPS) concentrations from 1.0-10% (w/v), Tween 20 concentrations from 0.10-1% (w/v), Tween 80 concentrations from 0.10-1% (w/v), pH ranges from 5-10, NaCl concentrations from 100-500 mM, and dextrose concentrations from 5.0-10% (w/v). Molar ratios of SC-CBU1910:ST-E2 monomer ranged from 0.5-3. Reaction temperatures and times ranged from 4-25 °C and 30 min-24 h, respectively. The soluble and insoluble fractions of these reactions were separated by centrifuging at 18000 x g for 5 min and analyzed using DLS and SDS-PAGE densitometry.

*A.1.5. Loading C. burnetii peptide antigen onto E2 nanoparticles (Relevant to section 3.4.5.)*

Given the desire to elicit a robust adaptive immune response towards the pathogen of *C. burnetii*, we conjugated peptide antigen epitopes to the E2 nanoparticle, a strategy which has been implemented by our cancer vaccines.<sup>2-4</sup> Using a CBU1910 peptide, HYLVDNHPEVLVEASQ (CBU1910p), that has been shown to be a T cell specific epitope, the CBU1910p-CpG-E2 formulation was synthesized.<sup>5,6</sup> Optimization of the peptide conjugation was necessary to synthesize well loaded and stable constructs. To increase its physical stability and prevent aggregation, the final formulation contained 0.005% (v/v) Tween 20. Conjugation of CBU1910p was supported by ~1.8 kDa incremental increases to E2 monomer molecular weight seen on SDS-PAGE. Using a BMPH linker, aldehyde modified CpG was conjugated in the core of the E2 nanoparticle. Loading of CpG was confirmed by a ~7 kDa increase in E2 monomer molecular

weight from ~28 kDa to ~35 kDa. SDS-PAGE and mass spectrometry were used to determine the loading of CBU1910p and CpG per nanoparticle.

*A.1.6. Loading Pam3CSK4C lipopeptide, CSIINFEKL peptide, and CpG DNA onto E2 nanoparticles (Relevant to section 4.4.9.1.)*

The Pam3CSK4C lipopeptide and CSIINEKL peptide were conjugated to the E2 (D381C) NP mutant, which contains 60 cysteines in its internal cavity, using a strategy which has been implemented by our cancer vaccines.<sup>2-4</sup> To synthesize stable low-density Pam3-E2 NPs a Pam3CSK4C:E2 monomer molar ratio of 1:1 was used. To conjugate both Pam3CSK4C and CSIINFEKL onto the same E2 NP all components were combined together at the Pam3CSK4C:CSIINFEKL:E2 monomer molar ratio of 2:2:1 and allowed to react for 2h at room temperature followed by 12-16h at 4°C. Conjugation of Pam3CSK4C and CSIINFEKL are supported by ~1.6 and ~1.1 kDa incremental increase, respectively, to E2 monomer molecular weight seen on SDS-PAGE. Using a BMPH linker, aldehyde modified CpG was conjugated in the core of the E2 nanoparticle. Attachment of CpG was confirmed by a ~7 kDa increase in E2 monomer molecular weight from ~28 kDa to ~35 kDa. SDS-PAGE were used to determine the loading of Pam3CSK4C, CSIINFEKL and CpG per nanoparticle. DLS was used to characterize the size of constructed nanoparticles.

*A.1.7. Reaction optimizations to improve high-density Pam3-E2 formulation stability (Relevant to section 4.4.9.1.)*

Molar ratio of Pam3CSK4C:E2 monomer was 5:1 to achieve high-density Pam3-E2 NPs. Investigated excipients included NaCl concentration of 500 mM, Tween 20 concentrations from 0.001-1% (w/v), Tween 80 concentrations from 0.001-1% (w/v), Sarkosyl (SLS) concentrations from 0.05-0.1% (w/v), DMSO concentration of 10% (v/v), sucrose concentrations from 1-10% (w/v), dextrose concentrations from 1-10% (w/v), glycerol concentrations from 1-50% (v/v), 3-((3-

cholamidopropyl) dimethylammonio)-1-propanesulfonate (CHAPS) concentrations from 0.025-0.25% (w/v), and DMF concentration of 10% (v/v). The soluble and insoluble fractions of these reactions were separated by centrifuging at 18000 xg for 5 min and analyzed using DLS and SDS-PAGE densitometry.

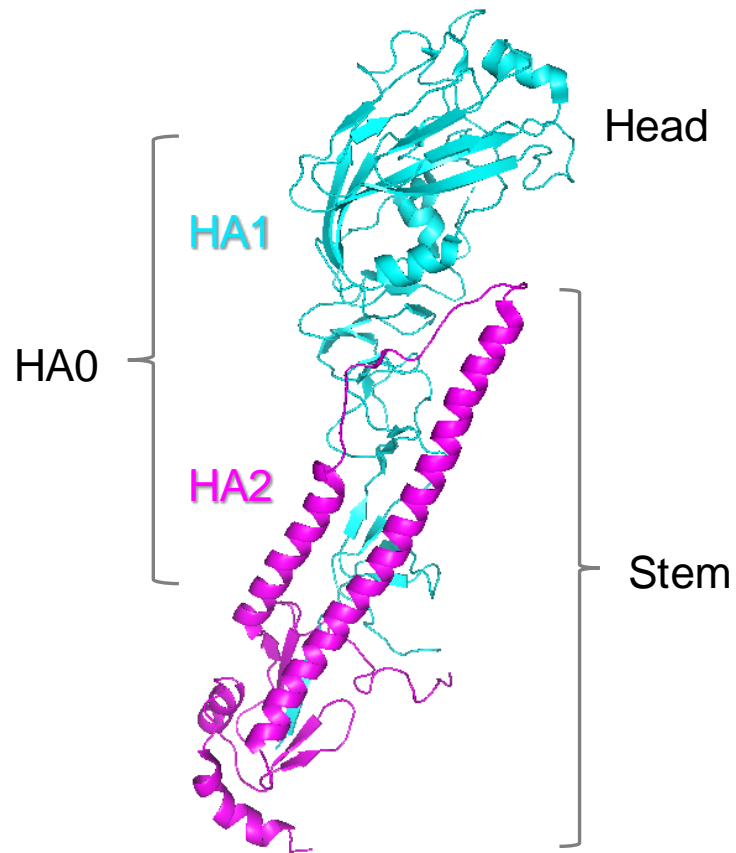
*A.1.8. In vitro characterization of Pam3CSK4 bioactivity (Relevant to section 4.4.9.2.)*

To characterize Pam3CSK4 bioactivity, we used the HEK-Blue hTLR2 reporter cell line (Invivogen), which overexpresses human TLR2 on its surface and contains an inducible secreted alkaline phosphatase (SEAP) gene. We followed the manufacturer's protocol using HEK-blue detection media to evaluate activation. Briefly, in a 96-well tissue culture plate at ~100,000 cells per well, we added concentrations of Pam3CSK4 ranging between 0.01-1000 ng/ml and incubated with HEK-blue detection media at 37 °C in a CO<sub>2</sub> incubator for 12h. The enzymatic activity of SEAP was measured using a spectrophotometer plate reader (SpectraMax M2) by absorbance at 630 nm.

## A.2. Additional descriptions, and protein and DNA sequences

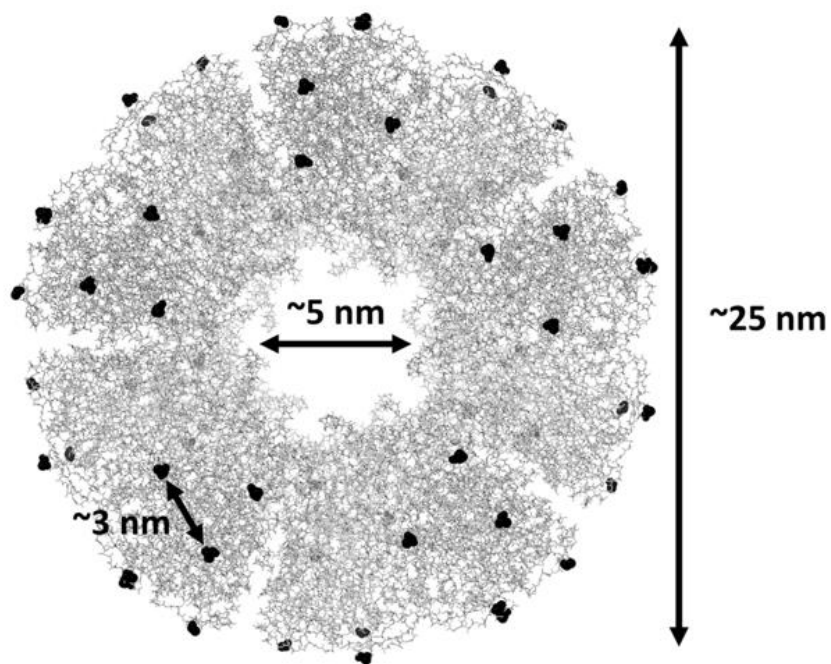
### A.2.1. Three-dimensional representation of the hemagglutinin (HA) monomer (Relevant to section 2.4.)

The head region (HA1) sequence shown in cyan and stem region (HA2) sequence in magenta (PDB: 3ztn). The HA0 description constitutes the HA1 and HA2 regions together.



*A.2.2. ChimeraX-generated three-dimensional structure of the E2 (E279C) nanoparticle (PDB: 1b5s) (Relevant to section 2.4.2.)*

Black spots are located at amino acid position 279, the site of the engineered cysteine residue (to yield mutant E279C), to which the mal-tNTA linker is attached allowing for conjugation of His-tagged protein antigens. The distance between each E279C residue is ~3 nm, which is considered during conjugation for steric hinderance assessments.



A.2.3. H1 HA0 and H1 HA1 variants printed on the protein microarray used for IgG, IgG1, and IgG2c antibody profiling of the H1-E2 nanoparticle vaccine (Relevant to section 2.4.3. and 2.4.4.)

(A) H1 HA0 descriptions: influenza strain, type, and subtype. (B) H1 HA1 descriptions: influenza strain, type, and subtype.

**A**

Influenza Strain/Control ID	Influenza Type	Subtype
A/Beijing/22808/2009	A	H1N1
A/Texas/05/2009	A	H1N1
A/England/195/2009	A	H1N1
A/New York/18/2009	A	H1N1
A/Ohio/07/2009	A	H1N1
A/California/07/2009	A	H1N1
A/Solomon Islands/3/2006	A	H1N1
A/swine/Guangxi/13/2006	A	H1N2
A/California/04/2009	A	H1N1
A/California/04/2009	A	H1N1
A/Brisbane/59/2007	A	H1N1
A/Brevig Mission/1/1918	A	H1N1
A/Ohio/UR06-0091/2007	A	H1N1
A/mallard/Ohio/265/1987	A	H1N9
A/New York/1/1918	A	H1N1
A/New Caledonia/20/99	A	H1N1
A/WSN/1933	A	H1N1
A/duck/NZL/160/1976	A	H1N3
A/Beijing/262/1995	A	H1N1
A/US SR/90/1977	A	H1N1
A/Puerto Rico/8/34	A	H1N1

**B**

Influenza Strain/Control ID	Influenza Type	Subtype
A/Ohio/07/2009	A	H1N1
A/California/04/2009	A	H1N1
A/New York/18/2009	A	H1N1
A/California/06/2009	A	H1N1
A/Beijing/22808/2009	A	H1N1
A/Texas/05/2009	A	H1N1
A/England/195/2009	A	H1N1
A/mallard/Ohio/265/1987	A	H1N9
A/Brevig Mission/1/1918	A	H1N1
A/Ohio/UR06-0091/2007	A	H1N1
A/New York/1/1918	A	H1N1
A/US SR/90/1977	A	H1N1
A/swine/Guangxi/13/2006	A	H1N2
A/Egyptian goose/South Africa/AI1448/2007	A	H1N8
A/Texas/36/1991	A	H1N1
A/duck/NZL/160/1976	A	H1N3
A/New Caledonia/20/99	A	H1N1
A/Solomon Islands/3/2006	A	H1N1
A/Puerto Rico/8/34	A	H1N1
A/Brisbane/59/2007	A	H1N1
A/WSN/1933	A	H1N1

A.2.4. Abbreviations and descriptions of *Coxiella burnetii* vaccine components (Relevant to section 3.4.1.)

Abbreviations of vaccine components and how each correlate to a specific conjugation strategy (i.e. sulfo-SMCC linker, SpyTag/SpyCatcher, recombinant fusion, and Ni-NTA/HisTag coordination bond). N/A denotes "not applicable".

Abbreviation	Description	Attachment strategy
CBU1910	<i>C. burnetii</i> protein antigen	N/A
E2	E2 protein nanoparticle	N/A
NP	Nanoparticle	N/A
VLP	Virus-like particle	N/A
E2(D381C)	E2 with internal cavity mutation of Asp to Cys	sulfo-SMCC linker
CBU1910p	<i>C. burnetii</i> peptide antigen	sulfo-SMCC linker
CBU1910p-E2	CBU1910p attached to E2 nanoparticle via ST/SC	sulfo-SMCC linker
CpG-E2	CpG attached to E2 nanoparticle	sulfo-SMCC linker
CpG-ST-E2	CpG attached to ST-E2 nanoparticle	ST/SC
CBU1910p-CpG-E2	CBU1910p and CpG attached to E2 nanoparticle	sulfo-SMCC linker
E2_152(D381C)	E2 with 20 amino acid N-terminus "tail" and internal cavity mutation of Asp to Cys	Recombinant fusion
E2_158(D381C)	E2 with 14 amino acid N-terminus "tail" and internal cavity mutation of Asp to Cys	Recombinant fusion
CBU1910-E2_152(D381C)	CBU1910 attached to E2_152(D381C) nanoparticle via genetic fusion	Recombinant fusion
CBU1910-E2_158(D381C)	CBU1910 attached to E2_158(D381C) nanoparticle via genetic fusion	Recombinant fusion
E2(E279C)	E2 with external surface mutation of Glu to Cys	Ni-NTA / His
tNTA	Tris-Nitrilotriacetic acid with maleimide functional group	Ni-NTA / His
tNTA-E2	tNTA linker attached to E2(E279C) nanoparticle	Ni-NTA / His
Ni-tNTA-E2	Ni loaded tNTA linker on E2 nanoparticle	Ni-NTA / His
CBU1910-(His) <sub>6</sub>	Histidine tagged CBU1910	Ni-NTA / His
CBU1910-E2	CBU1910 attached to E2 nanoparticle via Ni-tNTA linker	Ni-NTA / His
ST	SpyTag	ST/SC
SC	SpyCatcher	ST/SC
ST-E2	SpyTag fused to E2 monomer	ST/SC
SC-CBU1910	SpyCatcher fused to CBU1910	ST/SC
CBU1910-E2	CBU1910 attached to E2 nanoparticle via ST/SC	ST/SC
CBU1910-CpG-E2	CBU1910 and CpG attached to E2 nanoparticle	ST/SC

A.2.5. DNA and protein sequences of E2 nanoparticle mutants and antigen mutants used for *Coxiella burnetii* vaccine development. (Relevant to section 3.3.2. and 3.3.6. and 3.4.1.1.)

Abbreviation	Description: DNA (top) and protein (bottom) sequences	Attachment strategy
<b>CBU1910</b>	<p>ccgcagcaagtcaaagacattcagtcaatcgttcatcattacctggcaatcacc  cggaagtcctggtgaagccagccaggcactgcagaagaaaaccgaagctc  agcaagaagaacatgctcagcaagcgatcaaagaaaacgcgaaaaaact  gttcaacgatccggcatcaccggtcgcaggaaccgcgatggaatgtcacct  ggtggaatcttcgactatcagtcggccactgtaaagctatgaattcgggtattc  agggcatcggttaaacagaaacaaaaatctgcgtgtggttttaagaactgccga  ttttcggcggtcagagtcaatacgcggccaaagtctccctggcagctgcgaaa  cagggcaaatattacgcttttcacgatgcgctgctgagcgtggacggcgaactgt  ctgaacagattaccctgcaaacggccgaaaaagttggcctgaacgtcgcaca  gtgaaaaaagatatggacaatccggccatccagaaacaactgcgcgataa  cttcagctggccaaagtctgcagctggcaggcaccgccgcttctgtattggt  aacaagcgtgaccaaattcggtttcattccgggcgcaacgtcgcaacaaa  acctgcaaaaagaaattgaccgtgctgaaaaataa</p> <p>PQQVKDIQSIVHHYLVNHPEVLVEASQALQKKTEAQQEE  HAQQAIKENAKKLFNDPASPVAGNPHGNVTLVEFFDYQC  GHCKAMNSVIQAIKQNKNLRVVFKELPIFGGQSQYAAK  VSLAAAKQGKYAFHDALLSVDGQLSEQITLQTAEKVGL  NVAQLKKDMDNPAIQKQLRDNFQLAQSLLAGTPTFVIG  NKALTKFGFIPGATSQQNLQKEIDRVEK</p>	N/A
<b>E2_152(D381C)</b>	<p>gctagcaccggcaaaaatggtcgtgctgaaagaagacattgatgcgtttct  ggcggggcggcgcgaaaccgggcccgtgctgcagaggaaaaggctgctc  cagcggctgcgaaaccggctactactgaaggatgaattccctgaaaccgtga  aaaaatgtctggtatccgtcgtgcaatcgcgaaagccatggtcactctaaaca  caccgcgccacacgttaccctgatggatgaagcagacgttaccaaaactggtg  cgcaccgtaaaaaattcaaggcattgcggcggaaaaaggatcaaaactga  ccttctgccgtacgtgttaaagctctggttcggctctgctgtaataccggttct  gaacaccttattgacgacgagaccgaagaaatcatccagaaacactactac  aacatcggatcgtcgcggacactgatcgtggtcgtggtcctctgtgattaaca  cgcggaccgtaaacccgatctcgcgctcgtcaggaaatcaacgaactggctg  agaaagctcgtgacggtaaactgactcctggtgaaatgaaaggcgcgtcttgc  actattaccaacatcggctctgcagggtggtcagtggtcaccagttatcaacc  accgggaagtgcgatcctgggtattggtcgtatagccgaaaaagccgatcgttc  gttgcgggtgaaatcgttgctgctccgatgctggccctgtctcttctgatcatcg  tatgattgatggcgcgaccgcacagaaagccctgaaccacatcaaacgtctg  ctgtccgaccggaactgctgctgatggaagctaa</p> <p>ASTGKNRVLKEDIDAFLLAGGAKPGPAAAEKKAAPAAK  PATTEGEFPETREKMSGIRRAIAKAMVHSHKHTAPHVTLM  DEADVTKLVAHRKKFKAIKAAEKGIKLTFLPYVVKALVSALR  EYPVLNTSIDDETEEIIQKHYYNIGIAADTDRGLLVPVIKHA  DRKPIFALAQEINELA EKARDGKLTGEMK GASCTITNIG</p>	Recombinant fusion



	SAGGQWFTPVINHPEVAILGIGRIA EKPIVRCGEIVAAPML ALSLSFDHRMIDGATAQKALNHIKRLSDPELLLMEA	
<b>E2_158(D381C)</b>	<p>gctagcgtgctgaaagaagacattgatgcggttctggcgggcggcgcaaac ccgggcccgtgctgcagaggaaaaggctgctccagcggctgcgaaaccgg ctactactgaaggtgaattccctgaaacccgtgaaaaaatgtctggatccgtcg tgcaatcgcgaaagccatggtcactctaaacacaccgcgccacacggtacc tgatgatgaagcagacgttaccaaactggtgcgaccgtaaaaaattcaag gcgattgcggcggaaaaaggatcaaactgaccttctgacctgacgtgtgtaa gctctggttcggctctgctgaatacccggttctgaacacctctattgacgacga gaccgaagaaatcatccagaaacactactacaacatcggatcgtgctggac actgatcgtggtctgctggtcctgtgattaacacgcggaccgtaaccgatctt cgcgctcgtcaggaaatcaacgaactggctgagaaagctcgtgacggtaaa ctgactcctggtgaaatgaaaggcgcgtcttgactattaccaacatcggctctg cagtggtcagtggtcaccagttatcaaccaccggaagtgcgatcctgg gtattggtcgtatagccgaaaagccgatcgttcgtg<b>cg</b>ggtgaaatcgtgctgct ccgatgctggccctgctctgctttcgatcatcgtatgattgatggcgcgaccgca cagaaagccctgaaccacatcaaactgctgctgaccgaccggaactgctgct gatggaagctaa</p> <p>ASVLKEDIDAFLAGGAKPGPAAAEKAAAPAAAKPATTEG EFPETREKMSGIRRAIAKAMVHSKHTAPHVTLMDEADV KLVAHRKKFKAIKAEKGIKLTFLPYVVKALVSALREYPVLN TSIDDETEEIIQKHYYNIGIAADTDRGLLPVIKHADRKPIF ALAQEINELAEKARDGKLTGEMK GASCTITNIGSAGGQ WFTPVINHPEVAILGIGRIA EKPIVRCGEIVAAPMLALSLSF DHRMIDGATAQKALNHIKRLSDPELLLMEA</p>	Recombinant fusion
<b>CBU1910- E2_152(D381C)</b>	<p>ccgcagcaagtcaaagacattcagcaatcgttcattaccctggtcaatcacc cggaagtcctggtgaagccagccagcactgcagaagaaaaccgaagtc agcaagaagaacatgctcagcaagcgtcaaaagaaaacgcgaaaaaact gttaacgatccggcatcaccggtcgcaggaaccgcgatggaatgaccct ggtggaatcttcgactatcagtgccgactgtaaagctatgaattcgggtattc aggcgtcgttaaacagaaacaaaaatctgcgtgtggttttaagaactgccga tttcggcggcagagtcatacgcggccaaagtctccctggcagctgcgaaa cagggcaaatattacgctttcacgatgcgctgctgagcgtggacggcaactgt ctgaacagattaccctgcaaacggccgaaaaagttggcctgaacgtgcaca gctgaaaaaagatatggacaatccggccatccagaaacaactgcgcgataa ctccagctggccaaagtctgcagctggcaggcaccggcagcttctgattggt aacaagcgtgaccaaattcggttcattccgggcgcaacgtgcgcaacaaa acctgcaaaaagaaattgaccgtgctgaaaaagctagcaccggcaaaaatg gtcgtgctgaaagaagacattgatgcgttctggcgggcggcgcaaaccc gggcccgtgctgcagaggaaaaggctgctccagcggctgcgaaaccggct actactgaaggtgaattccctgaaacccgtgaaaaaatgtctggtatccgtcgtg caatcgcgaaagccatggtcactctaaacacaccgcgccacacggtaccctg atggatgaagcagacgttaccaaactggtgcgaccgtaaaaaattcaagg cgattgcggcggaaaaaggatcaaactgaccttctgacctgacgtgtgtaaag ctctggttcggctctgctggaatacccggttctgaacacctctattgacgacgag</p>	Recombinant fusion

	<p>accgaagaaatcatccagaaacactactacaacatcggtatcgctgaggaca  ctgatcgtggtctgctggttctctgtgattaacacgcggaccgtaaaccgatctc  gcgctcgctcaggaaatcaacgaactggctgagaaagctcgtgacggtaaac  tgactcctggtgaaatgaaaggcgcgtcttgactattaccaacatcggctctgc  aggtggtcagtggtcaccacagttatcaaccaccggaagttgcgatcctggg  tattggtcgtatagccgaaaagccgatcgttcgtcgggtgaaatcgttgctgctc  cgatgctggccctgtctgtctttcgatcatcgatgattgatggcgcgaccgcac  agaaagccctgaaccacatcaaacgtctgctgtccgaccggaactgctgctg  atggaagcttaa</p> <p>PQVKDIQSIVHHYLVNHPEVLVEASQALQKKTEAQQEE  HAQQAIKENAKKLFNDPASPVAGNPHGNVTLVEFFDYQC  GHCKAMNSVIQAIKQNKNLRVVFKELPIFGGQSQYAAK  VSLAAAKQGKYYAFHDALLSVDGQLSEQITLQTAEKVGL  NVAQLKKDMDNPAIQKQLRDNFQLAQLSLQLAGTPTFVIG  NKALTKFGFIPGATSQQNLQKEIDRVEKASTGKNGRVLK  EDIDAFLAGGAKPGPAAAEKAAPAAAKPATTEGEFPET  REKMSGIRRAIAKAMVHSKHTAPHVTLMDEADVTKLVAH  RKKFKAIAAEKGIKLTFLPYVVKALVSALREYPVLSIDD  ETEEIIQKHYYNIGIAADTDRLVPIKHADRKPIFALAQE  INELAEKARDGKLTGEMKASCTITNIGSAGGQWFTPV  INHPEVAILGIGRIAEKPIVRCGEIVAAPMLALSLSFDHRMI  DGATAQKALNHIKRLSDPELLLMEA</p>	
<p><b>CBU1910- E2_158(D381C)</b></p>	<p>ccgcagcaagtcaaagacattcagtaaatcgttcatcattacctggtcaatcacc  cggaaagtcctggtgaaagccagccaggcactgcagaagaaaaccgaagctc  agcaagaagaacatgctcagcaagcgaatcaagaaaacgcgaaaaaact  gtcaacgatccggcatcaccggctgcaggaaccgcgatggaatgacaccct  ggtggaattttcgactatcagtgccgactgaaagctatgaattcgggtgattc  aggcgtcgttaaacagaaacaaaaatctgcgtgtggttttaagaactgccga  tttccggcgtcagagtaatacgcggccaaagtctccctggcagctgcgaaa  cagggcaaataattacgcttttcacgatgcgctgctgagcgtggacggtaactgt  ctgaacagattaccctgcaaacggccgaaaaagttggcctgaacgtgcaca  gctgaaaaaagatatggacaatccggccatccagaaacaactgcgcgataa  cttcagctggccaaagtctgcagctggcaggcaccggcagctttgtgattggt  aacaagcgtgaccaaattcggttcattccgggcaacgtgcgaacaaa  accctgaaaaaagaaattgaccgtgctgaaaaagctagcgtgctgaaagaag  acattgatgcgtttctggcgggcgcgaaaccgggcccgcgtgctgcaga  ggaaaaggctgctccagcggctgcgaaccggctactactgaaggtgaattc  cctgaaaccgtgaaaaatgtctggtatccgtcgtgcaatcgcgaaagccat  ggtcactctaaacacaccgcgccacacgttaccctgatggatgaagcagacg  ttaccaaactggtgctgcaccgtaaaaaattcaaggcgattgcggcgaaaa  aggatcaaaactgacctctcgcgtacgtgttaagctcgtgttcggctctgcg  tgaatacccggttctgaacacctctattgacgacgagaccgaagaaatcatcc  agaaactactacaacatcggatcgcgtcgggacactgatcgtggtctgctgg  ttcctgtgattaacacgcggaccgtaaaccgatcttcgcgctcgtcaggaaa  tcaacgaactggctgagaaagctcgtgacggtaaaactgactcctggtgaaatg  aaaggcgcgtcttgactattaccaacatcggctctgcaggtggtcagtggtca  cccagttatcaaccaccggaagttgcgatcctgggtattggtcgtatagccg  aaaagccgatcgttcgtcgggtgaaatcgttgctgctccgatgctggccctgct</p>	<p>Recombinant fusion</p>

	<p>ctgtctttcgatcatcgatgattgatggcgcgaccgcacagaaagccctgaac  cacatcaaacgtctgctgctccgacccggaactgctgctgatggaagcttaa</p> <p>PQQVKDIQSIVHHYLVNHPEVLVEASQALQKKTEAQQEE  HAQQAIKENAKKLFNDPASPVAGNPHGNVTLVEFFDYQC  GHCKAMNSVIQAIVKQNKNLRVVFKELPIFGGQSQYAAK  VSLAAAKQGKYAFHDALLSVDGQLSEQITLQTAEKVGL  NVAQLKKDMDNPAIQKQLRDNFQLAQLSLQLAGTPTFVIG  NKALTKFGFIPGATSQQNLQKEIDRVEKASVLKEDIDAF  AGGAKPGPAAAEKAAPAAAKPATTEGEFPETREKMSGI  RRAIAKAMVHSKHTAPHVTLMDEADVTKLVAHRKKFKAI  AAEKGIKLTFLPYVVKALVSALREYPVLNTSIDDTEEIIQK  HYYNIGIAADTDRGLLVPVIKHADRKPIFALAEINELA  ARDGKLTGEMKASCTITNIGSAGGQWFTPVINHPEVA  ILGIGRIAEKPIVRCGEIVAAPMLALSLSFDHRMIDGATAQ  KALNHIKRLSDPELLLMEA</p>	
<p><b>E2 (E279C)</b></p>	<p>atgctgtctgtcctggctccgctgctgcagaggaaaaggctgctccagcggct  gcaaaccggctactactgaaggtaattcctgaaaccctgaaaaaatgct  tggtatccgctgcaatcgcaagccatggtcactctaaacacaccgccc  acacgttaccctgatggatgaagcagacgttaccaaactggtgcccaccgta  aaaaattcaaggcgattgcccggaaaaggatcaactgacctcctgccc  gtacgttgtaaaagctctggttcggctctgctggaatacccggtctgaacacctc  tattgacgactgcaccgaagaaatcatccagaaacactactacaacatcggt  tcgctgcggacactgatcgtggtctgctggtcctgtgattaacacgcccggaccg  taaaccgatcttcgctcgcctcaggaaatcaacgaactggctgagaaagctc  gtgacggtaaaactgactcctggtgaaatgaaaggcgcgtctgactattacca  acatcggctctgcagggtgctggtcagtggtcaccagttatcaaccaccggaag  ttcgatcctgggtattggtcgtatagccgaaaagccgatcgttcgtgacgggta  aatcgttgctgctccgatgctggccctgtctctgtctttcgatcatcgatgattgatg  gcgcgaccgcacagaaagccctgaaccacatcaaacgtctgctgctccgacc  cggaactgctgctgatggaagcttaa</p> <p>MLSVPGPAAAEKAAPAAAKPATTEGEFPETREKMSGIR  RAIAKAMVHSKHTAPHVTLMDEADVTKLVAHRKKFKAI  EKGIKLTFLPYVVKALVSALREYPVLNTSIDDCTEEIIQKH  YYNIGIAADTDRGLLVPVIKHADRKPIFALAEINELA  RDGKLTGEMKASCTITNIGSAGGQWFTPVINHPEVAI  LGIGRIAEKPIVRDGEIVAAPMLALSLSFDHRMIDGATAQK  ALNHIKRLSDPELLLMEA</p>	<p>Ni-NTA / His</p>

<b>E2 (D381C)</b>	<p>atgctgtctgttcttggtcccgctgctgcagaggaaaaggctgctccagcggct  gcaaaccggctactactgaaggtgaattccctgaaaccctgaaaaaatgct  tggatccgctgcaatcgcgaaagccatggtcactctaacacaccgccc  acacgttaccctgatggatgaagcagacgttaccaaactggtgctgacccgta  aaaaattcaaggcgattgctggcggaaggtatcaaactgaccttctgccc  gtacgttgtaaaagctctggttcggctctgctggaatacccggtctgaacacctc  tattgacgacgagaccgaagaaatcatccagaaacactactacaacatcgggt  atcgctgctggacactgatcgtggtctgctggttctgtgattaacacgctggacc  gtaaaccgatcttgcgctcgcctcaggaaatcaacgaactggctgagaaagct  cgtgacggtaaaactgactcctggtaaatgaaaggcgctctgactattacc  aacatcggctctgcaggtggtcagtggtcaccacagttatcaaccacccgga  gttgcgatcctgggtattggtcgtatagccgaaaagccgatcgttctgctgggtg  aaatcgttgctgctccgatgctggccctgtctctgctttcgatcatcgtatgattgat  ggcgacccgacagaaagccctgaaccacatcaaactgctgctgctccgac  ccggaactgctgctgatggaagcttaa</p> <p>MLSVPGPAAAEKKAAPAAAKPATTEGEFPETREKMSGIR  RAIAKAMVHSHKHTAPHVTLMDADVTKLVAHRKKFKAI  EKGIKLFLPYVVKALVSALREYVNLNTSIDDETEEIIQKH  YYNIGIAADTDRLVPIKHADRKPIFALAEINELA  RDGKLTGEMKASCTITNIGSAGGQWFTPVINHPEVAI  LGIGRIAEKPIVRCGEIVAAPMLALSLSFDHRMIDGATAQK  ALNHIKRLSDPELLLMEA</p>	ST/SC
<b>ST</b>	<p>gccacatcgttatggtggatgcctacaagccaactaaa</p> <p>AHIVMVDAYKPTK</p>	ST/SC
<b>SC</b>	<p>atgctgtactaccatcaccatcaccatcacgattacgacatccaacgaccg  aaaacctgtatcttcagggcgccatggttgataccttatcaggttatcaagtgag  caaggtcagtcgggtgatgacaattgaagaagatagtgtacctatattaaa  ttctcaaaactgtaggagcggcaagaggttagctggtgcaactatggagttg  cgtgattcatctggtaaaactattagtagatggattcagatggacaagtgaag  atttctacctgtatccaggaaaataacatttgcgaaaccgacgaccagacg  gttatgaggtagcaactgctattacctttacagtaaatgagcaaggtcaggttact  gtaaattggcaagcaactaaaggtgacgctcatatt</p> <p>MSYYHHHHHHHDYDIPTTENLYFQGAMVDTLSGLSSEQG  QSGDMTIEEDSATHIKFSKRDEDGKELAGATMELRDSSG  KTISTWISDGQVKDFYLYPGKYTFVETAAPDGYEVATAIT  FTVNEQGQVTVNGKATKGAHI</p>	ST/SC

<p><b>ST-E2</b></p>	<p>atggccacatcgttatggtggatgcctacaagccaactaaaggttcaggaac  agcaggtggtgggtcaggttcctgtctgttctgggtcccgtgctgcagaggaa  aaggctgtccagcggctgcgaaaccggctactactgaaggtgaattccctga  aaccctgtaaaaaatgtctggatccgtcgtgcaatcgcgaaagccatggtca  ctctaacaacaccgcccacacgttaccctgatggatgaagcagacgttacca  aactggtgcgaccgtaaaaaattcaaggcgattgcggcggaaaaaggtat  caactgaccttctgcccgtacgttgtaaaagctctggttcggctctgctgaata  cccgttctgaacacctctattgacgacgagaccgaagaaatcatccagaaa  cactactacaacatcggatcgtcgcggacactgatcgtggtctgctggttctgt  gattaaacacgaggaccgtaaacccgatcttcgctcgcctcaggaaatcaac  gaactggctgagaaagctcgtgacggtaaacgactcctggtaaatgaaag  gcgctctgactattaccaacatcggctctgcaggtggcagtggtcaccccc  agttatcaaccaccggaagttgcgatcctgggtattggtcgtatagccgaaa  gccgatcgttctgagcgggtaaatcgttctgctccgatgctggccctgctctgtc  ttcgtatcgtatgattgatggcgcgaccgcacagaaagccctgaacca  catcaaacgtctgctgccgaccggaactgctgctgatggaagctaa</p> <p>MAHIVMVDAYKPTKSGTAGGGSGSLSVPGPAAAEKA  APAAKPATTEGEFPETREKMSGIRRAIAKAMVHSHKHTA  PHVTLMDEADVTKLVAHRKKFKAIAAEKGIKLTFLPYVVK  ALVSALREYVPLNTSIDDETEEIIQKHYYNIGIAADTDRGL  LVPVIKHADRKPIFALAEINELAEKARDGKLTTPGEMKGA  SCTITNIGSAGGQWFTPVINHPEVAILGIGRIAEKPIVRCG  EIVAAPMLALSLSFDHRMIDGATAQKALNHIKRLLSPELL  LMEA</p>	<p>ST/SC</p>
<p><b>SC-CBU1910</b></p>	<p>atgtcgtactaccatcaccatcaccatcacgattacgacatccaacgaccg  aaaacctgtatttcagggcgccatggtgatacctatcaggttatcaagtgag  caaggtcagtcgggtgatgacaattgaagaagatagtctaccatattaaa  ttctcaaacgtgatgaggacggcaaagagttagctggtgcaactatggagttg  cgtgattcatctggtaaaactattagtagcatggattcagatggacaagtgaag  attctacctgtatccaggaaaatatacatttgcgaaaccgcagcaccagacg  gttatgaggtagcaactgctattacctttacagttaatgagcaaggtcaggttact  gtaaattggcaaagcaactaaaggtgacgctcatattgctagcgggtcaggaac  agcaggtgggtgggtcaggtccccgcagcaagtcaaagacattcagtcaatcg  ttcatattacctggtcaatcaccggaagtctggttgaagccagccaggcact  gcagaagaaaaccgaagctcagcaagaagaacatgctcagcaagcgatc  aaagaaaacgcgaaaaaactgtcaacgatccggcatcaccggtcgcaggt  aaccgcatggtaatgtcacctggtggaattttcgactatcagtgcggccact  gtaaagctatgaattcgggtgattcagggcagcgttaaacagaaacaaaaatctgc  gtgtggttttaagaactgccgattttcggcggcagagtcatacgcggccaa  agtctccctggcagctgcgaaacagggcaaatattacgctttcacgatgcgct  gctgagcgtggacggtaactgtctgaacagattaccctgcaaacggccgaa  aaagttggcctgaacgtcgcacagctgaaaaaagataggacaatccggcc  atccagaaacaactgcgcgataactccagctggcccaaagtctgcagctggc  aggcaccggcaggtttgtgattggaacaaagcgtgaccaaattcgggttcatt  ccggcgcaacgtcgcacaaaacctgcaaaaagaaattgaccgtgctgaa  aataa</p> <p>MSYYHHHHHDYDIPTTENLYFQGAMVDTLSGLSSEQG  QSGDMTIEEDSATHIKFSKRDEDGKELAGATMELRDSSG</p>	<p>ST/SC</p>

KTISTWISDGQVKDFYLYPGKYTFVETAAPDGYEVATAIT  
FTVNEQQQVTVNGKATKGDHIASGSGTAGGGSGSPQ  
QVKDIQSIVHHYLVNHPEVLVEASQALQKKTEAQEEHA  
QQAIKENAKKLFNDPASPVAGNPHGNVTLVEFFDYQCG  
HCKAMNSVIQAIVKQNKNLRVVFKELPIFGGQSQYAAKV  
SLAAAKQGKYYAFHDALLSVDGQLSEQITLQTAEKVGLN  
VAQLKKDMDNPAIQKQLRDNFQLAQLQLAGTPTFVIGN  
KALTKFGFIPGATSQQNLQKEIDRVEK

A.2.6. DNA and protein sequences of flagellin mutants and antigen mutant used for H5 influenza vaccine development (Relevant to section 4.3.2.)

Abbreviation	Description: DNA (top) and protein (bottom) sequences
SC-FliCc (N-terminus truncated SpyCatcher fused with cysteine-modified flagellin)	<p>ATGTCGTA ACTACCAT CACCATC ACCATC ACGATT ACGACAT CCCCA ACGACCG AAAACCT GTATTT TCAGGG CGATAG TGCTAC CCCATAT TAAATT CTCAAA ACGTG ATGAGG ACGGCA AAGAG TTAGCT GGTG CAACT ATGGAG TTGCGT GATTC ATCTG GTAAA ACTAT TAGTAC ATGG ATTTCT ACCTG TATCC CAGGA AAATA CACAT TTGT CGAA ACCG CAGC ACCAG ACGG TATG AGGT AGCA ACTG CTATT ACCT TTAC AGTT AATG AGCA AAGG TCAG GTTAC TGTA AATG GC AAAG CAACT AAAG GTGAC CGCT CATAT TGCT AGCA TGGG ATCAG GGGG GATC AGGT GGCAG CGGA ATACA AGTG ATTAA TACAA ACAG CCTG TCGCT GTTG ACCC CAGA ATAA CCTG AACAA ATCCC AGTCC CGCT CTGG GCACC GCTAT CGAG CGTCT GTCT TCCGG TTGCC GTAT CAAC AGCG CGAA AGAC GATG CGGC CAGGT CAGG CGATT GCTA ACCG TTTT ACCG CGAAC ATCAA AGGT CTGAC TCAG GGC TTCCC GTAAC GCTAAC GACGG TATCT CCATT GCGC AGACC ACTGA AAGG CGCG CTGA ACGAA TCAACA CAAC CCTGC CAGCG TGTG CGTGA ACTCC CAGT CTGAC CTCC ATCC CAGG CTGAA AGTCC TGCC ACAC GACGG TGAA ACTAT CGAT ATCG ATCT GAAG CAGAT CAACT CTCA GACC CTGG GTCT GGATA CGCT GAAT GTGCA ACAAAA ATATA AAGT TCAG CGATA ACGG CTGCA ACTG TTAC AGGAT ATGCC GATA CTAC GATT GCTTT TAGACA ATAG TACT TTTT AAAG CCTC GGCT ACTG GGTCT TTGG TACT GACC AGAAA ATTG ATGG CGAT TTAAA ATTT GATG ATAC GACT GGAAA ATATT ACGCC AAAG TTACC GTTAC CGGG GGGA ACG TGGT AAAG ATGG CTATT ATGA AGTT TCCG TTGATA AGAC GAAC GTGAG GTGACT CTTG CTGG CGGT GCGACT TCCCC GCTT ACAG GTGG ACTAC CTGCG ACAG CAACT GAGG ATGT GAAAA ATGT ACAAG TTGCA AATG CTGAT TTGAC AGAG GCTAA AGCC GCATT GACAG CAGCA GCAGG TGTT ACCG GCAC AGCAT CTGTT GTTA AGAT CTCT TATA CTGATA ATAAC CGGTA AAACT ATTG ATGG TGGTT TAGC AGTT AAGG TAGG CGAT GATT ACTT CTGCA ACTCAA AATA AAGAT GGTT CCATA AGTAT TAATA CTAC GAAATA CACT GCAG ATGAC GGTAC ATCC AAA ACTG CACT AAACA AACT GGGT GGCG CAGAC CGGCA AAAAC CGAAG TTGTT TCTAT TGGT GGTAA AACT TACG CTGCA AGTAA AGCC GAAG GTCA CAACT TTAA AGCAC AGCCT GATCT GGCG GAAG CGGCT GCTACA AACCA CCGAAA ACCC GCTG CAGAAA ATTG ATGCT GCTTT GGC ACAG GTTG ACAC GTTAC GTTCT GACCT GGGT GCGGT ACAGA ACC GTTT CAACT CCGCT ATTAC CAAC CTGG GCAAC ACCG TAAACA ACCTG ACTT CTGCCC GTAG CCGT ATCT GTGAT TCCG ACTAC GCGAC CGAAG TTTCCA ACAT CTCT CGCG CGCAG ATTCT GCAG CAGGCC GTAC CTCC GTTCT GGCG CAGGCC GAACC AGGT TCCG CAAA ACGT CCTCT CTTT ACTG CGTT AA</p>

	<p>MSYYHHHHHDYDIPTTENLYFQGDSATHIKFSKRDEDGKELAGAT  MELRDSSGKTISTWISDGQVKDFYLYPGKYTFVETAAPDGYEVATAI  TFTVNEQQQVTVNGKATKGDASHIASMGGSGGGSGIQVINTNSLSL  LTQNNLNKSQSALGTAIERLSSGCRINSAKDDAAGQAIANRFTANIK  GLTQASRNANDGISIAQTTEGALNEINNNLQRVRELAVQSANSTNS  QSDLDSIQAEITQRLNEIDRVSGQTQFNGVKVLAQDNTLTIQVGAND  GETIDIDLKQINSQTLGLDTLNVQQKYKVSDDAATVTGYADTTIALDN  STFKASATGLGGTDQKIDGDLKFDDTTGKYAKVTVTGGTGKDG  YEVSVDKTNGEVTLAGGATSPLTGGLPATATEDVKNVQVANADLTE  AKAALTAAGVTGTASVVKISYTDNNGKTIDGGLAVKVGDDYYSATQ  NKDGSISINTTKYTADDGTSKTALNKLGGADGKTEVVSIGGKTYAAS  KAEGHNFKAQPDLAEEAATTTENPLQKIDAALAQVDTLRSDLGAVQ  NRFNSAITNLGNTVNNLTSARSRICDSYATEVSNISRAQILQQAGT  SVLAQANQVPQNVLSLLR*</p>
<p>SC-FliC (N-terminus truncated SpyCatcher fused with wild-type flagellin)</p>	<p>ATGTCGTACTIONACCATCACCATCACCATCACGATTACGACATCCCA  ACGACCGAAAACCTGTATTTTCAGGGCGATAGTGCTACCCATAT  TAAATTCTCAAACCGTGATGAGGACGGCAAAGAGTTAGCTGGTG  CAACTATGGAGTTGCGTGATTCATCTGGTAAAACCTATTAGTACAT  GGATTTAGATGGACAAGTGAAAGATTTCTACCTGTATCCAGGA  AAATATACATTTGTGCAAACCGCAGCACCAGACGGTTATGAGGT  AGCAACTGCTATTACCTTTACAGTTAATGAGCAAGGTCAGGTTAC  TGTAATGGCAAAGCAACTAAAGGTGACGCTCATATTGCTAGCA  TGGGATCAGGGGGATCAGGTGGCAGCGGAGCACAAGTGATTAA  TACAAACAGCCTGTGCTGTTGACCCAGAATAACCTGAACAAAT  CCCAGTCCGCTCTGGGCACCGCTATCGAGCGTCTGTCTTCCGG  TCTGCGTATCAACAGCGCGAAAGACGATGCGGCAGGTCAGGCG  ATTGCTAACCGTTTTACCGCGAACATCAAAGGTCTGACTCAGGC  TTCCCGTAACGCTAACGACGGTATCTCCATTGCGCAGACCACTG  AAGGCGCGCTGAACGAAATCAACAACCTGCAGCGTGTGCG  TGAACGGCGGTTGAGTCTGTAACAGCACCAACTCCCAGTCTG  ACCTCGACTCCATCCAGGCTGAAATCACCCAGCGCCTGAACGAA  ATCGACCGTGTATCCGGCCAGACTCAGTTCAACGGCGTGAAAGT  CCTGGCGCAGGACAACACCCTGACCATCCAGGTTGGTGCCAAC  GACGGTGAAACTATCGATATCGATCTGAAGCAGATCAACTCTCA  GACCCTGGGTCTGGATACGCTGAATGTGCAACAAAAATATAAGG  TCAGCGATACGGCTGCAACTGTTACAGGATATGCCGATACTACG  ATTGCTTTAGACAATAGTACTTTTAAAGCCTCGGCTACTGGTCTT  GGTGGTACTGACCAGAAAATTGATGGCGATTTAAAATTTGATGAT  ACGACTGGAAAATATTACGCCAAAGTTACCGTTACGGGGGGAAC  TGGTAAAGATGGCTATTATGAAGTTTCCGTTGATAAGACGAACG  GTGAGGTGACTCTTGCTGGCGGTGCGACTTCCCCGCTTACAGG  TGGACTACCTGCGACAGCAACTGAGGATGTGAAAAATGTACAAG  TTGCAAATGCTGATTTGACAGAGGCTAAAGCCGCATTGACAGCA  GCAGGTGTTACCGGCACAGCATCTGTTGTTAAGATGTCTTATACT  GATAATAACGGTAAAACCTATTGATGGTGGTTTAGCAGTTAAGGTA  GGCGATGATTACTATTCTGCAACTCAAATAAAGATGGTTCCATA  AGTATTAATACTACGAAATACACTGCAGATGACGGTACATCCAAA  ACTGCACTAAACAAACTGGGTGGCGCAGACGGCAAACCGAAG  TTGTTTCTATTGGTGGTAAAACCTTACGCTGCAAGTAAAGCCGAAG  GTCACAACTTTAAAGCACAGCCTGATCTGGCGGAAGCGGCTGCT</p>



	<p>ACAACCACCGAAAACCCGCTGCAGAAAATTGATGCTGCTTTGGC  ACAGGTTGACACGTTACGTTCTGACCTGGGTGCGGTACAGAACC  GTTTCAACTCCGCTATTACCAACCTGGGCAACACCGTAAACAAC  CTGACTTCTGCCCGTAGCCGTATCGAAGATTCCGACTACGCGAC  CGAAGTTTTCCAACATGTCTCGCGCGCAGATTCTGCAGCAGGCC  GGTACCTCCGTTCTGGCGCAGGCCGAACCAGGTTCCGCAAACG  TCCTCTCTTTACTGCGTTAA</p> <p>MSYYHHHHHDYDIPTTENLYFQGDSATHIKFSKRDEDGKELAGAT  MELRDSSGKTISTWISDGQVKDFYLYPGKYTFVETAAPDGYEVATAI  TFTVNEQGQVTVNGKATKGDASHMSGSGGSGGSGAQVINTNSLS  LLTQNNLNKSQSALGTAIERLSSGLRINSAKDDAAGQAIANRFTANIK  GLTQASRNANDGISIAQTTEGALNEINNNLQRVRELAVQSANSTNS  QSDLDSIQAEITQRLNEIDRVSGQTQFNGVKVLAQDNTLTIQVGAND  GETIDIDLKQINSQTLGLDTLNVQQKYKVSDDAATVTGYADTTIALDN  STFKASATGLGGTDQKIDGDLKFDTTGKYYAKVTVTGGTGKDG  YEVSVDKTNGEVTLAGGATSPLTGGLPATATEDVKNVQVANADLTE  AKAALTAAGVTGTASVVKMSYTDNNGKTIDGGLAVKVGDDYYSAT  QNKDGSISINTTKYTADDGTSKTALNKLGGADGKTEVVSIGGKTYAA  SKAEGHNFKAQPDLAEEAATTTENPLQKIDAALAQVDTLRSDLGAV  QNRFNSAITNLGNTVNNLTSARSRIEDSDYATEVSNMSRAQILQQA  GTSVLAQANQVPQNVLSLLR*</p>
<p>SC-H5 (N-terminus  truncated SpyCatcher  fused with H5  hemagglutinin)</p>	<p>ATGTACAGGATGCAACTCCTGTCTTGCATTGCACTAAGTCTTGCA  CTTGTACAAACAGTCATCATCACCATCATCACCATCACCATTCA  GGAGGAGGATCAGGAGGAGGAATCGAGGGAAGGGATAGTGCTA  CCCATATTAATTCTCAAACGTTGATGAGGACGGCAAAGAGTTA  GCTGGTGCAACTATGGAGTTGCGTGATTCATCTGGTAAACTATT  AGTACATGGATTTTACAGATGGACAAGTGAAAGATTTCTACCTGTAT  CCAGGAAAATATACATTTGTGCAAACCGCAGCACCAGACGGTTA  TGAGGTAGCAACTGCTATTACCTTTACAGTTAATGAGCAAGGTCA  GGTTACTGTAAATGGCAAAGCAACTAAAGGTGACGCTCATATTG  CTAGCGGTTTACAGAACAGCAGGTGGTGGGTGAGGTTCCGATCA  GATTTGCATTGGTTACCATGCAAACAACCTCGACAGAGCAGGTTG  ACACAATAATGGAAAAGAACGTTACTGTTACACATGCCCAAGACA  TACTGGAAAAGACACACAATGGGAAGCTCTGCGATCTAGATGGA  GTGAAGCCTCTAATTTTGTAGAGATTGTAGTGTAGCTGGATGGCT  CCTCGGAAACCAATGTGTGACGAATTCATCAATGTGCCGGAAT  GGTCTTACATAGTGGAGAAGGCCAATCCAGTCAATGACCTCTGT  TACCCAGGGGATTTCAATGACTATGAAGAATTGAAACACCTATTG  AGCAGAATAAACCATTTTGTAGAAAATTCAGATCATCCCCAAAAGT  TCTTGGTCCAGTCATGAAGCCTCATTGGGGGTGAGCTCAGCATG  TCCATACCAGGGAAAGTCCTCCTTTTTTTCAGAAATGTGGTATGGCT  TATCAAAAAGAACAGTACATACCCAACAATAAAGAGGAGCTACAA  TAATACCAACCAAGAAGATCTTTTGGTACTGTGGGGGATTACCC  ATCCTAATGATGCGGCAGAGCAGACAAAGCTCTATCAAAACCCA  ACCACCTATATTTCCGTTGGGACATCAACACTAAACCAGAGATTG  GTACCAAGAATAGCTACTAGATCCAAAGTAAACGGGCAAAGTGG  AAGGATGGAGTTCTTCTGGACAATTTTAAAACCGAATGATGCAAT  CAACTTCGAGAGTAATGGAAATTTTATTGCTCCAGAATATGCATA</p>

CAAAATTGTCAAGAAAGGGGACTCAACAATTATGAAAAGTGAATT  
GGAATATGGTAACTGCAACACCAAGTGTCAAACCTCCAATGGGGG  
CGATAAACTCTAGCATGCCATTCCACAATATACACCCTCTACCA  
TCGGGGAATGCCCAAATATGTGAAATCAAACAGATTAGTCCTT  
GCGACTGGGCTCAGAAATAGCCCTCAACGAGAGACGCGAGGAT  
TATTTGGAGCTATAGCAGGTTTTATAGAGGGAGGATGGCAGGGA  
ATGGTAGATGGTTGGTATGGGTACCACCATAGCAACGAGCAGG  
GGAGTGGGTACGCTGCAGACAAAGAATCCACTCAAAAGGCAATA  
GATGGAGTCACCAATAAGGTCAACTCGATTATTGACAAAATGAAC  
ACTCAGTTTGAGGCCGTTGGAAGGGAATTTAACAACCTTAGAAAG  
GAGAATAGAGAATTTAAACAAGAAGATGGAAGACGGGTTCCCTAG  
ATGTCTGGACTTATAATGCTGAACTTCTAGTTCTCATGGAAAACG  
AGAGAACTCTAGACTTTCATGACTCAAATGTCAAGAACCTTTACG  
ACAAGGTCCGACTACAGCTTAGGGATAATGCAAAGGAGCTGGGT  
AACGTTGTTTTCGAGTTCTATCATAAATGTGATAATGAATGTATG  
GAAAGTGTAAAGAAACGGAACGTATGACTACCCGCAGTATTCAGA  
AGAAGCAAGACTAAAAAGAGAGGAAATAAGTGGAGTAAAATTGG  
AATCAATAGGAATTTACCAAATATAA

MYRMQLLSCIALSLALVTNSHHHHHHHHHSGGGSSGGGIEGRDSAT  
HIKFSKRDEDGKELAGATMELRDSSGKTISTWISDGQVKDFYLYPG  
KYTFVETAAPDGYEVATAITFTVNEQGQVTVNGKATKGDHIASGS  
GTAGGGSGSDQICIGYHANNSTEQVDTIMEKNVTVTHAQDILEKTH  
NGKLCDLDGVKPLILRDCSVAGWLLGNPMCDEFINPEWSYIVEKA  
NPVNDLCYPGDFNDYEELKHLLSRINHFEEKIIPKSSWSSHEASLG  
VSSACPYQGKSSFFRNVVWLIKKNSTYPTIKRSYNNTNQEDLLVLW  
GIHHPNDAAEQTKLYQNPTTYISVGTSTLNQRLVPRIATR SKVNGQS  
GRMEFFWTILKPNDAINFESNGNFIAPEYAYKIVKKGDSTIMKSELEY  
GNCNTKCQTPMGAINSSMPFHNIHPLTIGECPKYVKS NRLVLATGL  
RNSPQRETRGLFGAIAGFIEGGWQGMVDGWYGYHHSNEQGSYA  
ADKESTQKAIDGVTNKVNSIIDKMNTQFEAVGREFNLERRIENLNK  
KMEDGFLDVWTYNAELLVLMENERTLDFHDSNVKNLYDKVRLQLR  
DNAKELGNGCFEFYHKCDNECMESVRNGTYDYPQYSEEARLKRE  
EISGVKLESIGIYQI\*

*A.2.7. H5 variants printed on the protein microarray used for IgG, IgG1, and IgG2c antibody profiling of the H5-E2 nanoparticle vaccine (Relevant to section 4.3.7., 4.4.4., and 4.4.6.)*

H5 descriptions: variant number, Sino Biological catalog number, influenza strain, subtype, and type, expression system, protein sequence.

Variant #	Sino Biological Catalog #	Influenza Strain/Control ID	Subtype	Influenza Type	Expression System	Protein Sequence
1	11710-V08H	A/Cambodia/R0405050/2007	H5N1	A	HEK293 Cells	Met1-Gln531
2	11713-V08H	A/HongKong/213/2003	H5N1	A	HEK293 Cells	Met1-Gln531,28Ser/Trp
3	40088-V08H	A/chicken/Yamaguchi/7/2004	H5N1	A	HEK293 Cells	Met1-Gln530
4	11697-V08H	A/Egypt/2321NAMRU3/2007	H5N1	A	HEK293 Cells	Met1-Gln531
5	11062-V08H1	A/Vietnam/1194/2004	H5N1	A	HEK293 Cells	Met1-Gln531
6	11689-V08H	A/HongKong/483/1997	H5N1	A	HEK293 Cells	Met1-Gln531
7	11712-V08H	A/chicken/India/NIV33487/2006	H5N1	A	HEK293 Cells	Met1-Gln531
8	11690-V08H	A/goose/Guiyang/337/2006	H5N1	A	HEK293 Cells	Met1-Gln531
9	40001-V08H	A/duck/HongKong/P46/1997	H5N1	A	HEK293 Cells	Met1-Gln539
10	11709-V08H	A/whooperswan/Mongolia/244/2005	H5N1	A	HEK293 Cells	Met1-Gln531
11	40026-V08H	A/Cambodia/S1211394/2008	H5N1	A	HEK293 Cells	Met1-Gly341
12	11698-V08H	A/duck/Hunan/795/2002	H5N1	A	HEK293 Cells	Met1-Gln531
13	11694-V08H	A/japanesewhiteeye/HongKong/1038/2006	H5N1	A	HEK293 Cells	Met1-Gln530
14	40004-V08H	A/Xinjiang/1/2006	H5N1	A	HEK293 Cells	Met1-Gln531
15	11700-V08H	A/commonmaggpie/HongKong/2256/2006	H5N1	A	HEK293 Cells	Met1-Glu530
16	11702-V08H	A/Egypt/N05056/2009	H5N1	A	HEK293 Cells	Met1-Gln530
17	40044-V08H	A/commonmaggpie/HongKong/5052/2007	H5N1	A	HEK293 Cells	Met1-Gln530
18	40117-V08B	A/barheadedgoose/Qinghai/1A/2005	H5N1	A	Baculovirus-Insect Cells	Met1-Gln527
19	40015-V08H	A/Hubei/1/2010	H5N1	A	HEK293 Cells	Met1-Gln530
20	40024-V08B	A/goose/Guangdong/1/1996	H5N1	A	Baculovirus-Insect Cells	Met1-Gln531
21	40022-V08H	A/Vietnam/UT31413II/2008	H5N1	A	HEK293 Cells	Met1-Gln530
22	11062-V08B-B	H5N1 (A/Vietnam/1194/2004) Hemagglutinin / HA Protein (His Tag), Biotinylated	H5N1	A	Baculovirus-Insect Cells	Met1-Gln531
23	11048-V08H4	A/Anhui/1/2005	H5N1	A	HEK293 Cells	Met1-Gln530
24	40372-V08B	A/chicken/Jilin/9/2004	H5N1	A	Baculovirus-Insect Cells	Met1-Gln531
25	40160-V08B	A/barnswallow/HongKong/D101161/2010	H5N1	A	Baculovirus-Insect Cells	Met1-Gln531
26	40158-V08B	A/chicken/Vietnam/NCVD016/2008	H5N1	A	Baculovirus-Insect Cells	Met1-Gln532
27	11060-V08B1	H5N1 (A/Indonesia/5/2005) Hemagglutinin / HA-specific B cell probe (His Tag)	H5N1	A	Baculovirus-Insect Cells	Met1-Ile519
28	11060-V08B1	H5N1 (A/Indonesia/5/2005) Hemagglutinin / HA-specific B cell probe (His Tag)	H5N1	A	Baculovirus-Insect Cells	Met1-Ile519

### A.3. References

1. Lata, S.; Reichel, A.; Brock, R.; Tampe, R.; Piehler, J., High-affinity adaptors for switchable recognition of histidine-tagged proteins. *J. Am. Chem. Soc.* **2005**, *127* (29), 10205-10215.
2. Molino, N. M.; Anderson, A. K. L.; Nelson, E. L.; Wang, S.-W., Biomimetic Protein Nanoparticles Facilitate Enhanced Dendritic Cell Activation and Cross-Presentation. *ACS Nano* **2013**, *7* (11), 9743-9752.
3. Molino, N. M.; Neek, M.; Tucker, J. A.; Nelson, E. L.; Wang, S.-W., Viral-mimicking protein nanoparticle vaccine for eliciting anti-tumor responses. *Biomaterials* **2016**, *86*, 83-91.
4. Neek, M.; Tucker, J. A.; Kim, T. I.; Molino, N. M.; Nelson, E. L.; Wang, S.-W., Co-delivery of human cancer-testis antigens with adjuvant in protein nanoparticles induces higher cell-mediated immune responses. *Biomaterials* **2018**, *156*, 194-203.
5. Chen, C.; Dow, C.; Wang, P.; Sidney, J.; Read, A.; Harmsen, A.; Samuel, J. E.; Peters, B., Identification of CD4+ T Cell Epitopes in *C. burnetii* Antigens Targeted by Antibody Responses. *PLOS One* **2011**, *6* (3), e17712.
6. Xiong, X.; Qi, Y.; Jiao, J.; Gong, W.; Duan, C.; Wen, B., Exploratory Study on Th1 Epitope-Induced Protective Immunity against *Coxiella burnetii* Infection. *PLOS ONE* **2014**, *9* (1), e87206.

## **APPENDIX B**

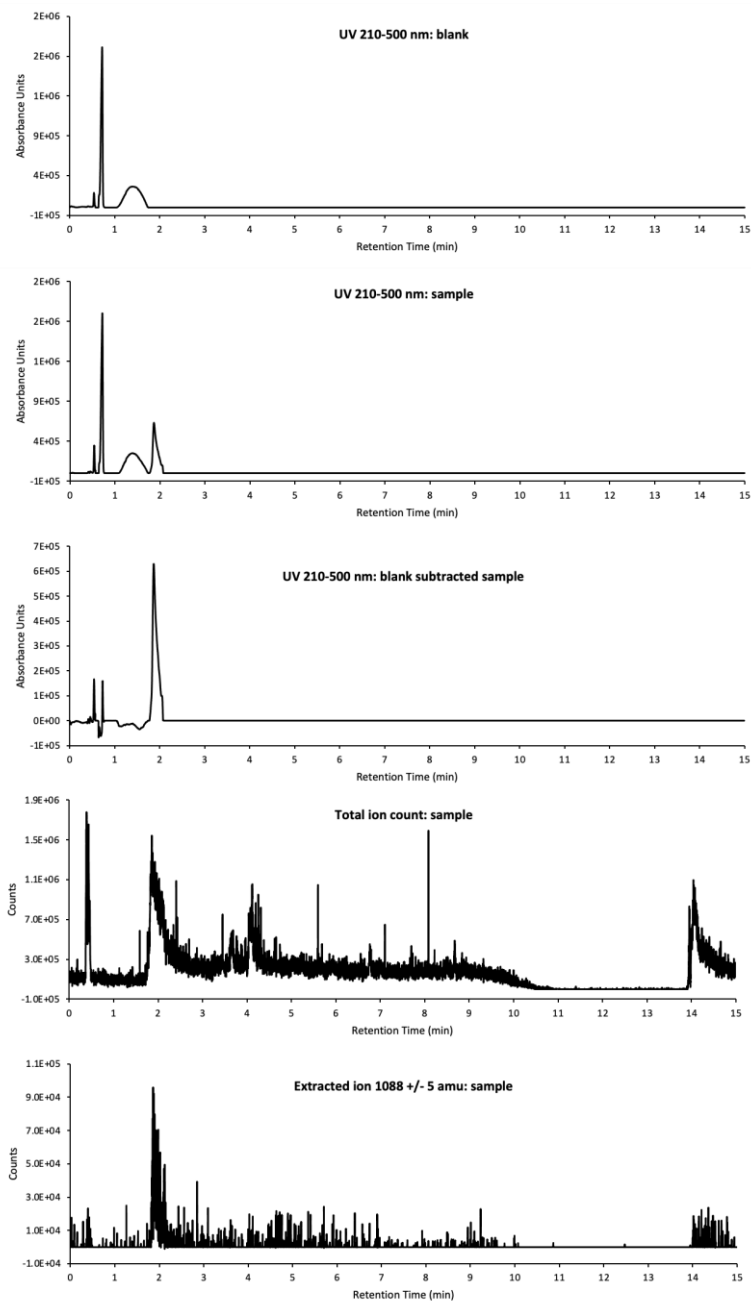
### **ADDITIONAL RESULTS**

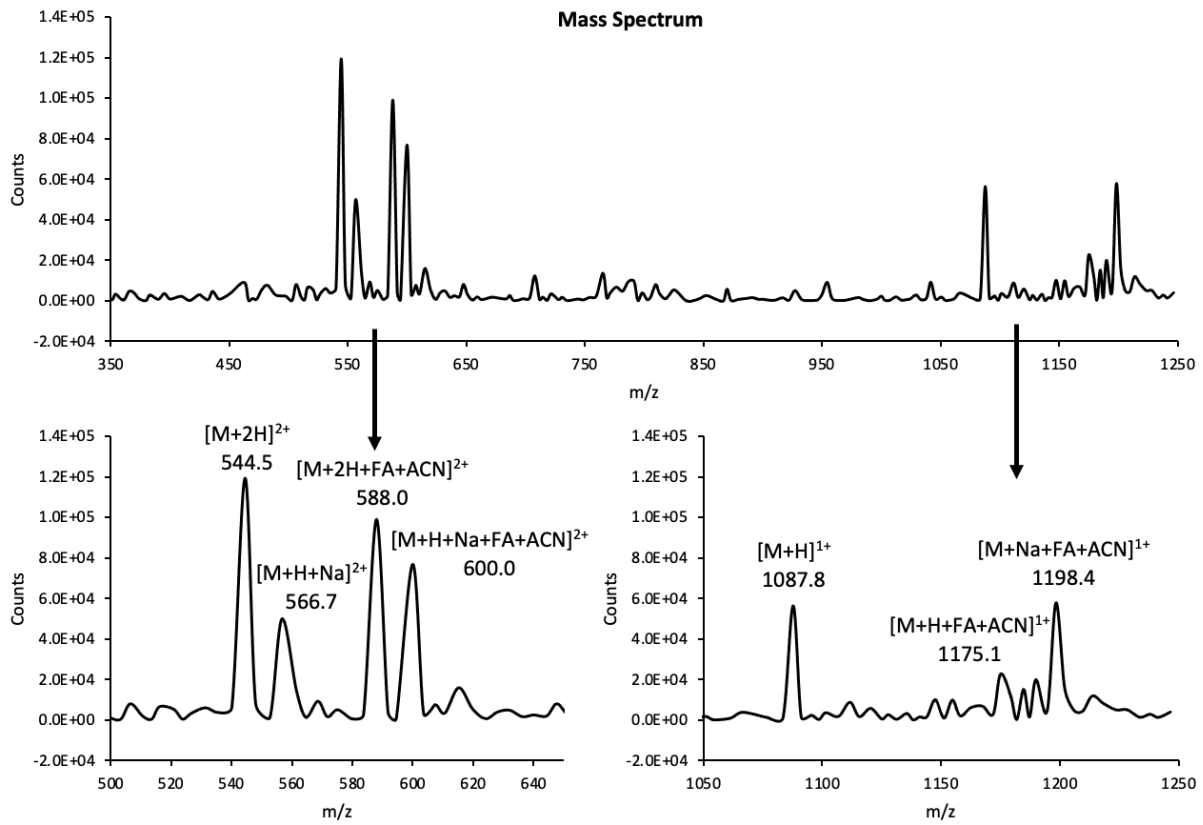
## B. Additional Results

### B.1. Liquid chromatography–mass spectrometry (LC-MS) data of maleimido tris-NTA (mal-tNTA) (Relevant to section 2.4.1.)

(A) Traces show chromatograms from final product UV and ions detected. (B) Mass spectrum of main peak, confirming identity of mal-tNTA.

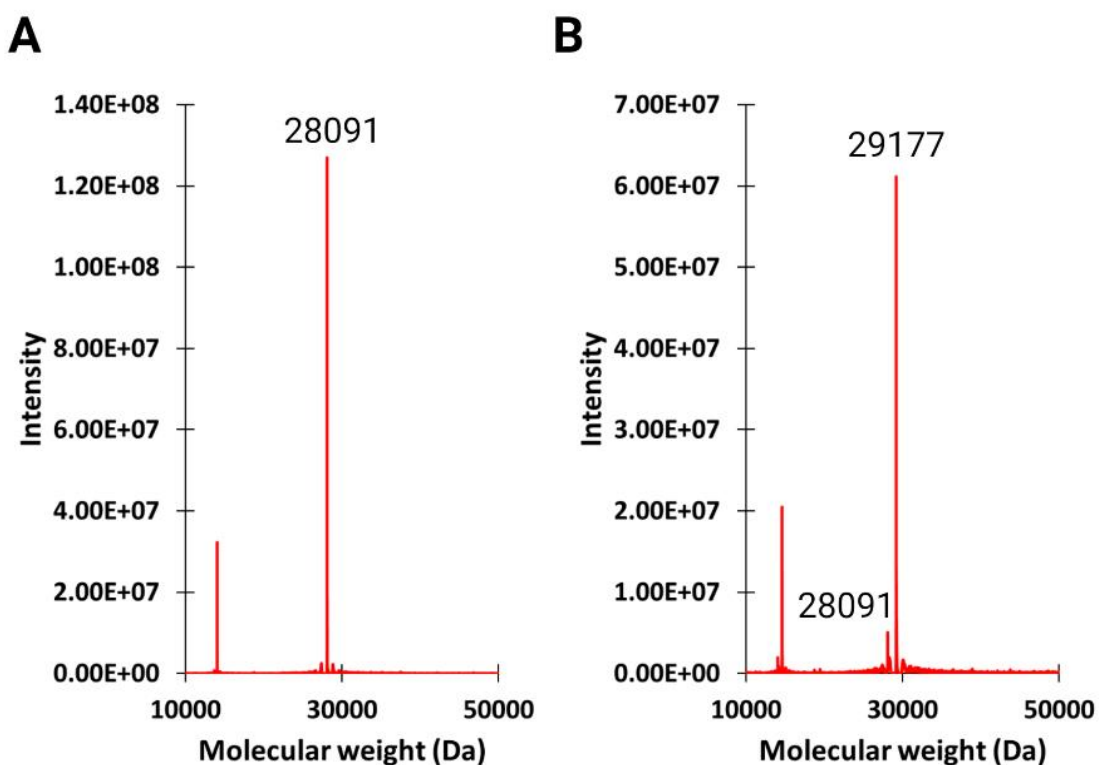
A



**B**

*B.2. Representative mass spectrometry data for E2 (E279C) and tNTA-E2 proteins (Relevant to section 2.4.2. and 3.3.5.)*

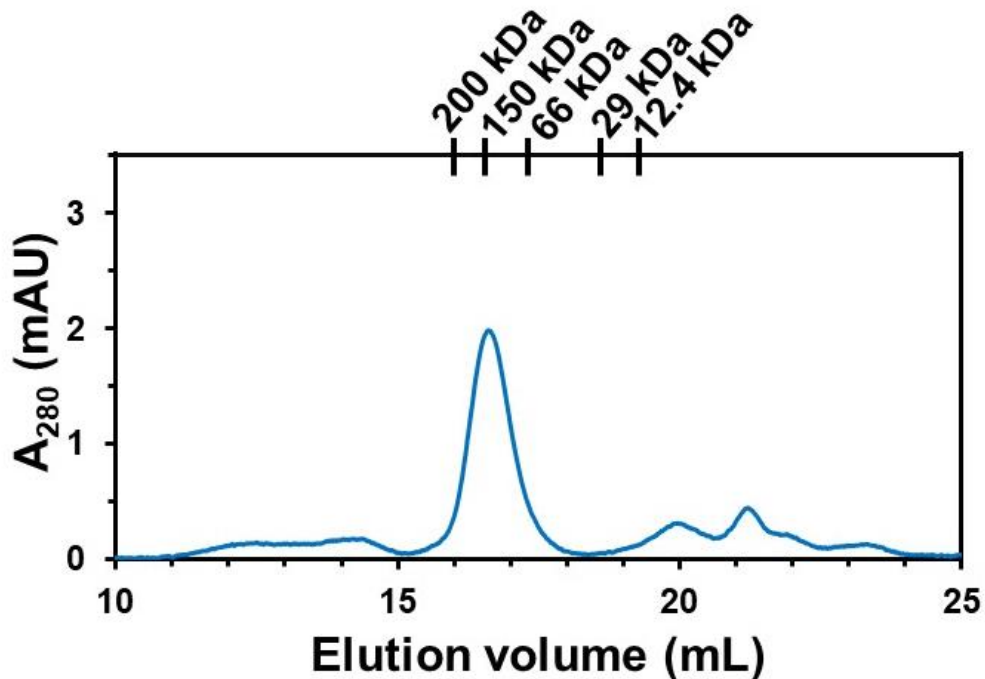
(**A**) E2 protein (E279C E2) and (**B**) E2 conjugated with mal-tNTA (tNTA-E2).  $MW_{E2 (E279C)} = 28091$  Da,  $MW_{\text{mal-tNTA}} = 1087$  Da,  $MW_{\text{tNTA-E2}} = 29177$  Da. Data shows near-complete conjugation of the tNTA linker for each protein monomer. Because the 60-mer nanoparticle is assembled via non-covalent intermolecular interactions, the use of relatively high-energy, non-native conditions in the ESI-MS instrument dissociates the protein nanoparticles into its monomers, yielding monomeric molecular weight values.





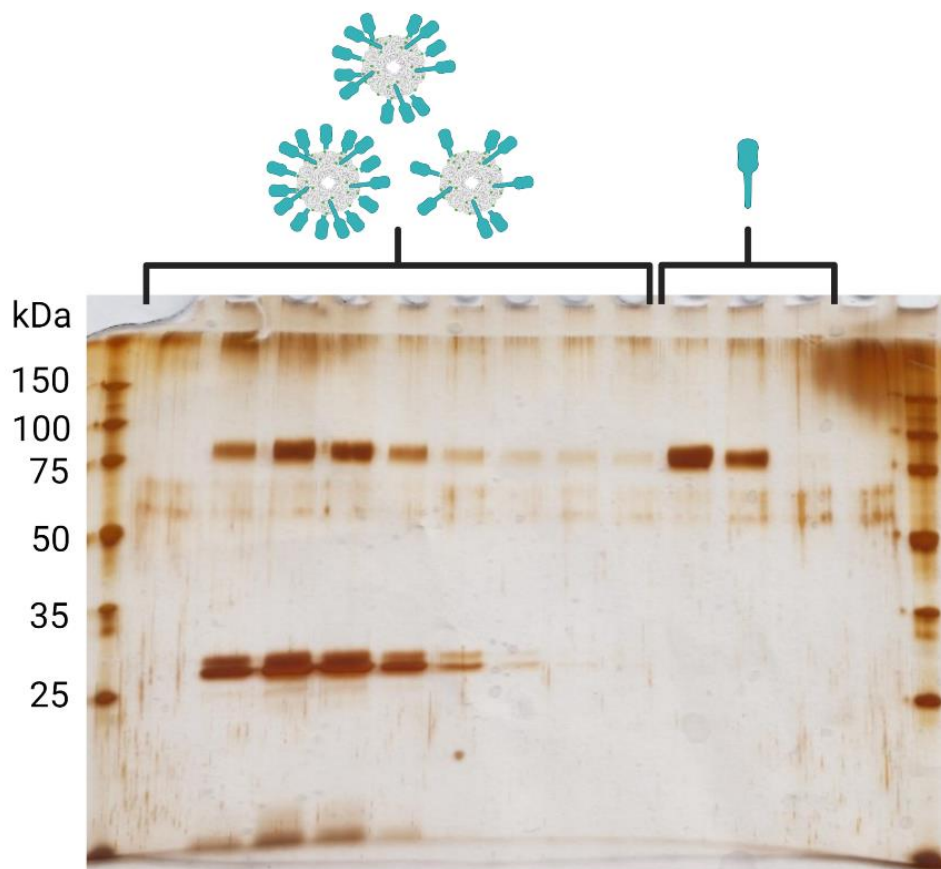
### B.3. Size exclusion chromatography (SEC) of H1 (Relevant to section 2.4.2.)

H1 is shown as solid blue line. Elution volumes of molecular weight (MW) standards are marked at the top of the chromatogram. The SEC elution peak of our soluble H1 (as-received) is located between 66 and 150 kDa, and this is consistent with other studies reporting monomeric HA proteins (with trimeric forms eluting at molecular weights >400 kDa).<sup>1-4</sup> MW standards included:  $\beta$ -amylase (200 kDa), alcohol dehydrogenase (150 kDa), albumin bovine serum (66 kDa), carbonic anhydrase (29 kDa), and cytochrome c (12.4 kDa). MW standards were run according to manufacturer's suggestions (Sigma Aldrich Cat#: MWGF200), on a Superose™ 6 increase 10/300 GL analytical column (Cytiva). A comparison of our H1 elution profile with H1 monomer and H1 trimer elution profiles from McMillan *et al.*<sup>2</sup> supports that our H1 protein is in monomeric form. No significant  $A_{280}$  signal was observed from 0-10 ml.



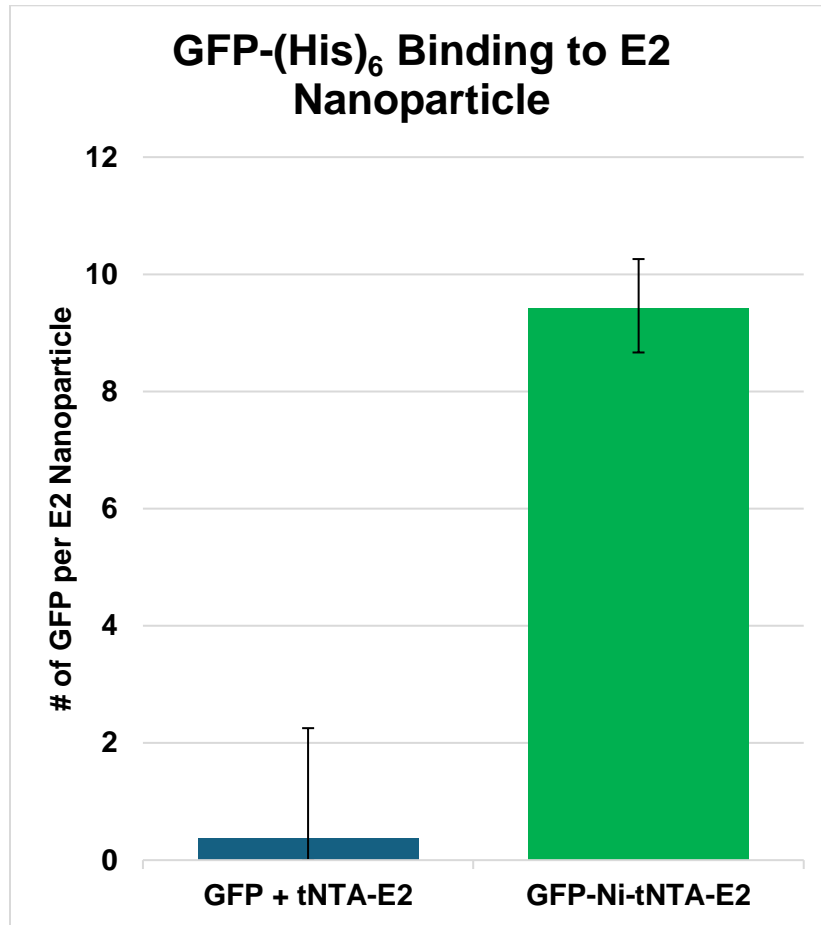
*B.4. SDS-PAGE with silver stain of fractions collected from analytical SEC used to separate H1-E2 from unbound H1 (Relevant to section 2.4.2.)*

Each collected fraction was analyzed with SDS-PAGE, and confirmed H1-bound E2 in the first SEC peak and unbound H1 in the second peak.  $MW_{E2(E279C)} = 28091$  Da,  $MW_{iNTA-E2} = 29177$  Da,  $MW_{H1} = 59000$  Da. Due to its glycosylation H1 runs at ~66-95kDa on SDS-PAGE under reducing conditions.



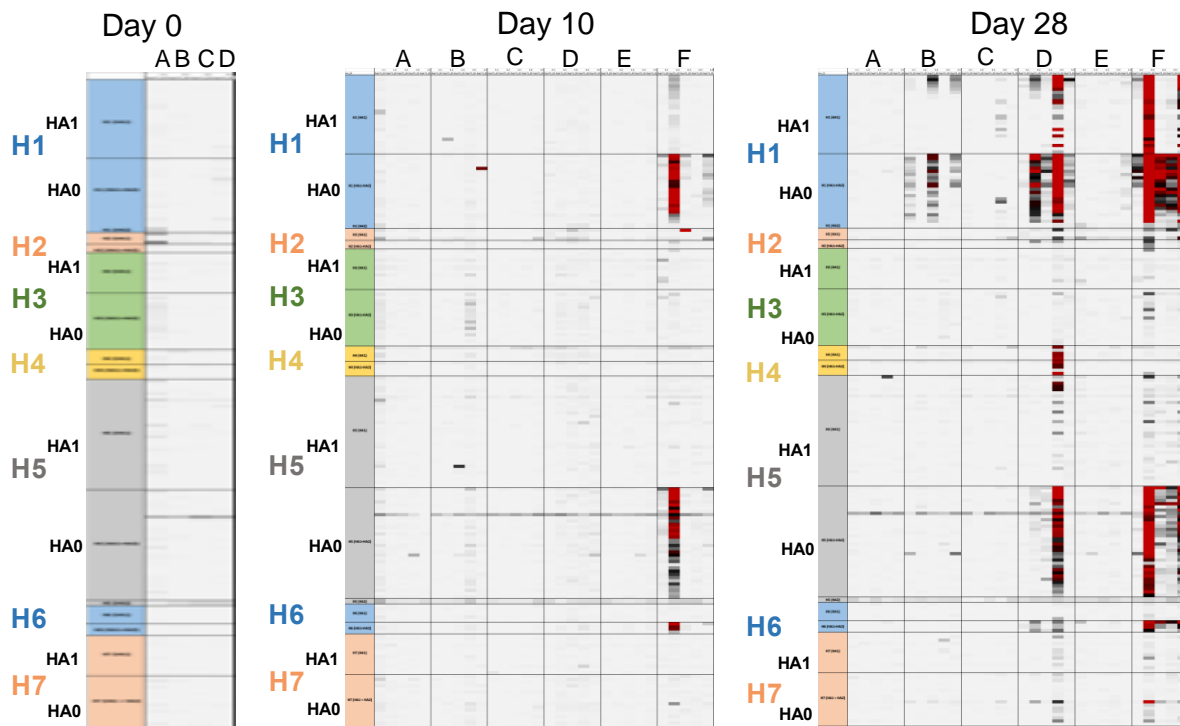
*B.5. GFP attachment to E2 (Relevant to section 2.4.2.)*

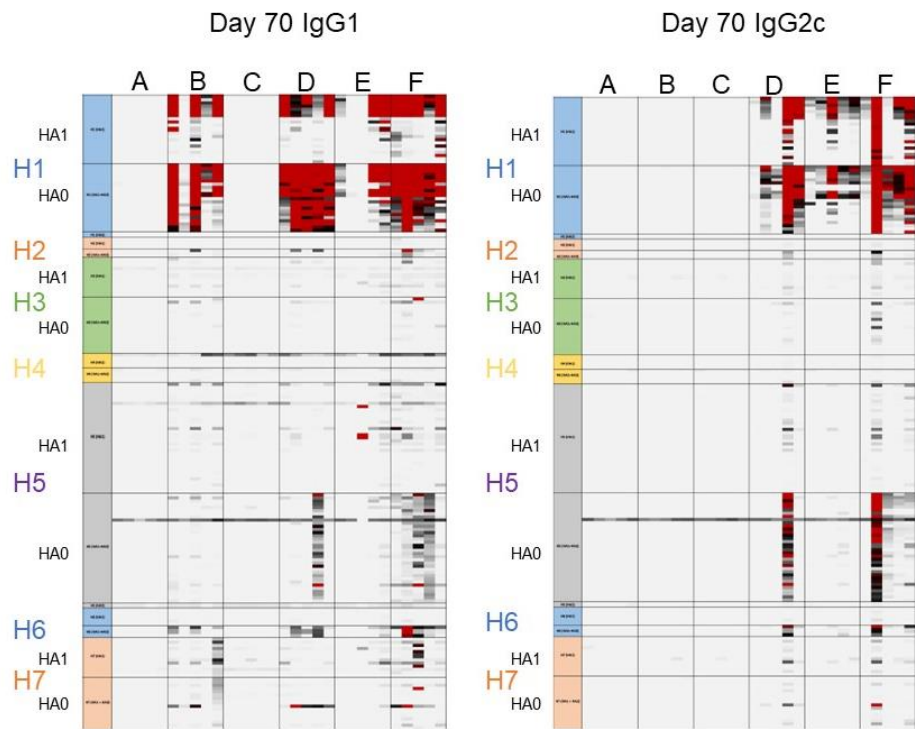
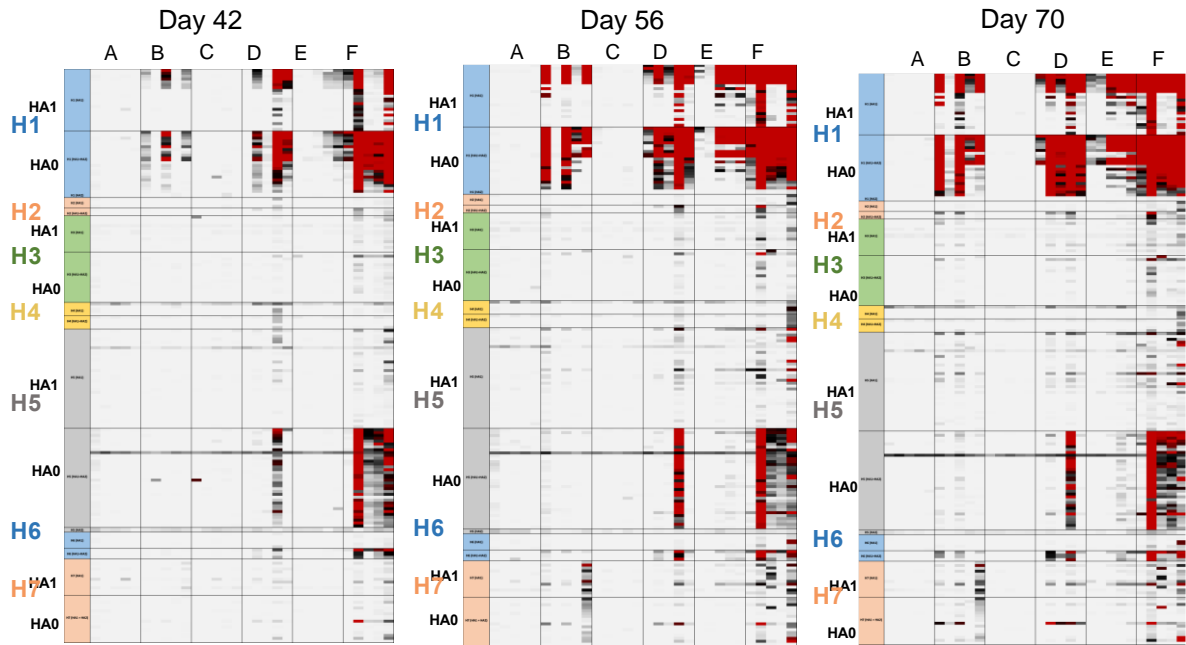
Bar graph of the number of GFP bound to Ni-tNTA-E2 after high affinity Ni-tNTA + (His)<sub>n</sub>-protein conjugation. tNTA-E2 is not loaded with Ni, thus no binding is expected. Ni-tNTA-E2 is loaded with Ni, thus binding is expected.



*B.6. Antibody arrays from sera of immunized mice (Relevant to section 2.3.8. and 2.4.3. and 2.4.5.)*

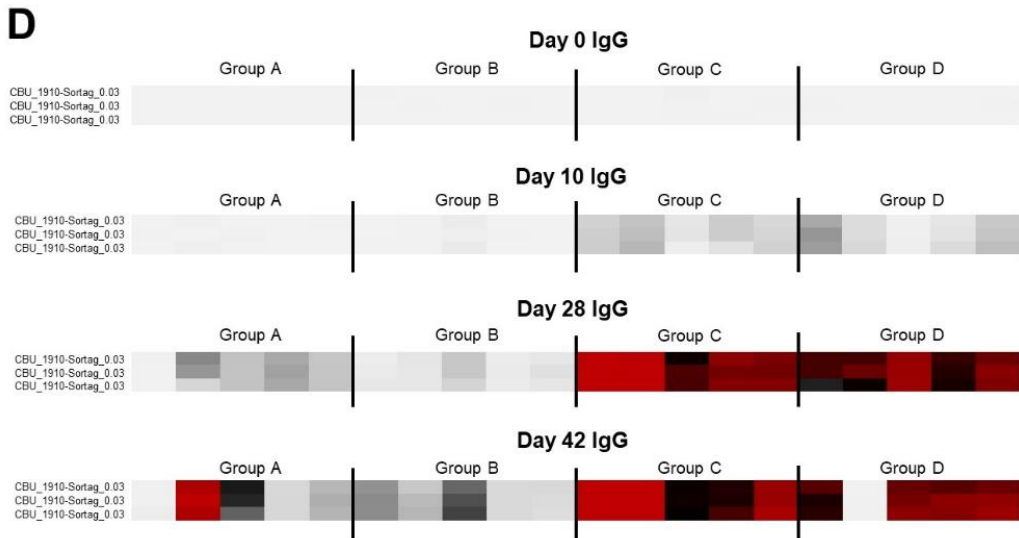
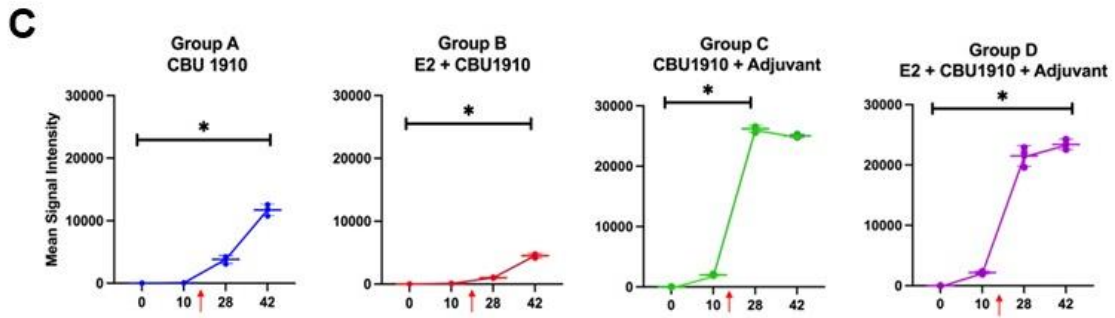
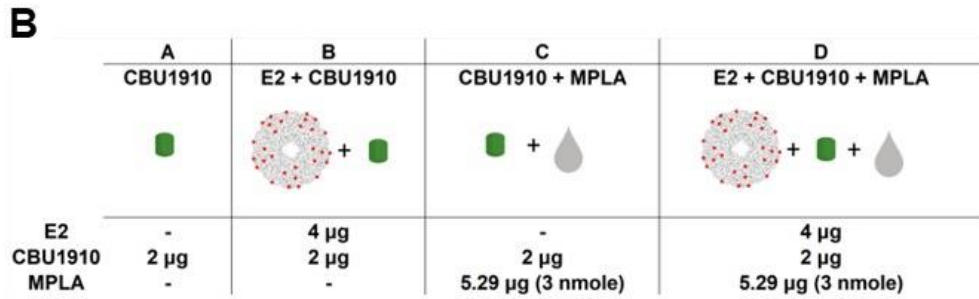
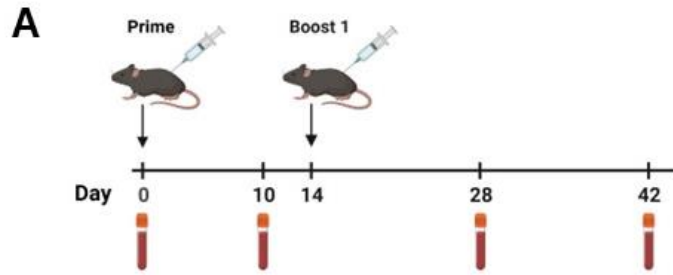
Six groups of 5 B6 mice (Groups A to F) were administered different formulations on d0 and boosted on d14 and d49. IgG, IgG1, and IgG2c signal intensities were determined at different time points post-prime against HA variants displayed on protein microarrays (Signals to H1 through H7 variants are shown). Microarray data was compiled into heat map compilations with columns representing immunized mice groups and rows representing individual HA variants and their specific HA1 and HA0 domains (red = high amount of binding, white = low amount of binding). Within each HA1 and HA0 row were the individual domains of homosubtypic HA variants (i.e., 23 variants of H1 were analyzed). Group A: PBS, Group B: H1, Group C: H1 + E2, Group D: H1 + E2 + MPLA, Group E: H1-E2, Group F: H1-E2 + MPLA. Day 0 sera = naive mice.





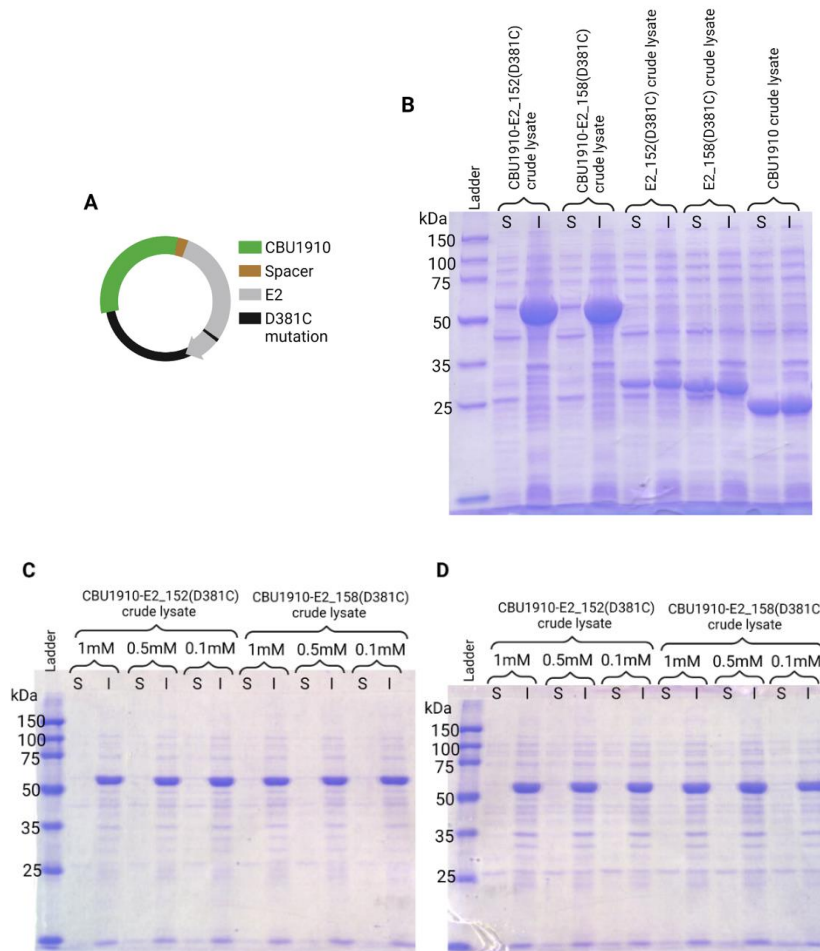
*B.7. CBU1910-specific IgG profiling by protein microarray shows potential antibody suppression from co-mixing of E2 with protein target antigen, CBU1910 (Relevant to section 2.4.3.)*

(A) Timeline of immunizations and plasma collection. (B) Table summarizing the vaccine groups and dose amounts per injection. Group A) CBU1910 only; Group B) E2 nanoparticle and CBU1910 (unconjugated); Group C) CBU910 with MPLA (TLR4 agonist); Group D) E2 nanoparticle and CBU1910 (unconjugated), with MPLA (TLR4 agonist). (C) CBU1910-specific IgG profiling by protein microarray. Four groups of 5 B6 mice (Groups A to D) were administered different formulations as indicated and boosted on d14 (red arrows). Array data are shown as dots plots of IgG signal intensities at different time points post-prime against CBU1910 displayed on a *Coxiella burnetii* protein microarray; each dot represents a replicate (of 3) of CBU1910 (mean of 5 mice) with lines connecting the means ( $\pm$  SD error bars). One-way ANOVA (non-parametric) comparisons using a Kruskal-Wallis test were made between both pre- and post-boost time points: \* $p < 0.05$ . (D) Microarray raw data was compiled into heat map compilations with columns representing immunized mice groups and rows representing CBU1910 (red = high amount of binding, white = low amount of binding). Abbreviations: MPLA, monophosphoryl lipid A.



**B.8. Direct recombinant fusion of CBU1910 onto E2 protein nanoparticles (Relevant to section 3.4.1.1.)**

**(A)** Plasmid construction of genetically fused CBU1910-E2 mutant in pET11a vector. **(B)** SDS-PAGE of expression studies of CBU1910-E2 mutants in BL21(DE3) *E. coli*. Expression at 37°C and induced with 1 mM IPTG. S: soluble fraction, I: insoluble fraction **(C)** SDS-PAGE of expression studies at 37°C induced with different concentrations of IPTG. S: soluble fraction, I: insoluble fraction, 1 mM: 1 mM IPTG induction, 0.5 mM: 0.5 mM IPTG induction, 0.1 mM: 1 mM IPTG induction. All samples diluted 1/10 when loaded into SDS-PAGE gel. **(D)** SDS-PAGE of expression studies at 20°C induced with different concentrations of IPTG. S: soluble fraction, I: insoluble fraction, 1 mM: 1 mM IPTG induction, 0.5 mM: 0.5 mM IPTG induction, 0.1 mM: 1 mM IPTG induction.





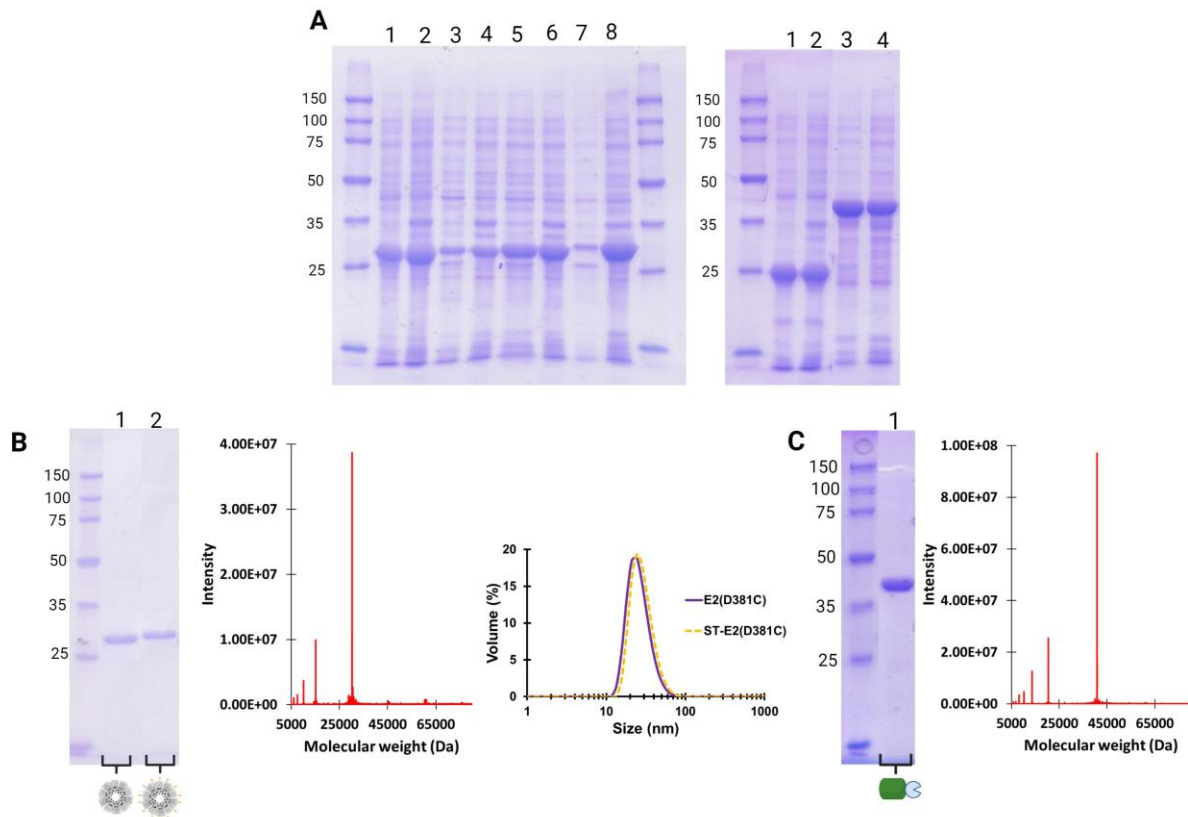
B.9. *tNTA-Ni + CBU1910 conjugation conditions optimization (Relevant to section 3.3.5. and 3.4.1.2.)*

Table of excipients tested to stabilize CBU1910-E2 constructs during tNTA-Ni/HisTag conjugation. Aggregation/precipitation and intact nanoparticle structure were determined based on DLS analysis. +++: high percentage of monodispersed particles; ++: mixture of monodispersed and aggregated particles; +: extreme aggregation of particles. A high NaCl concentration of 360 mM in a HEPES buffer system using low CBU1910:E2 molar ratios demonstrated the most consistent ability to alleviate aggregation during conjugation.

<b>E2:CBU1910 molar ratio</b>	<b>Buffer</b>	<b>Additive</b>	<b>Concentration of Additive</b>	<b>DLS</b>
1:2	Phosphate buffer (pH = 7.4)	Salt (NaCl)	10 mM	+
			100 mM	+
			200 mM	+
			360 mM	+
1:1	Phosphate buffer (pH = 7.4)	Salt (NaCl)	5 mM	+
			100 mM	+
			200 mM	+
			360 mM	+
1:0.5	Phosphate buffer (pH = 7.4)	Salt (NaCl)	15 mM	+
			100 mM	+
			200 mM	++
			360 mM	++
			450 mM	++
			550 mM	++
	HEPES buffer (pH = 7.3)	Salt (NaCl)	150 mM	++
			250 mM	+++
			360 mM	++
			450 mM	+++
			550 mM	++
			Sucrose Dextrose	10% (w/v) 5% (w/v)
1:0.3	HEPES buffer (pH = 7.3)	Salt (NaCl)	360 mM	+
		Salt (NaCl) + Tween 80	360mM + 0.004% (v/v)	+
		Salt (NaCl) + Tween 80	360mM + 0.004% (v/v)	+
1:0.1	HEPES buffer (pH = 7.3)	Salt (NaCl)	360 mM	+++
		Salt (NaCl) + Tween 80	360mM + 0.004% (v/v)	+++

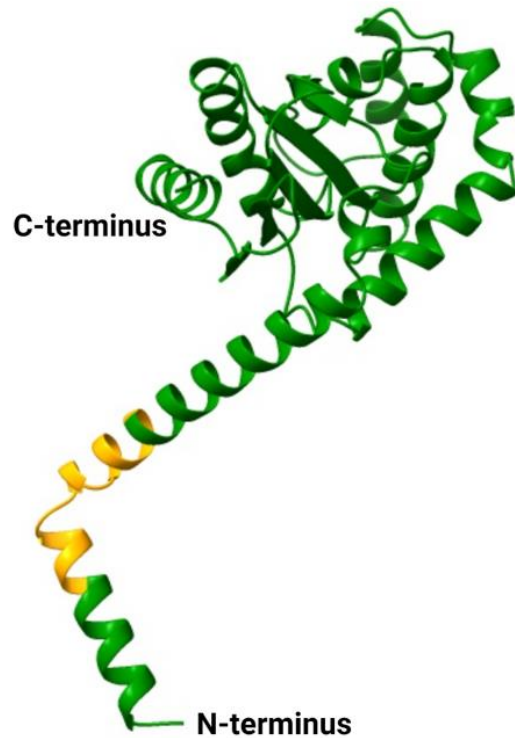
*B.10. Expression and characterization of ST-E2 and SC-CBU1910 (Relevant to section 3.4.1.3.)*

(A) SDS-PAGE from small scale expression studies of ST-E2 and SC-CBU1910. (left) 1: E2(D381C) soluble fraction; 2: E2(D381C) insoluble fraction; 3: E2\_152(D381C) soluble fraction; 4: E2\_152(D381C) insoluble fraction; 5: ST-E2(D381C) soluble fraction; 6: ST-E2(D381C) insoluble fraction; 7: ST-E2\_152(D381C) soluble fraction; 8: ST-E2\_152(D381C) insoluble fraction (right) 1: CBU1910 soluble fraction; 2: CBU1910 insoluble fraction; 3: SC-CBU1910 soluble fraction; 4: SC-CBU1910 insoluble fraction. (B) Characterization of ST-E2(D381C). Representative (left) SDS-PAGE, (middle) protein mass spectrometry showing ~2 kDa increase in E2 monomer when ST is recombinantly fused to its N-terminus, and (right) DLS indicating ~1 nm increase in diameter when ST is added to surface of E2 nanoparticles. (C) Characterization of SC-CBU1910. Representative (left) SDS-PAGE and (right) protein mass spectrometry showing final result of protein-protein with a molecular weight of ~40.8 kDa.



*B.11. Alphafold2 Colab to predict the folded structure of CBU1910 (Relevant to section 3.4.1.3.)*

The amino acid sequence of the transmembrane truncated form of CBU1910 was input into Alphafold2 and its output .pdb file was viewed on ChimeraX. Orange highlighted region = CBU1910p sequence.



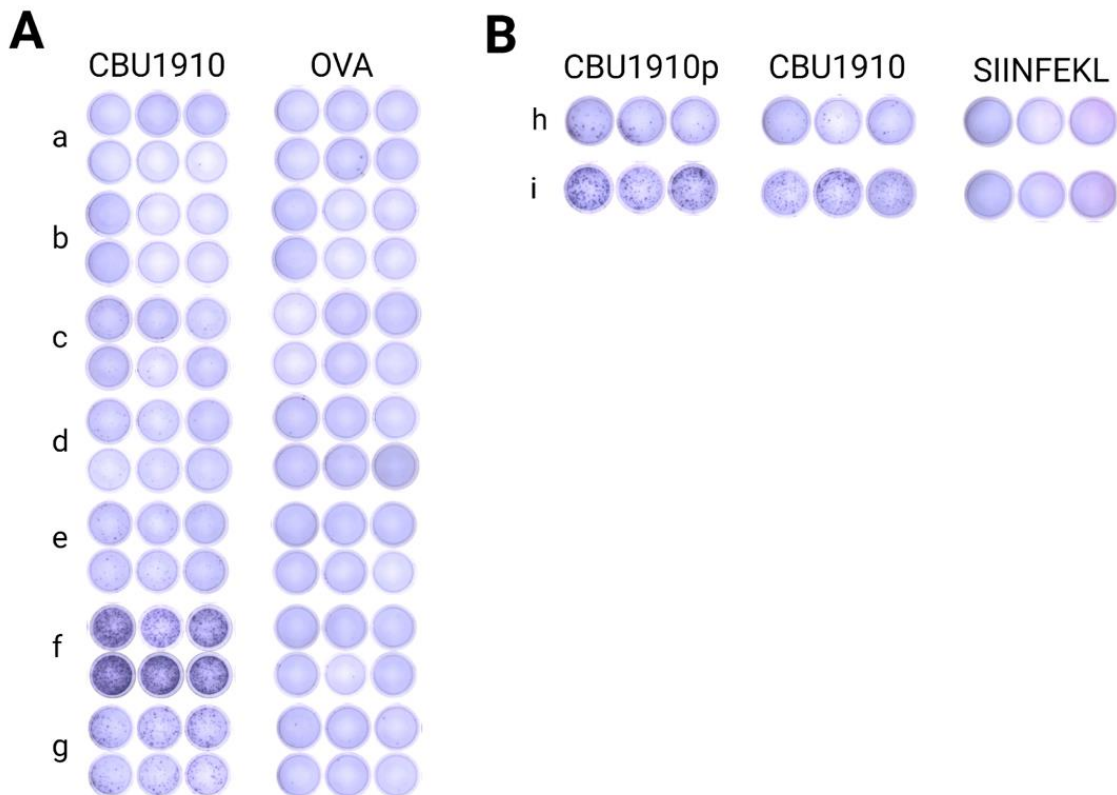
B.12. ST/SC reaction conditions optimization for CBU1910-E2 nanoparticles (Relevant to section 3.4.1.3.)

Table of excipients tested to stabilize CBU1910-E2 constructs during ST/SC reaction. Aggregation/precipitation and intact nanoparticle structure were determined based on SDS-PAGE and DLS analysis. +++X: highly soluble but disassembled particles; +++: high percentage of monodispersed particles; ++: mixture of monodispersed and aggregated particles; +: extreme aggregation of particles. A 0.08-0.0875% (w/v) Sarkosyl (SLS) condition demonstrated consistent ability to alleviate aggregation while keeping nanoparticles intact.

E2:CBU1910 molar ratio	Buffer	Additive	Concentration of Additive	DLS
1:0.5	Phosphate buffer (pH = 7.4)	None		+
		CHAPS	1% (w/v)	++
			2% (w/v)	++
			10% (w/v)	+
		Tween 20	0.1% (w/v)	+
			1% (w/v)	+
		Tween 80	0.1% (w/v)	+
			1% (w/v)	+
		pH	pH=4-5	+
			pH=9-10	+++X
		Salt (NaCl)	250mM	+
			500mM	++
		SLS	0.1% (w/v)	+++X
			0.09% (w/v)	+++
			0.0875% (w/v)	+++
			0.085% (w/v)	+++
			0.08% (w/v)	+++
			0.0775% (w/v)	++
			0.075% (w/v)	++
			0.0725% (w/v)	+
0.07% (w/v)	+			
0.0675% (w/v)	++			
0.065% (w/v)	+			
0.06% (w/v)	+			
0.055% (w/v)	+			
0.05% (w/v)	+			

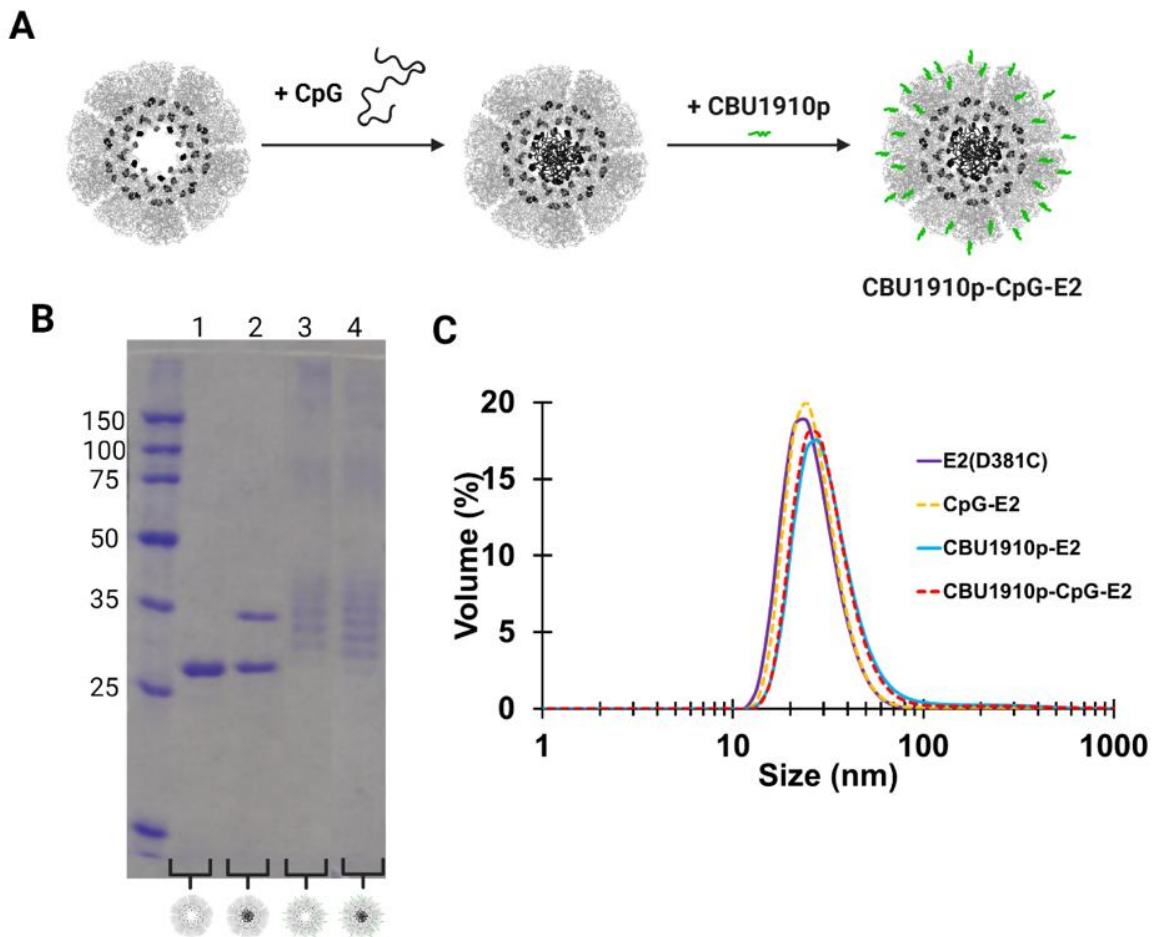
*B.13. ELISpot analysis of splenocytes after immunizations with CBU1910 and CBU1910p formulations (Relevant to section 3.4.5.)*

(A) Representative ELISpot data from splenocytes of immunized groups (a-g, CBU1910-E2 groups), pulsed *ex vivo* with relevant protein (CBU1910) or irrelevant protein (OVA) and analyzed for antigen-specific IFN- $\gamma$  secretion. (B) Representative ELISpot data from splenocytes of immunized groups (h = CBU1910p and i = CBU1910p-CpG-E2), pulsed *ex vivo* with relevant peptide or protein (CBU1910p or CBU1910) or irrelevant peptide (SIINFEKL) and analyzed for antigen-specific IFN- $\gamma$  secretion.



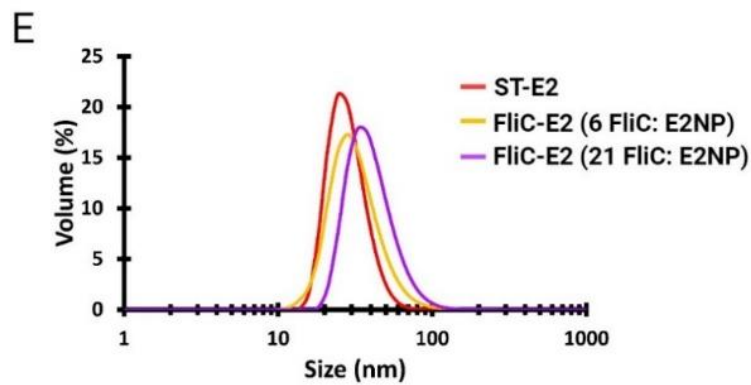
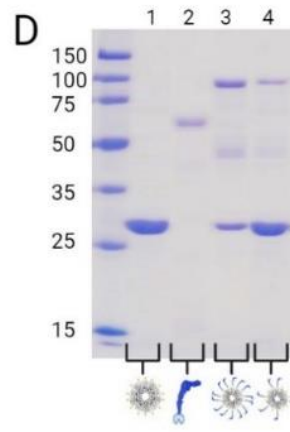
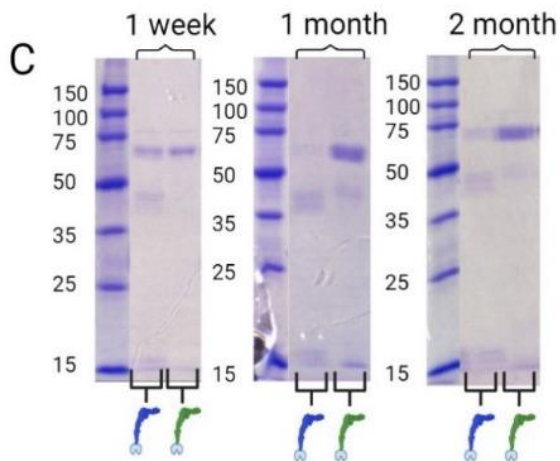
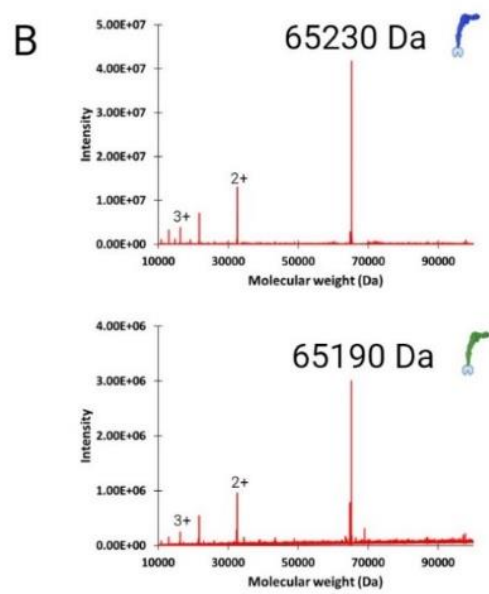
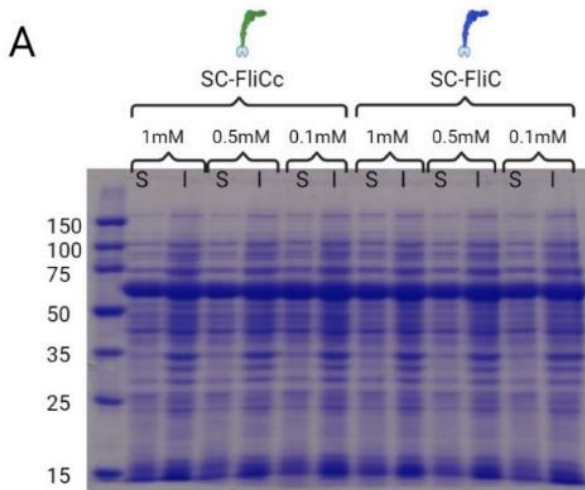
*B.14. Conjugation of CBU1910p onto E2 nanoparticles (Relevant to section 3.4.5.)*

(A) Structure of E2(D381C) with representative 60 cysteine groups in black. Schematic of CpG1826 and CBU1910p conjugation onto E2. (B) SDS-PAGE of formulation synthesis. 1: E2; 2: CpG-E2; 3: CBU1910p-E2; 4: CBU1910p-CpG-E2. Quantification indicated  $22.3 \pm 1.5$  CpG 1826 molecules were conjugated internally and  $166 \pm 11.2$  CBU1910p peptides were conjugated externally per 60-mer E2 nanoparticle, similar to previous E2 formulations.<sup>5</sup> (C) Hydrodynamic diameters of E2 constructs after CpG and CBU1910p conjugations. The average hydrodynamic diameter of CpG-E2, CBU1910p-E2 and CBU1910p-CpG-E2 nanoparticles was  $27.1 \pm 0.4$  nm,  $35.4 \pm 2.7$  nm, and  $31.9 \pm 1.7$  nm, respectively.



*B.15. Characterization of the purity and stability of SC-FliC and SC-FliCc, and the FliC-E2 nanoparticle (Relevant to section 4.4.1.)*


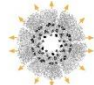


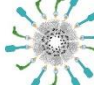
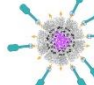
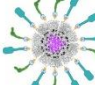
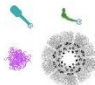
(A) Expression of SpyCatcher fused wild type (FliC) and cysteine stabilized (FliCc) flagellin at 37°C induced with 1, 0.5, and 0.1 mM IPTG.  $MW_{\text{Flagellin}} = \sim 65$  kDa. S: soluble; I: insoluble. (B) Mass spectrometry of purified SC-FliC (top, blue) and SC-FliCc (bottom, green). (C) SDS-PAGE comparing stability of SC-FliCc and SC-FliC after 1 week, 1 month, and 2 months at 4°C. (D) SDS-PAGE showing nanoparticles with  $\sim 6$  and  $\sim 21$  SC-FliC loaded on the external surface.  $MW_{\text{ST-E2}} = 30.2$  kDa,  $MW_{\text{SC-FliC}} = 65.2$  kDa,  $MW_{\text{FliC-E2}} = 95.4$  kDa. Lanes: 1. ST-E2; 2. SC-FliC; 3. FliC-E2 (6 FliC: E2NP); 4. FliC-E2 (21 FliC: E2NP). (E) Hydrodynamic diameters of FliC-E2 NPs with  $\sim 6$  and  $\sim 21$  FliC loaded on the external surface.





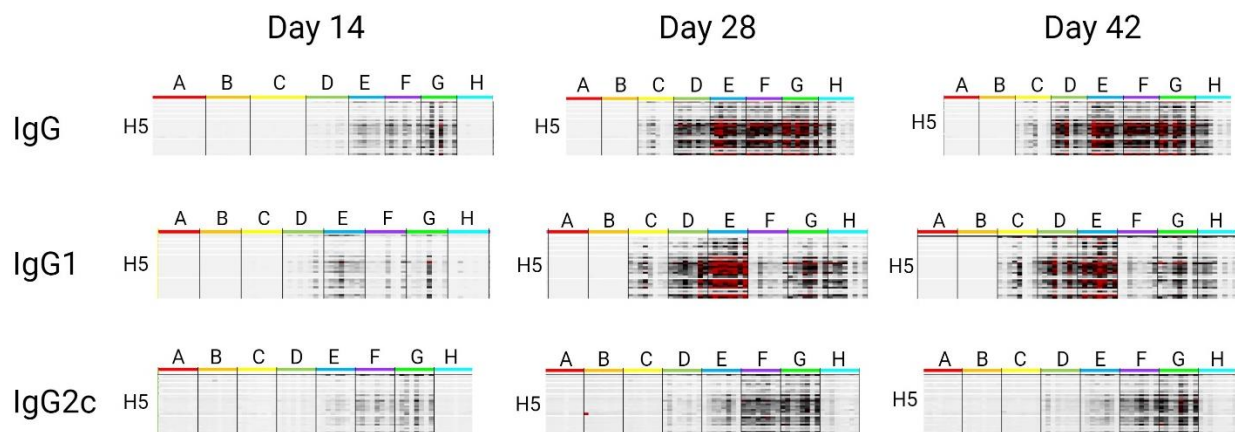
B.16. Table describing each H5 formulation and its individual components in mass and mole amounts per immunization (Relevant to section 4.4.4.)

3.5 µg of E2 is equivalent to 0.12 nmol of E2. 0.2 µg of CpG is equivalent to 0.03 nmol of CpG. 0.6 µg of FliCc is equivalent to 0.01 nmol of FliCc. 2 µg of H5 is equivalent to 0.03 nmol of H5.

	A	B	C	D	E	F	G	H
	PBS	ST-E2	SC-H5	H5-E2	H5-FliCc-E2	H5-CpG-E2	H5-FliCc-CpG-E2	SC-H5 + SC-FliCc + CpG + E2
								
E2	-	3.5 µg (0.12 nmol)	-	3.5 µg (0.12 nmol)	3.5 µg (0.12 nmol)	3.5 µg (0.12 nmol)	3.5 µg (0.12 nmol)	3.5 µg (0.12 nmol)
CpG	-	-	-	-	-	0.2 µg (0.03 nmol)	0.2 µg (0.03 nmol)	0.2 µg (0.03 nmol)
FliCc	-	-	-	-	0.6 µg (0.01 nmol)	-	0.6 µg (0.01 nmol)	0.6 µg (0.01 nmol)
H5	-	-	2 µg (0.03 nmol)	2 µg (0.03 nmol)	2 µg (0.03 nmol)	2 µg (0.03 nmol)	2 µg (0.03 nmol)	2 µg (0.03 nmol)

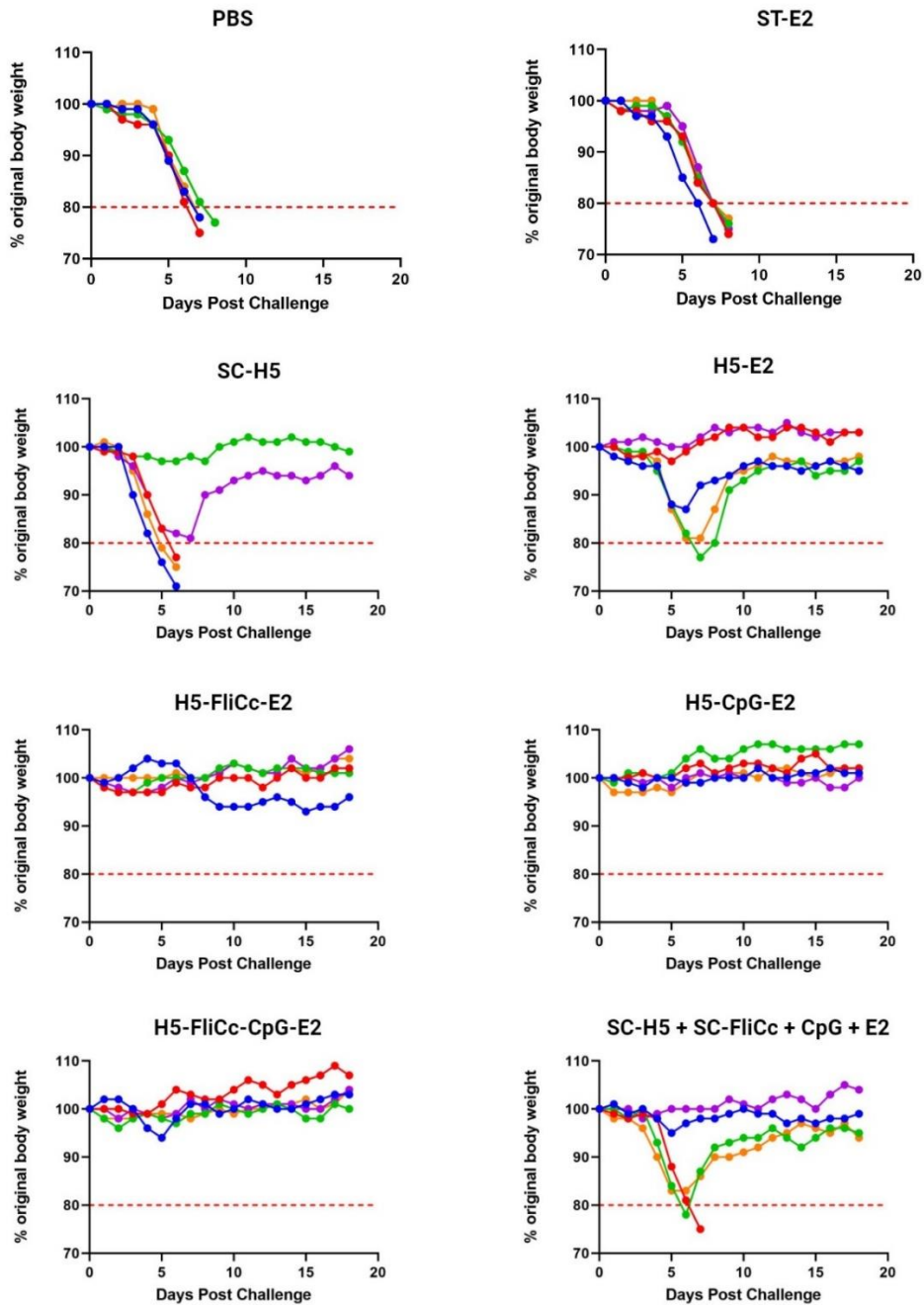
*B.17. Antibody arrays from sera of immunized mice (Relevant to section 4.3.7. and 4.4.4.)*

Eight groups of 8 mice (Groups A to H) were administered different formulations on day 0 and boosted on day 14. IgG, IgG1, and IgG2c signal intensities were determined at different time points post-prime against H5 variants displayed on protein microarrays. Microarray data was compiled into heat map compilations with columns representing immunized mice groups and rows representing individual H5 variants (i.e., 28 variants of H5 were analyzed) (red = high amount of binding, white = low amount of binding). Group A: PBS, Group B: ST-E2, Group C: SC-H5, Group D: H5-E2, Group E: H5-FliCc-E2, Group F: H5-CpG-E2, Group G: H5-FliCc-CpG-E2, Group H: SC-H5 + SC-FliCc + CpG + E2.



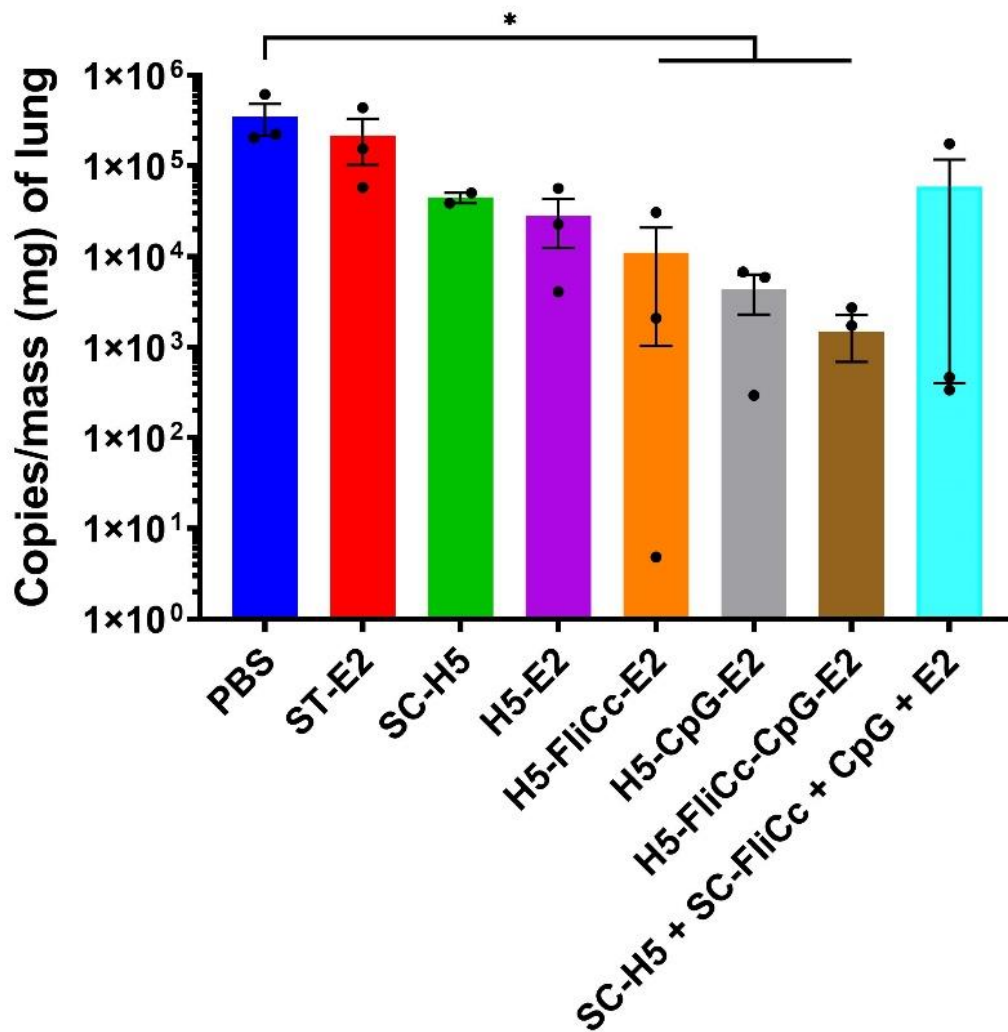
B.18. Individual weight curves of mice during H5N1 challenge (Relevant to section 4.4.8.)

Mice weights and physical state were monitored over 18 days after H5N1 virus inoculation. Each group had 5 mice. One mouse from the PBS group was evaluated to be an outlier using Grubb's outlier test comparing maximum weight loss between mice. The red dotted line indicates 20% weight loss.



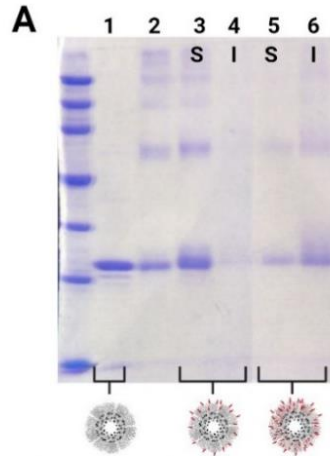
B.19. Viral loads in lungs four days post H5N1 challenge (Relevant to section 4.4.8.)

Influenza hemagglutinin H5 gene quantification by qPCR, represented as gene copies of hemagglutinin H5 normalized to the weight of the lungs. Each group had 3 mice. (Data of one sample from the SC-H5 group could not be acquired. Data of one sample from the H5-FliCc-CpG-E2 group was between 0-1 copy/mg of lung.). Statistical significance was determined by one-way ANOVA followed by a Tukey multiple comparisons test. \* $p < 0.05$ .



*B.20. Optimizing reaction conditions to improve solubility of higher-density Pam3-E2 nanoparticles (Relevant to section 4.4.9.1.)*

(A) SDS-PAGE comparing the solubility of low-density and high-density Pam3-E2 NPs. 1: E2 (D381C); 2: SMCC-E2; 3&4: low-density Pam3-E2; 5&6: high-density Pam3-E2. S: soluble, I: insoluble. (B) Table of excipients tested to stabilize Pam3-E2 constructs during conjugation reaction. Mixing additive and E2 together then adding Pam3 (Additive + E2 mixing); Mixing additive and Pam3 together then adding E2 (Additive + Pam3 mixing); Mixing additive with E2 and additive with Pam3 then combining mixtures (Additive + E2 + Pam3 mixing). Aggregation/precipitation and intact nanoparticle structure were determined based on SDS-PAGE and DLS analysis. +++X: highly soluble but disassembled particles; ++X: mixture of aggregated and disassembled particles; +++: high percentage of monodispersed particles; ++: mixture of monodispersed and aggregated particles; +: extreme aggregation of particles. A 0.01% (w/v) SLS condition demonstrated the ability to alleviate aggregation while keeping nanoparticles intact.

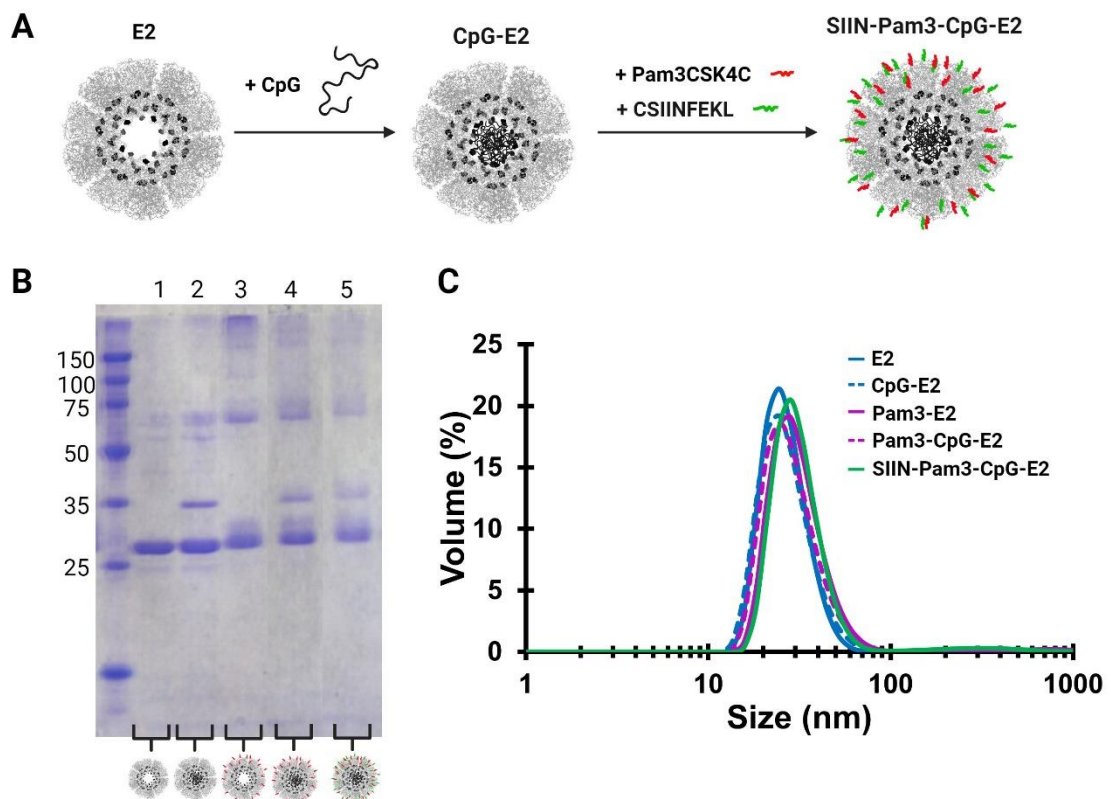


**B**

E2:Pam3CSK4 molar ratio	Buffer	Additive	Concentration of Additive	Degree of solubilization from additive mixing technique		
				Additive + E2	Additive + Pam3	Additive + E2 + Pam3
1:5	Phosphate buffer (pH = 7.4)	None		+	+	+
		NaCl	500 mM	+	++	+
		Tween 20	1% (v/v)	++X	++X	++X
			0.1% (v/v)	+	+	+
			0.001% (v/v)	+	+	+
		Tween 80	1% (v/v)	++X	++X	++X
			0.1% (v/v)	+	+	+
			0.001% (v/v)	+	+	+
		Sarkosyl (SLS)	0.1 (w/v)	+++	+++	+++
			0.05 (w/v)	++	+	++
		DMSO	10% (v/v)	+	+	+
		Sucrose	10% (w/v)	+	+	+
			1% (w/v)	+	+	+
		Dextrose	10% (w/v)	+	+	+
			1% (w/v)	+	+	+
		Glycerol	50% (v/v)	+	+	+
			10% (v/v)	+	+	+
			1% (v/v)	+	+	+
		CHAPS	0.25% (w/v)	+	++	+
			0.025% (w/v)	+	+	+
DMF	10% (v/v)	+	++	+		

*B.21. Characterization of Pam3CSK4C and CSIIINFEKL conjugated onto E2 nanoparticles (Relevant to section 4.4.9.2.)*

(A) Structure of E2(D381C) with representative 60 cysteine groups in black. Schematic of CpG1826, Pam3CSK4C (Pam3), and CSIIINFEKL (SIIN) conjugation onto E2. (B) SDS-PAGE of formulation synthesis. 1: E2; 2: CpG-E2; 3: Pam3-E2; 4: Pam3-CpG-E2; 5: SIIN-Pam3-CpG-E2. Quantification indicated ~30 Pam3CSK4 lipopeptides and ~15 SIINFEKL peptides were conjugated externally per 60-mer E2 nanoparticle. (C) Hydrodynamic diameters of E2 constructs after CpG, Pam3, and SIIN conjugations. The hydrodynamic diameters of CpG-E2, Pam3-E2 and Pam3-CpG-E2, and SIIN-Pam3-CpG-E2 nanoparticles were ~27.3 nm, ~31.3 nm, and ~29.2 nm, and ~31.1 nm, respectively.



## B. References

1. Milder, F. J.; Jongeneelen, M.; Ritschel, T.; Bouchier, P.; Bisschop, I. J. M.; de Man, M.; Veldman, D.; Le, L.; Kaufmann, B.; Bakkers, M. J. G.; Juraszek, J.; Brandenburg, B.; Langedijk, J. P. M., Universal stabilization of the influenza hemagglutinin by structure-based redesign of the pH switch regions. *Proc. Natl. Acad. Sci. U. S. A.* **2022**, *119* (6).
2. McMillan, C. L. D.; Cheung, S. T. M.; Modhiran, N.; Barnes, J.; Amarilla, A. A.; Bielefeldt-Ohmann, H.; Lee, L. Y. Y.; Guilfoyle, K.; van Amerongen, G.; Stittelaar, K.; Jakon, V.; Lebas, C.; Reading, P.; Short, K. R.; Young, P. R.; Watterson, D.; Chappell, K. J., Development of molecular clamp stabilized hemagglutinin vaccines for Influenza A viruses. *npj Vaccines* **2021**, *6* (1).
3. Maciola, A. K.; Pietrzak, M. A.; Kosson, P.; Czarnocki-Cieciura, M.; Smietanka, K.; Minta, Z.; Kopera, E., The Length of N-Glycans of Recombinant H5N1 Hemagglutinin Influences the Oligomerization and Immunogenicity of Vaccine Antigen. *Frontiers in Immunology* **2017**, *8*.
4. Pietrzak, M.; Maciola, A.; Zdanowski, K.; Protas-Klukowska, A. M.; Olszewska, M.; Smietanka, K.; Minta, Z.; Szewczyk, B.; Kopera, E., An avian influenza H5N1 virus vaccine candidate based on the extracellular domain produced in yeast system as subviral particles protects chickens from lethal challenge. *Antiviral Research* **2016**, *133*, 242-249.
5. Molino, N. M.; Anderson, A. K. L.; Nelson, E. L.; Wang, S.-W., Biomimetic Protein Nanoparticles Facilitate Enhanced Dendritic Cell Activation and Cross-Presentation. *ACS Nano* **2013**, *7* (11), 9743-9752.